NASA Tech Briefs

National
Aeronautics and
Space
Administration

High-density circuit boards for a commercial microfilm
storage and retrieval unit are made possible by wiring
concepts originally developed for spacecraft electronics. Two
such techniques — stitchbonding and parallel gap welding —
have found their way into several commercial products, where
they reduce package size and weight and help to lower
production costs. [See the bottom of page A1.]

About the NASA
Technology Utilization Program

The National Aeronautics and Space Act of 1958, which established NASA and the United States civilian space program, requires that "The Administration shall provide for the widest practicable and appropriate dissemination of information concerning its activities and the results thereof."

To help carry out this objective, NASA's Technology Utilization (TU) Program was established in 1962. Now, as an element of NASA's Technology Transfer Division, this program offers a variety of valuable services to help transfer aerospace technology to nonaerospace applications, thus assuring American taxpayers maximum return on their investment in space research; thousands of spinoffs of NASA research have already occurred in virtually every area of our economy.

The TU program has worked for engineers, scientists, technicians, and businessmen; and it can work for you.

NASA Tech Briefs

Tech Briefs is published quarterly and is free to engineers in U.S. industry and to other domestic technology transfer agents. It is both a current-awareness medium and a problem-solving tool. Potential products . . . industrial processes . . . basic and applied research . . . shop and lab techniques . . . computer software . . . new sources of technical data . . . concepts . . . can be found here. The short section on New Product Ideas highlights a few of the potential new products contained in this issue. The remainder of the volume is organized by technical category to help you quickly review new developments in your areas of interest. Finally, a subject index makes each issue a convenient reference file.

Further Information on Innovations

Although some new technology announcements are complete in themselves, most are backed up by Technical Support Packages (TSP's). TSP's are available without charge and may be ordered by simply completing a TSP Request Card found at the back of this volume. Further information on some innovations is available for a nominal fee from other sources, as indicated. In addition, Technology Utilization Officers at NASA Field Centers will often be able to lend necessary guidance and assistance.

Patent Licenses

Patents have been issued to NASA on some of the inventions described, and patent applications have been submitted on others. Each announcement indicates patent status, if applicable.

Other Technology Utilization Services

To assist engineers, industrial researchers, business executives, city officials, and other potential users in applying space technology to their problems, NASA sponsors Industrial Applications Centers. Their services are described on page A6. In addition, an extensive library of computer programs is available through COSMIC, the Technology Utilization Program's outlet for NASA-developed software.

Applications Program

NASA conducts applications engineering projects to help solve public-sector problems in such areas as safety, health, transportation, and environmental protection. Applications teams, staffed by professionals from a variety of disciplines, assist in this effort by working with Federal agencies and health organizations to identify critical problems amenable to solution by the application of existing NASA technology.

Reader Feedback

We hope you find the information in *NASA Tech Briefs* useful. A reader-feedback card has been included because we want your comments and suggestions on how we can further help you apply NASA innovations and technology to your needs. Please use it; or if you need more space, write to the Director, Technology Transfer Division, P. O. Box 8757, Baltimore/Washington International Airport, Maryland 21240.

NASA Tech Briefs

COVERS: The photographs on the front and back covers illustrate developments by NASA and its contractors that resulted in commercial and nonaerospace spinoffs. You can use the TSP Request Card at the end of this issue to learn more about the Wiring Techniques [Circle 90] and the Sewage Treatment Plant [Circle 91].

About This NASA Publication

NASA Tech Briefs, a quarterly publication, is distributed free to qualified U.S. citizens to encourage commercial application of U.S. space technology. For information on publications and services available through the NASA Technology Utilization Program, write to the Director, Technology Transfer Division, P. O. Box 8757, Baltimore/Washington International Airport, Maryland 21240.

Change of Address

If you wish to have NASA Tech Briefs forwarded to your new address, use one of the Subscriptions cards enclosed in the back of this volume of NASA Tech Briefs. Be sure to check the appropriate box indicating change of address.

Communications Concerning Editorial Matter

For editorial comments or general communications about NASA Tech Briefs, you may use the Feedback card in the back of NASA Tech Briefs, or write to: The Publications Manager, Technology Transfer Division (ETD-6), NASA Headquarters, Washington, DC 20546. Technical questions concerning specific articles should be directed to the Technology Utilization Officer of the sponsoring NASA Center (addresses listed on page A4).
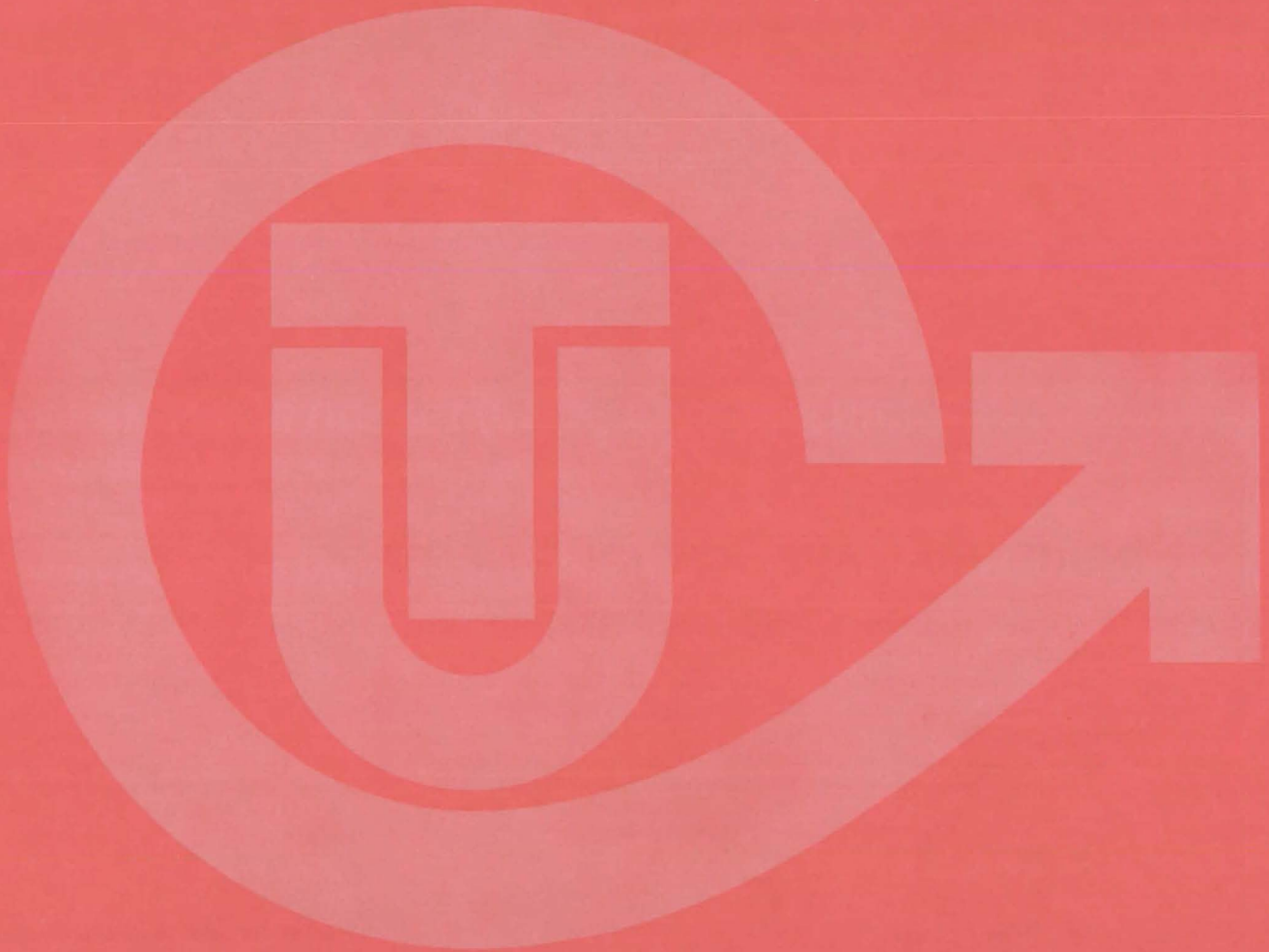
1978 Index

To obtain a copy of the 1978 Index to NASA Tech Briefs, Circle 92 on the TSP Request Card at the back of this issue. (Supplies are limited.)

Acknowledgements

NASA
TU SERVICES

NASA TECHNOLOGY UTILIZATION NETWORK

★ TECHNOLOGY UTILIZATION OFFICERS

Charles C. Kubokawa
Ames Research Center
Code AU: 240-2
Moffett Field, CA 94035
(415) 965-5333

Gussie Anderson
Hugh L. Dryden Flight Research Center
Code OD/TU Office - Room 2015
Post Office Box 273
Edwards, CA 93523
(805) 258-3311, Ext. 787

Donald S. Friedman
Goddard Space Flight Center
Code 702.1
Greenbelt, MD 20771
(301) 344-6242

John T. Wheeler
Lyndon B. Johnson Space Center
Code AT-3
Houston, TX 77058
(713) 483-3809

Raymond J. Cerrato
John F. Kennedy Space Center
Code AA-SA-1
Kennedy Space Center, FL 32899
(305) 867-2780

John Samos
Langley Research Center
Mail Stop 139A
Hampton, VA 23665
(804) 827-3281

Paul Foster
Lewis Research Center
Mail Stop 3-19
21000 Brookpark Road
Cleveland, OH 44135
(216) 433-4000, Ext. 6422

Aubrey D. Smith
George C. Marshall Space Flight Center
Code AT01
Marshall Space Flight Center, AL 35812
(205) 453-2224

D. W. Orrick
NASA Headquarters
Code ETD-6
Washington, DC 20546
(202) 755-2244

John H. Warden
NASA Pasadena Office
4800 Oak Grove Drive
Pasadena, CA 91103
(213) 354-6420

Gilmore H. Trafford
Wallops Flight Center
Code OD
Wallops Island, VA 23337
(804) 824-3411, Ext. 201

● INDUSTRIAL APPLICATIONS CENTERS

Aerospace Research Applications Center
1201 East 38th Street
Indianapolis, IN 46205
E. G. Buck, director
(317) 264-4644

**Computer Software Management
and Information Center (COSMIC)**
Suite 112, Barrow Hall
University of Georgia
Athens, GA 30602
(404) 542-3265

Kerr Industrial Applications Center
Southeastern Oklahoma State University
Durant, OK 74701
Robert Oliver, director
(405) 924-0121, Ext. 413

NASA Industrial Applications Center
LIS Building
University of Pittsburgh
Pittsburgh, PA 15260
Edmond Howie, director
(412) 624-5211

**New England Research Applications
Center**
Mansfield Professional Park
Storrs, CT 06268
Daniel Wilde, director
(203) 486-4533

**North Carolina Science and
Technology Research Center**
Post Office Box 12235
Research Triangle Park, NC 27709
Peter J. Chenery, director
(919) 549-0671

Technology Applications Center
University of New Mexico
Albuquerque, NM 87131
Stanley Morain, director
(505) 277-3622

Western Research Applications Cent
University of Southern California
University Park
Los Angeles, CA 90007
Robert Mixer, acting director
(213) 741-6132

■ STATE TECHNOLOGY APPLICATIONS CENTERS

**NASA/University of Florida
State Technology Applications Center**
311 Weil Hall
University of Florida
Gainesville, FL 32611
Ronald J. Thornton, director
Gainesville: (904) 392-6760
　　Orlando: (305) 275-2706
　　Tampa: (813) 974-2499

**NASA/University of Kentucky
State Technology Applications Program**
109 Kinkead Hall
University of Kentucky
Lexington, KY 40506
William R. Strong, manager
(606) 258-4632

◆ PATENT COUNSELS

Robert F. Kempf
Asst. Gen. Counsel for patent matters
NASA Headquarters
Code GP-4
400 Maryland Avenue, S.W.
Washington, DC 20546
(202) 755-3954

Darrell G. Brekke
Ames Research Center
Mail Code: 200-11A
Moffett Field, CA 94035
(415) 965-5104

Paul F. McCaul
Hugh L. Dryden Flight Research Center
Code OD/TU Office - Room 2015
Post Office Box 273
Edwards, CA 93523
(213) 354-2734

John O. Tresansky
Goddard Space Flight Center
Mail Code: 204
Greenbelt, MD 20771
(301) 344-7351

Marvin F. Matthews
Lyndon B. Johnson Space Center
Mail Code: AM
Houston, TX 77058
(713) 483-4871

James O. Harrell
John F. Kennedy Space Center
Mail Code: SA-PAT
Kennedy Space Center, FL 32899
(305) 867-2544

Howard J. Osborn
Langley Research Center
Mail Code: 279
Hampton, VA 23665
(804) 827-3725

Norman T. Musial
Lewis Research Center
Mail Code: 500-311
21000 Brookpark Road
Cleveland, OH 44135
(216) 433-4000, Ext. 346

Leon D. Wofford, Jr.
George C. Marshall Space Flight Center
Mail Code: CC01
Marshall Space Flight Center, AL 35812
(205) 453-0020

Monte F. Mott
NASA Pasadena Office
Mail Code: 180-601
4800 Oak Grove Drive
Pasadena, CA 91103
(213) 354-2700

▲ APPLICATION TEAMS

William N. Fetzner, director
Advisory Center for Medical Technology and Systems
University of Wisconsin
1500 Johnson Drive
Madison, WI 53706
(608) 263-2735

Edmund R. Bangs, director
IIT Research Institute
10 West 35th Street
Chicago, IL 60616
(312) 567-4191

Doris Rouse, director
Research Triangle Institute
Post Office Box 12194
Research Triangle Park, NC 27709
(919) 541-6256

Tom Anyos, director
SRI International
333 Ravenswood Avenue
Menlo Park, CA 94026
(415) 326-6200, Ext. 2864

Eugene Schmidt, program coordinator
Stanford University School of Medicine
Cardiology Division
Biomedical Technology Transfer
703 Welch Road, Suite E-4
Palo Alto, CA 94304
(415) 497-5353

David MacFadyen, project director
Technology + Economics
2225 Massachusetts Avenue
Cambridge, MA 02140
(617) 491-1500

TECHNOLOGY UTILIZATION OFFICERS

Technology transfer experts can help you
apply the innovations in NASA Tech Briefs.

The Technology Utilization Officer
at each NASA Field Center is an
applications engineer who can help
you make use of new technology
developed at his center. He brings you
NASA Tech Briefs and other special
publications, sponsors conferences,
and arranges for expert assistance in
solving technical problems.

Technical assistance,
in the form of further information about
NASA innovations and technology, is
one of the services available from the
TUO. Together with NASA scientists
and engineers, he can often help you
find and implement NASA technology
to meet your specific needs.

Technical Support Packages (TSP's)
are prepared by the center TUO's.
They provide further technical details
for articles in NASA Tech Briefs. This
additional material can help you
evaluate and use NASA technology.
You may receive most TSP's free of
charge by using the TSP Request Card
found at the back of this issue.

Technical questions about articles
in NASA Tech Briefs are answered in
the TSP's. When no TSP is available,
or you have further questions, contact
the Technology Utilization Officer at
the center that sponsored the re-
search [see page A4].

NASA INVENTIONS AVAILABLE FOR LICENSING

Over 3,500 NASA inventions are available for licensing
in the United States — both exclusive and nonexclusive.

Nonexclusive licenses
for commercial use of NASA inven-
tions are encouraged to promote
competition and to achieve the widest
use of inventions. They must be used
by a negotiated target date but are
usually royalty-free.

Exclusive licenses
may be granted to encourage early
commercial development of NASA
inventions, especially when consider-
able private investment is required.
These are generally for 5 to 10 years
and usually require royalties based on
sales or use.

Additional licenses available
include those of NASA-owned foreign
patents. In addition to inventions
described in NASA Tech Briefs,
"NASA Patent Abstract Bibliography"
(PAB), containing abstracts of all
NASA inventions, can be purchased
from National Technical Information
Service, Springfield, VA 22161. The
PAB is updated semiannually.
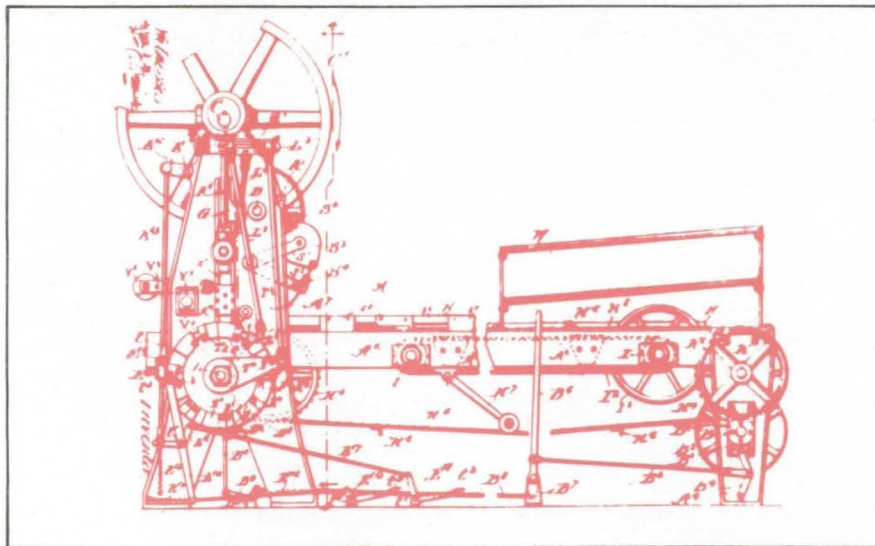
Patent licenses for Tech Briefs
are frequently available. Many of the
inventions reported in NASA Tech
Briefs are patented or are under
consideration for a patent at the time
they are published. The current patent
status is described at the end of the
article; otherwise, there is no state-
ment about patents. If you want to
know more about the patent program
or are interested in licensing a
particular invention, contact the
Patent Counsel at the NASA Field
Center that sponsored the research
[see page A5]. Be sure to refer to the
NASA reference number at the end of
the Tech Brief.

APPLICATION TEAMS
Technology-matching and problem-solving
assistance to public-sector organizations

Application engineering projects
are conducted by NASA to help solve
public-sector problems in such areas
as safety, health, transportation, and
environmental protection. Some appli-
cation teams specialize in biomedical
disciplines; others, in engineering and
scientific problems. Staffed by profes-
sionals from various disciplines, these
teams work with other Federal agen-
cies and health organizations to

identify critical problems amenable to
solution by the application of existing
NASA technology.

Public-sector organization
*representatives can learn more about
application teams by contacting a
nearby NASA Field Center Technology
Utilization Office [see page A4].*

INDUSTRIAL APPLICATIONS CENTERS
Computerized access to nearly
10 million documents worldwide

Computerized information retrieval
from one of the world's largest banks
of technical data is available from
NASA's network of Industrial Applica-
tions Centers (IAC's). The IAC's give
you access to 1,800,000 technical
reports in the NASA data base and to
more than 10 times that many reports
and articles found in 140 other
computerized data bases.

The major sources include:
* *750,000 NASA Technical Reports*
* *Selected Water Resources Abstracts*
* *NASA Scientific and Technical
  Aerospace Reports*
* *Air Pollution Technical Information
  Center*
* *NASA International Aerospace
  Abstracts*
* *Chem Abstracts Condensates*
* *Engineering Index*
* *Energy Research Abstracts*
* *NASA Tech Briefs*
* *Government Reports
  Announcements*

and many other specialized files on
food technology, textile technology,
metallurgy, medicine, business, eco-
nomics, social sciences, and physical
science.

The IAC services
range from tailored literature searches
through expert technical assistance:

* *Retrospective Searches:* Published
  or unpublished literature is screened,
  and documents are identified accord-
  ing to your interest profile. IAC engi-
  neers tailor results to your specific
  needs and furnish abstracts consid-
  ered the most pertinent. Complete
  reports are available upon request.
* *Current-Awareness Searches:* IAC
  engineers will help design a program
  to suit your needs. You will receive
  selected monthly or quarterly ab-
  stracts on new developments in your
  area of interest.

* *Technical Assistance:* IAC engineers
  will help you evaluate the results of
  your literature searches. They can
  help find answers to your technical
  problems and put you in touch with
  scientists and engineers at appropri-
  ate NASA Field Centers.

Prospective clients
*can obtain more information about the
services offered by NASA IAC's by
contacting the nearest IAC [see page
A4] or by checking the IAC box on a
TSP Request Card in this issue.*

STATE TECHNOLOGY APPLICATIONS CENTERS

Technical information services for industry
and state and local government agencies

Local government and industry

in Florida and Kentucky can utilize the services of NASA's State Technology Applications Centers (STAC's). The STAC's differ from the Industrial Applications Centers described on page A7, primarily in that they are integrated into existing state technical assistance programs and serve only the host state, whereas the IAC's serve multistate regions.

Many data bases,

including the NASA base and several commercial bases, are available for automatic data retrieval through the STAC's. Other services such as document retrieval and special searches are also provided. (The STAC's normally charge a fee for their services.)

To obtain information

about the services offered by NASA STAC's, write or call the STAC in your state [see page A4].

COSMIC®

An economical source of computer programs
developed by NASA and other government agencies

A vast software library

is maintained by COSMIC — the Computer Software Management and Information Center. COSMIC gives you access to approximately 1,600 computer programs developed for NASA and the Department of Defense and selected programs for other government agencies. Programs and documentation are available at reasonable cost.

Available programs

range from management (PERT scheduling) to information science (retrieval systems) and computer operations (hardware and software). Hundreds of engineering programs perform such tasks as structural analysis, electronic circuit design, chemical analysis, and the design of fluid systems. Others determine building energy requirements and optimize mineral exploration.

COSMIC services

go beyond the collection and storage of software packages. Programs are checked for completeness; special announcements and an indexed software catalog are prepared; and programs are reproduced for distribution. Customers are helped to identify their software needs; and COSMIC follows up to determine the successes and problems and to provide updates and error corrections. In some cases, NASA engineers can offer guidance to users in installing or running a program.

Information about programs

described in NASA Tech Briefs articles can be obtained by completing the COSMIC Request Card at the back of this issue. Just circle the letters that correspond to the programs in which you are interested.

NEW PRODUCT IDEAS

NEW PRODUCT IDEAS are just a few of the many innovations described in this issue of NASA Tech Briefs and having promising commercial applications. Each is discussed further on the referenced page in the appropriate section in this issue. If you are interested in developing a product from these or other NASA innovations, you can receive further technical information by requesting the TSP referenced at the end of the full-length article or by writing the Technology Utilization Office of the sponsoring NASA center (see page A4). NASA's patent-licensing program to encourage commercial development is described on page A8.

Seal for High and Low Temperatures
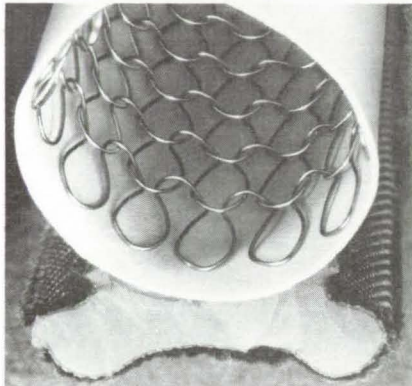
A composite seal for freezers, refrigerated vehicles, aircraft doors, and other applications sustains temperatures between -423° and 500° F. Made of a tubular spring core surrounded by a flow barrier of polytetrafluoroethylene or polyolefin, the seal outperforms many conventional seals made of silicon rubber or other elastomers. (These conventional seals lose their resiliency at very low temperatures or decompose at high temperatures.) The knitted-wire tubular spring is resilient and can be deflected to an extreme without deforming. It can be adjusted for specific applications by varying the wire diameter and density.
(See page 429.)

Flame-Resistant Textiles
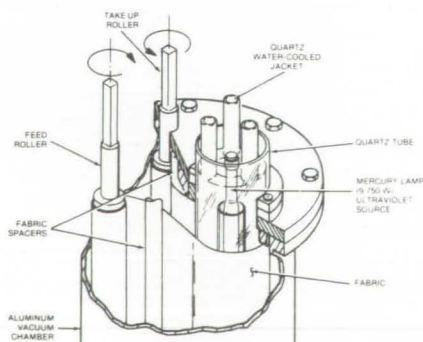
Textiles are made flame resistant in a new processor already tested successfully on one aromatic polyamide fabric. Included in the processor are feed and take-up rollers, a 9,750-watt ultraviolet lamp for generating fluorocarbon acceptor sites, and a vacuum chamber containing a gaseous halo-olefin mixture. Fluorocarbon grafts applied in the processor make the fibers flame resistant in oxygen-enriched atmospheres, without sacrificing their color or physical properties. The typical processing time for ten yards of fabric is about 3 to 4 hours.
(See page 369.)

Slip Sensor

A compact magnetic sensor, originally developed for a mechanical-claw manipulator, detects slippage of one surface relative to another. A sphere of nonmagnetic material embedded with magnetic pins is mounted in a bearing at the tip of the new sensor.
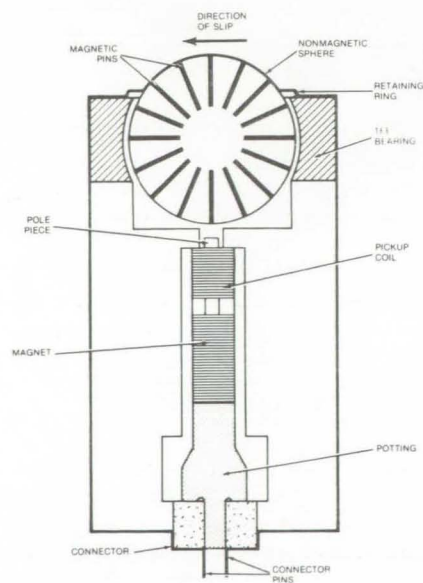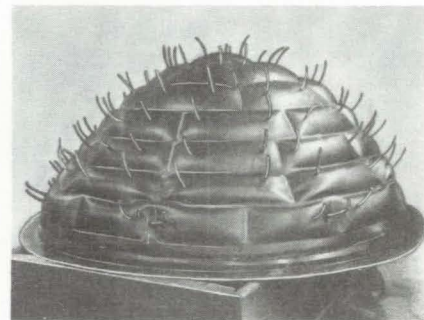

When the sphere rotates in any direction, the pins move past a magnetic pickup that generates a

series of electrical pulses. If the sensor is pressed against a surface, slippage of the surface turns the sphere, and the pulses actuate a warning light, buzzer, or slip-control circuit.
(See page 422.)

Pillowed Airbags for Conformal Cushions

A rubber airbag composed of many small air "pillows" can be used as a cushion for equipment during shipment. Pressure in the pillows can be adjusted individually to suit a given cargo. A novel four-step procedure fabricates the pillowed bag from two sheets of rubber. The sheets are bonded together only at the boundaries of the individual pillows. Holes are cut in the top sheet, and rubber tubing is inserted and bonded to the sheet with an adhesive. The pillows can be inflated through the tubes, which are then sealed. Other possible uses for the pillowed airbag are in applying uniform pressure during the fabrication of plastics and composites.
(See page 439.)

Long-Wearing TFE/Metal Bearings

Durable bearing surfaces are formed by a new process for applying a thin coating of polytetrafluoroethylene. Effective on a wide range of metals and complex surface contours, the technique is more versatile than previous pressed-powder methods.

The surface to be treated is first roughened by grit-blasting and then sprayed with a TFE dispersion. After the coating is dried and fused at high temperature, it is burnished and feathered flush over the grit-blasted area. The result is a low-friction surface with TFE embedded in grit-eroded pits. Developed to protect valve surfaces on the Space Shuttle, the coating has potential applications in automotive gears, ball joints, and roller-chain components. Other possible uses include release coatings for dies and molds and unlubricated bearings for industrial processes. (See page 425.)

Solid-State Power Controller

Up to 20 amperes at 28-Vdc are switched by a new power controller that measures only 5 by 5 by 3 cm. Activated by a low-voltage signal at its control input, the hybrid unit also features current limiting and delayed trip after 2 or 3 seconds of overload.
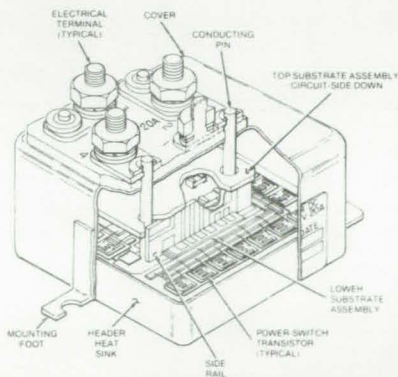
Novel use is made of special aluminum/magnesium wire in the emitter circuits of the output transistors. These wires increase in resistance nonlinearly with current and automatically limit the current without adding significant voltage drops that can reduce efficiency. Intended for applications where convection cooling is not efficient or not practical, the controller includes its own heat sink for attachment to a water-cooled plate or other temperature stabilizer. (See page 325.)

Detecting O2 in H2 and H2 in O2

Small amounts of oxygen in hydrogen or hydrogen in oxygen are detected by a new catalytic sensor.
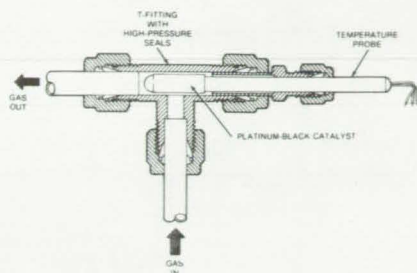
Whereas previous devices for sensing combustible gas mixtures were limited to low-pressure samples, the new unit can be installed directly in a high-pressure gas stream. Potentially explosive amounts of one gaseous species in the other at 415 psia are detected by a platinum-sheathed temperature-sensing probe. The platinum catalyzes the reaction of hydrogen and oxygen, and the heat of reaction is measured by the temperature sensor. Potential applications of the sensor are in gas-detection and measurement instruments, particularly for gases generated by electrolysis. (See page 380.)

Post-Processing Flame Retardant for Polyurethane
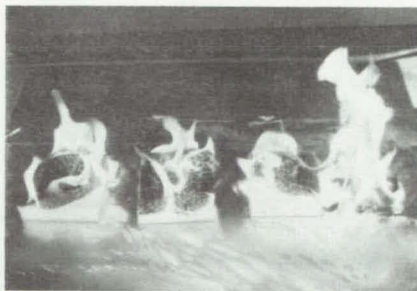
Polyurethane foam can be made fire-resistant without altering its lightness, flexibility, and resiliance by treating it with a new elastomeric formulation. In contrast to the conventional method of adding flame-retardants before the polyurethane is foamed, the new composition is dissolved in acetone and sprayed or otherwise applied on finished foam. Other advantages of the coating are that it does not deteriorate in Sunlight or generate smoke or toxic gases in a fire. By forming a protective char that stops combustion once the ignition source is removed, the coating can protect furniture cushions, mattresses, and other foam items. (See page 376.)

Precise Etching of Crystal Surfaces

Surface layers are removed from crystals and other samples with a precision of ± 1 Å by a new wet-chemical-etching apparatus. A gas-driven turbine rotates the crystal at up to 100,000 rpm as small droplets of etchant are dispensed on the surface.
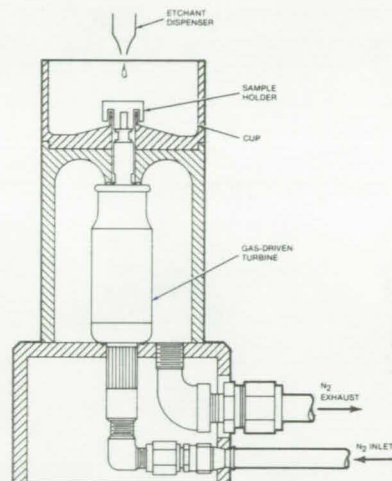
The drops spread into a film and evaporate, etching away a thin surface layer. The material-removal rate is controlled by adjusting the spin frequency, the etchant viscosity, the droplet size, and other parameters. Depth profiles of Si/SiO_2 samples have been exposed for study by the apparatus, which can be adapted for other materials as well. (See page 379.)

Compact Microbial Filter
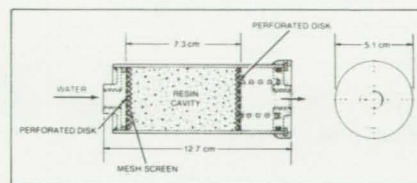
A compact microbial filter for potable water is packed with new iodine-saturated microbicidal resins. The recently tested resins give more stable iodine concentrations than previous formulations and do not impart objectionable odor or taste to the treated water. A typical filter is less than 13 cm long and only 5 cm in diameter. It is installed in series with

the water line where contamination by microorganisms is to be prevented. By releasing controlled amounts of iodine, the resin-filled cartridge kills bacteria, fungi, and viruses with essentially 100-percent efficiency. The filter operates on flows in either direction, with only a small loss of flow pressure.
(See page 392.)

## Rheometer for Coal and Other Multiphase Materials
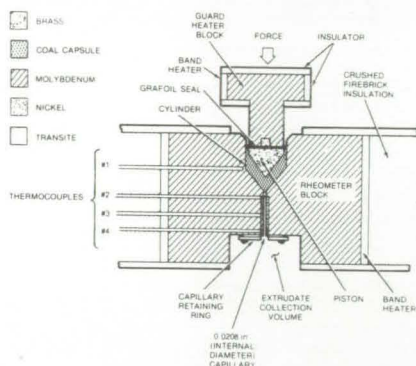
An improved rheometer measures the viscosity of coal and other materials heated to a molten or plastic state. Samples are heated rapidly and compressed by a piston through a capillary opening. The force applied by the piston is directly proportional to the sample viscosity. Tests may be run at pressures of up to 3,000 psig and temperatures as high as 470° C. The molybdenum housing includes thermocouples at various test points and a disposable nickel lining on the inside of the capillary. The nickel has high thermal conductivity, permitting accurate thermocouple readings. It is replaced after each test by removing a retaining ring.
(See page 380.)

Energy Saver for Industrial Lighting

Offices and industry can save energy by adopting a compact, inexpensive monitor that varies room
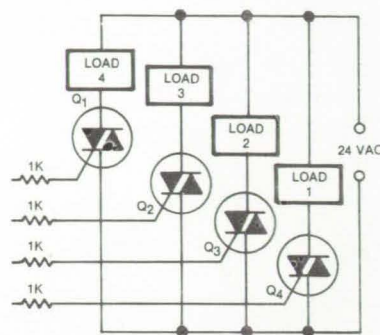

illumination according to the amount of Sunlight available. Consisting of a photosensitive cell, a few IC's, and solid-state switches, the monitor serves essentially the same function for lighting that a thermostat serves for a heating system. The photocell is mounted on the ceiling and pointed to an area where the illumination is representative of the entire room; changes in the cell output actuate the switching circuit, which controls power to artificial lighting. Consuming little current and being idle most of the time, the monitor is itself energy efficient.
(See page 407.)

Limiting Amplifier for Microwaves

Phase distortion in microwave traveling-wave tubes is prevented by a compact, lightweight, limiting amplifier. Using gallium arsenide field-effect transistors in four balanced radio-frequency stages, the limiter
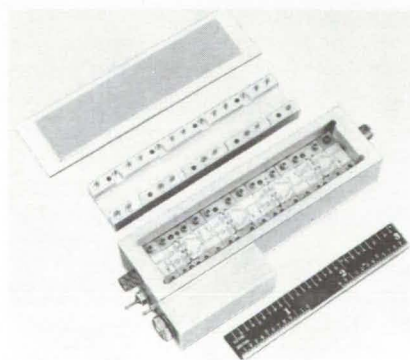
delivers a constant-amplitude drive signal to a Ku-band TWT. Since the FET limiter also introduces gain, TWT efficiency is enhanced for a given output power. The limiter is fabricated by conventional microstrip techniques and housed in an hermetically sealed package. The RF signal enters and leaves through metal-to-metal compression-seal connectors. Bias voltages enter via glass-to-metal feedthroughs. A separate voltage regulator is mounted in a small adjacent enclosure.
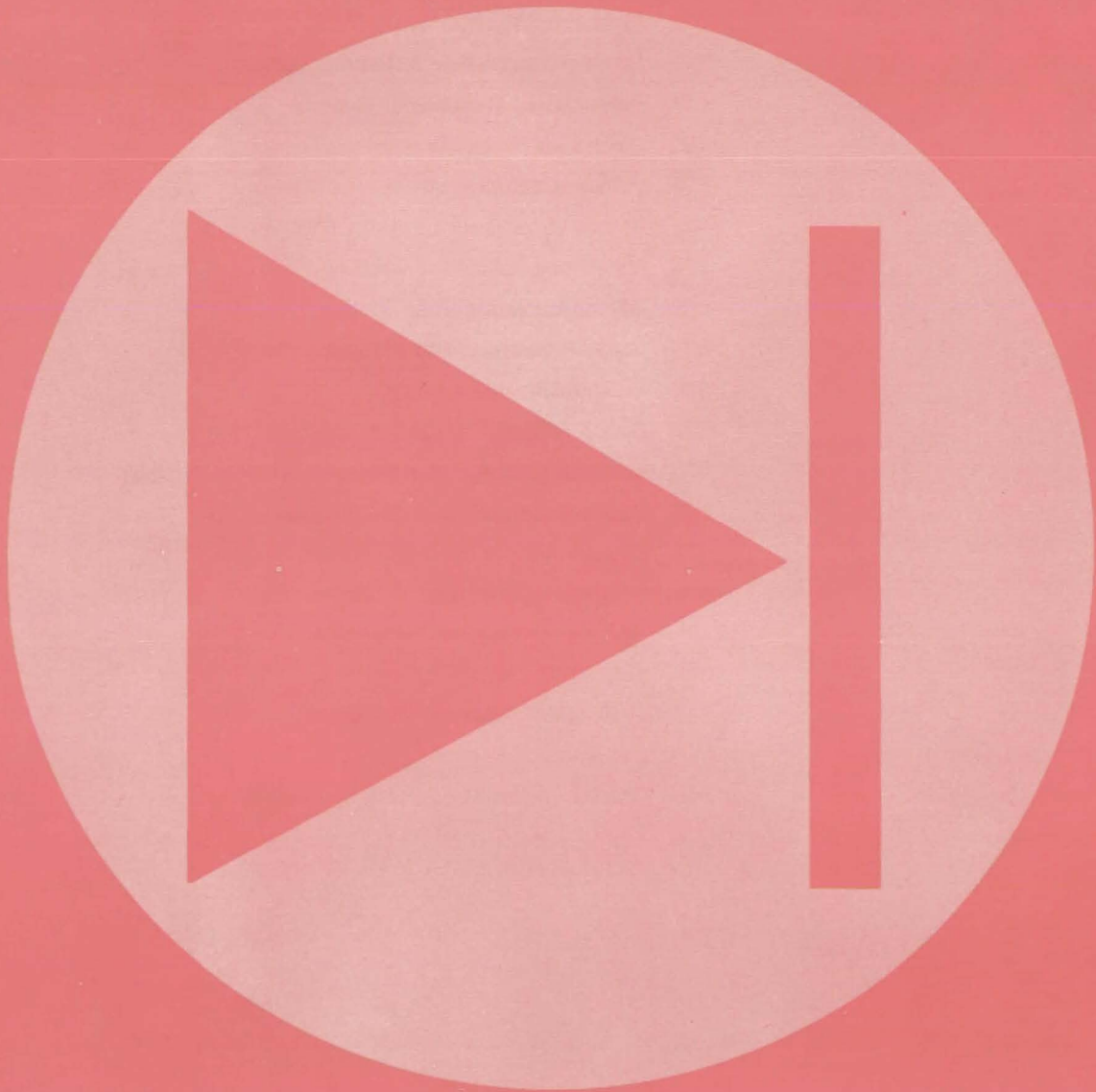(See page 337.)

Temperature Controller for Crystal Resonators
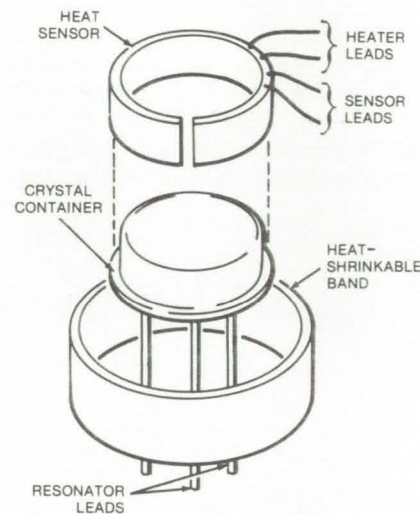
A tiny temperature controller for quartz crystal resonators slips over commercial TO-8 crystal packages and is held by a heat-shrinkable band. Temperature control is accurate to 0.7° C; and the low mass of the unit makes its time constant for temperature adjustment very short. An energy-efficient control circuit assembled from standard components is used with the heater/temperature sensor. Overall power consumption is under 5 W over the ambient operating temperature range of -55° to 80° C.
(See page 320.)

Electronic
Components
and Circuits

Hardware, Techniques, and Processes

Books and Reports

Inductorless Tuned Circuit for High Frequencies

Two-transistor connection is adaptable to filters,
amplifiers, and oscillators in integrated circuits.

Goddard Space Flight Center, Greenbelt, Maryland

A tuned circuit that uses no inductors can function as a filter, an amplifier, or an oscillator at radio frequencies. The circuit is based on two directly-coupled transistor stages in which the transistors are operated near their transition frequency F_t (the frequency at which transistor beta equals unity). In this frequency range, the inductive and capacitive reactances of the transistors allow them to function as active tuning elements, replacing inductive passive tuning elements. The inductorless tuned circuit can be fabricated as an integrated circuit on a single silicon chip.

The center frequency of operation must be in the rolloff portion of the beta-vs.-frequency curve of the transistors; in this operating region the transistors have reactive impedance and negative resistance if circuit parameters are properly adjusted. In the inductorless tuned amplifier in the figure, for example, transistors T_1 and T_2 have F_t of 4 MHz, and beta rolloff starts at 100 kHz. The amplifier produces a voltage gain of 200 when it is operated at 2 MHz. The 3-dB points of the band-pass curve are 8 kHz apart, indicating a circuit Q of 250.

T_1 and its associated circuitry form a common-base amplifier. T_2 and its associated circuitry form a common-emitter stage. (T_3 is a buffer stage that isolates T_1 and T_2 from the outut load and prevents load changes from affecting center frequency, Q, and gain.) Capacitor C_1 and resistor R_1 are connected to the base of T_1 for tuning that transistor, while capacitors C_3 and C_4 (connected to the base of T_2) and C_6 and C_7 (connected to the emitter of T_2) tune transistor T_2.

The circuit characteristics are essentially linear, largely because the input signal is applied to the emitter of one of the two transistors and the base of the other transistor. This arrangement causes F_t to change with input signal amplitude, which in turn causes changes in Q, gain, and center frequency.
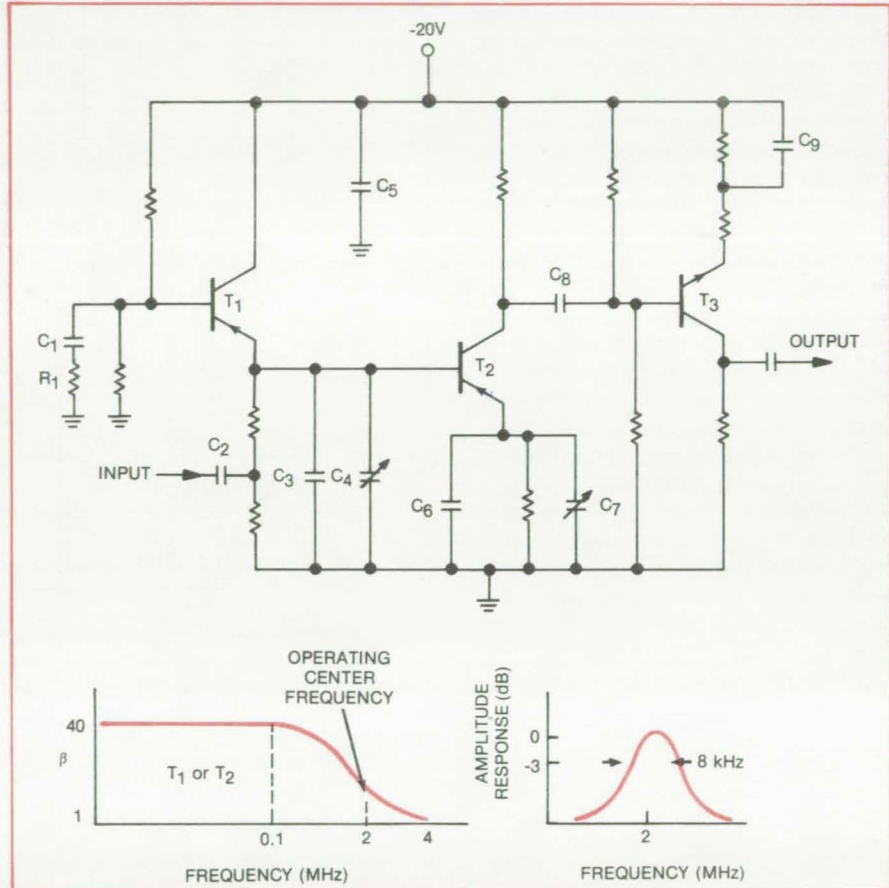
Inductorless Tuned Amplifier employs a direct-coupled two-transistor combination, T_1 and T_2. The input signal may be applied to the emitter side of either transistor.

The basic circuit can be operated as an oscillator by adjusting the values of R_1, C_3, C_4, C_6, and C_7 and of transistor collector current. The circuit can also be operated as a high-frequency crystal oscillator by using a crystal as the signal source. In one application, an overtone crystal with frequency in the 150- to 200-MHz range is placed in a circuit containing transistors with F_t in the region of 300 to 400 MHz. The result is a stable high-frequency oscillator that employs no unductors and is far easier to implement than a conventional high-frequency series-mode oscillator.

The F_t's of the two transistors in any application should be approximately equal. This fact makes the circuit particularly suitable for integration on a silicon chip, because both transistors will then be subjected to the same process conditions and will have virtually identical characteristics.

Temperature Controller for Crystal Resonators

An ultrafast, precise, low-cost control
unit for electronic filters and oscillators

NASA's Jet Propulsion Laboratory, Pasadena, California

A new temperature controller for quartz crystal resonators operates on less tha 5 W prime power and can heat a crystal from -10° C to +75° C in less than 45 s. Temperature control is accurate to within 0.7° C. This low-cost unit is more accurate and faster than other inexpensive controllers and faster than the costly but very precise controllers in vacuum flasks.

The short time constant of this temperature-controller is due to its reduced mass and smaller separation between the heater and the sensor. Its temperature error is reduced by an exceptionally high-gain circuit.

The unit consists of a heater/sensor crystal assembly and a high-gain control circuit. The nickel-iron wire used as a sensing/heating element has a highly stable resistance-versus-temperature characteristic. It dissipates 5 W. The assembly is arranged as an open ring (Figure 1) that fits over commercial TO-8 crystal containers.
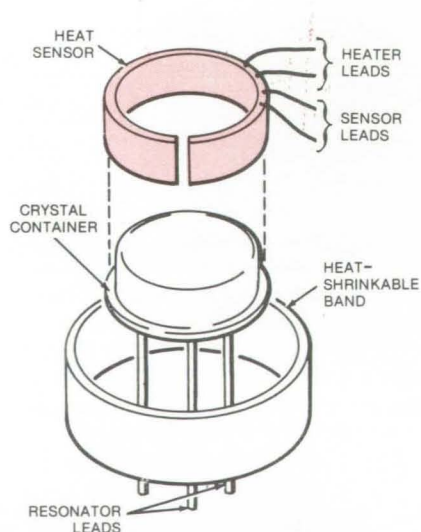

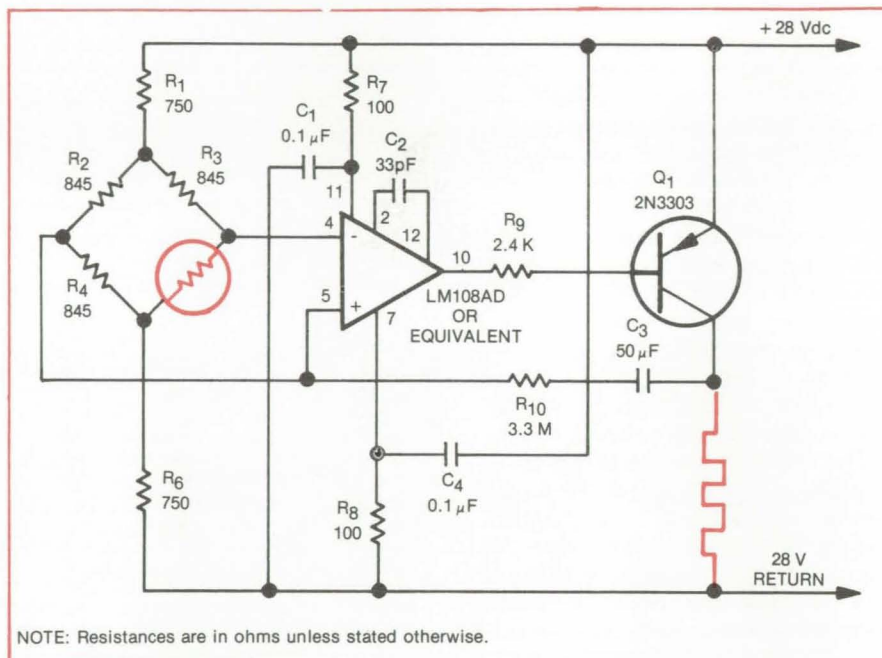NOTE: Resistances are in ohms unless stated otherwise.

Figure 2. The **Control Circuit** converts temperature error between the heater and the sensor into a voltage error. The bridge incorporates temperature sensor R_5. The values of resistors R_2, R_3, and R_4 are selected to match the value of R_5 at the desired control temperature, 75° C in this case.

Figure 1. **Thin Heater/Sensor** fits a standard TO-8 quartz-crystal package and is held in place with a heat-shrinkable band.

A film of room-temperature-vulcanized compound applied between the heater and the container assures good thermal conduction between the two. The heater is tied to the container surface with a lacing cord, and a heat-shrinkable band is placed over the heater as a constrictive cover.

The control circuit (see Figure 2) incorporates a sensor, an operational amplifier, and a power transistor. The sensor R_5 connected to a bridge circuit (R_2, R_3, R_4, and R_5) converts the temperature error into voltage error using a 20-mV/°C transfer function developed for this circuit. Resistors R_2, R_3, and R_4 are selected to equal the value of R_5 at the desired regulation temperature, and $R_1 = R_6$. The latter (R_1 and R_6) limit current through the bridge to keep the bridge elements from overheating.

The bridge error voltage is applied to an operational amplifier that has a static gain of 3×10^5 V/V. Resistors R_7 and R_8 with capacitors C_1 and C_4 filter the ripple on the prime voltage supply (+28 Vdc), while capacitor C_2 is selected to compensate the amplifier according to the manufacturer's specification. In addition, resistor R_9 is used to limit base current into transistor Q_1 so that full voltage swings of the amplifier output do not drive Q_1 into saturation.

The temperature controller works over an ambient temperature range of from -55° to 80° C. Its measured heat loss is 20 mW/° C.

This work was done by Thomas R. Turlington of Westinghouse Electric Co. for **NASA's Jet Propulsion Laboratory.** *For further information, Circle 2 on the TSP Request Card.*
NPO-14507

Direct-Current Drive for ac Motors

Windings of dual-wound motor replace
the transformer of the usual inverter.

NASA's Jet Propulsion Laboratory, Pasadena, California
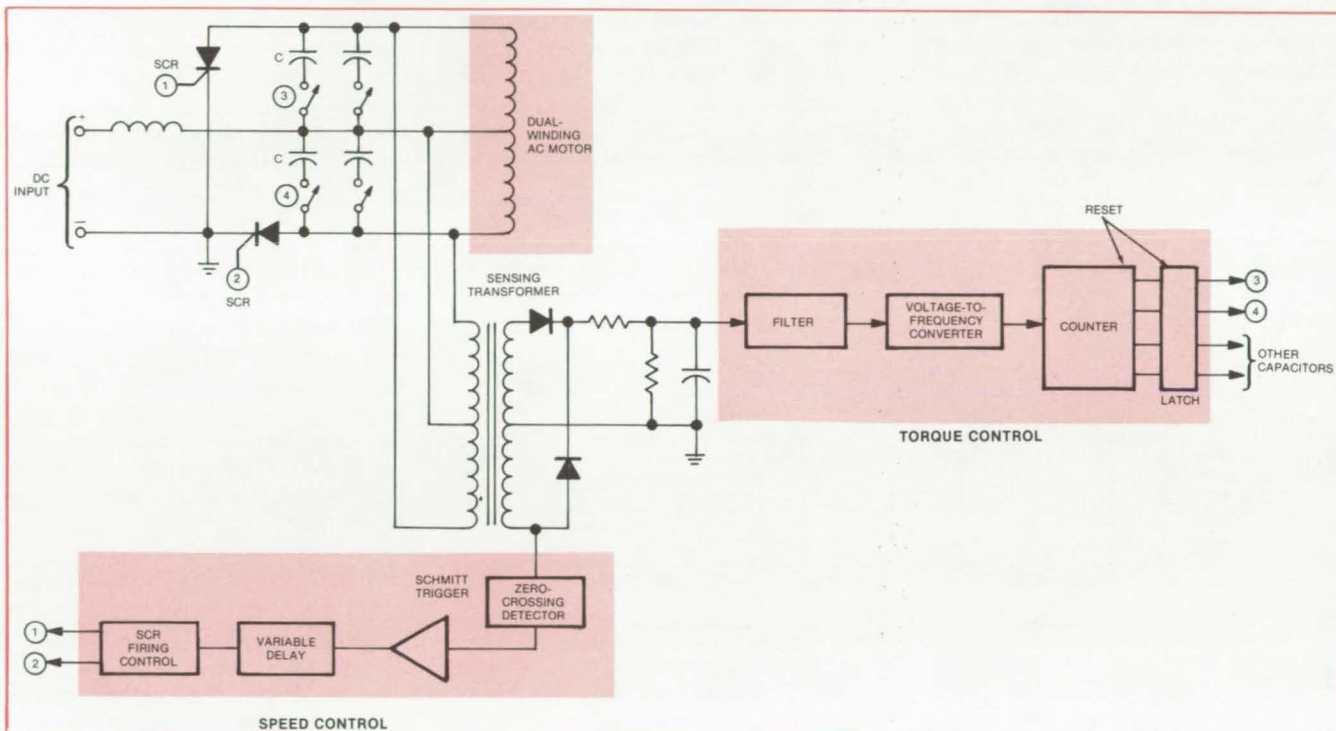
In **A dc-Driven ac Motor,** the dual windings of the motor serve as the output transformer for dc/ac inversion. Speed is controlled by the firing of the SCR's, and torque is controlled by inverter capacitance.

Dual-wound ac motors can be operated from dc connected through rectifiers to the ac motor windings. This use of the motor windings in place of inverter transformer windings makes it possible to use low-cost, commutatorless ac motors instead of more-complicated and expensive dc motors. Thus, readily-available ac motors can be powered by solar energy, batteries, and other dc sources. Moreover, because the motor speed is not fixed by a 60-hertz supply, motors can be operated at higher speeds and thus can be made smaller so that they require less material.

The dc is applied to the ends and center of the motor windings (see figure). The silicon controlled rectifiers (SCR's) individually pass current only on alternate half cycles, as in a full-wave rectifier, so that there is current in only one of the dual windings at any given instant.

The speed of the motor can be varied by varying the switching frequeny of the SCR's. The motor torque can be controlled by automatic switching of capacitors in the motor circuit. The variable-speed, controlled-torque operation is especially attractive in electric vehicles.

A sensing transformer monitors load variations via connections to the motor windings. For automatic speed control, the output of the center-tapped secondary of the sensing transformer is applied to a full-wave rectifier, the output of which is, in turn, applied to a zero-crossing detector. When it senses a change in load current, it turns on a Schmitt-trigger circuit that actuates a suitable response from an SCR firing-control circuit. A variable-delay network interposed between the Schmitt trigger and the SCR firing control allows the speed

to be set manually at some desired number of revolutions per minute. The sensing transformer and its associated control circuitry then maintain the speed at that setting.

Automatic torque control is provided by a filter, a voltage-to-frequency converter, and a counter connected to the sensing-transformer rectifier. The filtered dc voltage output of the rectifier is proportional to torque variations. That voltage is converted to a frequency change, which is fed to an up/down counter. The counter controls the capacitance in the inverter, switching capacitors in or out as torque is increasing or decreasing.

Measuring Signal-to-Noise Ratio Automatically

Fast bit-error-rate measurements are the basis of the
S/N calculations for digital communication channel.

NASA's Jet Propulsion Laboratory, Pasadena, California

An automated method of measuring signal-to-noise ratio in digital communication channels is more precise and 100 times faster than a previously used method. The new method can be used with cable, microwave radio, or optical-fiber links. It measures burst noise and channel capacity as well as signal-to-noise ratio and takes into account the effects of band limiting, crosstalk, timing jitter, and power level.

The new method is based on bit-error-rate (BER) measurement. As in other BER techniques, the channel is stimulated with a pseudorandom digital signal with spectral characteristics resembling those of an actual data signal.

Unlike earlier BER methods, however, the new method varies the "slicing" threshold in the decision stage of the receiver — the level at which a bit is regarded as a 0 rather than a 1. Although this level is customarily fixed in a receiver, in the new method it is swept from its optimum value to the 1 level, while a pseudorandom signal is sent through the link, until a specified BER is obtained. At that point, most of the errors are from noise superimposed on the 1 level, and thus the magnitude of the 1 level may be ascertained (Figure 1). From that magnitude, the signal-to-noise ratio can be computed by a simple formula. Signal-to-noise measurements accurate within ± 0.01 dB can be made in a minute or less.

A pseudorandom data generator drives the channel to be measured (Figure 2 illustrates the setup for an optical-fiber link). The data pass through the link where they are corrupted by noise, band-limited, regenerated, and finally transferred to a pseudorandom data receiver. The receiver contains a data generator identical to the one in the pseudorandom data transmitter and runs in synchronism with the data coming out of the link. The receiver makes a bit-by-bit comparison of the data coming out of the link and those generated in the receiver. When a discrepancy occurs, the receiver
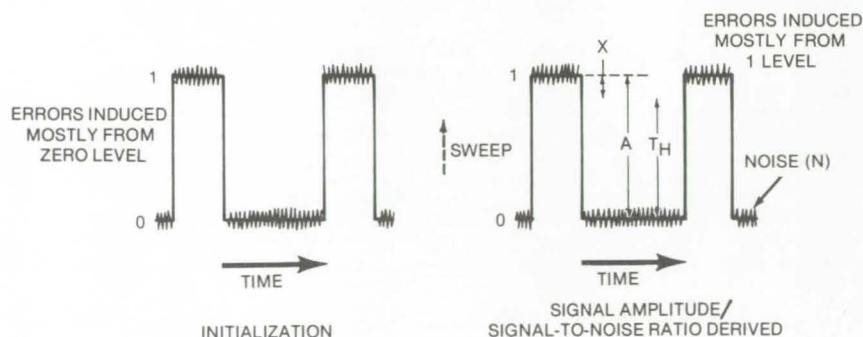

Figure 1. **Zero/One Threshold** is swept towards the one level during the bit-error-rate (BER) measurement. When a predetermined BER is reached, the distance X separating the one level and threshold is then known, permitting the determination of the signal level: $A = X + T_H$. The signal-to-noise ratio is calculated by using the signal amplitude (A) and the noise amplitude (N); N can be determined at initialization (low threshold).

INPUT PARAMETERS VARIED

* Receiver Threshold Level
* Data Stream Bit Rate
* Receiver Calibration Signal

OUTPUT PARAMETERS RECORDED:

* Receiver Threshold Level
* Burst Error Rates
* Temperature

CALCULATED SYSTEM PARAMETERS:

* Link Loss
* Link Bandlimiting
* Scintillation Effects
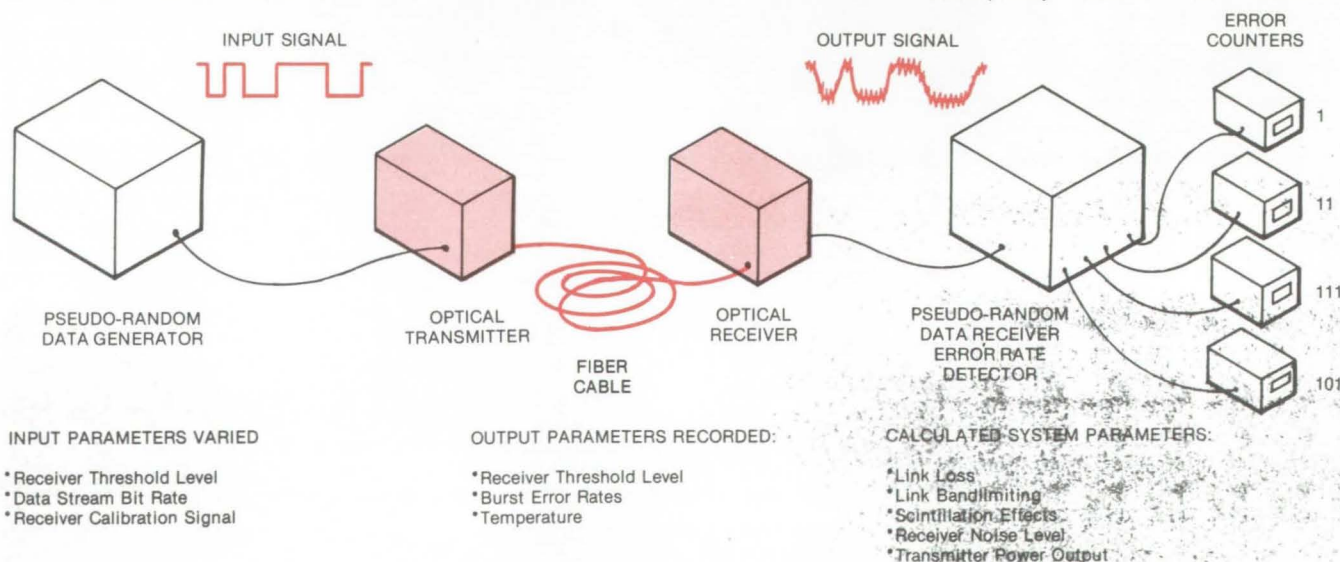* Receiver Noise Level
* Transmitter Power Output

Figure 2. Basic setup for **Measurements on a Fiber-Optic Channel** allows a comparison of the transmitted data with received data. In addition to signal-to-noise ratio, burst noise and channel capacity may also be measured simultaneously by employing multiple error counters.

sends an error pulse to a counter. The measurement is usually terminated when the counter accumulates 100 errors; this total provides a sample size large enough for accurate determination of bit-error rate.

The procedure is repeated for a range of threshold values so that the signal-to-noise ratio can be calculated. In addition, various other calculations of channel performance can be made, such as burst noise and channel capacity. The measurement setup can be automated by a microprocessor, which controls the test variables, monitors the data-collection process, and formats the data.

The prototype automated test system is contained on five circuit boards: a high-speed bit-error-rate test block, a central processing unit, a power controller, a temperature-sensor array, and the fiber-optic link terminal module. The circuitry employs 140 integrated circuits. An important practical advantage of the BER approach is that most of the test circuitry is digital, reducing calibration and temperature-stabilization requirements to a minimum.

Low-Common-Mode Differential Amplifier

Common-mode feedback suppresses phase and amplitude inequality over a wide frequency range.

Lyndon B. Johnson Space Center, Houston, Texas

The outputs of a new differential amplifier are excellently matched in phase and amplitude over a wide range of frequencies. A common-mode feedback loop offsets differences between the two signal paths. One implementation of the circuit has shown excellent response up to 5 MHz, and a wider bandwidth is obtainable through simple component substitutions. Possible applications of the circuit are in oscilloscopes, integrated-circuit logic testers, and other self-contained instruments.

As shown in the figure, the common-mode output signal is amplified by a gain K. It is then summed with the positive and negative values of the output of the low-gain input-amplifier stage G_1. The common-mode loop gain is a function of K and of the gains of the output-stage amplifiers G_2 and G_3. Detailed circuit analysis shows that as long as the common-mode loop gain is greater than 1, the common-mode feedback loop reduces the common-mode output voltage.

The amplifier input stage, G_1, uses differential field-effect transistors (FET's) that produce a relatively low gain. A pnp differential amplifier with capacitive feedback is the second stage. The capacitance and the transconductance of the FET's yield a bandwidth of 8.84 MHz for the signal loop (as distinguished from the common-mode loop).

Each output of the second stage drives one of the current amplifier

NOTE: Differential Output = $E_2 - E_3$
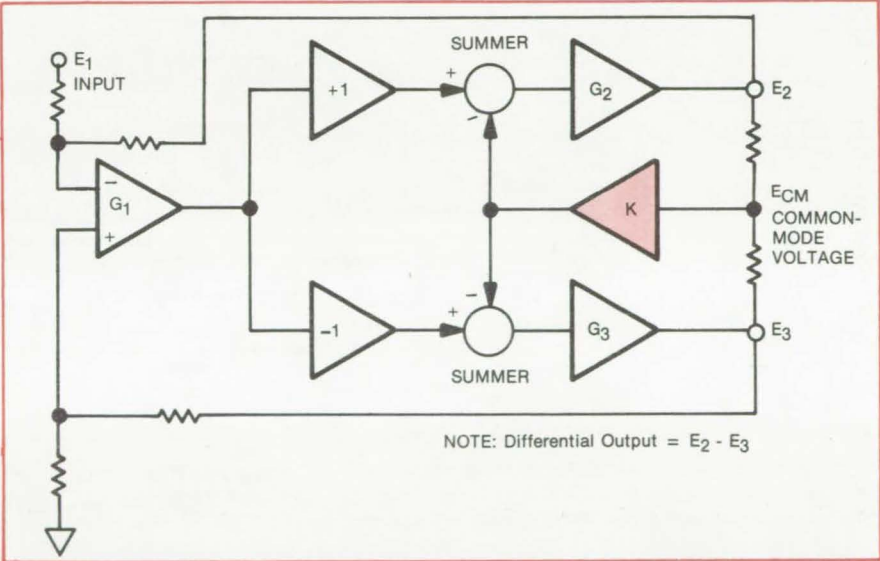
Common-Mode Feedback is furnished to the output stages G_2 and G_3 through amplifier K. The feedback offsets common-mode voltage caused by mismatch in the two signal paths. A breadboard model gives less than 0.36 dB amplitude difference between the two outputs up to 5 MHz. The phase difference departs by less than 3.0° from the nominal 180°.

outputs (G_2 and G_3) containing a push-pull transistor pair that is biased to prevent crossover distortion. The outputs of the current amplifier stages are summed to sample the common-mode signal and are fed to the operational amplifier K. The output of K drives a load network connected to the common-emitter nodes of the second stage.

A positive dc common-mode signal is amplified and inverted by amplifier K, causing the collector currents of the middle stage to be reduced. The collector voltages thus become less positive, changing the outputs in a direction that drives the common-mode output to zero.

As the signal frequency is increased, a common-mode voltage is produced by differences in the response of two signal paths. This voltage is sensed not only as a difference in amplitude but also as a difference in phase. The common-mode feedback loop minimizes these quantities as long as the gain around the loop is greater than unity. The gain values in the new circuit have been

selected to ensure that common-mode loop gain is greater than 1 up to a frequency of 10 MHz, although the unity-gain crossover frequency can be chosen higher or lower to meet specific circuit requirements.
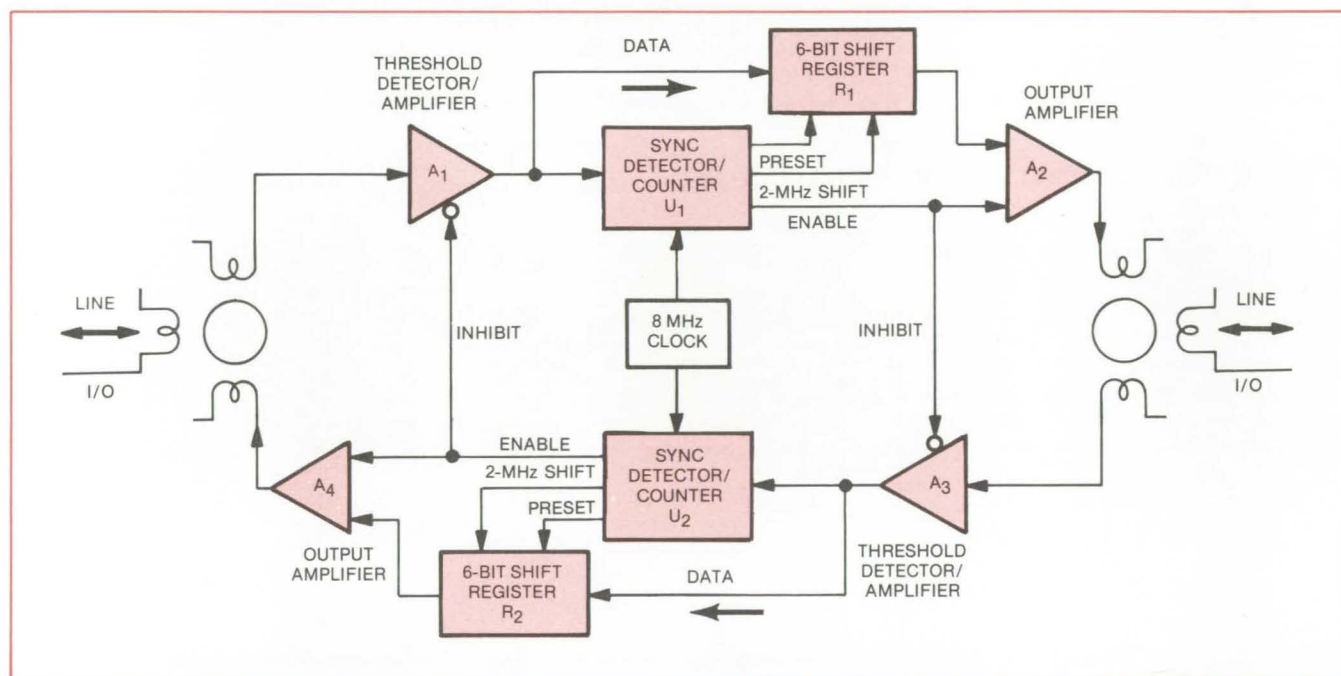
Bidirectional Manchester Repeater

Circuit detects, amplifies, and transmits bidirectional Manchester II signals.

Lyndon B. Johnson Space Center, Houston, Texas

The **Bidirectional Manchester Repeater** is activated by a sync pulse from either direction. The circuit reconstructs and transmits the sync, inhibits data flow in the reverse direction, and then amplifies and relays the Manchester data field. The circuit is transformer-coupled to the 75-ohm twisted-pair line.

Manchester II coded signals, often used in flight-simulator and computer-to-computer communications, are usually transmitted serially over a single bidirectional twisted-pair transmission line. To relay the signals over longer lines, and to restore faded signal strengths, a new bidirectional Manchester repeater may be inserted at periodic intervals along the line. The repeater includes amplifying circuitry to detect a signal in either direction and registers that reproduce the Manchester sync pulse and pass the data field while inhibiting data flow in the opposite direction. Requiring only 18 TTL 7400-series IC's, some line receivers and drivers, and a handful of passive components, the circuit is simple and relatively inexpensive to build.

As shown in the figure, a transformer-coupled 1-MHz Manchester II coded signal (consisting of a 3-microsecond sync pulse followed by twenty 1-microsecond bits of data) is applied to detector/amplifier A_1, which detects the presence of the signal above a preset noise threshold and amplifies it. The amplified signal is applied to sync detector/counter U_1 and to the input of a 6-bit shift register R_1. When A_1 recognizes a sync pulse, it enables the U_1 counter, which is clocked by an 8-MHz oscillator. U_1 also enables output amplifier A_2 and inhibits detector/amplifier A_3 to block data flow in the reverse direction.

The counter generates shift pulses at 2 MHz. The register is preloaded with a bit pattern of "000111," which regenerates the sync pulse. Following the sync, the register shifts the data from the incoming signal.

An identical circuit section detects and transmits data in the reverse direction. The repeater can be easily modified for the detection of other sync-pulse shapes, for increase or decrease in word length, and for different data rates.

Solid-State Power Controller

A circuit breaker that features current limiting
and delayed trip is switched by low-level voltage.

Lyndon B. Johnson Space Center, Houston, Texas

A compact, solid-state electric-power controller switches power on and off at a remote load, limits the current drawn by the load, and shuts off (with a 2- to 3-second trip time) in case of a short circuit. The hybrid unit operates at 28 volts dc and at maximum currents of from 3 to 20 amperes.

Originally designed for spacecraft electrical systems, the hermetically sealed controller (see Figure 1) is compact, lightweight, and efficient. Since it operates in the hard vacuum of outer space, where convection cooling is not possible, the controller is cooled by conduction through a beryllia cold plate maintained at between 25° and 125° F (-4° and 52° C).

The remote power controller contains power transistors on the beryllia base and logic circuits on an upper alumina plate. A block diagram of the circuit is shown in Figure 2. Output transistor Q_4 is actually an array of parallel output transistors, with one transistor for each ampere of current rating (that is, a 10-ampere unit contains 10 transistors). The unit is turned on by a low-level voltage (typically 9 to 12 volts) at the control input. With proper modifications, the control input can be made TTL-compatible.

The beryllia base is installed on a water-cooled plate, which removes heat during steady-state operation. The base is large enough to act as a thermal buffer that absorbs excess heat generated when the unit is limiting current to the load. Beryllia was selected because it has high thermal conductivity and high heat capacity, yet is light in weight.

The circuit output transistors are connected in parallel and, ideally, would share the current load equally. However, differences in transistor gains would cause unequal current sharing, with the consequence that a transistor could be overloaded and fail. One such failure would then cause other transistors in the parallel chain to fail.
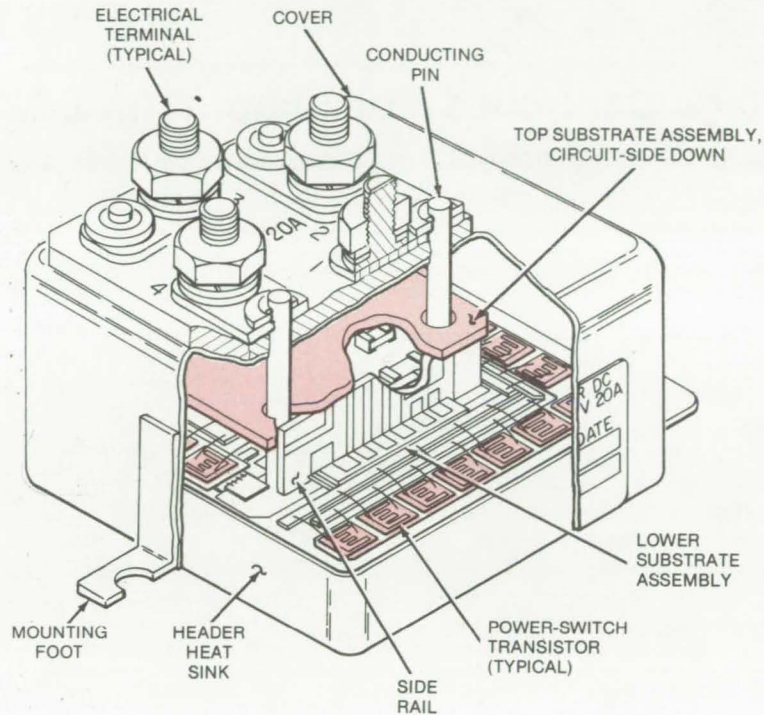
Figure 1. A **20-Ampere Remote Power Controller** measures only 4.8 by 4.8 by 3 centimeters and weighs only 5 ounces (141 grams). It uses CMOS logic and 30-ampere, mesa output transistors.
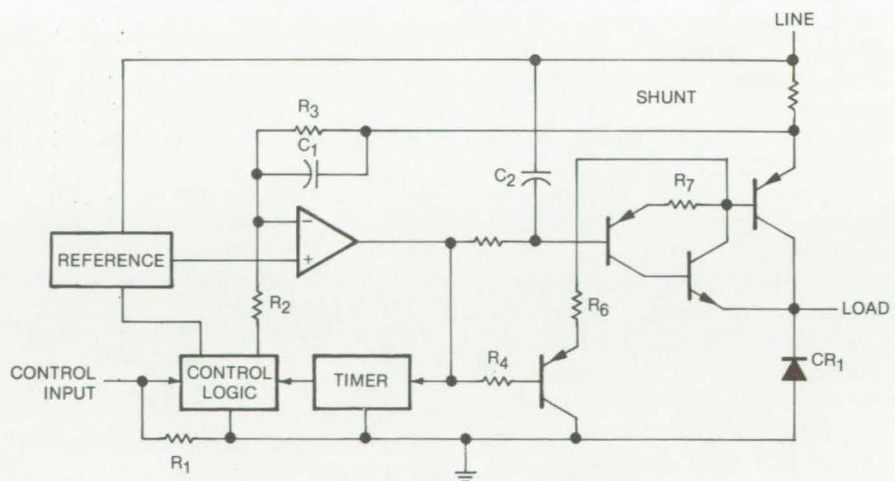

Figure 2. The **Power Controller Circuit** operates from a 24- to 34-Vdc line. Current limiting begins when the voltage across R_8 exceeds the reference voltage. At that point, the output of Z_1 begins to go positive, turning off Q_1 and Q_4. As the voltage across Q_4 begins to rise above 1.5 volts, transistors Q_2 and Q_3 become active and respond to current through R_5. The change in circuit gain as Q_2 and Q_3 are activated results in a sharp rise at the output of Z_1. This signal is used to trigger the 2- to 3-second timer, which ultimately trips the control logic.

Ordinarily, a large resistor would be connected to the emitter of each transistor to mask the effects of individual transistor gain differences, but this reduces efficiency. Instead, use is made of the resistance-vs.-temperature characteristics of the bonding wires that connect one transistor to another. These wires, 3 mils (0.76 millimeter) in diameter, which are composed of aluminum with 1 percent magnesium, increase non-linearly in resistance as the current through them increases. Therefore, if a paralleled transistor begins to draw excessive current, its bond-wire voltage drop will increase significantly, forcing the current down.

The bond wires are carefully cut to the same length for each transistor. At rated current (1 ampere) for each transistor, each wire produces only a small voltage drop (about 60 milli-volts).

This work was done by David A. Fox and James S. Fullemann of Westinghouse Electric Corp. for **Johnson Space Center.** *For further information, Circle 7 on the TSP Request Card.*
MSC-16661

Voltage-Controlled Attenuator With Low Phase Shift

A 5-MHz RF attenuator made from a quadrature hybrid and an optically variable resistance exhibits little phase shift.

NASA's Jet Propulsion Laboratory, Pasadena, California

A 5-MHz RF (radio-frequency) signal attenuator utilizes an RF quadrature hybrid and a variable-resistance load controlled by light intensity from a lamp circuit. The lamp circuit includes a current limiter that eliminates phase reversal of the RF signal as it passes through the quadrature hybrid. The circuit was designed to help distribute a standard RF signal, of controlled amplitude and phase, throughout a complex of facilities including frequency synthesizers and digital processors. It could also be useful with precision test equipment and communications electronics.

The attenuator circuit as shown incorporates a commercially-available 5-MHz quadrature hybrid and a variable-resistance load in the form of a dual photoconductive cell connected to output ports 2 and 4. The intensity of a long-life 5-V lamp, coupled to the photoconductor circuit, is controlled to vary the resistance of each cell from about 50 ohms to more than 1 megohm.

The variable-load circuit has two capacitors, C_1 and C_2, connected across each hybrid output, and series-compensation resistors R_1 through R_4 that match the dual cell characteristics. The capacitors tune out the inductive reactance of the hybrid, thus eliminating any phase change due to a change in the R-L time constant when the resistance of the dual photo-conductive cell is varied.

The derived attenuation is a function of dc voltage controlling the light intensity. An upper limit is imposed on the lamp by the current-limiting
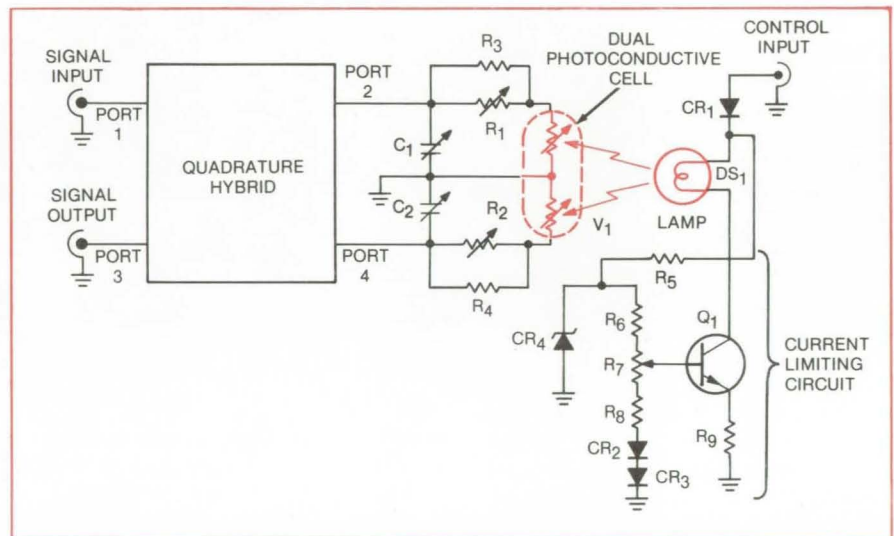
This **RF Attenuator** is controlled by a lamp circuit that limits its attenuation level to 30 dB. A current-limiting circuit controls the lamp output that irradiates a dual photoconductive cell. Phase reversal is prevented by keeping the cell resistance above the characteristic quadrature-hybrid impedance.

circuit. When the lamp is off, the photoconductive cells have maximum resistance of 1 megohm, forming effectively an open circuit. The applied RF signal power (port 1) then is totally reflected off output ports 2 and 4 and appears at the hybrid output port attenuated by about 0.5 dB, a minimum level.

The maximum attenuation of the RF signal would occur when the photo-conductive cells match the impedance of the quadrature hybrid (in this case, about 70 dB). However, as the resistance of the cells is adjusted through the characteristic impedance of the quadrature hybrid, a 180° phase reversal occurs. To eliminate this problem, a current limiter is included

in the lamp circuit to limit attenuation to 30 dB, so the attenuator never goes through the minimum attenuation part of the curve where phase reversal occurs.

Additional phase changes may occur.due to impedance changes at ports 1 and 3 because of transmission-line characteristics of the quadrature hybrid. However, since the attenuator will be located in series with a stabilized line, this phase shift will be largely canceled.

This work was done by George F. Lutes, Jr., of Caltech for **NASA's Jet Propulsion Laboratory.** *For further information, Circle 8 on the TSP Request Card.*
NPO-14347

Improved Insulator Layer for MIS Devices

Insulating layer of a superionic conductor allows increased capacitance in metal/insulator/semiconductor devices.

Langley Research Center, Hampton, Virginia

An insulating layer of a superionic conductor, such as LaF_3, has been shown able to impart improved electrical properties to photocapacitive detectors and promises to improve other metal/insulator/semiconductor (MIS) devices; e.g., MOSFET's and integrated circuits. MIS devices are normally fabricated by using SiO_2 technology. Insulating layers of SiO_2 are used with silicon-based devices; with other semiconductors, nonnative oxides are generally used.

These structures require relatively-thick insulating films. Furthermore, the typically-used insulating oxides have comparatively-low dielectric constants, and the upper limit on their capacitance restricts the performance and properties of the final device. In addition some presently used insulators are degraded by humidity.

LaF_3 is an ionic conductor and forms blocking contacts with other solids. Thin dipole layers form at the LaF_3 surfaces. At low frequencies, the equivalent circuit of the LaF_3 layer is two capacitors coupled by a resistor. The capacitors are the surface dipole layers, and the resistance results from the bulk ionic conductivity. At high frequencies, the LaF_3 layer behaves as a bulk capacitor with a dielectric constant of about 14.

Test devices were fabricated on silicon wafers. Layers of silicon dioxide 250 Å thick were thermally grown on the wafers. This served as the substrate for 250-Å layers of LaF_3 formed by electron-beam deposition. Metal field plates were evaporated by using a shadow mask to make multilayer MIS diodes.

An insulating layer of LaF_3 has a capacitance of $\sim 1\ \mu F/cm^2$, and in composite layers with SiO_2 the breakdown voltage is increased markedly. In a test of LaF_2/SiO_2 composite-layer devices, the breakdown voltage was increased by a factor of 30 with no degradation of the C/V characteristics. Resistance to humidity is increased because of the LaF_3 is chemically inert.
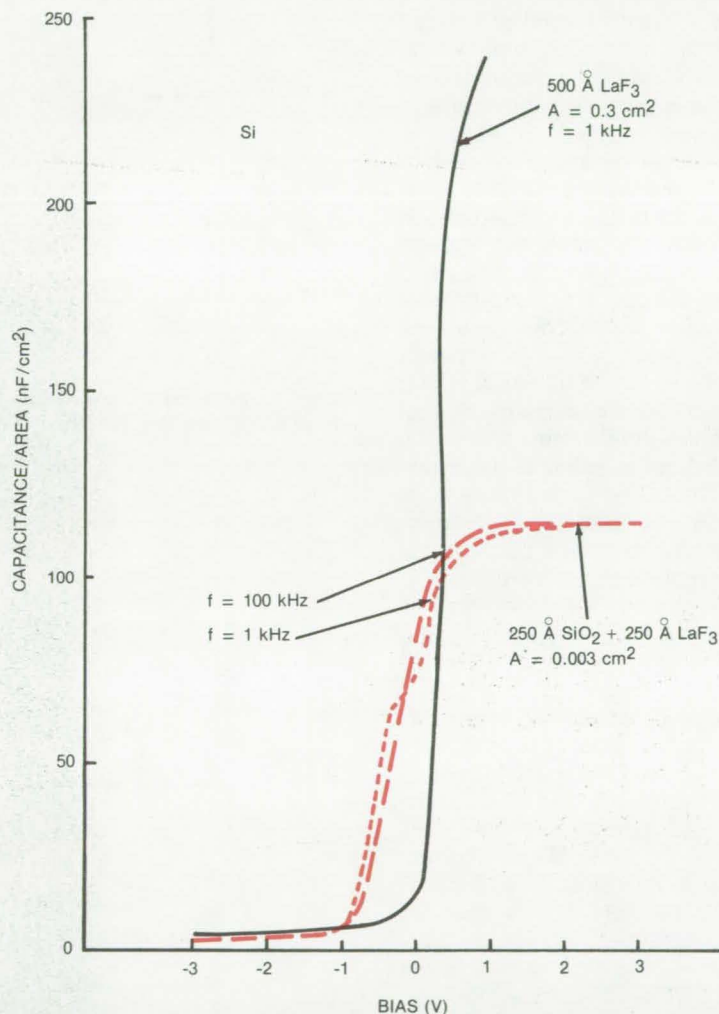
C/V Characteristics are shown for the LaF_3 insulating layer at 1 kHz and for SiO_2/LaF_3 composite insulation at 1 and 100 kHz.

Devices with only LaF_3 insulators on Si and GaAs have also been fabricated. These structures exhibit exceedingly-sharp, nearly-hysteresis-free C/V characteristics. While for n-type material they withstand moderately-large negative voltages (~ 3 to 9 volts) with little leakage, they begin to leak at positive voltages in excess of ~ 0.8 volt. Examples of the C/V characteristics of two samples are shown in the figure; one has an SiO_2/LaF_3 composite insulator and the other an LaF_3-only insulator.

Minimizing Spikes in Switching-Regulator Circuits

Addition of an inductor and a diode prevents harmful
current surges from damaging the switching transistors.

NASA's Jet Propulsion Laboratory, Pasadena, California

Current spikes, a cause of premature transistor failure in switching regaulators, are minimized by a circuit that employs a tapped inductor to back-bias the rectifying diodes and an extra diode to commutate the current.

The circuit diagram in Figure 1 shows a switching regulator with a pulse-width-modulating (PWM) converter in a push/pull arrangement. If such a converter does not include tapped inductor L_1 and commutating diode CR_3, the opposing currents from the two rectifier diodes are not necessarily equal when both power transistors are turned off. As a result, the opposing diode currents do not cancel in the transformer; the difference is enough to saturate the transformer core as shown in Figure 2(a), causing current spikes in the transistors. Spiking also occurs because the diode currents are not zero prior to transistor turn-on; the diode that is being turned off acts as a short circuit, letting a high current flow in the power transistor.

In the modified circuit, however, tapped inductor L_1 back-biases the push/pull diodes CR_1 and CR_2 enough to keep them turned off. Because there is no current through CR_1 and/or CR_2, there is no current imbalance in the secondary of transformer T_1. Therefore its core does not saturate, as shown in Figure 2(b). Commutating current flows through diode CR_3. When this diode turns off, the spike current is limited by the inductance of section N_2 of inductor L_1. If the number of turns on N_2 is properly chosen, current spikes can be minimized as shown in Figure 2(c).

The proper turns ratio for the two sections of L_1 depends on the leakage inductance of transformer T_1. A C-core transformer, for example, has a much larger leakage inductance than one with a toroidal core. The higher the reverse voltage to CR_1 and CR_2, the faster unwanted leakage current falls to zero.

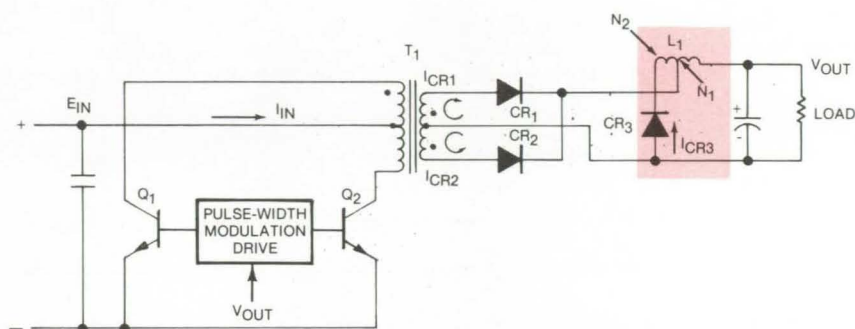*This work was done by Colonel W. T. McLyman of Caltech for* **NASA's Jet Propulsion Laboratory.** *For*

Figure 1. **Inductor L_1 and Diode CR_3** are added to the basic push/pull regulator circuit to protect the switching transistors against collector-current spikes.
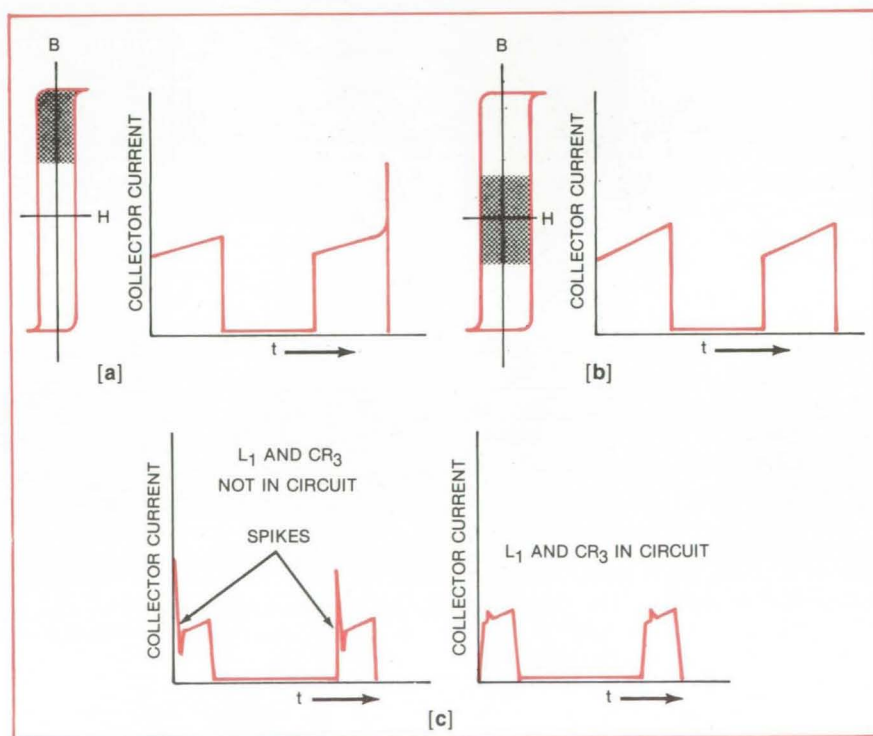

Figure 2. **Waveforms** show the spiking that occurs when unequal rectifier-diode currents saturate the transformer (a), and the absence of spiking when the rectifier diodes are biased off (b). The total effect of the tapped inductor with commutator is shown in (c).

further information, Circle 10 on the TSP Request Card.

This invention is owned by NASA, and a patent application has been filed. Inquiries concerning nonexclu-sive or exclusive license for its commercial sevelopment should be addressed to the Patent Counsel, NASA Resident Legal Office-JPL [see page A5]. Refer to NPO-14505.

Digital Automatic Gain Control

Digital circuit reduces gain error
to half that of analog AGC.

NASA's Jet Propulsion Laboratory, Pasadena, California

A digital integrator is the circuit best suited to digital automatic-gain control (AGC), according to a performance analysis that also evaluated digital low-pass filters and signal-averaging filters as AGC devices.

Digital circuitry makes it possible to alter the response of a receiver to match incoming signal conditions. For example, the AGC characteristics can be automatically modified to accept weak, noisy signals as well as strong, clear ones. As integrated circuits increase in complexity, digital AGC becomes more economical.

The frequency response and noise bandwidth of the digital-integrator AGC are equivalent to those of a conventional analog AGC circuit, and phase response and transient response are also comparable to those of an analog circuit.

The proposed digital-integrator AGC (see figure) employs a coherent amplitude detector (CAD) to extract gain information from the IF amplifiers in the receiver. A fast sample-and-hold circuit feeds a relatively-slow complementary-metal-oxide semiconductor (CMOS) analog-to-digital (A/D) converter. [Alternatively, transistor-transistor logic (TTL) could be used for faster A/D conversion without the S/H circuit. However, TTL requires more power than CMOS.]

A data stream that is 10 bits wide can give adequate resolution over a 110-dB dynamic range. The total time for the data conversion with CMOS circuitry is 180 microseconds or less.
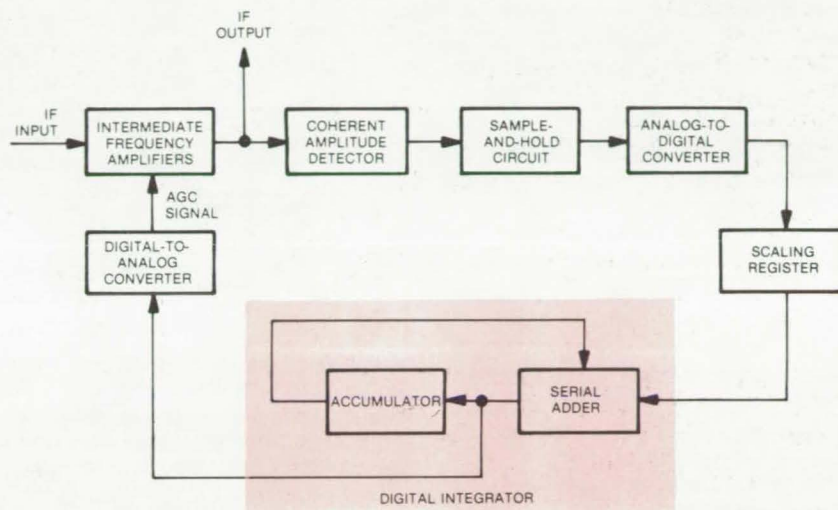
The **Signal From IF Amplifiers** is sampled every 200 microseconds. After the analog IF signal is converted to digital form, an error-correcting signal is developed in the digital integrator. The digital error signal is converted to analog form and applied to the IF amplifiers.

At a proposed sampling interval of 200 microseconds, a period of 20 microseconds is then available for such necessary operations as scaling, accumulating, and register transfers. These operations can be accomplished in a few tens of nanoseconds, so the 20-microsecond period is ample.

A scaling register adjusts the sampled valves to give the loop gain requred to achieve a desired AGC response. For a bandwidth of 0.9 Hz, the scaling factor is 1:256, produced by right-shifting a storage register by 8 places.

The output D/A converter applies a gain-correction signal to the IF amplifiers. The maximum error allowed by the digital AGC is expected to be ± 0.15 dB, which is about half that of an analog AGC. The digital AGC error is expected to be less dependent on temperature.

Eventual use of ultrahigh speed S/H amplifiers can eliminate the need for a physical CAD by directly sampling the IF carrier.

Surge Protection With Automatic Reset

An overvoltage protection circuit cuts off power
and then turns it on after a timed interval.

Lyndon B. Johnson Space Center, Houston, Texas

An automatic overvoltage-protection circuit turns off power when a voltage surge occurs and restores power when the voltage returns to normal. Originally designed for use aboard the Space Shuttle, the circuit

protects the components of a traveling-wave-tube (TWT) transmitter from transient overvoltages in the power supply. The automatic reset function allows the transmitter to resume operation quickly without intervention

by an operator. The same circuit can protect other equipment in an electrically noisy environment.

In the Shuttle application, the circuit turns off power for 0.5 second and

restores it if the overvoltage has passed. (Most overvoltages are the result of switching in the powerlines, and they typically last for less than 0.1 second.) However, when three transient overvoltages (or a continuous overvoltage) are sensed within 3.2 seconds, the protection circuit turns the power supply off permanently, since a serious failure may have occurred. When this happens, the operator must reset the equipment. Except for this condition, which is indicated by a light-emitting diode (LED), the operator is not aware that the protection circuit has turned power off and on.

In the Space Shuttle application shown in the circuit diagram, a power supply overvoltage appears as excessive body current or cathode voltage in the TWT transmitter. Either condition causes a high-to-low transition at an output of latch U_1 and generates a transmitter fault signal XF that latches U_1 (through the Q output of U_3).

This signal shuts off the TWT power supply immediately; it also triggers a 0.5-second timing pulse from multivibrator U_{2A}. The trailing edge of this pulse triggers a short (10-microsecond) pulse from multivibrator U_{2B} that resets the latch circuit so that the U_1 outputs can once again respond to the body current and cathode voltage inputs. If the excessive condition in these inputs has vanished, the power supply is turned on again; but if a fault still exists, signal XF is maintained.

A second fault signal XF* generated at the same time as XF starts a 3.2-
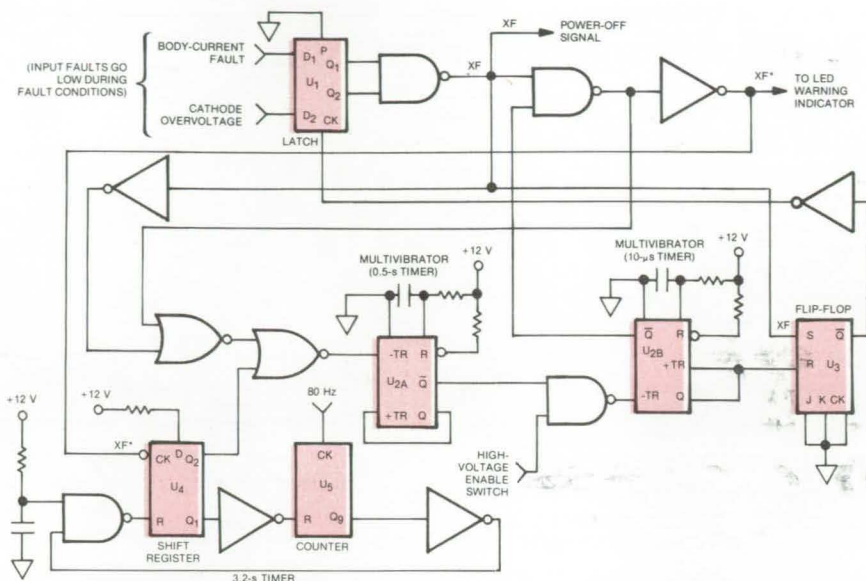
In this **Overvoltage Protection Circuit,** excessive body current or cathode voltage produces a fault signal that turns off power to a traveling-wave-tube transmitter. After 0.5 second, power is automatically restored unless: (1) the fault still exists; (2) three faults occur within a 3.2-second interval (timed by U_4 and U_5); or (3) a single fault lasts 3.2 seconds.

second timer (shift register U_4 and counter U_5). If a second XF* signal occurs within the 3.2-second "window," the Q_2 output of U_4 goes high and disables the 0.5-second timer (U_{2A}). Thus, a third XF* within the 3.2-second window cannot release the outputs of latch U_1, and the power supply remains off. In this state, the only way to turn on the power is manually to change the high-voltage enable switch from on to off to on.

If only one or two XF* signals are

registered during the window period, the Q_9 output of U_5 goes high, resetting the shift register and resetting and stopping the 0.5-second timer. The protection circuit is then in a quiescent state, monitoring the input for other faults.

*This work was done by Ronnie B. Chan and Marychristine C. Sinelli of Hughes Aircraft Co. for **Johnson Space Center.** No further documentation is available.*
MSC-18356

Bubble-Domain Detector

Transformer coupling simplifies detection
for bubble-domain memory device.

Langley Research Center, Hampton, Virginia

A new bubble-domain detector employs a transformer coupling for data retrieval. This makes multidetection practical by time-multiplexing. The multiplexer matrices can be scaled in 4 by 4, 4 by 8, 4 by 16, or other larger combinations without diode steering. This approach eliminates individual balancing of offset voltages, as in a voltage-amplification

detection scheme, and dc restoration circuits and component symmetry, as in a current-amplification scheme.

In Figure 1, when the transformer is driven by a current at the center tap position, any imbalance is coupled to the secondary side. When the balance is due to the nonsymmetry of bubble elements, an offset voltage is generated that can be of either polarity.

When the detector elements are imbalanced due to incremental resistance change in an active memory element (bubble data), this is reflected as a slope change on the offset voltage pedestal.

The transformer coupling ratio is 1:1 but can be step-up or stepdown, depending upon voltage amplitude
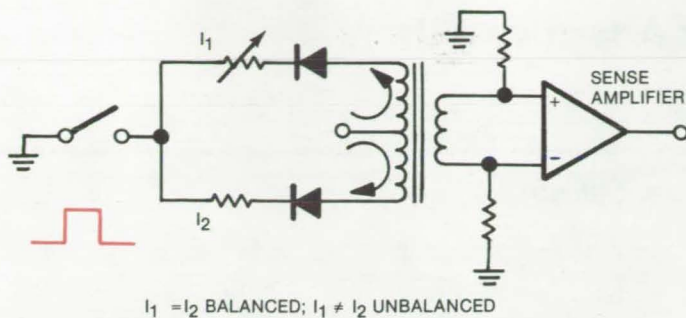
$I_1 = I_2$ BALANCED; $I_1 \neq I_2$ UNBALANCED

Figure 1. The **Basic Transformer Coupling** is used in bubble-domain detection to replace more complex balancing or restoration circuits used in voltage- and current-amplification detection schemes.
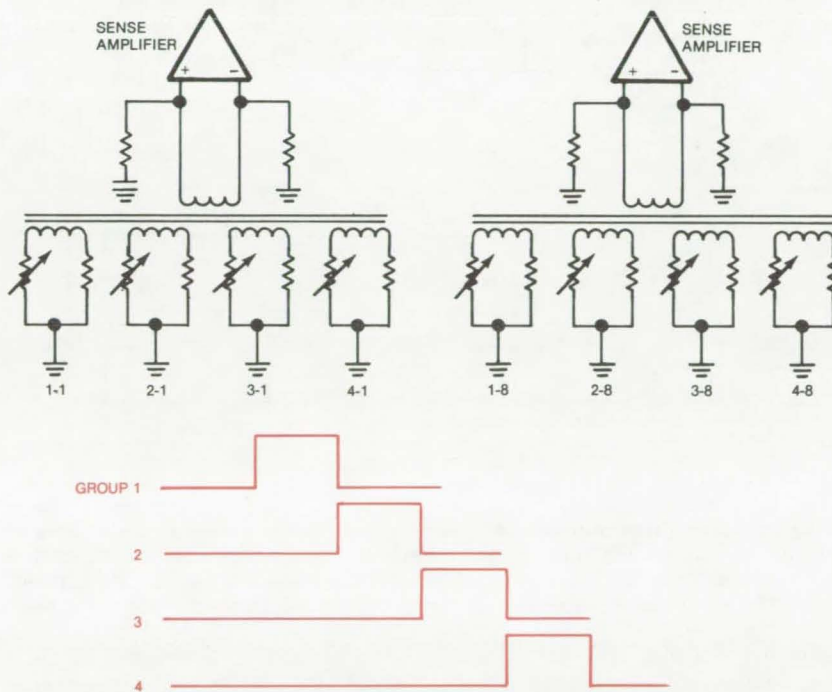

Figure 2. **Detector Matrix** employs transformer coupling only, to form a 4 by 8 array. When group 1 transformers are activated, groups 2, 3, and 4 are inhibited. The arrangement reduces crosstalk and reverse-bias leakage paths.

saturation, the transformer operates in a linear domain. A secondary termination of 200 ohms is used across each secondary lead and common ground. This is compatible with input base-to-emitter (V_{BE}) characteristics of a conventional sense amplifier.

The sense amplifier is capacitively coupled. Its typical input threshold is 1 mV, or larger, depending upon the input offset-voltage amplitude. A table gives threshold sensitivity changes as a function of offset voltages. As is evident, the offset voltages have minor influence on threshold response.

Offset [mV]	Threshold [mV]
0	1.0
10	1.1
20	1.4
40	2.0
60	3.2
80	4.8

Threshold Sensitivity is given as a function of offset voltages.

For a multiple detector operation, the number of primary windings is increased from one to four. Using this technique, a 4 by 4, 4 by 8, 4 by 16, or other detector matrix sizes may be constructed without the steering diodes.

Figure 2 shows a 4 by 8 matrix employing transformer coupling only. When group 1 transformers are activated, groups 2, 3, and 4 are inhibited. This reduces crosstalk in adjacent primary windings and completely eliminates reverse-bias leakage paths commonly encountered when diode matrices are used. The transformer can be driven as shown or with the detector elements operated from a fixed potential and common-ground pulse switched at the center-tap transformer location.

This work was done by Charles D. Nichols and Robert L. Stermer of **Langley Research Center.** *No further documentation is available.*

Inquiries concerning rights for the commercial use of this invention should be addressed to the Patent Counsel, Langley Reserach Center [see page A5]. Refer to LAR-12241.

requirements. The secondary termination is a function of the type of sense amplifier employed for level detection.

The primary inductance is typically in the range of 1 to 3 mH. This range of values results in a pulse waveform with a "droop" response that is less than 10 percent. "Droop" is related to primary inductance, input generator-source resistance, and output load resistance.

The volt-microsecond product of the transformer is 20 V-μs. When the bridge transformer combination is driven with a 6-V, 1.2-μs-wide pulse in 10-μs periods, a 1-V amplitude develops across each primary winding. Since that value is below core

CMOS Analog Switches for Adaptive Filters

CMOS switches reduce variations in switch
resistance in active low-pass filters.

*NASA's Jet Propulsion Laboratory, Pasadena, California*

Improved adaptive active low-pass filters incorporate CMOS (complementary metal-oxide semiconductor) analog switches (such as the 4066 switch) that reduce variations in switch resistance when the filter is switched to any selected transfer function. Conventional electromechanical switches used for the same purpose produce uncontrolled resistance variations that can alter the characteristic of the selected transfer function.

The illustration compares the conventional circuit (a) with the new CMOS modified circuit (b). Both circuits depict a low-pass network with high-frequency compensation. In (b), R_{S1}, R_{S2}, and R_{S3} represent the "on" resistances of the CMOS switches. The transfer function for the conventional circuit with the switches in the indicated position is

$$\frac{e_O}{e_{in}} = \frac{-R_{2a}}{R_{1a}} \times \frac{T_2 s + 1}{T_1 s + 1}$$

where $T_1 = (R_{2a} + R_{3a})C$, $T_2 = R_{3a}C$, and s is the characteristic root of the function. Here the low-frequency breakpoint (pole) of the response occurs at a frequency $\omega = 1/(R_{2a} + R_{3a})C$ and the high-frequency breakpoint (zero) occurs at $\omega = 1/R_{3a}C$ radians.

The problem with simply substituting CMOS switches for mechanical switches in the conventional configuration was that one of the filters called for resistance R_3 to be less than the maximum "on" resistance specified for the switch. Thus, the switch resistance would adversely affect the filter. The circuit resistance values could not be changed to make R_3 large compared to the switch resistance because the circuit dynamic-selection range already required resistances near the maximum allowed
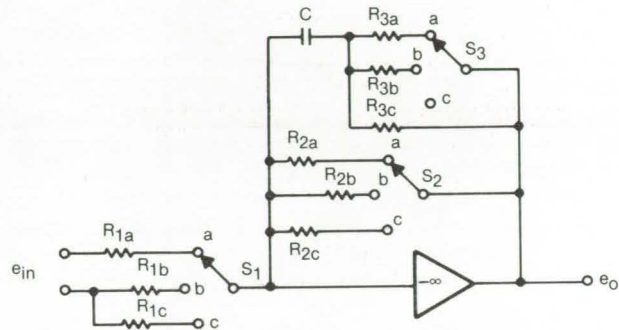
(a)
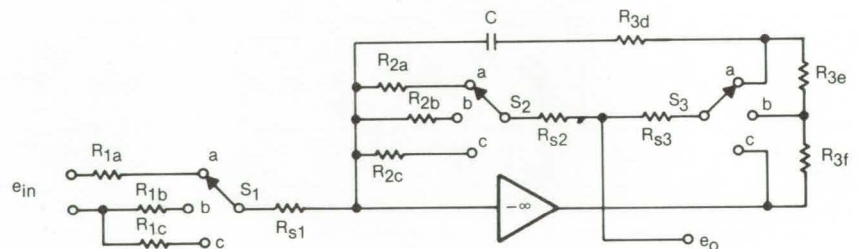
(b)

An **Adaptive Active Filter** utilizes CMOS analog switches to minimize the effects of switch resistances on the filter transfer function. The new circuit configuration shown in part (b) has the effect of switch resistance eliminated from its transfer function. The earlier version, shown in part (a), used electromechanical switches.

by capacitor leakage and amplifier-input bias-current considerations; and, the capacitor could not be switched because voltage transients could not be tolerated when switching from one circuit configuration to another.

The problem is corrected by the new circuit, which has the following transfer function:

$$\frac{e_O}{e_{in}} = -\frac{R_{2a} + R_{S2}}{R_{1a} + R_{S1}} \times \frac{T_2 s + 1}{T_1 s + 1}$$

where $T_1 = (R_{2a} + R_{S2} + R_{S3} + R_{3d})C$ and $T_2 = R_{3d}C$.

In this configuration, the function includes the effects of all three switch resistances, and R_1 and R_2 values are large compared to R_3 and to the switch resistance. The switch resistances in series with R_1 and R_2 and appearing in the T_1 definition have negligible effect. No switch resistance appears in the T_2 expression, and therefore R_{3d} can be made as small as desired with no limitation due to the switch characteristics.

Measuring Charge Nonuniformity in MOS Devices

Lateral nonuniformities of charge can be determined
by low-temperature capacitance measurements.

NASA's Jet Propulsion Laboratory, Pasadena, California

Part of the effort to improve the reliability and quality control of solid-state devices involves measuring surface-state concentrations caused by irradiation and electrical stress at metal-oxide-semiconductor (MOS) interfaces. However, inherent charge nonuniformities along silicon dioxide/ silicon boundaries may mask these effects; a convenient way of measuring the nonuniformities is needed.

In a new approach to this problem, capacitance of the interface is rapidly measured as a function of voltage at low temperature. The charge distribution is extracted by fast-Fourier-transform analysis of the capacitance/ voltage (C-V) measurements.

Mathematically, the C-V curve is the convolution of the ideal capacitance with a density function that depends on lateral charge nonuniformity:

$$C(V) = \int_{-\infty}^{\infty} C_o(V - V_{FB}) \, f(V_{FB}) dV_{FB}$$

where V_{FB} is the flatband voltage along the interface, $C_o(V - V_{FB})$ is the ideal capacitance, $C(V)$ is the measured capacitance, and $f(V_{FB})$ is the density function for the flatband distribution. $C_o(V - V_{FB})$ can be calculated from the known doping profile near the surface. Thus, by measuring $C(V)$ and
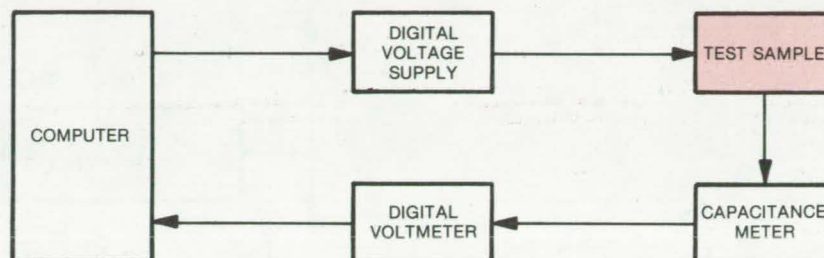
Test Apparatus outlined above is used for measuring charge uniformity in MOS devices. The test sample is cooled to liquid nitrogen temperatures to minimize changes in the occupancy of surface states.

applying a Fourier transform, $f(V_{FB})$ can be determined as

$$f(V_{FB}) = \mathbf{F}^{-1} \left[\frac{\mathbf{F}[C'(V)]}{\mathbf{F}[C_o'(V)]} \right]$$

where the prime signifies the derivative with respect to V and $\mathbf{F}$ and $\mathbf{F}^{-1}$ are the Fourier transform operator and its inverse.

The equipment for making the measurements (see figure) consists of a capacitance meter, a digital voltmeter, a digitally-programable power supply for biasing the interface, and a liquid nitrogen bath or a cold plate at liquid nitrogen temperature. The sample is cooled to liquid nitrogen temperature to minimize changes in the occupancy of surface states during the measurements.

First, the interface capacitor is biased in strong accumulation, to fill all interface states; then the measuring voltage is switched on for a few milliseconds, and the capacitance is measured. This procedure is repeated for other voltages until the complete C-V curve has been measured. An automated digital system collects the data. Since very little change in the C-V curve is found for longer measurement periods, the interface states are apparently "frozen" for purposes of these measurements. The density distribution can be converted to that at room temperature by simple calculations.

This work was done by Joseph Maserjian and Nasser Zamani of Caltech for **NASA's Jet Propulsion Laboratory.** *For further information, Circle 12 on the TSP Request Card.*
NPO-14585

Variable-Clock-Rate A/D Converter

Circuit uses different rates to optimize
performance in both searching and tracking.

Lyndon B. Johnson Space Center, Houston, Texas

An analog-to-digital (A/D) converter operates at two different rates so that low-amplitude noise is reduced without the loss of transient response. A slow clock rate is used while the converter is tracking a signal, and a fast clock rate is used when the converter is searching for a signal. During tracking, when sensitivity is

important, the slow clock reduces noise. In the search mode, when the signal may be changing rapidly, the fast clock ensures rapid response.

In previous A/D converters for low-frequency instrumentation, noise was reduced by adding a low-pass analog filter or by permanently reducing the clock rate. However, these methods

made the converter too slow.

In the new A/D converter (see figure), an up/down counter is forced to equal the analog input and then to track it. The slew rate, or bandwidth, of the converter is a function of the clock rate.

TRUTH TABLE FOR DIVIDER		
A	B	COUNT 2^n
0	0	8,192
1	0	256
0	1	1,024
1	1	65,536
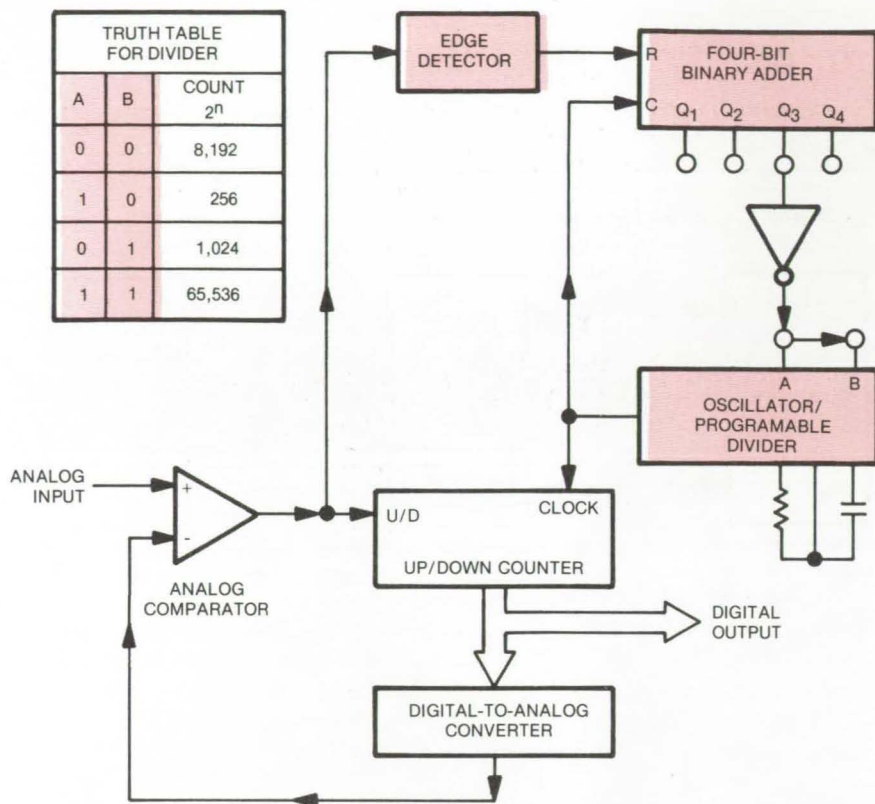
To Select the Clock Rate for this analog-to-digital converter, the combination of the edge detector and the 4-bit binary adder determines whether the converter is tracking a signal or searching for one.

Transistions at the output of an analog comparator are sensed by an edge detector. Transitions at the clock rate signify that the converter is tracking, while an absence of transitions signifies searching. When the converter is tracking, a 4-bit binary adder is constantly being reset, causing the converter to be clocked by a programable divider at f/65,536, where f is the oscillator frequency. If four successive clock pulses occur without an up/down transition being detected, the converter clock changes to f/8,192, or eight times the tracking rate. Of course, many other clock rates and track/search-rate ratios are possible, and the transitions from track to search can be made at absent-transition sums other than four.

This work was done by Phillip C. Lipoma of Lockheed Electronics Co., Inc., for **Johnson Space Center.** *No further documentation is available.*

Title to this invention has been waived under the provisions of the National Aeronautics and Space Act [42 U.S.C. 2457(f)], to the Lockheed Electronics Company, Inc., Houston, TX 77058.
MSC-18541

Strain Relief for Power-Cable Connectors

Grommet prevents strain from
distorting connector pins.

Lyndon B. Johnson Space Center, Houston, Texas
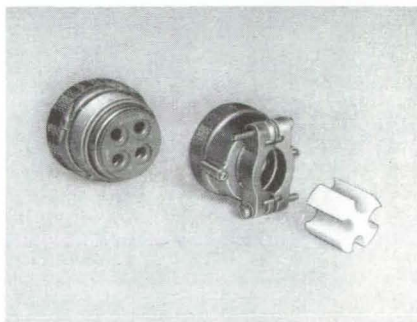
Cable-Support Grommet (left) fits in the back shell of a standard large-diameter cable connector and is secured by the cable clamp (right).
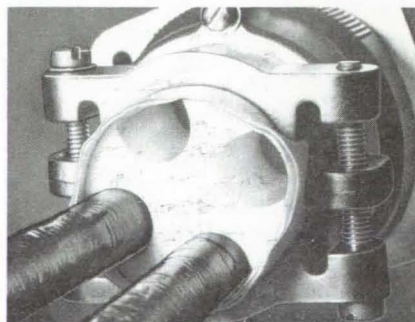
An easily-fabricated grommet for power-cable connectors relieves strain on the cables and thereby prevents the connector pins from angling outward. The connector plug can thus be readily inserted, removed, and reinserted in the connector receptacle.

The grommet is a polytetrafluoroethylene cylinder containing U-shaped channels equally spaced around its periphery (see figure). The cables, instead of being held directly by the connector clamp, pass through the grommet channels. Since the grommet is held by the clamp, it takes up much of the strain in the cables.

For 0-gage cables and a four-pin connector, the grommet is 1.375 in. (3.49 cm) in diameter and 1.06 in. (2.69 cm) in length. The channels are 0.474 in. (1.2 cm) wide. Grommets can also be used with other standard large-diameter cables. The grommet is potentially useful for electrical wiring in large residential and commercial buildings.

This work was done by William T. Dean III of Rockwell International Corp. for **Johnson Space Center.** *No further documentation is available.*
MSC-19497

# Interleaved Shielding for Cables

Counterwrapped foil strips shield more
effectively than a single wrapped strip.

Lyndon B. Johnson Space Center, Houston, Texas

SECTION A-A

SINGLE OVERLAPPING WRAP

SECTION B-B

INTERLEAVED COUNTERROTATING
DOUBLE-LAYER WRAP

SECTION C-C

NONINTERLEAVED COUNTERROTATING
DOUBLE-LAYER WRAP
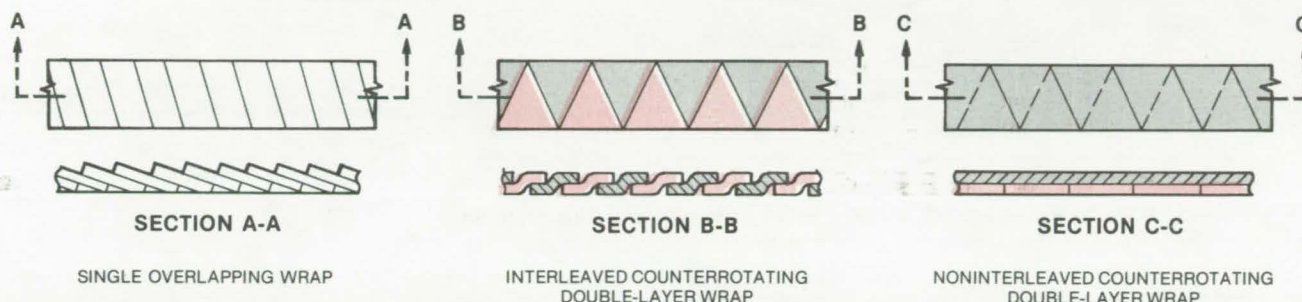
In an **Electromagnetic-Interference-Shielded Cable,** a single overlapped strip (left) requires as much material as two counterwrapped strips — whether machine-wrapped and interleaved (center) or hand-wrapped and noninterleaved (right) — but provides far less attenuation.

Interleaved wrapping of metal foil on cables gives more-effective shielding, without increasing the amount of material or weight. Instead of wrapping a cable with a single overlapping layer of aluminum-foil strip, it is wrapped by machine with two counterrotating interwoven strips of foil (compare figure, left, with figure, center). In either case, there are two thicknesses of metal at every point on the cable; but, whereas the single overlapping strip furnishes only 16.8 dB of shielding (at a given set of test conditions), the double interleaved strip gives 27.4 dB of shielding. The greater effectiveness of the interleaved wrap results from cancellation of the electromagnetic fields set up by

currents in the counterrotating strips.

The interleaved foil was tested for its effectiveness in shielding against interference caused by lightning strikes. The frequency range of interest is from 50 to 250 kHz, and the effects of simulated lightning-induced current pulses with risetimes from 0.5 to 5 microseconds were investigated. The interleaved foil gave consistently better attenuation than the unidirectional single-wrapped foil.

The two foil strips can be applied to cable by conventional wire-braid weaving machines, with relatively minor modifications. Although it would be difficult to wrap the interleaved strips by hand, simply wrapping the two foils in opposite directions without

interleaving produces almost the same level of attenuation of electromagnetic interference (26.6 dB). This manual method of wrapping foil (also shown in the figure, right) is therefore an acceptable alternative when a wrapping machine is not available. Whether implemented by hand or by machine, the new method protects against electromagnetic interference almost as well as woven braid (tested at 29.5 dB) but at substantially less weight.

This work was done by George R. Read of Rockwell International Corp. for **Johnson Space Center.** *No further documentation is available.*
MSC-18369

Isolator/Retainer for Connectors

Double cap secures a plug and receptacle
but prevents electrical contact.

Lyndon B. Johnson Space Center, Houston, Texas

A double-ended dust cap holds a mating plug and receptacle, preventing electrical contact between them when they are not in use. At the same time, the cap maintains a continuous electrical ground between plug and receptacle, thereby protecting against electromagnetic-interference pickup.

Besides isolating the mating connectors from each other, the dust cap

prevents them from hanging loosely and perhaps contacting other conductors. It also prevents loose parts from falling off the connectors. The cap is useful for isolating sensitive circuits from each other during storage, transit, or testing.

The double-ended dust cap consists of a riveted pair of conventional dust caps from mating connectors (see

figure). Three holes, 120° apart, are drilled through each of the caps. The caps are placed back to back. Spacers are inserted between them and riveted to the caps. Finally, silicone gaskets are inserted in the caps.

An optional retaining ring can be placed around the spacers to hold a warning streamer with a message
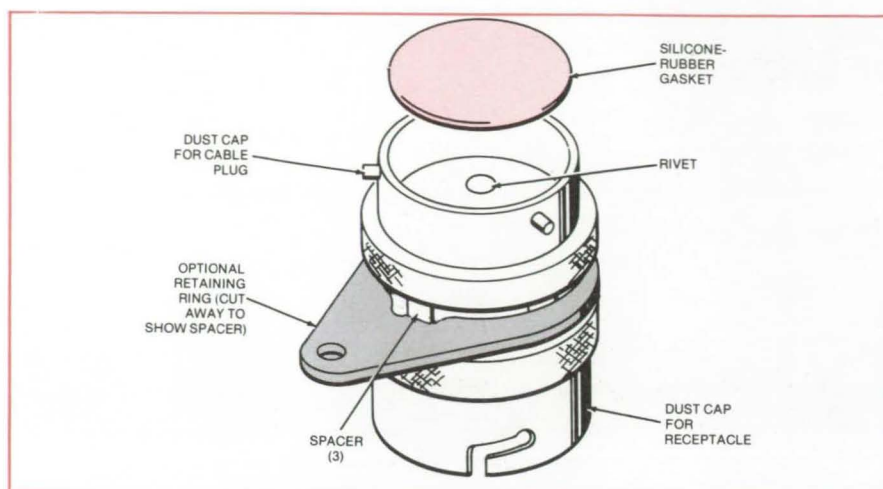
Double-Ended Cap mates with a plug (top) and a receptacle (bottom). The retaining ring holds a warning streamer.

such as "Remove Before Using Cables."

Previously, an unused cable plug was held by a clamp on a bulkhead, and an electrical ground wire was attached to the plug. The new cap is faster to connect and disconnect and requires fewer loose parts. It may be a bayonet type (as shown) or may be threaded, depending on the type of mating connectors.

Stable S-Band Power Amplifier

Amplifier with automatic level control
preserves transmitter modulation characteristics.

NASA's Jet Propulsion Laboratory, Pasadena, California

A relatively linear amplifier with automatic level control (ALC) preserves modulation characteristics of a phase-shift-key (PSK) modulated S-band transmitter. The PSK often used in RF transmission of commands or data, or in spreading the RF signal by pseudorandom noise (PN), creates a broad spectrum of modulation side lobes that can cause interchannel interference. Earlier use of a band-pass filter at the transmitter output caused center-frequency instability and reduced signal-power output. Another approach of using a modulator and filter at a lower center frequency had objectionable non-linearity.

The power amplifier shown in the illustration has successfully used ALC to produce low AM-to-PM conversion, which allows it to amplify the filtered PSK spectrum without negating the modulation side-lobe suppression provided by the modulation filter. The measured AM-to-PM conversion is 2.5°/dB of amplitude variation (1-watt power-output option). Typical data- or PN-induced amplitude variations are approximately 0.1 to 0.2 dB. The incidental PM contributions from the power amplifier are therefore less than 0.5°.
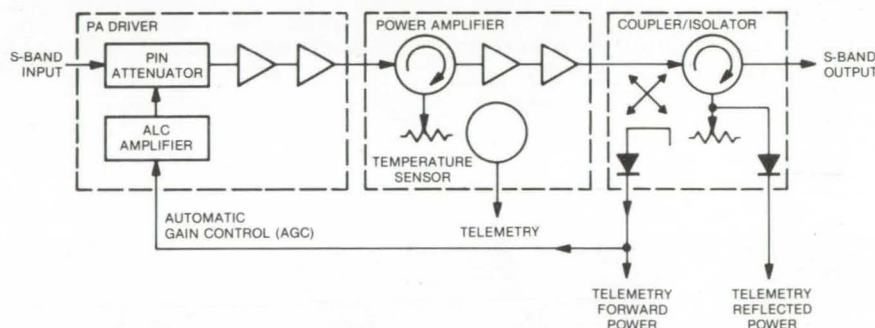
The **PA Circuit** used in the NASA standard tracking and data relay satellite-system (TDRSS) transponder incorporates a PA driver, a PA, and coupler/isolator subassemblies. The PA driver contains a PIN (p-intrinsic-n) diode level-controlling attenuator, two stages of class AB amplification, and an ALC loop amplifier/filter. The circuit features adequate linearily and AM-to-PM conversion characteristics. A small modulation side-lobe filter can be used in this circuit at one-eight the S-band output frequency.

The ALC loop also holds the transmitter S-band output power to within ±0.3 dB of nominal under all slowly varying conditions including full specified temperature and voltage variations. A benefit of this stable power output is that the dc input power is reasonably constant over the temperature range of variation and is less than the maximum required for the case where limiting is used to control power-output variations.

For maximum overall efficiency, the PA uses one or two stages of class C common-base amplification, depending on the power-output option selected for the specific application. The ALC loop holds the operating points of these stages below saturation, to maintain linear performance and low AM-to-PM conversion. A circulator/isolator at the input to the subassembly ensures that a low VSWR (voltage-standing-wave ratio) load is presented

to the driver and that a low VSWR source impedance is seen by the PA under all operating conditions.

The coupler/isolator subassembly includes a coupler and detector, which sample the forward power for both the ALC loop and telemetry purposes. In addition, the subassembly includes a circulator for output load isolation and a detector at the terminated port of the circulator for reflected-power telemetry.

The ALC amplifier drives the error signal for the ALC loop by comparing the forward-power detector voltage with an adjustable reference voltage. The amplified signal with suitable loop time constant controls the current through each of the PIN diodes in the "PI"-configuration constant-imped-ance alternator network and thereby controls the overall transmitter-output signal level.

This work was done by Charles E. Hermesmeyer of Motorola, Inc., for **NASA's Jet Propulsion Laboratory.** *For further information, Circle 13 on the TSP Request Card.*
NPO-14443

Limiting Amplifier for Microwaves
Field-effect transistors give level output
to prevent AM/PM conversion.

Lyndon B. Johnson Space Center, Houston, Texas

A limiting amplifier using field-effect transistors (FET's) delivers a constant-amplitude drive signal to a Ku-band traveling-wave tube (TWT), thus preventing phase distortion in the output from the TWT. The FET's are gallium arsenide devices.

TWT's convert amplitude modulation (AM) to phase modulation (PM) at a rate of about 8 degrees/dB. The FET limiting amplifier, by removing amplitude variations from a phase-modulated signal, prevents the TWT from introuducing phase distortion. The FET limiter itself introduces almost no AM-to-PM conversion.

The FET limiter contains four balanced radio-frequency (RF) stages. Interdigitated couplers at the input and output of each stage furnish a broad-band impedance match for splitting and combining power. Several FET amplifier stages can be cascaded to build up gain with a minimum of gain ripple caused by VSWR interactions. Because interstage isolators are not required, the limiter can be packaged in a small, lightweight unit (see figure).

The interdigitated couplers are fabricated by conventional photolith-ographic techniques on an alumina substrate 0.025 in. (0.635 mm) thick. The RF stages are hermetically sealed by a welded aluminum cover. The RF signal enters and leaves via metal-to-metal compression-seal connectors, and bias voltages enter via glass-to-metal-seal feedthrough terminals. A separate voltage regulator is mounted on a standard printed-wiring board
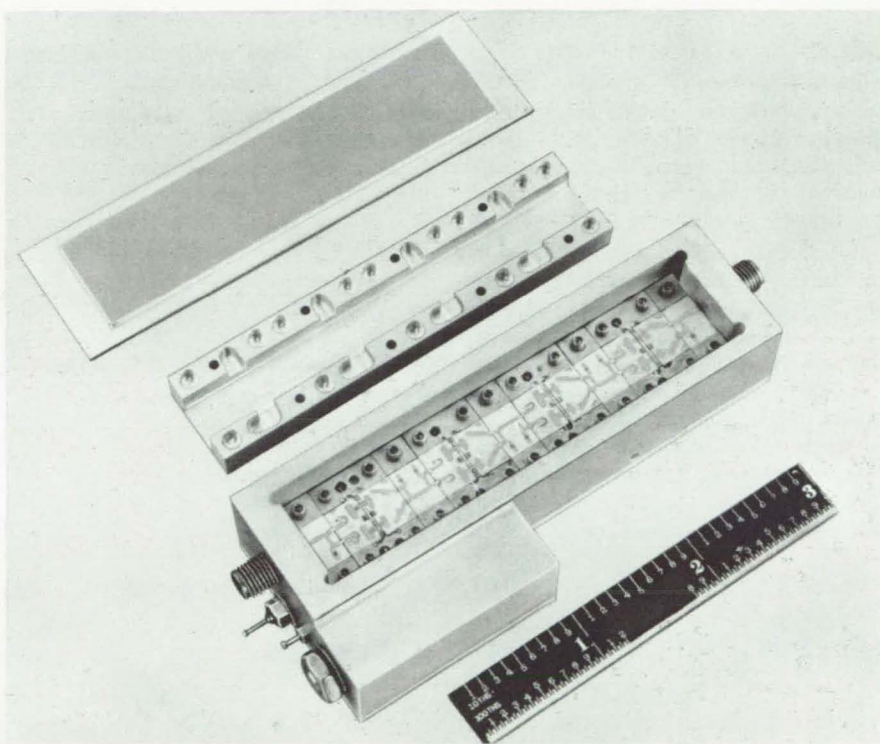
Four Balanced FET Stages on a microstrip circuit deliver 12 dBm at Ku band. The RF stages, here shown uncovered, are normally hermetically sealed in the enclosure by a welded cover plate. The smaller enclosure just below the RF stages contains voltage-regulator circuitry.

that is not hermetically sealed.

With 1.5 degrees/dB AM-to-PM conversion, the FET limiter introduces far less phase distortion than alternative limiters such as those incorporating PIN diodes. In addition, the FET limiter introduces gain, making it possible to operate the TWT more efficiently for a given output power.

This work was done by J. N. Owens of Hughes Aircraft Co. for **Johnson Space Center.** *For further information, including a schematic diagram of the circuit, Circle 14 on the TSP Request Card.*

Inquiries concerning rights for the commercial use of this invention should be addressed to the Patent Counsel, Johnson Space Center [see page A5]. Refer to MSC-18471.

Books and Reports

Moisture Penetration in Microcircuit Packages

A study of hybrid microcircuit packages in extreme temperature/humidity environments

A study finds adhesive-sealed hybrid microcircuit packages susceptible to moisture penetration. The result was uncovered by subjecting ceramic-packaged samples to four different temperature/humidity conditions: 25° C at 98 percent relative humidity (RH), 50° C at 60 percent RH, 60° C at 98 percent RH, and 85° C at 85 percent RH. Five package samples were tested under each condition. Two ceramic packages were sealed using one commercially available adhesive; two using another; and the fifth was metallurgically sealed (seam-sealed; i.e., brazed with gold/tin preforms) as a control sample.

The test program, described in a 74-page report, incorporated a commercially-available moisture sensor attached to the microcircuit substrate with pure indium solder. Each group of five sensors was calibrated at one of the four temperature settings over a moisture range of 200 to 10,000 p/m-vol. (parts per million-volume) and then was sealed, using the accepted sealing processes. All the packages were pretested for possible leaks prior to actual testing.

The tests were conducted for periods ranging up to 40 days for a 25° C, 98-percent RH environment and as short as 52 hours for the 85° C, 85-percent RH. Moisture was monitored every hour by using a multiplexer for sequentially monitoring all five samples.

Test results show that package susceptibility to moisture is affected more by high temperatures than by humidity. Worst cases were reported at 85° C and 85 percent RH. Apparently, package expansion at the elevated temperatures causes leaks to develop that do not exist at room temperature.

The ceramic packages using either type of commercial adhesive were more susceptible to moisture than the seam-sealed packages, although one adhesive showed better results than the other. Unexpectedly, it was found that seam-sealed packages were also susceptible in spite of their very low helium-leak rates as tested at room temperature. The results suggest that room-temperature tests are inadequate in evaluating the seal integrity without considering the seal deterioration at elevated temperatures.

This work was done by J. J. Licari and K. L. Perkins of Rockwell International Corp. for **Marshall Space Flight Center.** *To obtain a copy of the report, "Development of Low Cost, High Reliability Sealing Techniques for Hybrid Microcircuit Packages, Phase II — Supplement No. 1," Circle 15 on the TSP Request Card.*
MFS-25087

Electronic
Systems

Hardware, Techniques, and Processes

Video-Compression Scheme

Diagonal picture elements are transmitted serially, stored, and then reconstructed at the receiver.

Ames Research Center, Moffett Field, California
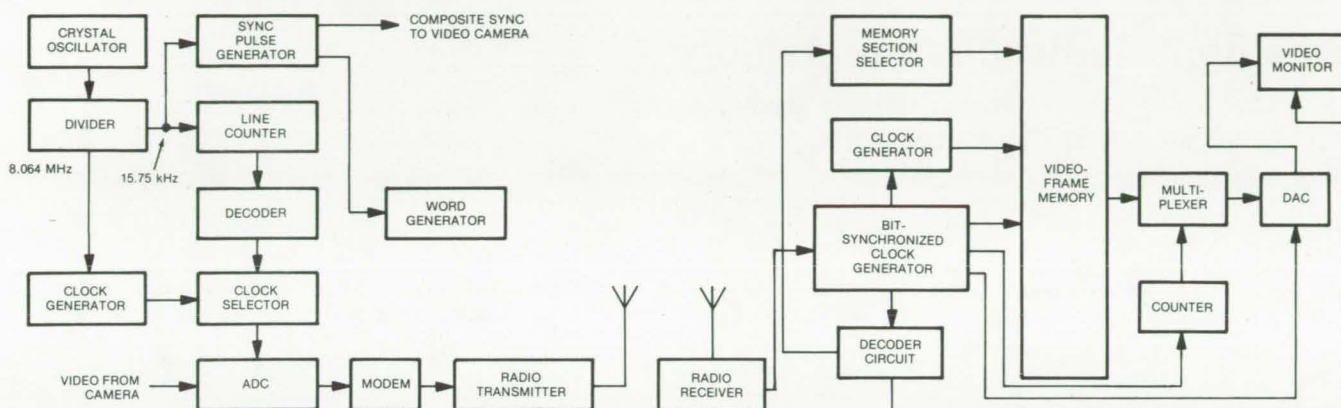
Figure 1. The Video-Compression Circuit divides a picture into elements that are transmitted at a reduced data rate. By sampling the elements along diagonals in N-by-N picture-element blocks, the system gives picture quality comparable to that of standard television and quality superior to most pseudorandom sampling schemes.

The channel bandwidth requirements for transmitting video pictures are reduced by a scheme that divides the picture into blocks containing a checkerboard pattern of picture elements. The elements are sampled along diagonal rows, converted to digital signals, and transmitted serially to the receiving station where they are stored in a video frame memory. The memory contents are continually updated as new picture elements are received. The standard bandwidth of 8.064 MHz for transmitting a 525-row by 512-column picture is reduced by factors of 4, 8, 16, or higher by the scheme.

The picture to be transmitted is imagined to be partitioned into blocks, each containing N-by-N picture elements. Thus, 512/N blocks span the horizontal width of the picture. The elements are transmitted by the circuit shown in Figure 1. A crystal oscillator in the transmitter is the origin of all synchronizing and sampling signals. Its output is divided to 15.75 kHz to develop horizontal and vertical synchronizing pulses and to 8.064 MHz to furnish the fundamental video-sampling signal. This 8.064-MHz signal clocks an N-bit recirculating shift register (in the clock generator) to produce N clock phases, all at 1/N of the fundamental frequency and all

equally shifted in phase from each other. (N is typically 4, 8, or 16.)

During each line scan, the combination of horizontal line counter, binary-to-one-of-N decoder, and clock selector routes one of the N clock phases to the storage command input of the analog-to-digital converter (ADC). For a typical scan, the nth picture element of each block on the line is transmitted. On the following

LOCATION OF SUCCESSIVE PICTURE ELEMENTS IN BLOCK
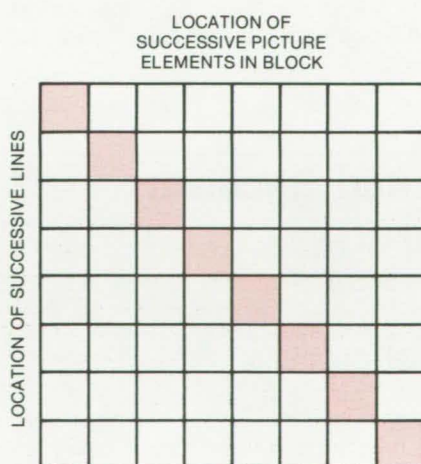
Figure 2. A Typical Picture-Element Block is shown after one frame scan. The shaded elements represent those that have been transmitted. The corresponding diagonals in other blocks have also been transmitted.

line scan, the next clock phase is selected, and the (n + 1)th picture element in each block is transmitted. In this way, all picture elements along corresponding diagonals in the blocks are transmitted.

Figure 2 shows one 8-by-8 picture-element block, with the squares in color indicating those that are sampled during a typical scan of all 8 lines. Since the 525 lines of the video frame are not an even multiple of 8, the diagonals will be displaced in each successive frame until every picture element is covered once.

The picture elements are transmitted to the receiving station where they are placed in the video frame memory. In the receiver, a bit-synchronized clock generator develops the 15.75-kHz synchronizing signal at the video line frequency and the 8.064-MHz video-information rate signal. The decoder circuit and memory section selector route each incoming image element into a section of the video frame memory. The memory has as many sections as the largest useful number of blocks (for example, 16). If N is chosen to be equal to this maximum number, each block goes into one section; if N is less than the maximum, the picture elements of each block are distributed in more than one section. At the memory

output, multiplexing circuitry selects consecutive sections of memory and transmits the picture elements in the proper temporal sequence to a digital-to-analog converter (DAC). The DAC feeds the analog video to the monitor and reconstructs the picture.

Analog Actuator-Piston Memory

A simple analog-control system resets digitially controlled drive following a power loss.

Lyndon B. Johnson Space Center, Houston, Texas

Frequently, a digitally controlled actuator, such as is used in an industrial process, must be automatically reset following a power shutdown so that the processes are resumed exactly at the point where they were interrupted. A simple and straightforward solution is to use the "stopped" position of the actuator as a "memory" and a potentiometer as the sensing element.

The proposed control (see figure) uses the actuator feedback loop and a comparator as an analog-to-digital converter. When the supply power is reapplied, a reload timer inhibits the drive to the actuator, while the up/down counter is reset to zero. The counter then counts up until the stop-count comparator indicates a null between the feedback potentiometer and the number reloaded into the up/down counter. After sufficient time has been allowed for the counter to assume a digital number equal to the potentiometer reading, the counter control is again restored to the normal
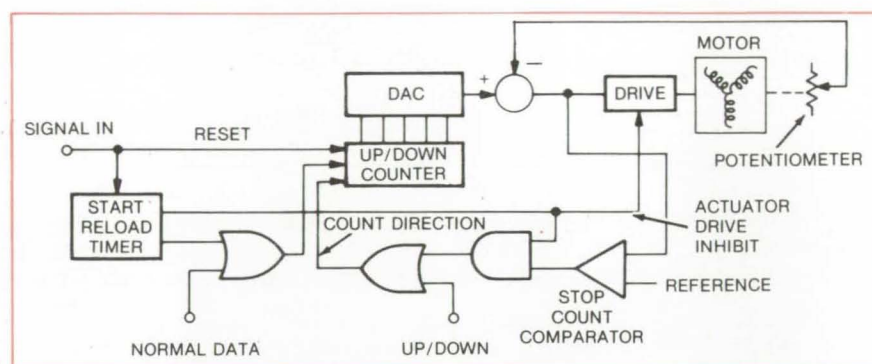
This **"Actuator Memory" Circuit** reloads a digital drive circuit to a value equal to its last position preceding a power loss. The circuit incorporates an actuator feedback loop and a comparator that effectively serve as an analog-to-digital converter. The circuit is not restarted until the counter assumes a digital number equal to the potentiometer reading. This control is important in large-scale production processes where the system must be restarted at the same point when it stopped during power shutdown.

data bus, and actuator power inhibit is removed. Using a reload data clock that is much faster than the normal data stream, the counter may be updated in a short time.

Microprocessor-Controlled Receiver

Radio receiver automatically acquires, tracks, demodulates, and synchronizes weak signals.

Ames Research Center, Moffett Field, California

A microprocessor and a radio receiver are combined in a new low-cost, high-performance, data-communications receiver. Originally developed for relay-link communications between two spacecraft on planetary exploration missions, the hybrid receiver automatically acquires and tracks UHF channels despite low

signal-to-noise ratios, fading signal strengths, and high Doppler offset. In addition, it performs the digital bit synchronization, which has traditionally required a separate unit.

A typical configuration is shown in the figure, where a conventional radio-frequency (RF) and intermediate-frequency (IF) front end is

combined with a microprocessor that is customized from bit-slice low-power Schottky logic. After the IF analog output of the receiver is converted to a digital signal, the microprocessor demodulates the signal, synchronizes the signal bits, and determines the signal power and frequency. The
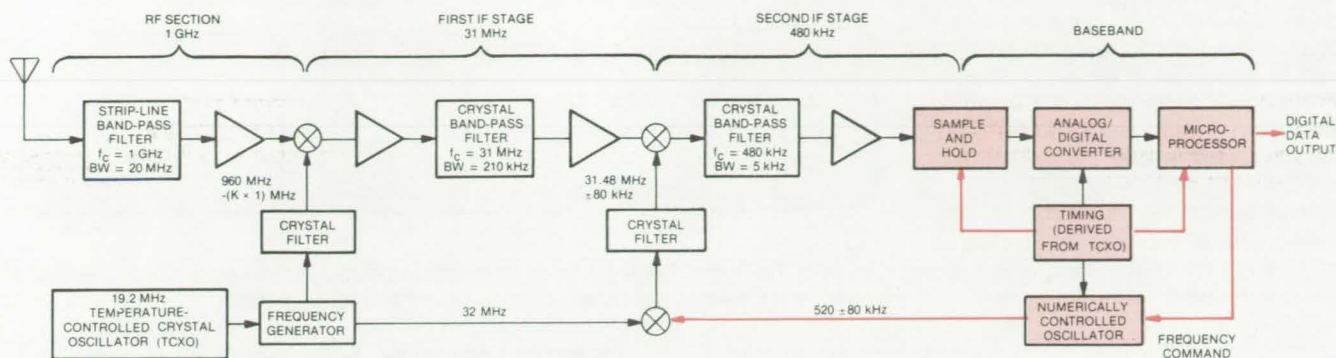
The **Microprocessor-Controlled Radio Receiver** is synchronized by a temperature-controlled crystal oscillator, which provides timing signals for the crystal filters, the sampling circuit, the digital-to-analog converter, and for digital processing. The hybrid circuit is presently undergoing breadboard tests and software debugging.

processor also controls the second-stage IF mixer frequency for acquiring and tracking signals. For other applications, it can be programed for different modulation types and bit rates.

The input to the microprocessor is produced by direct sampling of the 480-kHz IF. Sample pairs are taken in phase quadrature. After executing a program that distinguishes a signal from noise, the microprocessor transmits a frequency-command signal to a numerically controlled oscillator, which produces the up-to-±80-kHz

frequency variation necessary for tracking and acquiring a data channel. All the mixing and sampling frequencies are derived from a single reference oscillator.

The custom microprocessor is an 8-bit-parallel design, with two data buses to connect its arithmetic logic unit and separate hardware multiplier to its random-access memory and input/output ports. A special set of microinstructions was developed to generate the receiver functions. The instructions are stored separately from the data in a 32-bit-wide micropro-

gram stored in read-only memory. The processor architecture is dictated by the need for a short (400-ns) instruction cycle to process data signals in real time. The maximum data rate depends on the IF bandwidth and the amount of processing needed.

This work was done by Terry L. Grant and Yutaka Matsumoto of **Ames Research Center** *and Peter L. McAdam, Oliver W. Saunders, and Marvin S. Stone of TRW, Inc. For further informaton, Circle 17 on the TSP Request Card.*
ARC-11275

Centering Images in Split-Screen TV Displays

In two side-by-side images on a single TV screen,
each shows the center of its camera field of view.

Lyndon B. Johnson Space Center, Houston, Texas

A new circuit for creating "split-screen" television pictures allows an operator to select the portion of each image to be displayed without moving the TV cameras. Until now, a split-screen picture divided in half could show only the left half of the left image and the right half of the right image (Figure 1). If the area of interest occupied another part of either image, the operator had to redirect the camera to bring the area into view on the screen.

The new circuit for combining two video signals on a time-shared basis can display the center of the image from each video source (Figure 2). The circuit centers the images for all screen-splitting proportions, for a 1/3-to-2/3 division, for example, just as easily as for an equal half-and-half split.
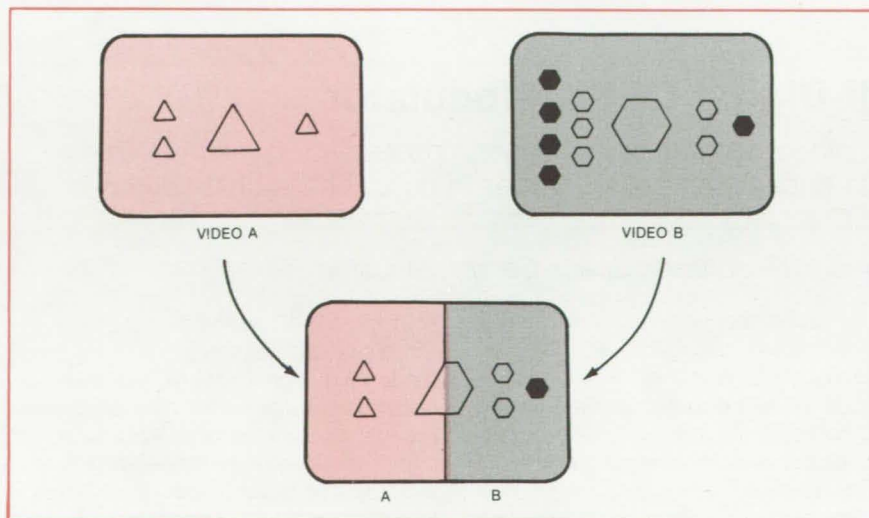
Figure 1. In a **Conventional Split-Screen Display,** the left portion of video signal A appears alongside the right portion of video signal B.

The area of interest in a video image is usually in the center of the camera field of view; but if it should happen that the prime-interest area is off to one side of an image, the video time-sharing circuit allows the operator to select an offcenter area for display — without redirecting the camera. The operator merely directs the display to roll through the field of view and stops the rollthrough at will (Figure 3).
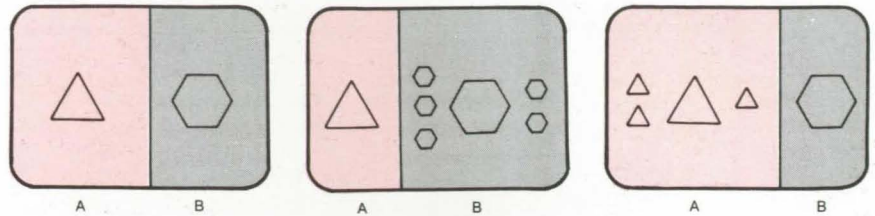
Figure 2. **The New Circuit** for video time-sharing displays the center of each video signal, regardless of the screen area assigned to each signal.
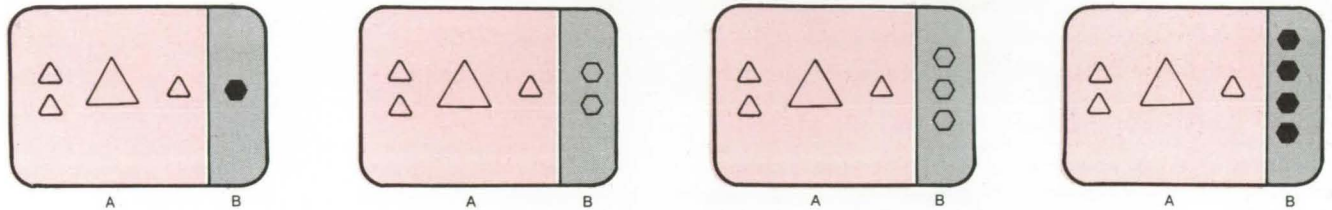
Figure 3. With an **Override of Automatic Centering,** the operator can display other areas of interest.

The video signals from the two sources are stored in separate registers and are released from each register in a staggered sequence; that is, the output clocking process for one register begins in advance of the output process for the other register. By coordination of the clock-start sequences, the desired portions of the stored video signals can be restructured so that they occupy the prescribed portion of each horizontal line. To keep storage requirements low, the signals are restructured line by line, and only active-video data are used (that is, horizontal synchronization pulses are not included). A storage capacity of only 569 memory elements is needed.

The restructuring is performed as follows: The two stored video lines are each subdivided into 64 sequential elements (the number of subdivisions is arbitrary). The beginning of a line is then at subdivision zero, and the end is at subdivision 64. For an equal split between Video A and Video B, a total of 32 increments is taken from each stored video signal. These increments are the 16 subdivisions on either side of the center of each line — that is increments 16 to 48 of Video A and of Video B.

If the display ratio between Video A and Video B is changed, the center portion of each is held on the screen because the circuit automatically alters the preclocking pause for Video A. (The preclocking pause for Video B is always the complement of that for Video A.) To move a displayed image away from the center portion, the operator turns a control know clockwise or counterclockwise from its automatic-center position.

This work was done by Jack B. Hopkins of Westinghouse Electric Corp. for **Johnson Space Center.** *For further information, including a schematic circuit diagram, Circle 18 on the TSP Request Card.*
MSC-18399

All-Digital QPSK Modulator

Simple low-power circuit superimposes two asynchronous data streams on an RF carrier in quadriphase-shift-key code.

Lyndon B. Johnson Space Center, Houston, Texas

A circuit consisting of only four components modulates a radio-frequency (RF) signal with two asynchronous digital data signals. Two of the components are integrated-circuit (IC) chips, and the other two are time-delay devices.

Previously, an analog circuit was used to modulate the carrier. The RF carrier was split into quadrature (sine and cosine) signals; each was phase-shift-key (PSK) modulated by one of the digital data streams, and the two modulated signals were summed to obtain the output. The new all-digital modulator has several advantages over its analog predecessor: It is virtually free of amplitude modulation; it is not subject to temperature effects from such components as power splitters, matched sets of diodes, quadrature hybrids, and tuned amplifiers; it is much simpler; and it dissipates less power.

The new circuit converts the RF carrier input into two complementary square waves that are 180° out of phase (labeled A and C in the figure). The delay elements shift A and C further, producing square waves B and D. The delay elements can be set for 90° phase shift (as illustrated) for a balanced quadriphase shift-key

(QPSK) modulation, or for less than 90° for an unbalanced QPSK output. The same circuit can be used for either balanced or unbalanced modulation, whereas the analog technique required a separate circuit for each form of modulation.

Two of the gates in the input integrated circuit and the four gates in the output IC form a four-to-one multiplexer that selects the output phase according to the combination of data bits at the input channels. For example, a 0 on channel 1 and a 1 on channel 2 produce phase A in the output; a 1 on both channels produces phase B in the output.

This work was done by Roger W. Burgess and Richard L. Julian of Hughes Aircraft Co. for **Johnson Space Center.** *No further documentation is available.*
MSC-16922
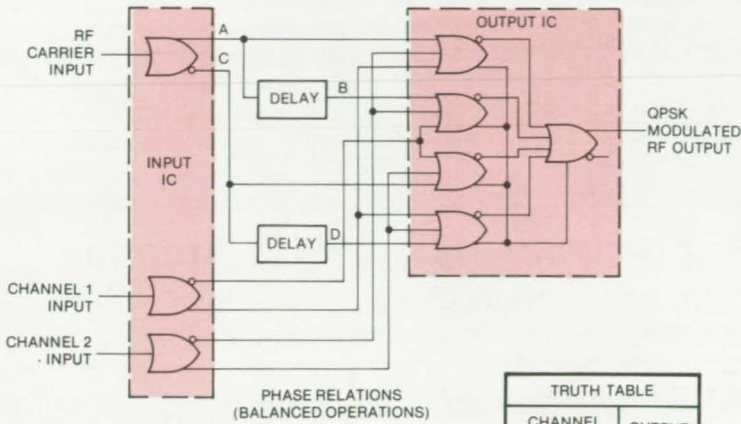
TRUTH TABLE

CHANNEL		OUTPUT PHASE
1	2	
0	1	A
1	1	B
1	0	C
0	0	D

This **Quadriphase-Shift-Key [QPSK] Modulator** uses only two logic integrated circuits and two time-delay devices. The output integrated circuit and two gates in the input IC make up a four-to-one multiplexer.

Low-Profile Communications Antenna

Compact antenna with low aerodynamic profile can be used for elliptical or circularly polarized signals.

Lyndon B. Johnson Space Center, Houston, Texas

A new antenna, shown in the illustration, has been designed with a low profile for aircraft and spacecraft. Its compact size and shape, along with other desirable features, may also make it useful for communications on trains and road vehicles.

The antenna element is elliptical for use with any circular polarization. The special cases right- and left-circular polarization can be selected by placement of the feedpoint. The desired frequency range is determined by the size of the antenna element; for instance, a relatively small version is ideal for the microwave region. It has been found that the radiation pattern of this antenna is nearly uniform over a solid angle of 2π steradians. Therefore, there should be very little interruption of signal when the vehicle on which it is mounted changes orientation.

The position of the feedpoint determines the impedance of the antenna as well as its polarization. To change the impedance, the feedpoint is moved along a radius of the disk; as the feedpoint is shifted closer to the edge of the disk, the impedance
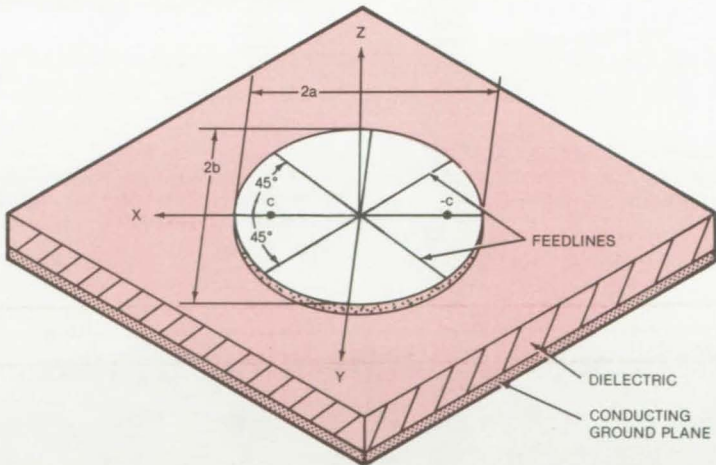
Low-Profile Antenna can be constructed using microstrip techniques. The operating frequency range is determined by the thickness of the dielectric layer and the size of the antenna element. The polarization characteristics are determined by the location of the feedpoint. For the special case of circular polarization, the feedpoint is placed on an azimuth 45° from a semimajor axis of the ellipse of the antenna disk. Placement 45° clockwise gives right-hand polarization, and counterclockwise produces left-hand polarization.

becomes lower. The polarization is changed by moving the azimuth of the feedpoint relative to the semimajor axis of the elliptical disk.

Microstrip techniques can be used to fabricate the antenna. For example,

the antenna disk could be formed by vapor deposition on a dielectric substrate. The side of the substrate opposite the antenna disk is covered with a conducting layer that acts as

the ground plane. An electrical connector (not visible in the illustration) couples the antenna disk with a center conductor, without electrically contacting the ground plane.

This work was done by I Ping Yu of

Lockheed Electronics Co., Inc., for **Johnson Space Center.** *For further information, Circle 19 on the TSP Request Card.*

This invention is owned by NASA, and a patent application has been

Dual-Frequency Microwave Antenna

A dichroic plate combines S-band and X-band components for transmission and separates them in reception.

NASA's Jet Propulsion Laboratory, Pasadena, California

A single antenna can accommodate two different microwave frequencies at the same time by using two feed horns — one for receiving and radiating X-band signals and one for S-band signals — in combination with an ellipsoid reflector and a dichroic plate (see figure). The dichroic plate passes X-band radiation with low attenuation, but reflects S-band radiation.

Thus, when combined X-band and S-band signals arrive at the antenna, the dichroic plate transmits the X-band portion to the X-band horn and reflects the S-band portion to the ellipsoid reflector, which in turn directs the signal to the S-band horn. For transmission, the process is reversed. Radiation from the X-band and S-band horns is superposed at the dichroic plate and is beamed as combined signals.

The dichroic plate is a sheet of aluminum or copper perforated with an array of holes with dimensions that correspond to X-band wavelengths. The plate is thus transparent to X-band

ANTENNA CASSEGRAINIAN ASSEMBLY
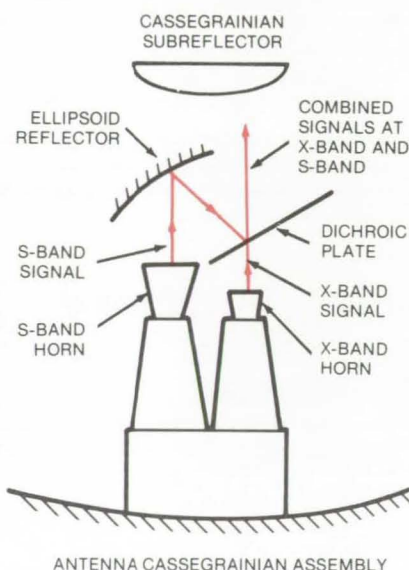
A **Dichroic Plate** in the dual-frequency antenna is transparent to radiation at X-band frequencies but is reflective to S-band radiation. Arrows indicate the directions of transmitted signals; for received signals, the directions are reversed.

frequencies. The ellipsoid reflector is a sheet of solid aluminum backed by a Z-section framework.

The dichroic plate and ellipsoid reflector distort the radiation pattern somewhat, so that it is no longer symmetrical about the beam axis. The distortion is small, however, amounting to no more than a 0.10-decibel degradation in gain.

The dual-frequency antenna was developed to make it possible to receive weak signals from deep space with a single 64-meter-diameter dish. [See also "Signal Separator for Dual-Frequency Antenna" (NPO-14022), *NASA Tech Briefs,* Vol. 4, No. 1, p. 23, and "Efficient Dichroic Plate for Microwaves" (GSC-12171), *NASA Tech Briefs,* Vol. 4, No. 1, p. 4.]

This work was done by Dan A. Bathker, Samuel A. Brunstein, Arthur C. Ludwig, and Philip D. Potter of Caltech for **NASA's Jet Propulsion Laboratory.** *For further information, Circle 20 on the TSP Request Card. NPO-13091*

Interferometer Antenna-Array System

A system immune from interference locates signals in space without ambiguity.

Goddard Space Flight Center, Greenbelt, Maryland

A new scannable beam-forming interferometer antenna-array system comprises a set of widely spaced antenna elements with selected spacings that are integral multiples of a fractional part of the received wavelength. The signals from each antenna element are processed through three mixing stages. With phase information

preserved, the resulting output spatial frequencies are coherently summed to synthesize a single beam, thus uniquely defining the direction of the arriving signal.

The approach (see figure) is demonstrated using a four-element, linear, antenna array. The signal arriving from an angular direction Θ is

received by the four elements spaced an integral multiple of half-wavelength distances apart. Using arbitrarily the first element as reference, the signal at the second element appears to be modulated by ψ_1, which is a spatial frequency determined by the spacing between antenna elements 1 and 2, and, in this case, corresponds to the

INCOMING SIGNAL

θ Ψ_1 Ψ_2 Ψ_4 Ψ_5 Ψ_3

1 2 3 4 ANTENNA ELEMENTS

$3\frac{1}{2}$ $10\frac{1}{2}$ $2\frac{1}{2}$

FIRST LOCAL OSCILLATOR

SECOND LOCAL OSCILLATOR

A_1 A_2 A_3 A_4 A_5 A_6 A_7 A_8 FIRST MIXERS AND BAND-PASS FILTERS

a_1 a_2 a_3 a_4 a_5 a_6 a_7 a_8 FIRST INTERMEDIATE-FREQUENCY TERMINALS

B_1 a_4 B_2 a_4 B_3 a_4 B_4 a_3 B_5 a_6 B_6 a_8 B_7 a_5 B_8 a_7 SECOND MIXERS AND BAND-PASS FILTERS
a_1 a_5 a_6 a_7 a_5 a_2 a_4

b_1 b_2 b_3 b_4 b_5 b_6 b_7 b_8 SECOND INTERMEDIATE-FREQUENCY TERMINALS

C_1 C_2 b_4 C_3 b_5 C_4 b_3 C_5 b_2 C_6 b_6 C_7 b_1 C_8 b_5 THIRD MIXERS AND BAND-PASS FILTERS
b_7 b_1 b_2 b_8 b_7 b_3 b_7

c_1 c_2 c_3 c_4 c_5 c_6 c_7 c_8 SPATIAL-HARMONIC OUTPUT TERMINALS

1st 3rd 5th 7th 9th 11th 13th 15th

A **Four-Element Linear Antenna** array locates signal position in space by processing the incoming signal into odd harmonics via three IF mixing stages. The second and the third stages are set up using interferometer pairs combined from the antenna element outputs. A coherent summation of the spatial harmonic output following the last stage is equivalent to a fully-filled antenna aperture pointing at the direction of the incoming signal.

third spatial harmonic due to 3 $\lambda/2$ separation. Similar harmonics are set up at elements 3 and 4, forming the 13th and 15th harmonics, respectively; the other intermediate harmonics are derived from signal processing.

The signals from each antenna element are divided into two parts and processed to the first intermediate-frequency (IF) signals using coherent local oscillators. Each antenna element feeds a pair of mixers; one of each pair (A_1, A_3, A_5, . . .) is connected to the first local oscillator operating at a certain frequency, and the other of each pair is (A_2, A_4, A_6, . . .) connected to the second local oscillator operating at another frequency. The oscillator frequencies may be above, below, or one above the other below the signal frequency. The mixed difference signals are fed to

power dividers a_1 through a_8.

Interferometer pairs are formed at the second mixing IF stage, B_1 through B_8. The input signals from the first IF terminals are paired from different antenna elements and fed to mixers B_1 through B_8. Connections are made so that identical frequencies are not mixed. Instead a set of normal and inverted functions is generated by alternate mixers. This second set is fed to a group of power dividers b_1 through b_8 that are again mixed to form additional interferometer pairs at the third mixing stage.

The third mixing stage is connected to form the odd spatial harmonics of the processes signal by properly combining the antenna outputs. Coherent summation of the spatial frequencies forms a single beam that uniquely defines the direction of the

arriving signal equal to a fully filled aperture of the same dimensions with antenna elements spaced 1/2 wavelength apart. The system can be made retrodirective without phase shifters, weighing circuits, or scan controllers by applying the processed spatial phase information to a fully-filled transmit array.

This work was done by Julius A. Kaiser, Jr., of **Goddard Space Flight Center.** *For further information, Circle 21 on the TSP Request Card.*

This invention is owned by NASA, and a patent application has been filed. Inquiries concerning nonexclusive or exclusive license for its commercial development should be addressed to the Patent Counsel, Goddard Space Flight Center [see page A5]. Refer to GSC-12365.

Lock Detector for Noise-Coded Signals

Circuit indicates when a receiver is
locked on a scrambled input signal.

NASA's Jet Propulsion Laboratory, Pasadena, California
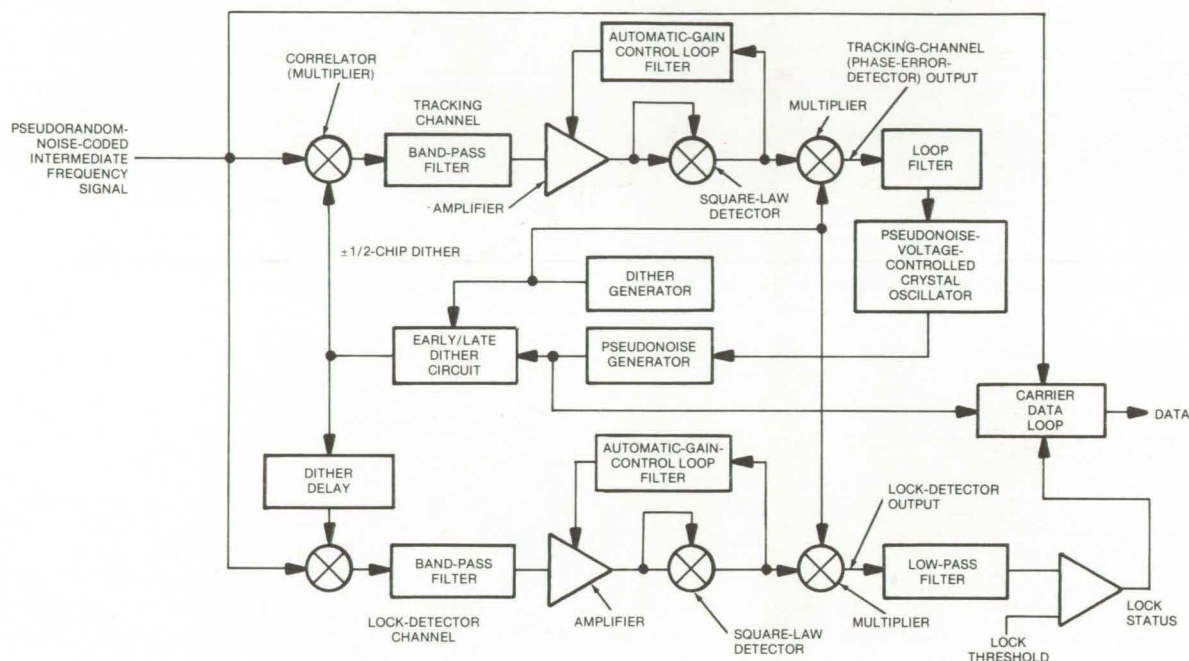
This Circuit Generates a Dithered Code, making it possible to detect when the receiver is locked to an incoming pseudorandom-noise signal. The circuit uses only one lock-detector channel, thus avoiding the balancing and offset problems associated with dual channels.

A circuit indicates when a receiver is locked on a pseudorandom-noise-coded signal. The circuit can be used for the reception of such digitally coded signals as scrambled voice messages (police communication) or scrambled video (subscription television). Such messages are intentionally disguised as noise for security. To decode the message, the receiver must generate an identical code and synchronize it with the received signal. The new circuit determines when the receiver code is correct and synchronized so that the receiver can track the signal.

The received signal enters two separate channels (see figure). In the tracking channel, the received signal is correlated with a "dithered" local pseudorandom-noise sequence; i.e., a pseudorandom-noise sequence that is alternately advanced and retarded by equal amounts in a shift register. When the received sequence and the local sequence are correlated, a partially decoded signal appears at the output of the tracking channel.

In the lock-detector channel, the received signal is correlated with another dithered signal — this one like the tracking-channel dither sequence, but delayed from it. When the optimum tracking point is reached (as controlled by the tracking channel), maximum correlation occurs in the lock-detector channel during the early part of its delayed dithered code, and virtually no correlation occurs during the late part of its dithered code.

A square-law detector in the lock-detector channel produces an output that is much greater during the early part of the code than during the late part. When the dc output from the square-law detector is multiplied by the dithering reference signal, the late voltage (produced by noise) is subtracted from the early voltage (produced by full code correlation). The subtraction yields a dc signal proportional to the degree of correlation.

The dc signal is compared with a dc reference level (the lock threshold). If the dc signal exceeds the lock threshold, the circuit produces a status signal that indicates that the receiver is locked to the incoming pseudorandom-noise signal.

The lock indication is essentially independent of the noise in the lock-detector channel. In addition, use of the single dithered lock-detector channel instead of separate "ontime" and "late" channels avoids the problems of balancing gain and offset created by a dual channel, and requires fewer components.

*This work was done by Lansing M. Carson of Motorola, Inc., for **NASA's Jet Propulsion Laboratory.** No further documentation is available.*

This invention is owned by NASA, and a patent application has been filed. Inquiries concerning nonexclusive or exclusive license for its commercial development should be addressed to the Patent Counsel NASA Resident Legal Office-JPL [see page A5]. Refer to NPO-14435.

Physical
Sciences

Transmitter/Receiver for Laser Imaging

Dual-mirror system reduces backscatter
and compensates for phase delay.

Lyndon B. Johnson Space Center, Houston, Texas

An improved two-mirror transmitter and receiver combination is used with a laser multispectral imaging system carried by low-flying aircraft. One mirror directs a laser beam in a scanning pattern over an area; the other is synchronized to receive the reflected laser beam.

The mirrors are positioned to prevent any significant amount of backscattered laser light from reaching the receiver and thereby creating false light levels in the received image. Their arrangement also compensates for the difference in scanning phase between the transmitter and receiver, created by the brief time interval between transmission and reception.

The two mirrors are ellipses mounted at an oblique angle on opposite ends of a shaft 2 ft (61 cm) long (see figure). They are angled so that axial rays from their centers converge to a common point 1,400 ft (430 m) below. Thus when the aircraft flies at an altitude of 1,400 ft, a laser beam (actually a combined beam from two lasers) coaxial with the mirror shaft is reflected by the transmitting mirror (mirror 1) to the ground below and is reflected from the ground back into the receiving mirror (mirror 2). The elliptical axes of the receiving mirror are twisted with respect to the axes of the transmitting mirror so that the mirrors are slightly but precisely out of phase with each other. This adjustment compensates for the difference in the scanning phases of the transmitted and received beams created by the 2,800-ft (850-m) round trip.

The two mirrors view the ground through separate line apertures (not shown in the figure). Their motion (scanning pattern) is controlled by the shaft that synchronizes the receiving mirror with the transmitter. The two apertures are spaced far enough apart that little or no transmitted laser light
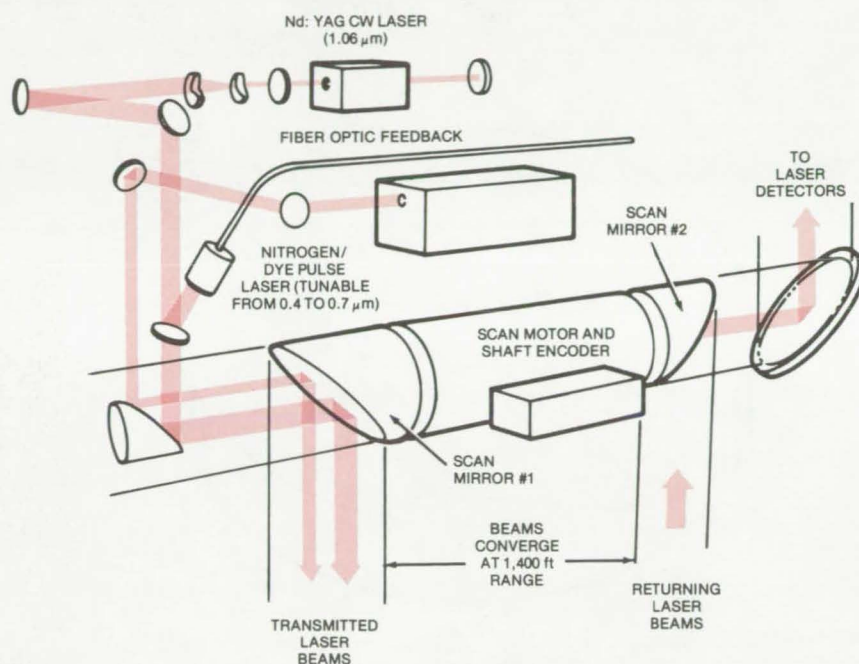
This **Scanning Device** is part of an imaging and spectrum analysis system used for Earth-resources studies. The left-hand mirror directs two laser beams of different wavelengths to Earth 1,400 feet below. The right-hand mirror receives the reflected beams and directs them into a laser detection system. (Simultaneously, the left-hand mirror receives Sunlight reflected from the ground and directs it into dispersing and detecting apparatus that is not shown here.)

is scattered by the air into the receiving aperture.

The transmitting mirror also performs another function: it receives reflected Sunlight from the ground and reflects it into a spectrometer, where it is analyzed in several wavelength bands between 0.4 and 14 micrometers. Thus the complete system includes passive scanning as well as the active (laser-beam) scanning.

[For a related article, see "Optical System for Multispectral Scanner" (MSC-18255), *NASA Tech Briefs*, Vol. 4, No. 1, p. 52.]

Fabricating Wedge-Shaped Beam Splitters

Steps to produce very
sharp beam splitters

Goddard Space Flight Center, Greenbelt, Maryland
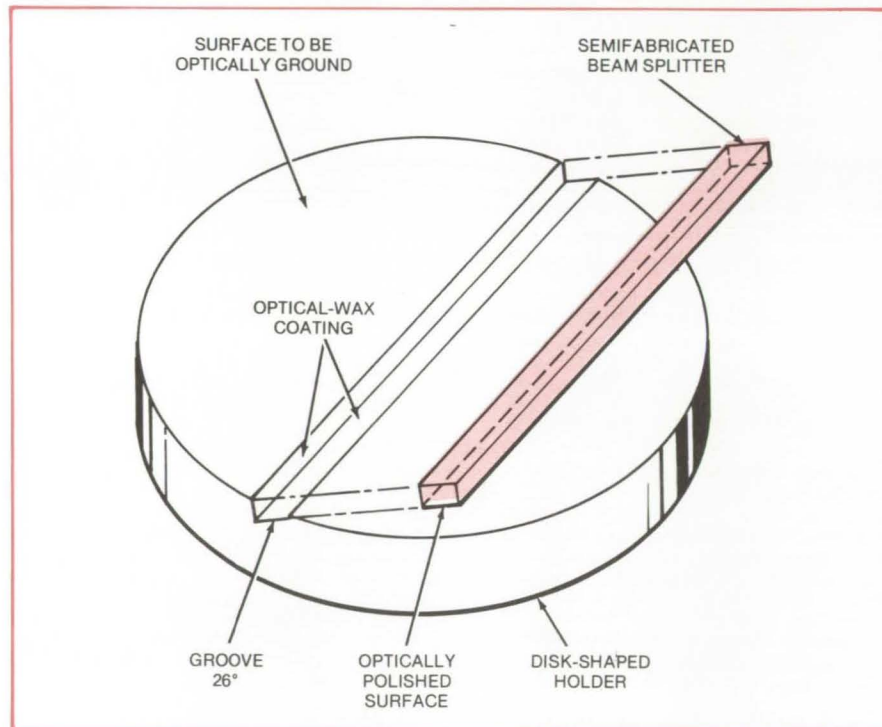
Figure 1. Initial steps in **Fabricating Sharp-Edged Beam Splitters** involve cutting glass strips from an optically-polished glass blank. Each strip is placed into a groove in a holding disk for subsequent grinding and polishing.

A fast and economical fabrication produces wedge-shaped beam splitters with a 0.3-μm edge, compared to conventional methods that have yielded 2-μm edges.

A typical beam splitter made by the new process is prism shaped, with a right-triangle cross section. One component of the split beam strikes the angled reflective surface (hypotenuse), while the other moves parallel to one leg of the triangle. Each component is picked up by a separate optical detector. This setup, for example, may be used in measuring the effect of magnetic fields on light beams; i.e., the well-known Zeeman effect.

The device may be fabricated from either glass or quartz. The first step is to pitch-polish one side of a disk-shaped glass blank. This surface will serve as the angled reflecting surface (hypotenuse) of the finished device. It is polished on a rotating apparatus,

using cerium oxide polishing compound mixed with water. The finished surface has a flatness of one-tenth the wavelength of the energy beam to be reflected by the surface.

The polished disk is cut into strips with a diamond cutter. Each of these strips may then be used to make the beam splitter. The next step is to prepare a holding mechanism (see Figure 1), which can be made from many materials, preferably, however, of the same glass as the device. The holding mechanism is disk shaped and is prepared by cutting a precisely-positioned right-angle groove in its surface, using a diamond saw. The groove is oriented to form a 26° angle with the disk surface.

After the groove is cut and its surfaces waxed with conventional optical wax, the glass strip is placed in the groove and held secure by the wax. The strip is oriented with its optically polished surface resting in-

side the groove forming one side of the 26° angle. This setup is placed on an optical grinding apparatus to remove the strip section protruding from the surface of the holding disk.

When the strip and the surface of the holding disk are coplanar, they are removed from the grinding apparatus for polishing, to sharpen the edge to final sharpness. The device is polished with a rotating felt pad moistened with cerium oxide, or ferric oxide, polishing compound. Only the felt pad rotates; the device is held stationary to prevent breakage or peeling with the desired sharp edge being the trailing edge when placed on polisher. Polishing normally takes several hours until the edge is sharpened to 0.3 μm; however, it depends on the pressure applied to the handle, the speed of the rotating pad, and the desired quality of the ground surface.

Before the beam splitter is finished, a support device is attached to its felt-polished surface, using optical wax. Next both the support and the holding disk are cut with a diamond saw on sides parallel to the longitudinal axis of the beam splitter. Then, they are ground down to a line shown in the figure. The finished beam splitter is
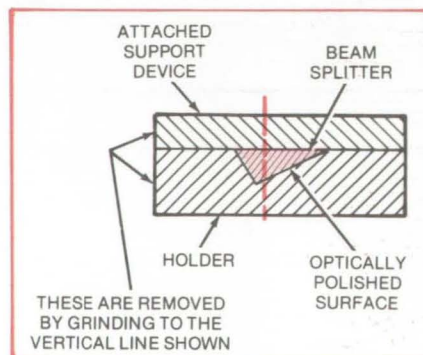
Figure 2. Before the **Beam Splitter Is Finished,** it is covered with a support device for final cutting and grinding so that the optically polished surface becomes a hypotenuse of the right triangle. This procedure may also be used to make very-sharp disposable surgical instruments.

removed from the holding disk and support. Its optically polished surface then forms the hypotenuse of the right triangle.

This work was done by Charles M. Fleetwood, Jr., and Stephen H. Rice

Field-Flattener Lens

Embedded reflective coating produces a plane image for a flat silicon detector.

Lyndon B. Johnson Space Center, Houston, Texas

A spherical lens that focuses light to a flat image has been proposed. The lens is intended for use as an optical scanner for a silicon light detector. It can scan a wide angle at low f-stops, producing a high-resolution image over a range of wavelengths from 0.4 to 14 micrometers.

Ordinarily, a spherical reflector would be used under such conditions, but spherical reflectors focus their images on a spherical surface. Because silicon detectors are necessarily flat (at least at their present stage of development), they are not compatible with spherical images. The new lens concept employs an image-flattening reflective surface within spherical refracting elements (see figure). It keeps spherical aberration to a minimum without external correcting lenses or reflectors.

After passing through a field stop, a collimated ray bundle from the field of view passes through a flat surface into the lens, where the refracting material reduces the field angle of the bundle. Striking a spherical surface within the lens, the ray bundle is reflected back to an embedded "field-flattener" coating, which reflects the ray bundle once more. This time the reflected bundle exits through a narrow slot in the first reflecting surface, converging on a plane image surface where the silicon detector is located.
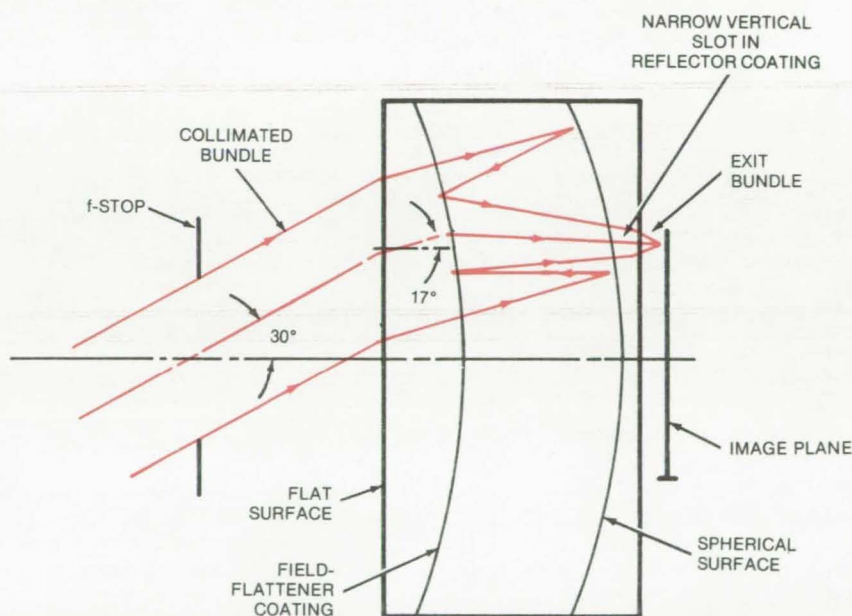
Light Rays Undergo Two Reflections from two spherical surfaces and converge to a flat (plane) image.

A possible alternative way of creating a flat image is to use a cluster of optical fibers as a lens. However, optical fibers are currently suited only to the shorter wavelengths in the 0.4- to 14-micrometer range.

This work was done by Fred Vicik of Barnes Engineering Co. for **Johnson Space Center.** Further information may be found in NASA CR-151753

High-Resolution Spectrometer

Instrument combines optical and imaging devices and cryogenic cooling for accurate measurements of infrared spectra.

NASA's Jet Propulsion Laboratory, Pasadena, California

A proposed spectrometer would measure infrared radiation in the 1- to 15-micrometer wavelength range with a spatial resolution of 1 arc-second and an average spectral resolution of about 0.1 cm^{-1}. It uses an echelle grating, a cross-dispersion grating, a Schmidt camera, and charge-coupled-device detectors. The optics are cooled to 152 K, and the detector arrays are held at 63.5 K. The new spectrometer, which was originally designed for astronomical measurements from a satellite, is suitable for high-resolution, high-sensitivity spectrometry in the laboratory or in the field. Pollution monitoring is one possible application.

Infrared (IR) radiation entering the spectrometer (see figure) is directed by a set of reflectors and aperture wheels to a collimating surface that reflects the IR in parallel rays to a cross-dispersion grating. The ordered IR is collimated by a second collimating surface and directed to an echelle grating. This grating, which has high dispersion and resolving power, sends as much as 80 percent of the IR into a particular order for a given wavelength.

The IR is reflected and focused by a Schmidt camera that was selected because it produces minimal coma and astigmatism. The Schmidt camera directs the IR, via a bending flat, to the detector array. By appropriately indexing only the cross-dispersion grating, at least 80 echelle orders can be focused on the detectors.

Two CCD detector arrays are used: one composed of indium antimonide for the wavelengths from 1 to 5 micrometers and the other composed of mercury cadmium telluride for the range from 5 to 15 micrometers. So that they conform to the spherical field
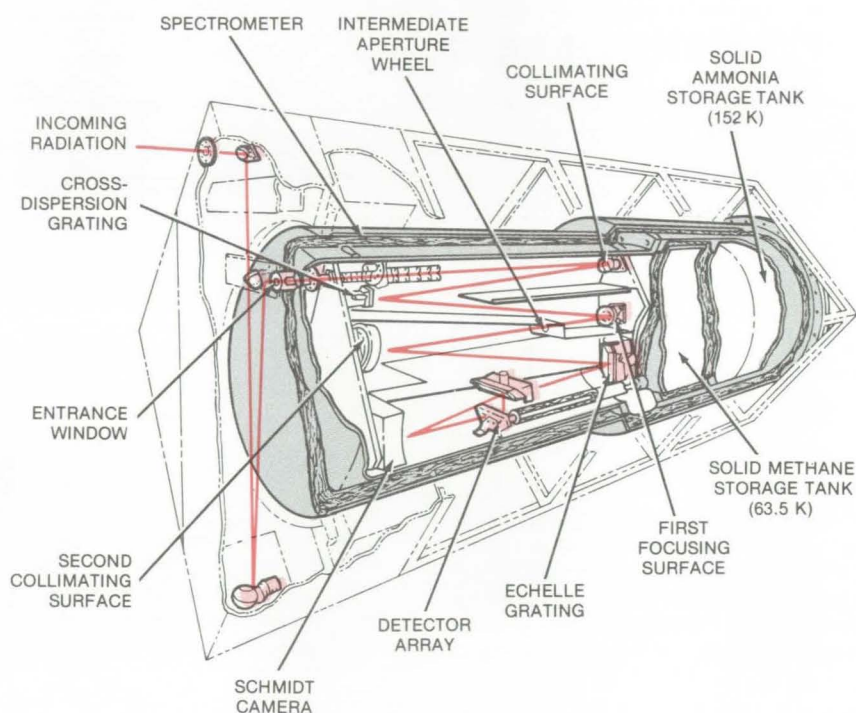
The **Infrared Spectrometer,** shown packaged for space telescope use, is relatively compact and lightweight. The length of the cryogenically cooled section is approximately 1 meter. Total weight is 300 kilograms, of which 100 kilograms are allocated to the cooling system.

of the Schmidt camera, the detector-array elements are arranged as a polygon that approximates a spherical dish.

The cryogenic cooling system includes a storage tank for solid ammonia at 152 K and another tank for solid methane at 63.5 K. The ammonia cools the optical elements, and the methane cools the detector arrays.

For astronomical measurements, the 1,024 elements in each array are scanned every 20 milliseconds. The charge packets are clocked out of the detector arrays, digitized, and summed in 1,024 parallel accumulators,

where they are held for the observation period. The spectrometer calibrates itself by making background scans and by taking readings of self-contained radiance standards.

This work was done by Reinhard Beer of Caltech for **NASA's Jet Propulsion Laboratory.** *For further information, Circle 23 on the TSP Request Card.*

This invention is owned by NASA, and a patent application has been filed. Inquiries concerning nonexclusive or exclusive license for its commercial development should be addressed to the Patent Counsel, NASA Resident Legal Office-JPL [see page A5]. Refer to NPO-14372.

Liquid/Liquid Heat Exchanger

Heat can be exchanged with high efficiency
by the direct contact of two immiscible liquids.

NASA's Jet Propulsion Laboratory, Pasadena, California

A conceptual design for a heat exchanger would utilize two immiscible liquids in direct contact. Since the concept would eliminate the walls or membranes that separate the media in conventional heat exchangers, heat could be transferred more efficiently. Moreover, if the liquids have dissimilar specific gravities, one can be made to rise through the other, improving the heat transfer and reducing the power required to circulate the liquids. Frictional losses would also be lower since the media do not have to be forced through long narrow tubes as in conventional heat exchangers.

The concept could be adapted for collecting heat from Sunlight or from geothermal brine. For instance, in a solar-collector, the immiscible-fluid exchanger could directly use the hot water from the solar collector instead of converting it to water vapor at the collector, as is sometimes done. The hot liquid can be transported through a small-diameter pipe to the heat exchanger, whereas the equivalent amount of vapor would require a much larger pipe.

In the solar-collector application, water would be circulated through the collector by a small pump that produces a pressure differential of about 2 psi (13.8×10^3 N/m²) across the collector (see figure). The water emerges from the collector at about 70° C, enters the heat-exchange chamber through its upper inlet, and falls to the bottom of the chamber through an immiscible fluid that is lighter than the water. Organic liquids such as butane or octane could be experimented with as possible heat-exchange fluids.

The light immiscible fluid is circulated by a pump and enters the chamber through its lower inlet. It rises through the lower zone of the chamber, which contains water at about 20° C, to the middle zone. As shown in the figure, the organic fluid in the middle zone has water drops falling through it.
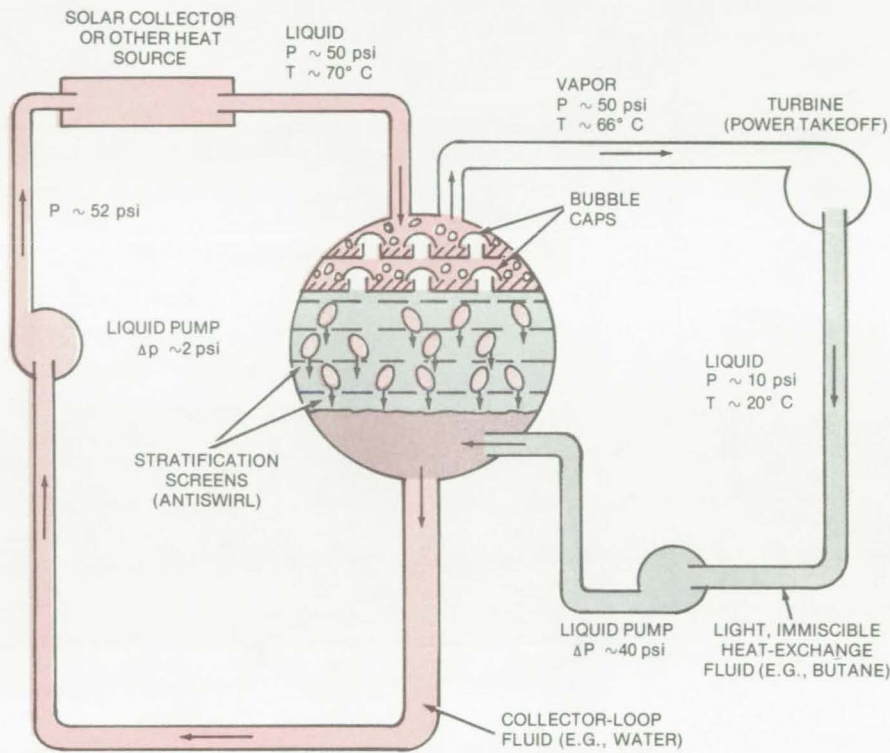
Liquid/Liquid Heat Exchanger would circulate hot water from a solar collector through a light immiscible fluid such as butane. The light fluid picks up heat, is vaporized, and can be used to drive a turbine.

An array of closely spaced screens in the middle zone decreases convection so that there is a temperature differential across the organic fluid. The temperature of the upper portion of the middle zone is approximately at the boiling point of the organic fluid; in the lower portion of the middle zone, the temperature is close to that of the water in the lower zone. An array of bubble caps or Raschig rings in the top portion of the chamber improves the contact between the two counter-flowing streams.

Tube-in-wall heat exchangers are usually considered for the extraction of heat from geothermal brine to prevent the corrosive brine from coming in contact with the turbine-generator blades. In the immiscible-fluid exchanger, butane could be circulated through the brine to absorb heat from it. The brine would then be discarded, and the butane could be fed to a turbine. A water wash might be included in the system to remove water-soluble gases that the butane may pick up from the brine. Depending on the pressure and the temperature of the brine, other fluids may be more satisfactory than butane. If the fluid has a higher density than brine, the connections to the heat-exchange chamber would have to be reversed so that the heavier liquid would be withdrawn from the bottom of the chamber.

This work was done by Charles G. Miller of Caltech for **NASA's Jet Propulsion Laboratory.** *For further information, Circle 24 on the TSP Request Card.*
NPO-14271

No-Reheat Air-Conditioning

System controls moisture content and temperature in computer room without recourse to overcooling and reheating.

Goddard Space Flight Center, Greenbelt, Maryland
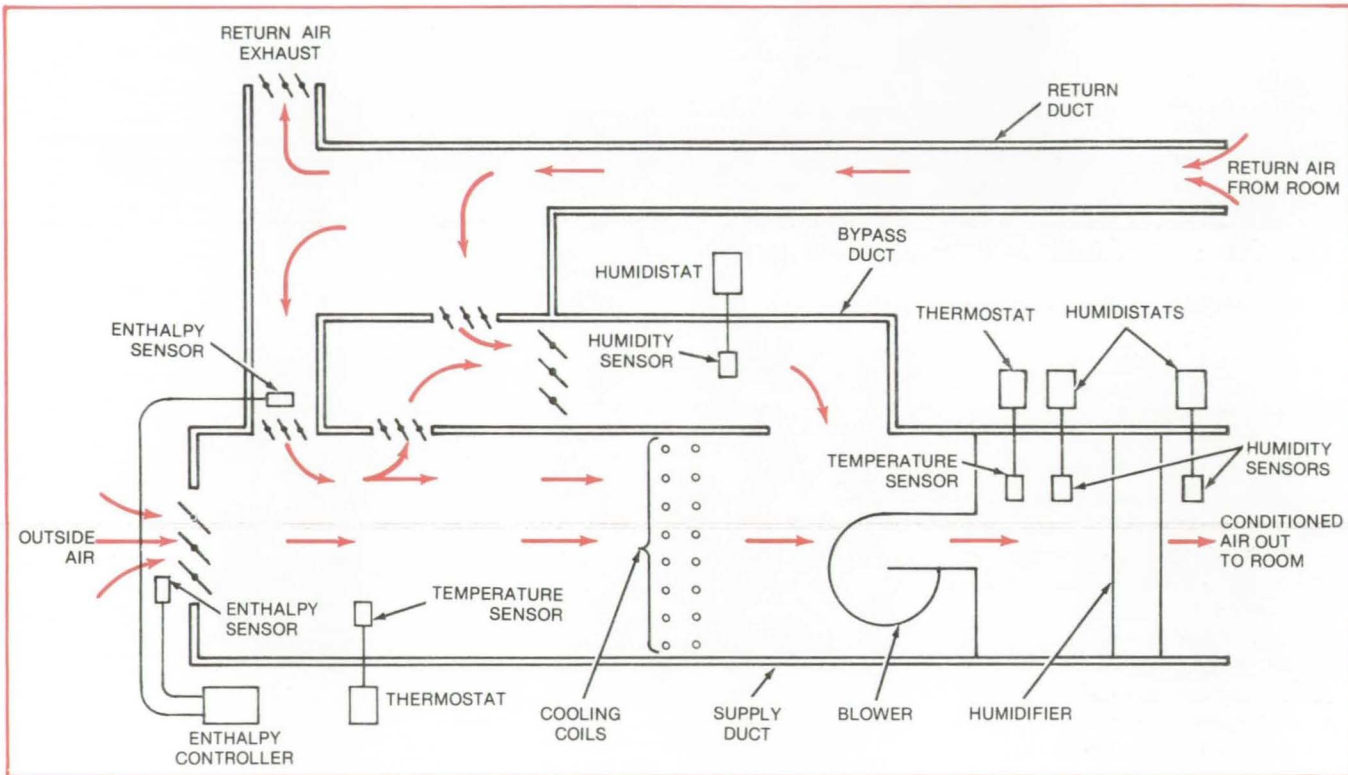
In this **Air-Conditioning System,** dampers, sensors, and controllers blend, divert, and cut off the outside air and / or the return air as necessary to maintain constant temperature and humidity.

An air-conditioning system for environmentally controlled areas containing sensitive equipment, computers, and the like regulates temperature and humidity without wasteful and costly reheating. The new system blends outside air with return air as dictated by various sensors; a portion of the return air bypasses the cooling coil to maintain low humidity and then is mixed with high-humidity cooled air in the proper amount to ensure the required humidity in the cooled space (such as a computer room).

In conventional air-conditioning systems, the cooled air often contains too much moisture. It is common practice to overcool the air to condense out its excess moisture, then to heat it so that it is not too cold for the cooled space. Energy is thereby wasted, both in overcooling the air and in reheating it. The bypass feature of the new system

avoids both overcooling and reheating and maintains essentially constant temperature and humidity.

The new system operates under four distinct outside-air conditions:

1. Outside-air temperature and humidity below the desired dewpoint of the air to be supplied to the room;
2. Outside-air humidity below the desired dewpoint and outside-air temperature at the low end of the range between the desired dewpoint and the enthalpy changeover point (the temperature at which the enthalpy, or heat content, of the outside air equals that of the return air);
3. Outside-air humidity above the desired dewpoint and outside-air temperature at the high end of the range between the desired dewpoint and the enthalpy changeover point; and

4. Enthalpy of the outside air higher than the enthalpy of the return air.

Suppose, for example, that the conditioned air is to be supplied at 60° F (16° C) with a dewpoint of 55° F (13° C), the return air is at 75° F (24° C), and the outside air is at 56° F (13° C). The temperature sensor and thermostat near the inlets to the supply duct (see figure) regulate dampers so that outside air flows in and the return air flows partly into the fresh-air duct and partly through the exhaust outlet. The sensor and thermostat monitor the temperature of the mixed supply air; if the temperature rises above a preset level, the thermostat changes the damper settings so that less return air flows into the supply duct and more return air is exhausted. If the temperature drops, the opposite action occurs.

The temperature sensor and thermostat just downstream from the

blower keep the flow of coolant to the coil turned off (because the supply air is mixed to the desired temperature) and also open the damper in the bypass duct so that air flows over the humidity sensor in that duct. If the dewpoint falls below 55° F, the bypass-duct humidistat opens the damper between the supply duct and the bypass duct and closes the return-to-bypass-duct damper.

Meanwhile, if the blower humidity sensor finds that the supply-air dew-point is too low, it activates the humidifier to add moisture to the air. The humidistat downstream of the humidifier turns it off if humidity rises too high.

Similar appropriate actions occur for the other outside-air conditions. For example, in typical hot summer weather (condition 4), the outside enthalpy sensor measures a higher value than the return-duct enthalpy sensor. Therefore the enthalpy controller closes the outside-air damper and return exhaust damper, so that only return air is treated and used for cooling.

This work was done by Henry D. Obler of **Goddard Space Flight Center.** *For further information, Circle 25 on the TSP Request Card.*

This invention is owned by NASA, and a patent application has been filed. Inquiries concerning nonexclusive or exclusive license for its commercial development should be addressed to the Patent Counsel, Goddard Space Flight Center [see page A5]. Refer to GSC-12191.

Improving Maser Frequency Stability

A coated multitube collimator reduces
the line width of a hydrogen maser.

Goddard Space Flight Center, Greenbelt, Maryland

A hydrogen-maser frequency standard has been made more stable by the addition of a special collimator. With the new collimator, the maser line width — a measure of long-term frequency stability — can be made extremely narrow. Line widths as narrow as 0.24 hertz have been measured in the laboraory, representing a fivefold improvement over a maser without the collimator.

The collimator is an assembly of capillary tubes made of Pyrex, or equivalent material. The tubes have a pore diameter of 0.020 millimeter and a length of 8 millimeters; the tube assembly is 13 millimeters in diameter. The cylindrical array of tubes is inserted in a round hole in the maser hydrogen-storage bottle, 7 inches (17.8 centimeters) in diameter, and is held in place by a retaining ring and a plastic collar (see figure).

The collimator guides atoms in a hydrogen beam into the storage bottle. At the same time, it prevents excited hydrogen atoms in the bottle from escaping. The insides of the tubes are coated with $(CF_3CH_2CH_2)_2SiCl_2$, also known as BCFT, which inhibits recombination and the loss of energy by the beam atoms when they strike the walls of the tube. The net result is a sizable increase in the efficiency of the maser, thus decreasing the effects
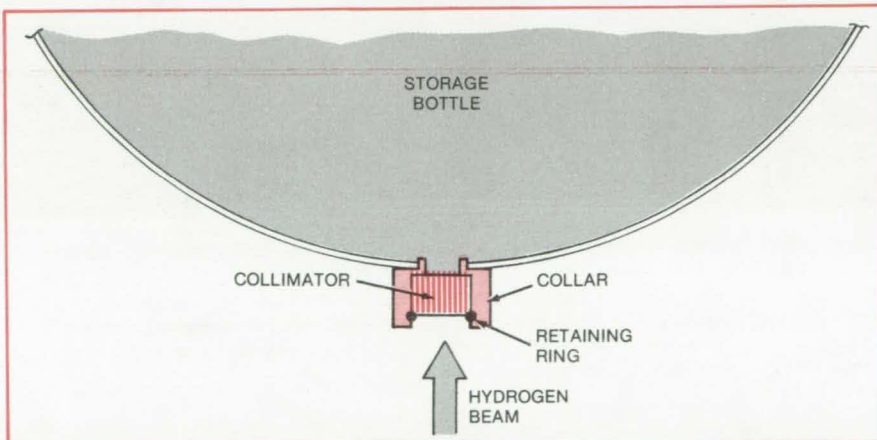
An **Array of Parallel Glass Tubes** assembled as a cylinder forms a collimator for the atoms in a hydrogen beam. A fluorocarbon coating in the tubes virtually eliminates energy loss in the collimator.

on frequency stability of unpredictable external influences such as stray magnetic fields.

The collimator pores are coated by the following procedure:

• The Pyrex tube array is soaked for several hours in undiluted BCFT, then drained on a clean, absorbent material such as a laboratory paper towel.

• The array is dipped and agitated for a few minutes in distilled water at a temperature between 40° and 50° C. The water reacts with the BCFT, re-moving any that has not been bound to the glass surface.

• Another agitated dip, this time in ethyl alcohol, removes the oily residue of the BCFT/water reaction.

• Finally, to remove particles that might block the pores, the array is blown out with a jet of dry, high-pressure nitrogen gas.

This work was done by Stuart B. Crampton of Williams College for **Goddard Space Flight Center.** *For further information, Circle 26 on the TSP Request Card.*
GSC-12400

Rotatable Microscope Stage

A simple microscope stage permits
sample inspection at various angles.

Lyndon B. Johnson Space Center, Houston, Texas
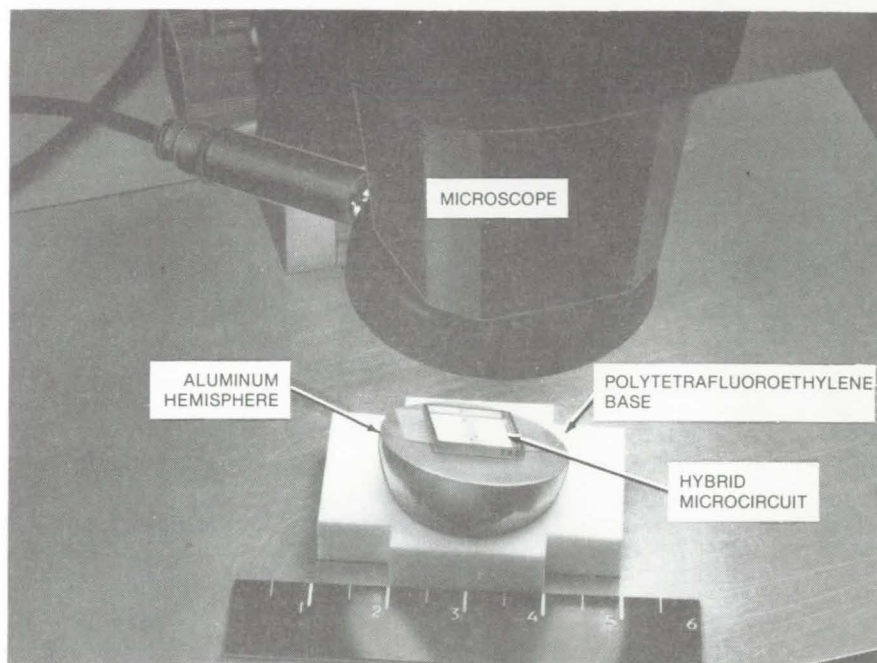
A **Simple Microscope Stage** is easily turned to any desired angle for optical inspection of hybrid microcircuits. As shown, the microcircuit is attached to a magnetic strip on the flat plane of the hemisphere. The hemisphere is simply twisted to any desired position for oblique viewing of the circuit details. Unsteady hand-holding of the sample or complex optical tube adjustments are no longer needed. The illustrated scale is in inches.

Samples mounted on a simply-constructed rotatable microscope stage can be viewed at various angles. The new stage is very convenient in inspecting hybrid microcircuits. Microcircuit inspection on conventional microscope stages designed for planar viewing is more difficult because the sample may have to be hand-held at various angles. The new stage permits the operator to orient the sample at selected fixed angles to view details.

The stage as shown consists of an aluminum hemisphere resting in a hemispherical cavity of a polytetra-fluoroethylene base. The microcircuit is attached to a magnetic strip cemented to the flat plane of the hemisphere. The stage is placed under the microscope and the microcircuit examined by turning the hemisphere to any desired angle. A typical inspection is carried out at 30 to 140 X magnifications.

This work was done by Joseph A. Ivanisko of Sperry Rand Corp. for **Johnson Space Center.** *No further documentation is available.*
MSC-18549

Microwave Measurement of Atmospheric Pressure

A satellite measures atmospheric pressure over
the oceans for long-range weather forecasting.

NASA's Jet Propulsion Laboratory, Pasadena, California

A proposed concept for measuring surface air pressure over the oceans utilizes three pairs of microwave signals transmitted from an orbiting satellite. For each pair of frequencies in and near the millimeter-wavelength absorption band of oxygen, signals of equal power are transmitted. The ratios of the returned-echo powers (differential absorption) are a measure of the total oxygen in the path and hence of the partial pressure of oxygen at the surface.

The primary pair of pressure-sensing frequencies lies on the lower wing of the broad oxygen-absorption band centered on 60 GHz. One of the pair is sufficiently far into the band to be significantly affected by changes in the total mass of oxygen in the transmission path, while the other is on the extreme wing of the band and, therefore, is affected very little by oxygen absorption.

Measurements at two additional pairs of frequencies are used to compensate for the atmospheric temperature profile, water-vapor content, cloud cover, and sea state. When the operating frequencies are chosen correctly, a combination of the three measured ratios depends only on the surface pressure. The principal operating frequency of the instrument should be around 52 to 53 GHz. Farther into the band, the effectiveness of the signal and the signal-to-noise ratio are reduced; at lower frequencies the effect of surface pressure on the signal is reduced.

The presence of water vapor in the atmosphere has both indirect and direct effects, modifying the pressure broadening of the lines within the oxygen band and contributing to absorption in the spectral band of interest. It can make a significant contribution to the total surface atmospheric pressure. With the exception of ozone, other atmospheric gases do not significantly absorb in this region of the spectrum; but clouds and rain both absorb and scatter. Numerous weak ozone lines exist throughout the microwave spectrum, but only close to line centers is the absorption strong enough to affect the results. These frequencies can be easily avoided.

Although the proposed method has been specifically designed for use over the oceans, similar measurements over land may give a valid indication of pressure, but only if a suitable average height can be used and if the surface has appropriate reflection characteristics. However, the existing network of weather-monitoring stations gives satisfactory coverage of most of the continental land masses, while the oceans covering some 70 percent of Earth's surface are almost totally neglected. Satellite surface-pressure data for the oceans will complement present land data.

For most sea states, it should be possible to make measurements with angles up to about 15° from the vertical. Such measurements away from the subsatellite path will allow the surface-pressure gradient to be determined, and this is of much greater value than pressure only along the orbit path. For a 1,000-km orbit altitude, the 15° limitation means that the swath width at the surface is about 500 km, across which significant pressure differences frequently occur.

Potentially, the proposed concept could be accurate to within 1 to 2 mbar of surface pressure without the accurate determination of temperature and water-vapor fields. Continuing research is directed toward selecting an optimum set of frequencies mostly to reduce the background effects. No great improvement in the sensitivity to pressure is expected, however, because that is limited by how close the operating frequencies are to the band center. The transmitter power in the range of several watts is deemed adequate for this application.

All-Glass Solar Collector

Maintenance-free
solar collector

Marshall Space Flight Center, Alabama

Conventional solar collectors incorporate a number of metal components. Much of the collector is metal tubing carrying the heated fluid. The metal is relatively expensive and may corrode with time.

A proposed alternative is an all-glass solar collector. The collector is designed for high efficiency; and because of its all-glass structure, it is virtually maintenance-free.

The proposed configuration as shown in the illustration is made from several plates of glass stacked on top of each other. The top plate is tempered glass, which admits incoming solar radiation. This glass has been treated to resist breakage from various wind-driven objects and to resist the effects of heat. Directly underneath is air that acts as a thermal barrier, preventing loss of the collected heat back to the environment. Below this space are two layers of heat-strengthened glass. The area between the two layers is grooved. A film of black solar fluid flows through the grooved area and is heated directly by solar radiation. A mirrored
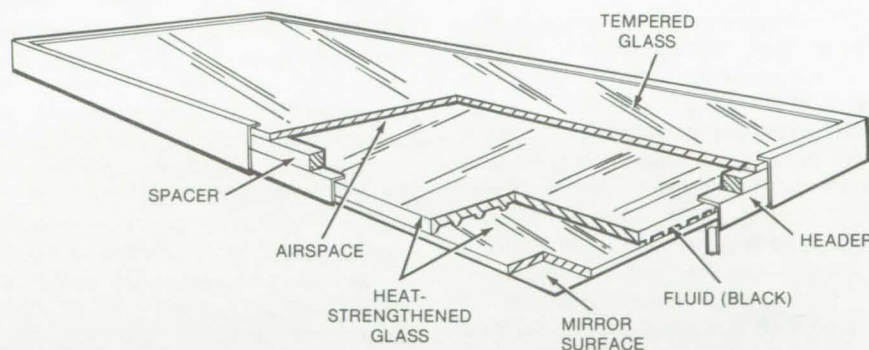
An **All-Glass Solar Collector** is corrosion-free and more economical without conventional fluid-carrying metal tubes. It utilizes black fluid to absorb solar heat. A mirrored surface on the bottom reflects any heat lost back to the fluid.

surface below the fluid reflects any lost energy back to the fluid.

The advantages of this type of construction include:
a. A practically maintenance-free collector without corrosion problems,
b. Reduced costs due to glass instead of metal,
c. The use of efficient black fluid to collect solar heat, and
d. The use of mirrored surface to return any lost energy back to the fluid.

Books and Reports

Solar-Heating System Design Package

System drawings and description are compiled in a 68-page report.

A commercial solar-heating system that meets government standards for installation in residential dwellings is described in a new report. The system is composed of a warm-air solar collector, a logic control unit, and a switching and transport unit.

The collector, which was originally designed as an integrated roof/wall system, serves both as a solar-energy converter and as a structural weather-resistant skin. It can be fabricated in any length from 12 to 24 feet (3.6 to 7.3 m).

The logic control unit receives input data from sensor probes in the collectors, in the heat-storage space, and in the living space. The logic maximizes the use of solar energy and minimizes the use of conventional energy. The transport and switching unit is a high-efficiency air handler equipped with valves that respond to outputs from the control system.

The 68-page report describes the system, its operation, and its performance specifications. Chapters are devoted to the collectors, the logic unit, the switching unit, and the energy-transport unit; and specifications for sizing the rock-bed thermal-storage unit are also given. The text is complemented by a comprehensive set of design drawings of the subcomponents.

This work was done by Contemporary Systems, Inc., for **Marshall Space Flight Center.** *To obtain a copy of the report, "Solar Heating System Final Design Package," Circle 28 on the TSP Request Card.*
MFS-25226

Test and Evaluation of a Solar-Heating System

Tests of the collectors, energy-transport module, and control panel

Evaluation tests on the components of a commercial solar-heating and hot-water system are documented in a new report. The subsystems tested were the solar collector, energy-transport module, and control panel.

The flat-plate collector was evaluated for its ability to withstand expected snow and wind loads and for its flame-spread and smoke classification. Two fire tests were carried out (intermittent and burning-brand). The collector meets applicable standards for all of these tests.

Solar-heating operation was simulated to test the energy-transport module. During the test, the blower end of the module was connected to a flow chamber to measure the air-delivery rate. Such parameters as motor current drain, winding temperature, and external static pressure were also monitored. Immediately following the operation test, a 60-Hz, 1,000-V signal was applied between a high-voltage part of the module and nearby "dead-metal" sections to check for dielectric breakdowns; none were found.

Thermocouples were placed on critical components of the control panel to check the temperatures during operation. The temperatures of three relay coils exceeded specifications when running with loads connected.

The main body of the report describes the tests and test results. A description of the solar collector is contained in an appendix.

This work was done by Fern Engineering Co., Inc., for **Marshall Space Flight Center.** *To obtain a copy of the report, "Test and Evaluation of Fern Engineering Company, Inc., Solar Heating and Hot Water System," Circle 29 on the TSP Request Card.*
MFS-25201

Installation Package for a Solar-Heating System

Includes installation, operation, and maintenance manuals for four subsystems

This package consists of installation, operation, and maintenance manuals for each of four commercial solar-energy subsystems:
• Solar Collectors,
• Thermal-Storage Unit (Pebble-Bed),
• Air-Handler Unit, and
• Controller for the Heat Pump and Off-Peak Storage.
The manuals, each about 15 pages in length, give design information, sizing data, specifications, drawings, and other material needed to install, operate, and maintain the subsystems.

The pebble-bed heat-storage unit consists of river gravel or other hard, dense rock, held in a reinforced-concrete or similar high-temperature-resistant container. It is sized for each installation and can be located on the building or buried.

The collectors are flat-plate devices with air as the transport medium. They are assembled in large arrays by coupling several 3- by 6-ft (0.9- by 1.8-m) sections. Information on pre-installation roof preparation, mounting hardware, input/output connections, and the attachment of temperature sensors is included.

The air handler is installed with filters and humidifiers, as required. Among its possible operating modes are: space heating, storing heat, and domestic-water heating. With properly installed temperature sensors and control circuits, a comfortable temperature is maintained, once the thermostat is set.

This work was done by Solaron Corp. for **Marshall Space Flight Center.** *To obtain a copy of the installation package, "Installation Package for the Solaron Solar Subsystem," Circle 30 on the TSP Request Card.*
MFS-25198

Verification Tests for a Solar-Heating System

Components, subsystems, and system were tested for performance, durability, safety, and other factors.

A 44-page report describes verification tests on a solar space-heating and hot-water system. The tests cover the development, qualification, and acceptance of the system, which has been installed in commercial buildings in California and Colorado.

Preliminary design information for this system is given in "Design Information for Solar-Heating Systems" (MFS-25097) on page 58 of NASA Tech Briefs, Vol. 4, No. 1. The solar collectors have aluminum absorber plates coated with an absorbent paint. Oil is the heat-transfer medium. A water-filled heat-storage tank is included for use during periods of low Sunshine and darkness. When the stored heat is depleted, an electrical-resistance auxiliary heater is activated. The system is regulated automatically by electrical and electronic controls.

The verification tests were made on the overall system, on mechanical and structural subsystems and components, and on the buildings and sites. Such important factors as leakge prevention, collector adjustment, structural load capacity, susceptibility to hail damage, and architectural esthetics were considered.

Attention was also given to safety (e.g., adherence to plumbing and electrical codes, the operation of fail-safe controls, and the presence of toxic and flammable fluids). Durability, reliability, and maintainability were analyzed.

The verification methods used were similarity comparisons, mathematical analyses, inspections, and tests. Tables and graphs complement the test material.

This work was done by Colt, Inc., for **Marshall Space Flight Center.** *To obtain a copy of the report, "Verification Test Report on a Solar Heating and Hot water System," Circle 31 on the TSP Request Card.*
MFS-25178

Residential Solar-Heating/ Cooling System

A report of progress on a system for single-family residences

A new report documents continuing work on the residential solar-heating and cooling systems described in "The Design of Solar-Heating and Cooling Systems" (MFS-25106) on page 210 of NASA Tech Briefs, Vol. 4, No. 2. At the 5-month mark in the anticipated 17-month program, the initial design is complete, and development and component testing has been initiated.

The system proposed for a single-family dwelling is a single-loop, solar-assisted, hydronic-to-warm-air heating subsystem with solar-assisted domestic-water heating and a Rankine-cycle air-conditioning unit. It uses flat-plate liquid solar collectors and a water tank for thermal storage.

A review of the "baseline" design is contained in section 3 of the 109-page report. It includes a diagram of the system and an overview of its operation.

Section 4 is a detailed discussion of the results of redesign and refinement of the baseline to reduce size, weight, maintenance requirements, and production costs, and to incorporate other modifications. Methods for selecting the most efficient working fluid for the Rankine cycle are described, along with a comprehensive computer-simulated cycle-optimization study. Design optimization studies of subcomponents (such as the evaporative condenser, the compressor, and the turbine) are presented. A description of marketing plans for the system is included as section 5 of the report.

This work was done by the Energy Resources Center of Honeywell, Inc., for **Marshall Space Flight Center.** *To obtain a copy of the report, "Preliminary Design Package for Residential Heating/Cooling System — Rankine Air Conditioner Redesign," Circle 32 on the TSP Request Card.*
MFS-25166

Installation Package for a Solar-Heating System

Package contains information for installing, operating, and maintaining an air-heating system.

An installation package for the prototype solar-heating system described in "Solar-Powered Hot-Air System" (MFS-23976) on page 511 of NASA Tech Briefs, Vol. 3, No. 4, is now available. It contains an operation and maintenance manual, hardware brochures, schematics, operating-mode descriptions, and drawings. The air-type system, which is installed at the Concho Indian School in Oklahoma, consists of solar collectors on the roof of the building, ductwork, fans, control devices, and a rock pit for heat storage. The package includes information for installing, operating, and maintaining the system components.

The operation and maintenance section gives simple instructions for changing from winter to summer operation. (In the summer, the system closes off ducts to the collectors and circulates outside air through the attic.) This section also contains recommendations for cleaning the filters and the collector cover plates. The manufacturers' brochures describe fans, blowers, motors, thermostats, zone-control devices, relays, damper actuators, timer, and airflow controller.

Drawings illustrate the airflow circuit for direct heating from the collectors, for heating from rock storage, for auxiliary heating from fossil fuel, and for summer (vented-attic) operation. Other drawings show the collectors, the collector mounting, ductwork in the attic and crawl space, duct connections, and instrumentation locations.

This work was done by Solar Engineering and Equipment Co., Inc., for **Marshall Space Flight Center.** *To obtain a copy of the installation package, "Installation Package for a Solar Heating System," Circle 33 on the TSP Request Card.*
MFS-25157

Liquid Solar Collector

Performances before and after natural weathering are compared.

A 38-page report documents evaluation tests on a commercial flat-plate solar collector. The collector uses water as the working fluid.

The collector is covered with two plates of low-iron glass and is insulated with polyurethane foam. It weighs 242.5 pounds (110.0 kilograms) and measures 48.8 by 120.8 by 4.1 inches (124.1 by 306.9 by 10.5 centimeters). The absorber consists of copper tubing soldered to a copper fin coated with black paint.

Collector performance was measured before and after exposure to the natural environment for 34 days. During the exposure, the collector orientation was adjusted continually to keep Sunlight within 5° of normal to the surface at solar noon. After the exposure, there was no evidence of deterioration in the cover plates, absorber, absorptive coating, collector enclosure, insulation, gaskets, caulking, and sealants.

Graphs included in the report show efficiency as a function of insolation in metric and in English units, compare efficiencies before and after weathering, and depict the incident-angle modifier (which represents efficiency as a function of Sunlight direction). Tables in metric and English units present data on test dates and times, air and working-fluid temperatures, waterflow, insolation, efficiency, and windspeed and direction. Appendixes describe the test facilities and test methods.

This work was done by the Florida Solar Energy Center for Marshall Space Flight Center. To obtain a copy of the report, "Thermal Performance Evaluation of the SEMCO [Liquid] Solar Collector," Circle 34 on the TSP Request Card.
MFS-25218

Final Report on the Concentric-Tube Solar Collector

A summary of a 26-month effort to optimize its performance

The results of a 26-month program to improve the performance of a commercial solar collector are documented in a recently released report. [See related articles "High-Performance Solar Collector" (MFS-25135) on page 198 of *NASA Tech Briefs*, Vol. 4, No. 2, and "Design Review of a Liquid Solar Collector" (MFS-25140 on page 212 of that issue.]

The improved collector consists of 72 concentric-tube elements with manifolding and a reflective backing surface. It can use either air or liquid as the heat-transfer medium. The 72-element module can operate continuously at exit air temperatures of up to 325° F (163° C), high enough to drive solar-powered air-conditioning equipment efficiently.

The 22-page report lists the program objectives, relates how they were accomplished, discusses problems encountered during fabrication and testing, and describes the final hardware. A performance certificate, verifying that the system meets applicable standards for solar-heating and cooling of private and commercial buildings, was obtained from an independent engineering firm. The certification test result is included in the report.

This work was done by John C. Parker of Marshall Space Flight Center. To obtain a copy of the report, "Development, Testing, and Certification of Owens-Illinois Model SEC-601 Solar Energy Collector Systems — Final Report," Circle 35 on the TSP Request Card.
MFS-25188

Collector Performance at Various Air-Channel Depths

Hot-air solar collector efficiency is measured at various airflow-channel depths.

A new report describes an evaluation of a hot-air solar collector at various flow-channel depths. The collector [see "Simple, Economical Solar Collector" (MFS-25109) on page 199 of *NASA Tech Briefs*, Vol. 4, No. 2] has a glass cover, a black-coated aluminum absorber plate, and a urethane molded body.

The collector thermal performance was measured in a solar simulator.

Airflow-channel depths of 3, 2, 1, and 1/2 inches (7.6, 5.1, 2.5, and 1.2 centimeters) were created by inserting spacers in the flow channel. During the measurements, data were recorded on absorber surface temperature, inlet air temperature, outlet air temperature, airflow rate, collector differential pressure, insolation rate, and windspeed. Collector efficiency was determined from the recorded data.

Test results are tabulated and plotted for each of the channel depths. Thermal efficiency was highest for shallow channels and high airflow rates.

This work was done by Wyle Laboratories for Marshall Space Flight Center. To obtain a copy of the report, "Thermal Performance Evaluation of MSFC Hot Air Collectors With Various Flow Channel Depths," Circle 36 on the TSP Request Card.
MFS-25159

Fin-Tube Solar Collectors

Three fin-tube designs were evaluated.

A new report presents test procedures and results of a thermal-performance evaluation of seven commercial fin-tube (liquid) solar-collector absorber plates. The indoor tests used the Marshall Space Flight Center solar simulator. They were carried out according to the Center test procedures and ASHRAE (American Society of Heating, Refrigerating, and Air-Conditioning Engineers) test requirements.

Each absorber plate is 5.9 in. (14.9 cm) wide by 83 in. (211 cm) long, with type-M copper tube of 0.569 in. (1.44 cm) inside diameter. No cover plates were used, and the absorber plates were removed from the collector enclosure.

Three fin-tube designs were evaluated: One design used an extruded aluminum fin that snapped around the tube; a second design used a wrap-around fin with pop rivets fastening the fin around the tube; and the third design was an integrated tube/fin element.

The tests obtained performance data at inlet temperatures of ambient and 50° and 100° F (28° and 56° C) above ambient, with a controlled liquid

flow rate of 0.15 gal/min (0.01 l/s). The tests were repeated at 0.30 gal/min (0.02 l/s). Data recorded were ambient temperature, solar flux, liquid flow rate, windspeed, and liquid inlet and outlet temperatures.

Test results are shown graphically, and tables show supporting test data and a summary of the test results, indicating efficiency as a function of inlet temperature. The snap-in fin with a black-chrome selectively coated absorber outperformed the other configurations.

This work was done by Wyle Laboratories for **Marshall Space Flight Center.** *To obtain a copy of the report, "Indoor Test for Thermal Performance Evaluation of Seven Elcam Fin-Tube Solar Collector Configurations," Circle 37 on the TSP Request Card.*
MFS-25238

Certification of the Concentrating Solar Collector

Extensive tests demonstrate its compliance with applicable standards.

The procedures and results of pre-certification testing of a concentrating solar collector (see related article on this page) are documented in a new report. In evaluating the collector, engineers carried out extensive operational, electrical, and mechanical checks, the results of which were compared with government performance standards and with contract specifications. No problems were uncovered, and the collector was certified as meeting applicable standards.

Parts 1 and 2 of the 183-page report contain the engineers' certification statements and the results of a computer evaluation of the collector design. The design study determined the effectiveness of the structure in supporting itself and in withstanding expected wind and ice loads. The results are summarized in a table of allowable and actual weight/thickness ratios for various structural members.

In part 3, the report describes the verification tests of the collector and its tracking drive. The tests included:

- thermal performance (efficiency);
- stagnation;
- pressure and vacuum loading of the absorber;
- vibration and noise;
- erosion/corrosion;
- the effectiveness of seals, selective coatings, glazing, and pressure-relief valve;
- tracking accuracy; and
- adherence to plumbing and electrical standards.

This work was done by Northrup, Inc., for **Marshall Space Flight Center.** *To obtain a copy of the report, "Certification and Verification for Northrup Model NSC-01-0732 Fresnel Lens Concentrating Solar Collector," Circle 38 on the TSP Request Card.*
MFS-25220

Collector Performance After Weathering

Retest results after 16-month exposure

A new report summarizes thermal performance tests on a flat-plate solar collector following long-term weathering. The collector was mounted on the weathering-test stand at Marshall Space Flight Center and exposed to the natural environment. It was held stagnant for approximately 16 months during the exposure.

The collector uses air as the heat-transfer fluid. It has a gross area of 19 ft^2 (1.77 m^2). The absorber plate is made of 24-gage steel, the coating is baked-on black paint, the cover consists of two sheets of low-iron tempered glass, and the insulation is fiberglass batting.

After weathering, a visual inspection of the collector revealed a slight film on the inner cover plate and significant discoloration of the absorber. The performance tests showed a lowering of efficiency, which is probably caused by a change in the absorptivity of the absorber plate. There was no obvious sign of a change in the transmissivity of the cover.

[See related article "Thermal Performance of a Hot-Air Solar Collector" (MFS-23924) on page 216 of *NASA*

Tech Briefs, Vol. 3, No. 2.]

This work was done by the Solar Energy Systems Division of Wyle Laboratories for **Marshall Space Flight Center.** *To obtain a copy of the report, "Long Term Weathering Effects on the Thermal Performance of the Solaron [Air] Solar Collector," Circle 39 on the TSP Request Card.*
MFS-25187

Concentrating Solar Collector — Final Design

The collector and its tracking drive meet government standards for public use.

The final report of a program to improve a commercially-available concentrating solar collector has been made available. The end product of the program is a collector that meets applicable government standards of structural design, plumbing, heating and cooling, electrical design, building codes, and other test criteria.

Each collector panel is an array of four troughlike enclosures covered by an acrylic Fresnel lens. Sunlight is focused on a copper absorber tube near the bottom of the trough. The tracking drive includes a Sun sensor, an electric motor, a drive train, and associated electronics.

The 27-page report describes the final hardware, discusses problems encountered during fabrication and testing, and presents certification statements of performance. Photographs of the collector, performance data (which are compared to specifications), and recommendations for future modifications are included.

[See related article, "Concentrating Solar Collector — Installation Package" (MFS-25068), on page 524 of *NASA Tech Briefs,* Vol. 3, No. 4.]

This work was done by John C. Parker of **Marshall Space Flight Center.** *To obtain a copy of the report, "Development, Testing, and Certification of the Northrup, Inc., ML Series Concentrating Solar Collector Model NSC-01-0732 — Final Report," Circle 40 on the TSP Request Card.*
MFS-25186

Weathering of a Flat-Plate Solar Collector

Collector performance after 14-1/2 months exposure is described.

A new report contains a performance evaluation after weathering of a flat-plate solar collector described in two previous articles in *NASA Tech Briefs*. [See "Thermal Performance of a Flat-Plate Liquid Solar Collector" (MFS-23890) on page 217 of Vol. 3, No. 2, and "Static Load Testing of a Liquid Solar Collector" (MFS-25115) on page 59 of Vol. 4, No. 1.]

The solar collector, which uses a liquid heat-transfer medium, was exposed to natural weathering for 14-1/2 months. After exposure, the inner cover glass was noticeably cloudy, probably because of gases given off by the insulation. The absorber plate was also slightly discolored.

The collector was performance-tested in a solar simulator at inlet liquid temperatures above ambient by 0°, 25°, 50°, and 110° F (0°, 14°, 28°, and 61° C). Measurements were made of ambient temperature, inlet temperature, outlet temperature, differential temperature, differential pressure, liquid flow rate, insolation rate, and windspeed.

Collector efficiency was calculated and plotted as a function of inlet liquid temperature. The slope of the efficiency curve decreased significantly (became more negative) after exposure, indicating an increase in the collector heat-loss coefficient.

The tested collector has a copper absorber plate 0.021 inch (0.53 millimeter) in thickness and a double cover of tempered glass 1/8 inch (3.2 millimeters) in thickness. The collector measures 3 by 7 feet by 4-3/4 inches (0.9 by 2.1 meters by 12.1 centimeters). It weighs 130 pounds (59 kilograms).

This work was done by Wyle Laboratories for **Marshall Space Flight Center.** *To obtain a copy of the report, "Long-Term Weathering Effects on the Thermal Performance of the Libbey-Owens-Ford [Liquid] Solar Collector," Circle 41 on the TSP Request Card.*
MFS-25160

Guide to Remote-Sensor Data Systems

Handbook contains extensive information on sensors for Earth-resource satellites.

A remote-sensing data handbook presents 469 pages of theoretical and practical information on spaceborne sensors and associated systems for Earth-resources applications.

The handbook covers:
• Synthetic-Aperture Radars,
• Altimeters,
• Scatterometers,
• Laser Radars,
• Multispectral and Mapping Cameras,
• Imaging Spectroradiometers,
• Atmospheric Sounders,
• Field-Measuring Sensors, and
• Infrared Detectors.

For each sensor category, the handbook provides an introduction discussing historical information, the principles of operation, the factors affecting (and limiting) performance, the nature of the data output and the system required to process the data, and the trends in research and development. The introductions also list references and prominent contributors to the technology.

The information on specific sensor systems is organized in data-sheet format. A data sheet comprises 13 "cells":

1. Sensor Name and Acronym: Identifies the sensor by its most commonly used title and by its acronym, if applicable;
2. Discipline: Relates the sensor to a primary field of application;
3. Subdiscipline: Relates the sensor to secondary disciplines;
4. Application and Objective: Describes how the sensor is used and its intended purpose;
5. Heritage/Key Personnel: Identifies the sensor predecessors and its representatives or sponsors;
6. Sensor Deployment: Describes the spacecraft on which the sensor is mounted;
7. Sensor Characteristics: Describes capabilities and constraints, active source characteristics, and detector measurement characteristics;

8. Data-Measurement and Transmission System: Provides a block diagram of inputs and outputs and of units between the detector and the downlink antenna (bandwidths and data rates are specified);
9. Measurement and transmission System — Narrative: Elaborates on the block diagram, furnishing the details of storage and pre-processing equipment, for example;
10. Sensor Data Reception and Processing: Shows a block diagram of the ground-based data processing;
11. Receiving and Processing — Narrative: Describes the block diagram of item 10 in words, giving added detail;
12. Distribution of Data From Ground Stations: Shows a block diagram of the distribution routes and time to users; and
13. Data Distribution — Narrative: Describes the distribution block diagram in words.

For example, from the data sheet for the coastal-zone color scanner (CZCS), one can learn that this sensor is employed in Earth observations, particularly ocean monitoring. It is a passive-imaging, scanning, visible/infrared, spectroradiometer. It gathers data for mapping chlorophyll concentration, sediment distribution, salinity, and the temperature of coastal waters and the open ocean. Built for the Nimbus-G satellite, the CZCS is similar to the Nimbus-5 surface-composition mapping radiometer.

Additional cells on the CZCS data sheet furnish a wealth of technical information on the operational characteristics of the sensor, the spectral characteristics of its silicon photo-diodes and mercury cadmium telluride photoconductor, and on its data-distribution network.

This work was done by R. R. DeWitt and James L. Ellison of New Technology, Inc., for **Marshall Space Flight Center.** *Further information may be found in NASA CR-150837 [N79-14499/NSP], "Remote Sensing Data Handbook [$14.50]. A copy may be purchased [prepayment required] from the National Technical Information Service, Springfield, Virginia 22151.*
MFS-25169

Computer Programs

Solar Insolation Model

Computes solar energy available to a surface of arbitrary orientation

Because of their economic advantages, fixed flat-plate solar collectors may become the solar-energy systems most widely used with residences and many other buildings. The designer of a fixed collector can increase its efficiency by choosing the best orientation for local conditions. A new computer program, SOLINS, helps engineers with this relatively complex task by modeling the average hourly solar insolation on a fixed but arbitrarily oriented surface.

The program considers the problems of array spacing, shadowing, and the use of augmentation reflectors to increase insolation at the collector surface.

SOLINS uses a modified version of the National Bureau of Standards model to calculate the direct, diffuse, and reflected components of total insolation on a tilted surface with a given azimuthal orientation. The model is based on the work of Liu and Jordan with corrections by Kusuda and Ishii to account for early-morning and late-afternoon absorption variations. A parametric description of the average-day solar climate is used to generate monthly average-day profiles, by the hour, of the insolation level on the collector surface.

The user can specify the ground and landscape reflectivities at the collector site. For roof- or ground-mounted tilted arrays, SOLINS will calculate insolation values that include the effects of shadowing and augmentation reflectors. One supplies the program with data on the array design and orientation, the month, the solar climate parameters, the ground reflectance, and printout control specifications. For a specified array and environmental conditions, SOLINS outputs the hourly insolation the array will receive on a typical day during the month specified, along with the total insolation the collector surface will receive over a typical 24-hour period.

This program is written in FORTRAN IV for batch execution and has been implemented on an IBM 370 computer with a central memory requirement of approximately 170K of 8-bit words using a FORTRAN G compiler option (IBM).

This program was written by Jeff H. Smith of Caltech for **NASA's Jet Propulsion Laboratory.** *For further information, Circle A on the COSMIC Request Card.*
NPO-14787

General Optics Evaluation Program

Ray tracing for optical component and system analysis

GENOPTICS is a generalized aid for the analysis and evaluation of optical systems that employ lenses, mirrors, diffraction gratings, and other geometrical surfaces. It can exactly trace up to 800 rays through as many as 40 surfaces. The surfaces may be planar, conic, toric, or polynomial shaped lenses, mirrors, or diffraction gratings and may not be rotationally symmetrical. The surfaces may also be tilted and off center. Paraxial ray tracing of two rays through as many as 39 surfaces is possible; the results can be used to compute third-order aberration coefficients including aspheric contributions.

Numerous output options are available, including image spot, radial energy distribution, and geometric modulation transfer function plots. An automatic focus option can be selected. GENOPTICS should be useful in the analysis of a large family of optical systems, including afocal systems.

The basic calculations use conventional ray-tracing methods. The ray is traced in a vector form with surfaces expressed in Cartesian coordinates. Special consideration has been taken in simplifying input requirements. The transformation matrix of a tilted and decentered surface is computed automatically when one specifies the surface geometry and the desired dislocation. Diffraction surfaces are treated by means of a vectorial diffraction equation. Rectangular and circular apertures may be specified.

Following the ray tracing, a number of image analysis functions are available. Where conventional ray tracing is not applicable, such as Fabry optics and radiative transfer studies, a skew ray-tracing option employs an equiangular lattice method, which has proved useful in many circumstances.

This program is written in FORTRAN IV and IBM OS Assembler for batch execution on the IBM 360 with a central memory requirement of approximately 185K of 8-bit bytes. For plotted output a CALCOMP plotting system is required.

This program was written by Barton J. Howell of **Goddard Space Flight Center.** *For further information, Circle B on the COSMIC Request Card.*
GSC-12439

Thermodynamic and Transport Properties of Fluids

A numerical interpolation procedure

FLUID, a computer program subroutine, calculates the thermodynamic and transport properties of pure fluids in liquid, gas, or two-phase (liquid/gas) conditions. The program determines the thermodynamic state from assigned values for temperature and density, pressure and density, temperature and pressure, pressure and entropy, or pressure and enthalpy. The Van der Waals equation of state is used to obtain approximate state values. These values are then corrected for real-gas effects by model

correction factors obtained from tables based on experimental data. Since the service tables for saturation conditions, specific heat, enthropy, and enthalpy are external to the FLUID subroutine itself, FLUID can calculate the thermodynamic and transport properties of any fluid for which a set of tables has been generated. FLUID was developed as a cost-saving measure and is much faster than older, more complex programs such as the heavily-used GASP and WASP programs.

The tables used support accurate compensation for the special circumstances that arise whenever phase conditions occur. Viscosity and thermal conductivity values are computed directly from the tables. Interpolation within tables is based on Lagrange's three-point formula. FLUID currently contains tables for nine fluids, including dry air and steam. The FLUID routine is structured so that it may easily be incorporated into engineering programs.

This package is written in FORTRAN IV, SFTRAN, and has been implemented on an IBM 360 with a central memory requirement of approximately 222K of 8-bit bytes. It was developed in 1977.

This program was written by Theodore E. Fessler of **Lewis Research Center.** *For further information, Circle C on the COSMIC Request Card.*
LEW-13127

Materials

Hardware, Techniques, and Processes

Books and Reports

Computer Programs

Flame-Resistant Textiles

Continuous process treats fabric by the
surface photoaddition of fluorocarbons.

Lyndon B. Johnson Space Center, Houston, Texas

A flame-resistance treatment for
polyamide fibers, previously tested on
small laboratory samples [see "Flame
and Acid Resistant Polyamide Fibers"
(MSC-16074) on page 353 of *NASA
Tech Briefs*, Vol. 2, No. 3], has been
scaled up to treat 10 yards (9.1 m) of
commercial-width [41-in. (1.04-m)]
fabric. The process involves the
photoaddition of fluorocarbons to the
surface of the fibers. Already tested
successfully on one aromatic polyam-
ide [poly(m-phenyleneisophthalam-
ide)], the process appears applicable
to other low-cost textiles (e.g., poly-
esters and polyamides).

Many organic fibrous products that
have a highly aromatic backbone self-
extinguish in air, even without the
surface modification. However, these
materials burn in oxygen-enriched
atmospheres. The fluorocarbon grafts
make the fibers flame-resistant in
atmospheres with high-oxygen content
[e.g., 27 to 31 percent oxygen at 10
psia (68.9×10^3 N/m^2)]. Moreover, the
color and physical properties of the
treated fibers are not sacrificed, and
they remain nonirritant and nonal-
lergenic.

The fabric processor, shown in the
figure, is a modification of the earlier
design for sample areas on the order
of a few square inches. As before, the
fabric is exposed to a gaseous mixture
of halo-olefins and a dilutant gas such
as nitrogen in a vacuum-sealed
chamber. (A typical composition is 1
percent tetrafluoroethylene, 4 percent
bromotrifluoroethylene, and 95 per-
cent nitrogen.) An ultraviolet source
irradiates the fabric during the process
to generate acceptor sites for the
fluorocarbon compound.

In the modified processor the fabric
unrolls from a feed roller, loops
around the outside of a quartz tube
surrounding the ultraviolet lamp, and
is taken up on another roller. To treat
large fabric samples in a reasonable
time, the original 50-watt ultraviolet
lamp was replaced by a 9,750-watt
lamp. A cooling jacket and high-
temperature vacuum seal were added
to keep the processor temperature in
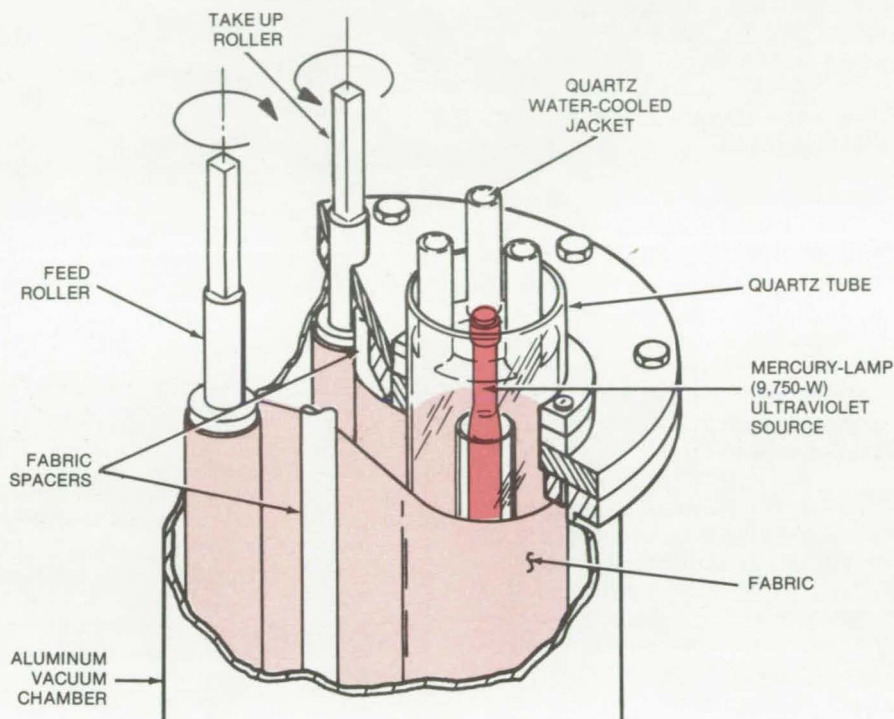
This **Fabric Processor** treats large samples of textiles by the surface photoaddition
of fluorocarbons. The vacuum chamber contains a mixture of halo-olefins and a
dilutant gas. Since the fabric is not in direct contact with the left side of the quartz
tube, the inner surface of the tube on that side is painted with a porcelain
compound. The compound prevents the ultraviolet from causing some cyclization
and polymerization of the monomers in the processor.

the range from 150° to 200° C.
(Higher or lower temperatures could
be used for other fabrics.) Processing
time for the 10-yard length of 41-in.-
wide fabric is 3 to 4 hours.

Water and aqueous solutions of
iodine, copper sulfate, and other com-
pounds were found to be adequate
coolants; however, they also decrease
the efficiency of the process by
absorbing some of the ultraviolet
radiation. A better coolant is trichloro-
trifluoroethane (TF). It is transparent
to ultraviolet, low in toxicity, and
readily available commercially (since
it is widely used as a cleaning agent).
It would significantly increase the
efficiency of the process in creating
fabrics that do not burn in high-oxygen
atmospheres. To convert to TF, the
cooling system would be modified to

prevent the buildup of contaminants
dislodged by the solvent capability of
TF.

Four-Step Reaction for Polytriazine Elastomers

A more precisely controlled reaction enhances
the quality and reproducibility of the final product.

Ames Research Center, Moffett Field, California

Cross-linked polyperfluoroalkyltriazines that are elastic at room temperature are made by an improved imidoylamidine reaction. The new reaction sequence expands the former one-step polymerization to four steps, allowing greater control of the molecular weight and the extent of cross-linking in the final product. The resulting polymers have superior elastomeric properties, lower glass-transition temperature, improved hydrolytic stability, and a broader temperature range. They can find uses in fuel-tank sealants, O-rings, wire enamels, pneumatic ducts, and many other applications.

The improved process (see figure) involves: (1) the reaction of ammonia with a perfluorodinitrile, (2) cyclization of the poly(imidoylamidine) with an acyl anhydride or an acyl halide, (3) a chain-lengthening reaction between the nitrile-group-terminated polytriazine molecules and ammonia, and finally, (4) heat-treating the product to cyclize the newly formed imidoylamidine linkages and to cross-link the polymer.

The previous one-step polymerization reactions of imidoylamidine and of preformed triazine derivatives gave products with molecular weights too low for good physical properties. The products were also very sensitive to the reaction conditions and therefore were not easily reproducible.

In the four-step reaction sequence, R_f represents identical bivalent perfluorinated organic radicals or a combination of radicals having structures that fall within a specified set of parameters. The linear polytriazines obtained from reaction 2 should have molecular weights ranging from 15,000 to 30,000, when the ring-closing agent is a derivative of trifluoroacetic acid. This range is considered optimal for forming an elastomeric network, following cross-linking in step 4.

This work was done by Robert W.
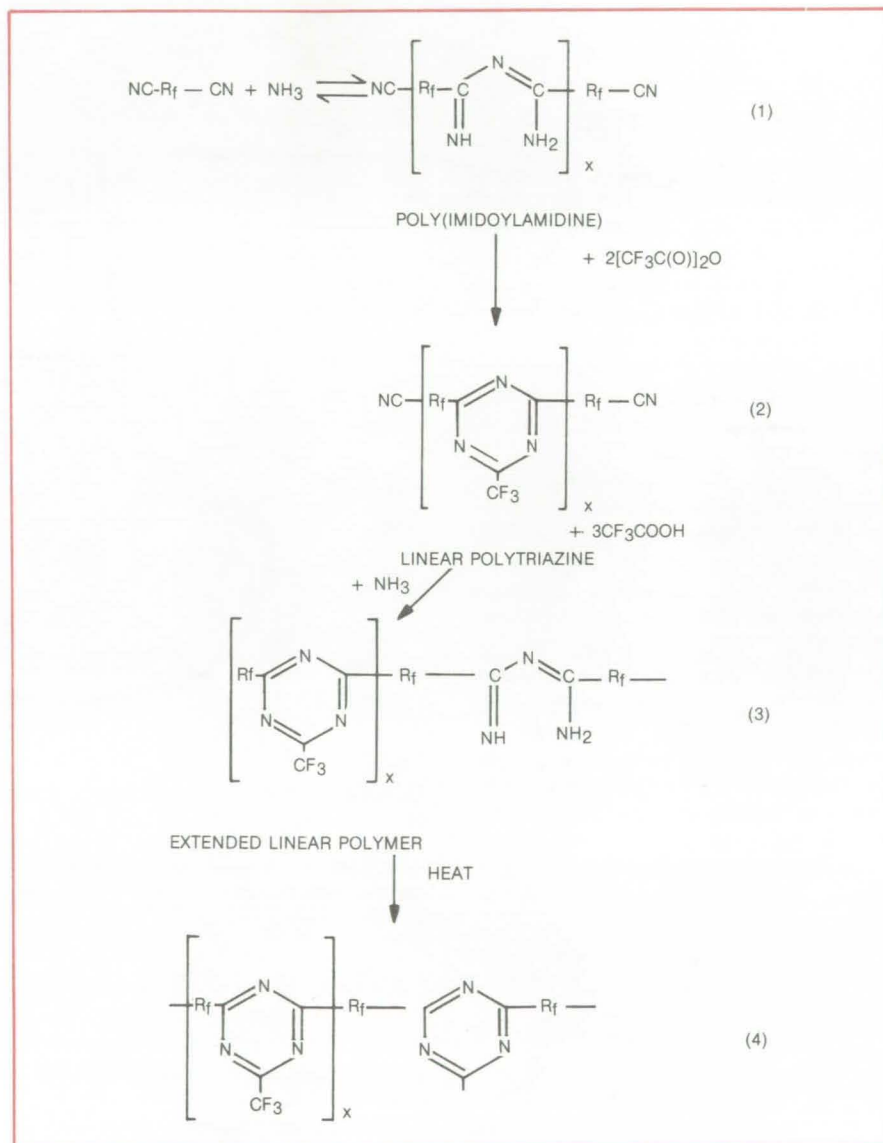
This **Four-Step Procedure** produces cross-linked elastomeric polytriazines with excellent physical and chemical properties. Other cyclizing agents, such as the acyl fluorides and acyl chlorides of perfluorinated lower aliphatic acids, can replace the trifluoroacetic acid in reaction 2.

*Rosser of **Ames Research Center** and Roger A. Korus of San Jose State University. For further information, Circle 42 on the TSP Request Card.*

This invention is owned by NASA, and a patent application has been filed. Inquiries concerning nonexclusive or exclusive license for its commercial development should be addressed to the Patent Counsel, Ames Research Center [see page A5] Refer to ARC-11248.

Heat- and Chemical-Resistant Oxadiazole Elastomers

Cross-linked 1,2,4-oxadiazole polymers
are prepared by thermal condensation.

Ames Research Center, Moffett Field, California

New heat- and chemical-resistant polymers with triazine cross links (see illustration) are prepared by heat-induced condensation reactions to form 1,2,4-oxadiazole linkages. The polymers are prepared from monomers containing amidoxime and nitrile or amidine groups. They can be compounded with a variety of fillers, extenders, and modifiers for numerous applications in which stability, impermeability to liquids and gases, and good plasticity and elasticity, or rigidity, are important. By selecting the monomer mix and altering polymerization conditions, the product polymers may be made into adhesives, caulking compounds, chemical sealants, fuel-tank liners, and the like.

In general, the monomer condensation reactions form linear oxadiazole linkages and tridimensional triazine linkages when carried out at temperatures of up to 200° C. The heating time depends on the amount of cure desired. Higher molecular weights are obtained by using longer cure times at elevated temperatures (see table). For example an elastomer having an average molecular weight of 35,000 is formed by curing at 150° C for 3-1/2 days. The process is completed during the 200° C postcure heating period.

The polymer properties will vary according to the type and proportion of monomer end groups present. For example, when an amidoxime/ amidine monomer is used, the resulting polymer has a theoretically equal

Temperature (°C)	Time (Days)	Molecular Weight
80 to 130	3	~ 3,000 (3,000 to 10,000)
150	1 to 1.75	10,000 to 35,000
150	3.5	~ 35,000+

The **Temperature and Time** determine the molecular weight of produced polymers.
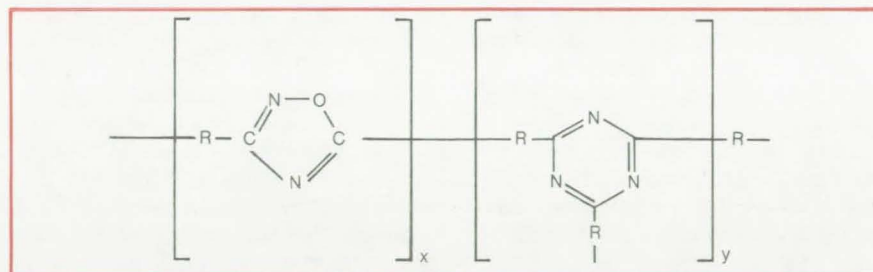
Cross-Linked 1,2,4-Oxadiazole Elastomers have been prepared with the formulas above, where x and y and the order of the oxadiazole and triazine linkages are randomly determined and are functions of the nature and the proportions of monomers present in the reaction mixture. The usable monomers are represented by $H_2N(HON)$-R-Q in which: (1) R is a bivalent, or a mixture of bivalent organic radicals, comprising $-(CX_2)_p$-, or $-CFY(OCF_2CFY)_mO(CX_2)_pO(CFYCF_2O)_nCFY$-, where X may be fluorine or hydrogen, Y may be fluorine or trifluoromethyl, p ranges from 1 to 18, and m + n ranges from 2 to about 7; and (2) Q is an amidoxime, nitrile, or amidine group.

number of oxadiazole rings and cross-linking triazine rings. By adding an amount of diamidoxime monomer, the proportion of oxadiazole linkages increases. In general when elasticity is desired, the ratio of oxadiazole ring-forming groups to the triazine ring-forming groups should be 9 or 10 to 1. A higher proportion of triazine linkages increases the polymer rigidity.

This work was done by Robert W. Rosser of Ames Research Center

and Hanoi Kwong and Ibrahim M. Shalhoub of San Jose State Foundation. For further information, Circle 43 on the TSP Request Card.

Synthesis of 2,4,8,10-Tetroxaspiro [5.5] Undecane

An improved process increases yield
and reduces preparation time.

Ames Research Center, Moffett Field, California

An improved method drastically reduces the preparation time of pentaerythritol diformal (2,4,8,10-tetroxaspiro [5.5] undecane). Pen-

taerythritol diformal is typically prepared under acidic conditions from pentaerythritol and aqueous formaldehyde, trioxane, or paraformaldehyde.

Reaction times, however, are several hours or days, and isolating the product is time consuming.

The new process has several advantages, including shortened reaction times in the order of 3 to 20 minutes, yields greater than 90 percent, the elimination of solvents, decrease in labor and energy needs, adaptability to continuous operations, and overall simplicity and convenience. The product is conventionally used as an intermediate in the synthesis of certain ethylenically unsaturated monomers, aphrogenic and pyrostatic phosphorylated derivatives, and other useful compounds.

In the improved process, a stirred mixture of pentaerythritol is heated with a slight excess of paraformaldehyde. This is done at a temperature of up to about 120° C in the presence of a catalytic quantity of acid and in the absence of any solvent except for a small quantity of water.

During heating, the mixture turns into a paste, progressively becoming more fluid as the temperature rises and finally turning into a clear liquid at about 110° C. Between about 105° and 115° C, the liquid boils as the water of reaction escapes; then it soon becomes quiescent.

The clear odorless liquid crystallizes into a solid mass of crystals on cooling. The product supercools rapidly, giving off appreciable heat during solidification. It also melts within the range of 35° to 48° C — in the lower end of the range if some monoformal is present, and in the upper range if the reaction has been properly carried out to minimize formation of the monoformal. Recrystallization from petroleum ether or distillation yields the pure compound, which melts at 50° C.

The reaction is best carried out in two steps. First, the reagents are heated to a maximum temperature of about 120° C for about 5 minutes to give the monoformal. After cooling to about 70° C and adding the second molar equivalent of paraformaldehyde, with about 1 percent excess, the mixture is heated again to about 120° C for about 5 minutes to convert the monoformal to the diformal. In this manner, the total heating time is still about 10 minutes, but formaldehyde losses are minimized and conversion is improved, with yields in excess of 90 percent in either case.

Catalytic quantities of acid, that is, about 0.1 to 1.0 mole percent, must be present. Examples of usable acids include hydrochloric, sulfuric, toluenesulfonic, and methanesulfonic acids, as well as boron trifluoride etherate and aluminum chloride. If anhydrous acids are used, a small quantity of water, about 1 percent of the total weight of the reactants, is beneficial in that the reagents convert into an easily stirrable fluid much faster. Heat transfer is thus greatly improved. Aside from this convenience, water is not essential for good yield of product.

*This work was done by Algirdas C. Poshkus of the National Research Council for **Ames Research Center**. For further information, Circle 44 on the TSP Request Card.*

This invention is owned by NASA, and a patent application has been filed. Inquiries concerning nonexclusive or exclusive license for its commercial development should be addressed to the Patent Counsel, Ames Research Center [see page A5]. Refer to ARC-11243.

Relating Viscosity to Polymer Concentration

An equation explicitly relates viscosity of polymer-solvent system with polymer concentration.

NASA's Jet Propulsion Laboratory, Pasadena, California

An equation developed by Van Dijk and first applied to the viscosity of Newtonian suspensions of rigid particles by Eilers is used to describe the intrinsic viscosity of dilute to moderately-concentrated polymer-solvent systems. The equation is rearranged to yield the intrinsic viscosity as an explicit function of polymer concentration. Experiments have shown this relationship valid for polymer solutions having relative viscosities ranging from 1 to 100.

Relative viscosity η_r of a Newtonian suspension is expressed by

$$\eta_r = \left(1 + \frac{1.25\varphi}{1 - \varphi/\varphi_m} \right)^2 \qquad (1)$$

where φ is the volume fraction of suspended particles and φ_m is the

maximum volume fraction to which the particles can pack. For large rigid suspended particles, the value of φ_m can be independently estimated from sedimentation experiments.

If φ is assumed to be proportional to the polymer concentration, then it may be expressed as $\varphi = kc$ where k is the constant of proportionality and c is the polymer concentration (the hydrodynamic spheres considered to be rigid). By substituting this expression into equation 1, the relative viscosity η_r can be given by

$$\eta_r = \left[1 + \frac{1.25kc}{1 - c/c_m} \right]^2 \qquad (2)$$

where c_m is a polymer concentration parameter that corresponds to φ_m.

For small c, equation 2 reduces to $\eta_r = 1 + 2.5kc$ and hence $2.5k = [\eta]$, the intrinsic viscosity. This result substituted into equation 2 becomes

$$\eta_r = \left[1 + \frac{[\eta]c}{2(1 - c/c_m)} \right]^2 \qquad (3)$$

which includes the key parameters $[\eta]$ and c_m.

For the purposes of testing, the expression is rearranged to form:

$$\frac{1}{2(\eta_r^{1/2} - 1)} = \frac{1}{[\eta]c} - \frac{1}{[\eta]c_m} \qquad (4)$$

A plot of the quantity on the left as a function of $1/c$ results in a linear response with slope equal to $1/[\eta]$ and intercept $-1/[\eta]c_m$.

The last equation can be rearranged to yield intrinsic viscosity explicitly:

$$[\eta] = 2(\eta_r^{1/2} - 1)(1/c - 1/c_m) \quad (5)$$

Once the value c_m is established for a given polymer/solvent system, $[\eta]$ can be calculated from a determination of η_r at a single polymer concentration c.

A plot applying existing data to equation 4 is shown in the figure. As expected, the response is linear. Equation 4 is very sensitive to the values of η_r in the dilute range; i.e., for values c less than about 1 gram per deciliter, because the quantity $1/2(\eta_r^{1/2} - 1)$ approaches infinity as c goes to zero. The general treatment in this case is to omit the data in the very dilute range and to fit the remaining data, using a least-squares fitting technique.

This work was done by Robert F. Fedors of Caltech for **NASA's Jet Propulsion Laboratory.** *For further information, Circle 45 on the TSP Request Card.*
NPO-14609
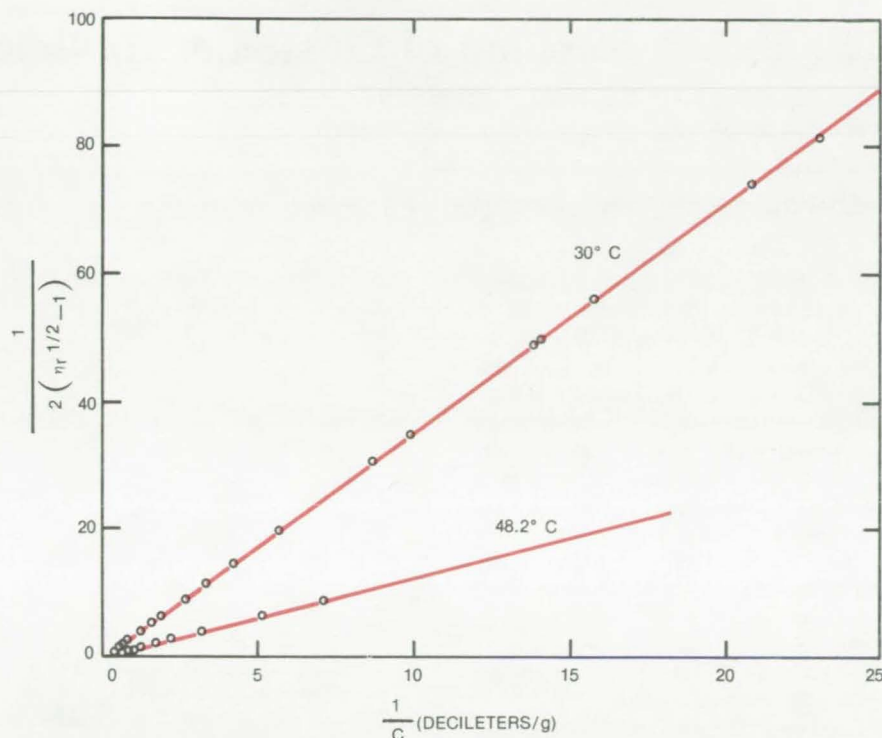
Polymer Viscosity-Concentration Data of polystyrene are shown for a fraction of molecular weight 1.46×10^5 g/mole in toluene at 30° C and at 48.2° C. The straight-line curve shows that the expression correlates with published experimental results shown as points.

Simple Estimate of Critical Volume

A new method that requires summation of no more than 18 incremental contributions gives 3 percent accuracy.

NASA's Jet Propulsion Laboratory, Pasadena, California

A new method for estimating the critical molar volume of a material is faster and simpler than previous procedures. The new method is based on the formula

$$V_c = 26.608 + \sum_i v_i$$

where V_c represents the critical volume and v_i represents the contributions from components of the chemical structure of the material. Previous methods employed formulas that required summing more than 40 contributions. [See "Determining Critical Temperatures and Volumes" (NPO-13405) on page 81 of *NASA Tech Briefs*, Vol. 2, No. 1.] The new formula sums no more than 18 different v_i contributions. It is just as accurate (within 3 percent) as the older methods.

The critical molar volume of a material at its critical pressure and temperature (where the gas and liquid phases have the same density) is important in chemical engineering and thermodynamics. However, it is a difficult quantity to measure, and experimental data on critical volume are available for only a few substances. Thus, the new method for accurately estimating V_c should expedite many thermodynamic design calculations.

A value of v_i is selected for each element in the molecule. Alternative values are used for oxygen and nitrogen when they occur in alcohols or amines. Similarly, values of v_i are selected from a table for structural features of the molecule; these v_i range from negative values for ring structures to sizable positive values for rings attached to other rings. All the v_i are summed algebraically and added to 26.608, as indicated by the formula, yielding the critical volume in cubic centimeters of 1 mole of the material.

This work was done by Robert F. Fedors of Caltech for **NASA's Jet Propulsion Laboratory.** *For further information, Circle 46 on the TSP Request Card.*
NPO-14464

Equilibrium Swelling of Elastomers in Solvents

Two equations relate elastomer swelling
with the type and concentration of filler.

NASA's Jet Propulsion Laboratory, Pasadena, California

Two empirical equations are proposed to characterize the relative modulus of filled elastomers as a function of filler content. The equations are directly developed from the original Eilers-VanDijk equation, which relates the viscosity of Newtonian suspensions with the volume fraction of particles. One equation describes equilibrium swelling for cases in which the fillers are composed of permanent aggregates of primary particles such as reinforcing carbon black. The other equation relates equilibrium swelling when the filler material is composed of non-aggregated particles such as large-size thermal blacks.

For fillers composed of permanent aggregates of primary particles, the equation describing equilibrium swelling data is given by

$$\nu_{e,rel} = \left(1 + \frac{1.25\,\varnothing}{\varnothing_{max} - \varnothing} \right)^2 \qquad (1)$$

where $\nu_{e,rel}$ is the relative network-chain concentration defined as the ratio of ν_e of the filled to that of the unfilled elastomer, $\varnothing_{max}$ is the maximum volume fraction to which the particles can pack, and $\varnothing$ is the volume fraction of the filler particles.

Figure 1 shows the data from various published experiments for both SBR (styrene-butadiene rubber) and natural rubber containing high-structure blacks, obtained in a variety of solvents and using a variety of curing systems. The curve has been derived from equation (1) and $\varnothing_{max}$ is assigned a value of 0.63 that corresponds to random packing of large spheres. As can be seen, the curve
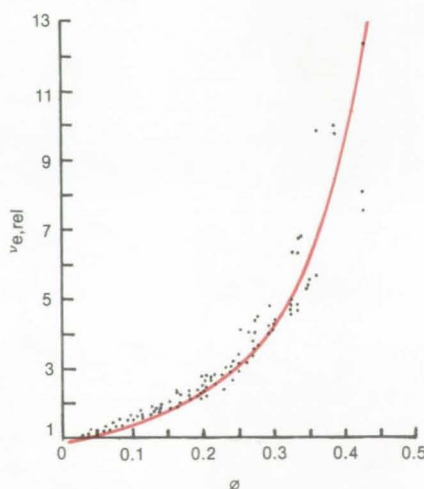
Figure 1. **Swelling of Rubber-Containing Permanent Aggregates** of primary particles, such as carbon black, as predicted by equation (1) is shown as the curve. Experimental data are denoted by the points.

Figure 2. **Swelling of Rubber-Containing Nonaggregated** filler particles, as predicted by equation (2) is shown by the curve. Experimental data are denoted by the points.

closely approximates the experimental data. The deviation at higher concentrations reflects the difficulties in mixing large concentrations of active carbon black in unsaturated rubbers.

When the filler is composed of nonaggregated particles such as the large-size thermal blacks, the relationship between the relative network-chain concentration and the volume fraction of filler becomes

$$\nu_{e,rel} = \left(1 + \frac{1.25\,\varnothing}{1 - \varnothing/\varnothing_{max}} \right)^2 \qquad (2)$$

Figure 2 shows the behavior of the relatively-nonreinforcing medium-thermal (MT) and fine-thermal (FT) carbon blacks and Graphon contained in both SBR and natural rubber vulcanizates.

The value of $\varnothing_{max} = 0.80$ required to fit the curve to the data is higher than expected for the random packing of spheres. However, if dewetting occurs, the true value of $\varnothing_{max}$ will be lower than the apparent value.

Double-Wall Tubing for Oil Recovery

Insulated tubing proposed as way of increasing the recovery of heavy oil from steam-injection oil wells.

NASA's Jet Propulsion Laboratory, Pasadena, California
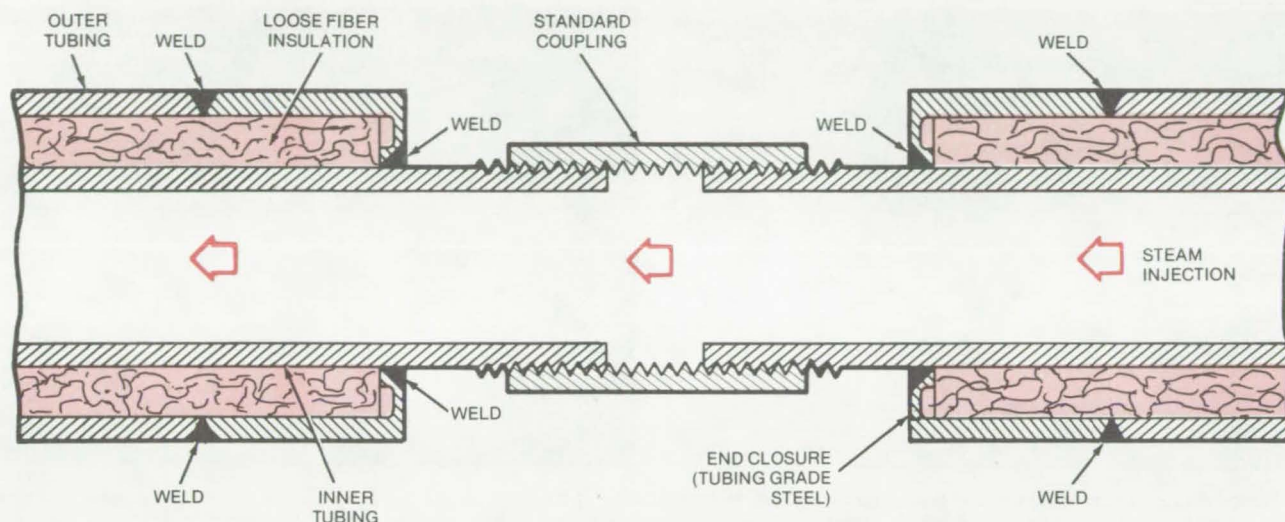
Figure 1. **Insulated Tubing** prevents heat losses in steam-injection process used for the recovery of heavy oil. The new tubing makes the process more economical and extends the recovery of oil from deeper wells that could no longer be exploited.

Insulated double-wall tubing designed for steam-injection oil recovery could reduce heat losses to the surrounding rock. Higher-quality wet steam could also be delivered to deeper wells, increasing heavy oil production. Steam-injection oil wells are presently limited by economics to depths of from 1,500 to 2,500 ft (450 to 750 m). With this process improvement, it might be possible to recover additional oil from known but previously-unworkable reservoirs.

Key features of the design are: (1) The insulation is sealed to prevent wetting by well-bore fluids, which would severely degrade its performance; and (2) standard couplings and standard techniques for running the tubing are used.

The proposed double-wall tubing incorporates loop or matted glass, or ceramic fibers, packed and sealed between the walls (see Figure 1). The outer pipe is cut a few inches shorter than the standard length of a 20- or 30-ft (6- or 9-m) inner tube, leaving both threaded ends of the inner tube exposed to coupling.

A low-conductivity, high-strength, stainless-steel end closure welded at each end of the pipe seals the insulation from well fluids. The closure cap
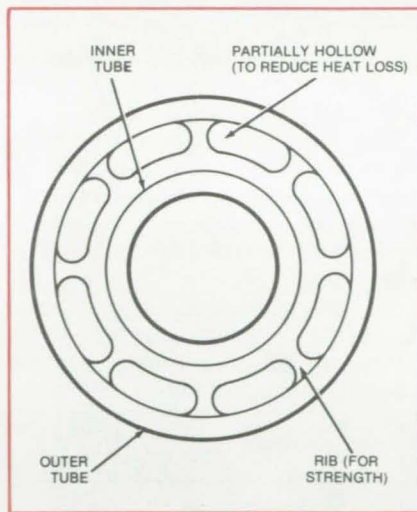
Figure 2. The **Steel End Closure** holds the insulation in place on both ends of the tube. Its rib-and-hollow cap minimizes heat losses in the coupling area.

(see Figure 2) is a rib and partially hollow structure designed to reduce heat leakage through the steel. At the same time it provides strength, pressure tightness, and corrosion resistance. The entire closure is welded to the circumferences of the inner and outer tubes and extends several

inches longitudinally along the pipe for maximizing insulating effectiveness. A prestress would be applied between the two tubes to reduce thermal stress.

The new tubing would be fabricated in standard 20- or 30-ft (6- or 9-m) sections and delivered to an oil well ready for installation. The tube sections are joined by standard threaded couplings tightened onto the inner tubes of adjacent sections. Short split halves of external insulation may be strapped onto the couplings to further reduce the heat losses.

The tube structure has another advantage. Because of the insulation, the thermal stresses in the cement casing surrounding the outer pipe are reduced, improving the casing life and correspondingly reducing maintenance.

[Also see related article "Water-Cooled Insulated Steam-Injection Wells" (NPO-14605) on page 383 of this issue].

This work was done by Lloyd H. Back, William F. Carroll, Leonard D. Jaffee, and Leonard D. Stimpson of Caltech for **NASA's Jet Propulsion Laboratory.** *For further information, Circle 48 on the TSP Request Card.* NPO-14606

Post-Processing Flame-Retardant for Polyurethane

Cushions, pads, and packing materials can be protected
against fire without compromising the resiliency of the foam.

Lyndon B. Johnson Space Center, Houston, Texas
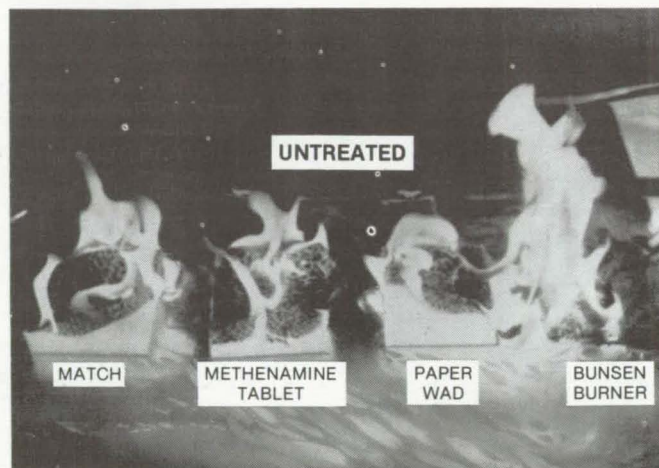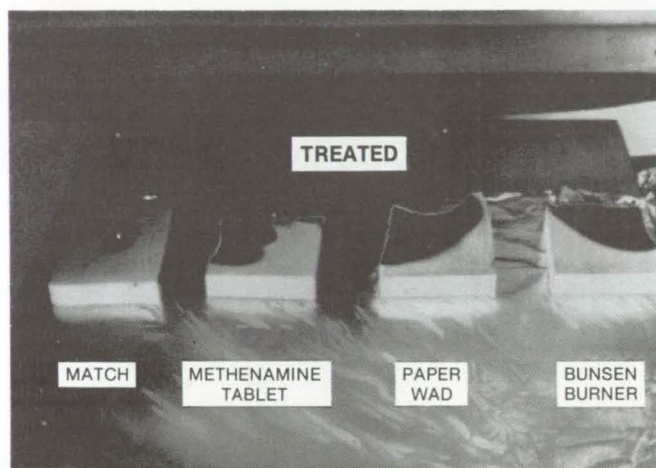
In a **Flame-Retardance Test,** treated polyurethane foam stopped burning as soon as the ignition source (a match, a methenamine tablet, or a bunsen burner) was consumed or extinguished. Untreated foam, on the other hand, continued to burn after removal of the ignition source.

Polyurethane foam can be made fire-resistant without altering its lightness, flexibility, and resilience by treating it with a new elastomer formulation after processing. In contrast to the conventional method of adding flame-retardant compounds to the polyurethane before it is foamed, the new method detracts little from the desirable physical properties of the finished product.

Because their cellular structure presents a large surface area to the oxygen in the atmosphere, polyurethane foams burn rapidly when they are ignited. With the new treatment, however, the foam develops a protective char that stops combustion, once the ignition source is removed (see figure). Moreover, the new treatment prevents molten particles from forming; such particles could drip from the foam and ignite adjacent materials. The new formulation does not deteriorate under prolonged exposure to Sunlight and generates no smoke or toxic gases in a fire.

The treatment can be used to protect furniture cushions, mattresses, and fabric backing, where it is particularly effective aginst small ignition sources such as cigarettes. The treatment is also highly effective in aircraft cushions, automobile crash pads, and protective packaging.

The flame-retardant formulation is composed of elastomeric binders, a thermally stable source of bromine, metal oxide catalyst/acid accepters, nitrogen-containing curing agents, phosphorus-containing fillers, and hydrated fillers, dispersed in an organic liquid such as acetone or hexane. A particularly effective version has the following composition:

Ingredient	Parts by Weight
Viton B	100
Lead Monoxide	15
Diak No. 1	1.5
Decabromobiphenyl Oxide	60
Antimony Oxide	30
Phoschek P-30	15

This formulation, dissolved in acetone, may be applied by either spray coating or saturation procedures to yield flame-retardant foam that generates minimum smoke when exposed to flame. After the liquid is evaporated off, a thin elastomeric coating remains on the surface. Alternatively, the foam can be saturated with the liquid dispersion, squeezed to remove excess liquid, and then dried. This latter procedure yields a foam that is uniformly treated throughout, not just on the surface.

Ozone Inhibits Corrosion in Cooling Towers

Ozone circulated in a cooling-tower
system inhibits scale and corrosion.

NASA's Jet Propulsion Laboratory, Pasadena, California

A commercially-available corona-discharge ozone generator fitted onto an industrial cooling tower significantly reduces the formation of scale (calcium carbonate) and corrosion. Ozone in the water is known to convert calcium carbonate to calcium bicarbonate, which is much more soluble. Also small quantities of acids, such as nitric-acid, form and subsequently act to remove scale already formed. The maintenance of scaled-clogged heat-exchanger tubes is reduced, and service life of the entire system is improved. Moreover, ozone is produced inexpensively in relatively non-toxic quantities. Because it is a well-known biocide/disinfectant, no additional compounds need be introduced as biocides or for algae control.

The system (see figure) consists of an ozone-generating and injection section, the cooling tower, and a heat exchanger. Water is cooled by a fan blowing air through water falling through grids and slats into a 678-gal (2,566-l) basin.

The water is ozonated by recirculating part of it from the basin through an ozone injection pump and discharging it back into the basin. Alternatively, ozone may be injected into the low-pressure end of the water-recirculation main pump.

Ozone may be generated either from air or oxygen. Normally, air is fed through a column containing silica gel desiccant, or a refrigeration system, to reduce humidity and thus enhance ozone production. The dried air then enters the corona-discharge ozone generator that, in turn, feeds the ozone to either one of the selected
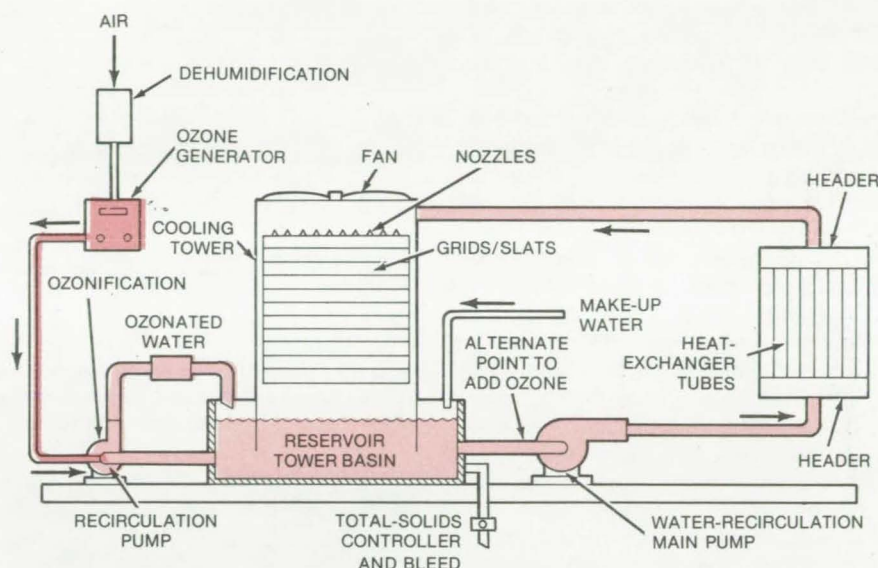
Cooling-Tower Water is ozonated by turbulence inside the recirculating pump, mixing water from the basin with ozone produced by the ozone generator. The ozonated water circulated through the entire system by the water-recirculation main pump inhibits corrosion, removes scale, and kills algae and bacteria. The process extends the life and reduces maintenance of the cooling-tower system.

pumps. Ozone is mixed with water by turbulence within the pump, and the treated water is pumped back into the system.

As the ozone and water are mixing, organic impurities are rapidly oxidized. Most of the micro-organisms are killed by the time the ozonated water reaches the basin. The remainder of the dissolved ozone remains in the basin and travels through the cooling circuit where it passivates metal surfaces, attacks slime or other bacterial deposits, and prevents and removes scale.

Measuring Coal Thickness

A noncontacting sensor promises fast and accurate
determination of overhead layer depth.

Marshall Space Flight Center, Alabama

A laboratory-tested concept for measuring the thickness of overhead coal may allow mining machines to remove virtually all the coal from mine roofs without the danger of cutting into the overlying rock. The concept proposes a jet of water to cut a hole in the overhead coal and an inexpensive optical device akin to the rangefinder in an automatic-focus camera to measure the depth of the hole.

The water jet is forced through a rotating nozzle (Figure 1) so that it cuts a circular groove as it impinges on the coal. The cylinder of coal then drops out under the pull of gravity (Figure 2). Only coal separates in this fashion; a cylinder of rock cut by the jet does not fall away from its surrounding rock. When the optical depth meter "looks" into the hole cut by the jet, it sees a reflecting surface of rock at the coal/rock interface and measures only the depth cut into the coal.

In laboratory tests of the method for cutting coal on sandstone, a 6,000-psi $(41 \times 10^6\text{-N/m}^2)$ jet of water, turning at about 750 rpm in a circle with a radius of 1 in. (2.54 cm), cut through more than 8 inches (20 cm) of coal to the sandstone in only 2 seconds. Only 1.3 quarts (1.2 liters) of water were needed to drill the hole.

For the laboratory experiments, an automatic optical rangefinder was removed from a commercial 35-mm camera and used as a depth meter. It was found that the electronic signal that controls the focal length of the camera gives a measure of the distance to the target. With the present apparatus, the measurement accuracy is about 1 in. (2.5 cm) at focal distances of greater than approximately 41 in. (103 cm); however, the system should give accuracies of better than 0.01 in. (0.025 cm) at closer ranges with suitable modifications to the electronics.

The coal cutter could be packaged in a relatively small volume. The
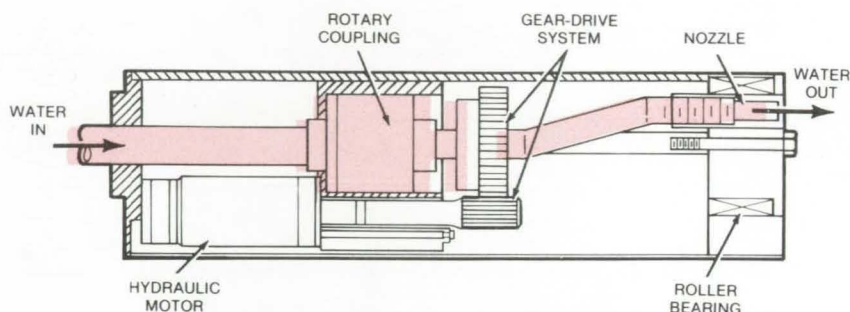
Figure 1. **Coal-Etching Water Jet** flows from a rotating nozzle. The high-pressure jet cuts a narrow circular slot 1 inch in radius. Water is supplied to the nozzle through a rotary coupling as the nozzle is turned, via gears, by a hydraulic motor.
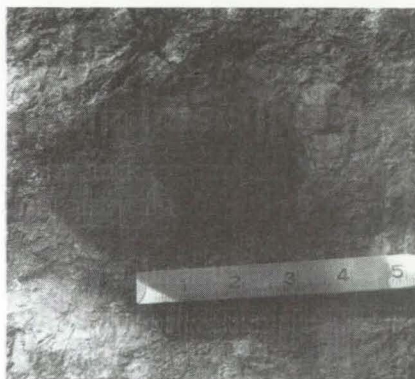
Figure 2. The **Water Jet Selectively Removes a Core of Coal,** leaving the overlying rock intact. The water penetrates planes in the coal core, weakening it enough that it drops away by gravity.

water-jet drill, for example, can be housed in an enclosure less than 7 inches (18 cm) in diameter and 1 foot (30 cm) long. The water jet can be pressurized from the mining-machine hydraulic system, which has power to spare. The optical depth meter can be housed in a 1- by 2- by 3-inch (2.5- by 5- by 5-cm) enclosure, just aft of the water-jet drill.

It is not necessary that the mining machine be halted while the hole is etched and the depth measurement is made. During the 2 to 3 seconds that it takes to etch a hole and measure its depth, the water-jet and depth-meter assembly can be moved automatically to compensate for the forward motion. Coal-thickness measurements can thus be made in 1-foot (0.3-meter) increments, if necessary.

Unlike the nucleonic sensors now used to measure coal thickness by backscattered gamma rays, the proposed instrument does not contact the coal surface, does not require calibration, and is unaffected by the density of the coal or the type of rock. The new instrument promises to be faster, measuring thickness in less than 3 seconds instead of the 10 seconds required by the nucleonic sensor. It is also potentially far more accurate, since it can determine coal thickness within 0.1 inch (2.5 millimeters) instead of 1 inch.

Precise Wet-Chemical Etching

A controlled amount of etchant applied to the surface of a rotating sample removes only a few angstroms of material.

NASA's Jet Propulsion Laboratory, Pasadena, California

Surface layers of crystals and other samples are removed with a precision of ±1 Å by a new wet-chemical-etching process. Thicknesses of the order of 10's of angstroms are etched away by mounting the sample on a rapidly spinning holder and dropping a measured amount of etchant on the rotating surface. Before it evaporates, the etchant removes a small amount of material without mechanically disturbing the sample or leaving a residue. The technique is suited to the study of chemical and crystal structures and is being used at NASA's Jet Propulsion Laboratory to expose depth profiles of Si/SiO_2 samples.

The etchant is dropped onto the rotating sample, as seen in the figure. (Each drop is allowed to evaporate before the next drop is dispensed.) The sample is maintained at a constant angular velocity of between 2,000 and 100,000 rpm by a dry-nitrogen-driven turbine. [The gas pressure is set between 12 and 95 psi (83×10^3 and 655×10^3 N/m^2).]

A chemical-resistant cup captures excess etchant thrown off the sample as it rotates. In the Si/SiO_2 studies, the cup is tetrafluoroethylene, the spinning head was made of polypropylene, and the etchant was an ethanol/hydrofluoric-acid solution. The acid converts SiO_2 to fluorides such as H_2SiF_6, and the fluorides dissolve in the ethanol.

Following dropwise addition of the appropriate amount of etchant, the sample is rinsed with ethanol and analyzed by X-ray photoelectron spectroscope. For calibration, the film thickness is independently measured by elliposometry.

When a droplet of liquid falls onto the center of the rotating sample, a film forms over its surface, and excess etchant is ejected against the cup walls. The thickness depends on the centrifugal force, the surface tension of the liquid, and the wettability of the surface.
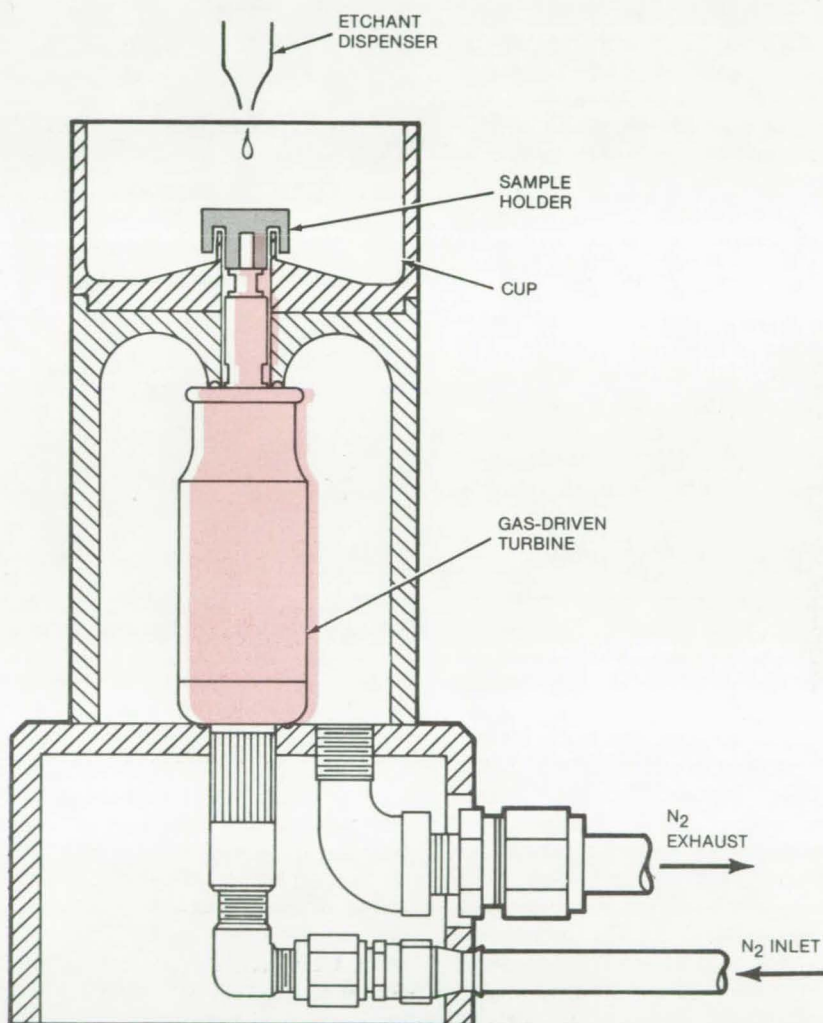
A **Dry-Nitrogen-Driven Turbine** rotates at from 2,000 to 100,000 rpm in this apparatus for precise wet-chemical etching. A controlled amount of etchant is dispensed on the sample and is evaporated to dryness.

In the SiO_2/HF system, a volatile reaction product can be formed (SiF_4), which is evaporated to a partially-fluoridated film residue. This residue can be partially solvated with additional ethanol.

The total residence time of the liquid film determines the removal rate. The rate can be varied through control of the spin frequency, liquid viscosity, droplet size, total etchant volume, and etchant concentration. After etching, the film is evaporated, and the substrate is rinsed with pure solvent to remove residual reaction products.

Detecting Oxygen in Hydrogen or Hydrogen in Oxygen

Catalytic sensor can operate in
high-pressure, moisture-laden gases.

Lyndon B. Johnson Space Center, Houston, Texas

A new sensor can detect small amounts of oxygen in hydrogen (or hydrogen in oxygen) at high pressures and is unaffected by moisture in the gases. It was developed for a life-support system in which water is decomposed by electrolysis to produce oxygen and hydrogen. The sensor detects potentially explosive amounts of one gaseous product in the other at 415 psia (2,860 kN/m^2). Previously available devices for sensing combustible gas mixtures are limited to much lower pressures and thus require that a small amount of high-pressure gas be bled off continuously for sampling. The new sensor, in contrast, can be positioned directly in the high-pressure gas stream.

Platinum black on the sheath of a temperature probe (see figure) serves as a catalyst for the recombination of hydrogen and oxygen. Thus trace amounts of oxygen in the hydrogen stream (and vice versa) combine at the platinum black, and the heat of reaction is detected by the platinum resistance-temperature probe inside the sheath. A porous film of polytetrafluoroethylene around the platinum black keeps out moisture but allows the gases to contact the catalyst. The film prevents water vapor in the gases from condensing on the probe and thus masking the small temperature rise created by hydrogen/oxygen recombination. The film allows the sensor to function in high-humidity gases and even with water forced into the sensor cavity.
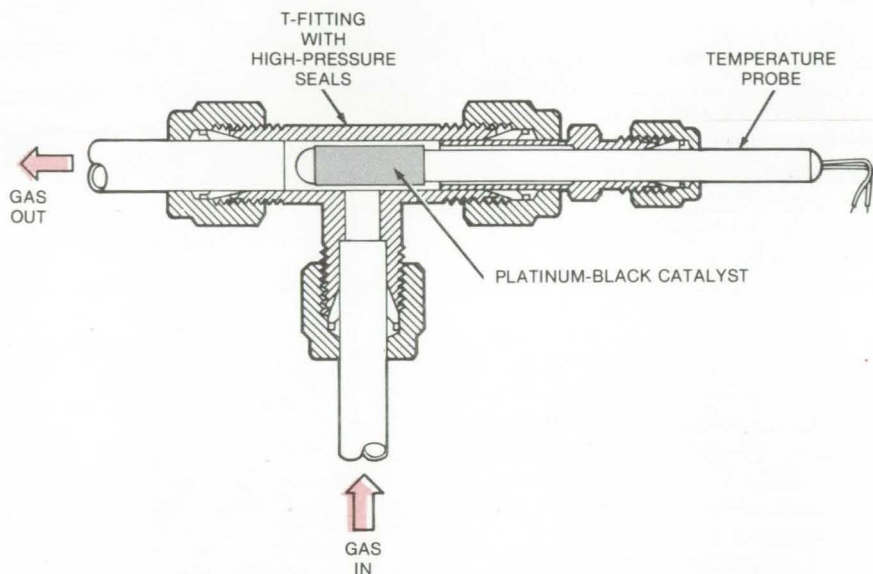
Gas Sensor can be inserted in a standard 3/8-inch (0.95-centimeter) tube in a flareless T-fitting. The gas mixture enters the vertical leg of the tee, impinges on the sensor, and exits through a horizontal leg of the fitting. The temperature probe detects the heat of recombination of hydrogen and oxygen at the platinum black catalyst; the probe resistance increases proportionally with the rise in temperature created by the recombination.

The catalyst structure is made from material that has been pressed under heat to a thickness of 0.005 inch (0.13 millimeter) and then cut to size. This foil is wrapped around the stainless-steel probe, 1/4 inch (0.64 centimeter) in diameter, 4 inches (10.2 centimeters) long, and is tack-welded in place.

The sensor has potential applications in gas-detection and measurement instruments, particularly for gases generated by electrolysis, because such gases may contain large amounts of moisture. It may also be useful in future hydrogen-energy systems.

This work was done by Albert C. Erickson of General Electric Co. for **Johnson Space Center.** *For further information, including parts list and operating data, Circle 52 on the TSP Request Card.*
MSC-18380

An Improved Capillary Rheometer

A device for measuring viscosity of heated
coal and other multiphase materials

NASA's Jet Propulsion Laboratory, Pasadena, California

An improved rheometer is used to measure the viscosity of coal samples heated to a molten, or plastic, state. Coal samples are heated rapidly in a cylinder and compressed by piston through a capillary opening. Force applied to the piston, measured by a separate instrument, is directly proportional to the sample viscosity. The device, primarily applied in designing efficient equipment for feeding coal into a combustion chamber, may be

readily used in other viscosity studies.

The rheometer (see figure) is made from molybdenum, known for its high heat-transfer properties and high-temperature strength. Coal samples ground and screened to less than 80 mesh and pressed at about 15,000 psi $(103.5 \times 10^6 \text{ N/m}^2)$ into capsules are introduced into the preheated cone-tipped cylinder.

A piston preheated by a band heater to the desired temperature is introduced into the cylinder, and the entire assembly is placed into the compression cage of an Instron, or an equivalent, testing machine. Force applied to the piston is recorded directly from the machine load cell. The temperatures are monitored at various test points by thermocouples connected to the cylinder and the capillary.

The tests may be run at conditions as high as 3,000 psig $(20.6 \times 10^6 \text{ N/m}^2)$ and 470° C. The coal-sample capsules are relatively thin and rapidly reach test temperatures because of the large area of exposure to the piston and cylinder walls.

Coal volatiles are completely contained inside the cylinder by a graphite seal. This seal, about 0.015 in. (0.38 mm) thick and made from commercially-available flexible graphite sheet material, is replaced after each test.

A separate disposable nickel tube lining the capillary is also replaced after each test by removing a lower retaining ring. Nickel, due to its high heat-transfer, permits accurate thermocouple readings.
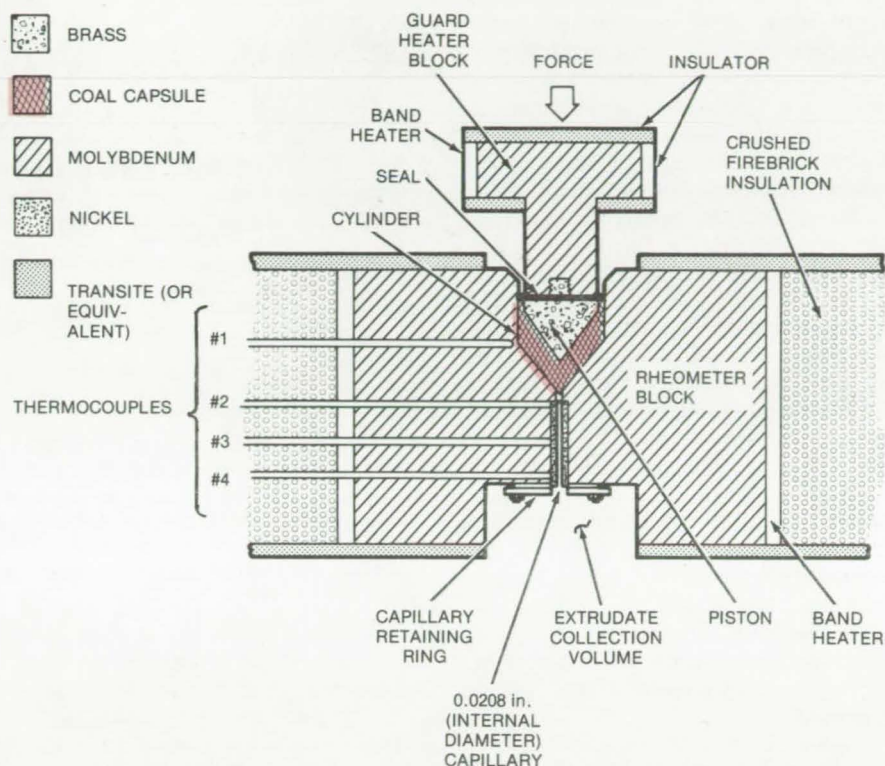
Capillary Rheometer incorporates a cone-tipped preheated piston to compress a plasticized coal sample through a narrow tube. The applied force is proportional to the viscosity and is recorded on a separate instrument. The samples are heated rapidly due to the large area of the cone surface.

This work was done by Samuel P. Feinstein of Caltech for NASA's Jet Propulsion Laboratory. For further information, Circle 53 on the TSP Request Card.

This invention is owned by NASA, and a patent application has been filed. Inquiries concerning nonexclusive or exclusive license for its commercial development should be addressed to the Patent Counsel, NASA Resident Legal Office-JPL [see page A5]. Refer to NPO-14501.

New Approach to Purifying Silicon

Silicon tetrafluoride gas removes metallurgical-grade impurities when passed over silicon in a quartz tube.

NASA's Jet Propulsion Laboratory, Pasadena, California

A technique now under investigation promises to allow an inexpensive increase in the throughput rate when purifying metallurgical grade silicon. Aluminum impurities are removed from a silicon charge, rather than purifying by removing the silicon.

As shown in the figure, a quartz tube is charged with 1- to 10-mm chunks of metallurgical-grade silicon and/or very pure quartz sand. The total charge ranges between 1 and 5 kg. The tube is evacuated and heated to between 800° and 1,350° C. Once the charge is heated, a stream of SiF_4 is passed over the charge at low pressure for not less than 20 hours.

Aluminum and boron impurities are removed according to

$$4Al + 3SiF_4 \xrightarrow{\Delta} 4AlF_3 + Si$$
and
$$4B + 3SiF_4 \xrightarrow{\Delta} 4BF_3 + Si$$
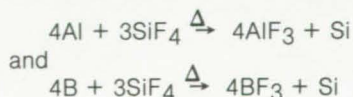
The 12 Al-F or B-F bonds are formed at the expense of 12 Si-F bonds.

Because the Al-F bond is 17 Kcal/mole and the B-F bond in BF_3 is 38 Kcal/mole stronger than the corresponding Si-F bonds in SiF_4, the reaction proceeds rapidly. When AlF_3 is formed, it will react on contact with a hot SiO_2 surface to form SiF_4 and Al_2O_3. The Al_2O_3 coats the quartz surface of the furnace tube. On the other hand, B, Cu, Ca, and Mg impurities are volatilized and concentrated in the cooler zones outside the furnace.

In tests, the new process has reduced Al impurity concentration from 5,000 ppm (0.5 percent) to 2 to 3 ppm, (a purification of greater than 3 orders of magnitude) as demonstrated by emission spectroscope analysis of silicon samples removed from four sections of the quartz tube. The removal of B, Ti, Be, Cu, Mg, and Ca impurities was not as great but did occur.

It is recommended that this process be combined with a second-step to remove transition series elements. It has also been suggested to obtain purer silicon by mixing CO gas with the SiF_4 as shown in the figure. Carbon monoxide is known to react with many of the transition metals to form volatile metal carbonyls at elevated temperatures. For example, Ni reacts with CO above 200° C to form $Ni(CO)_4$, a volatile gas. The other impurities, such as Fe, Mn, and Co, may be removed in the same manner.

This work was done by Robert E. Chaney, William M. Ingle, and
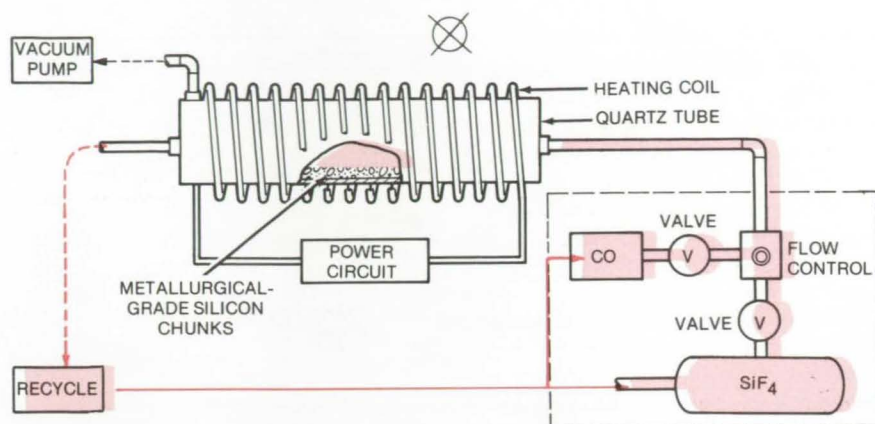
Metallurgical-Grade Silicon is purified in an evacuated quartz tube heated to temperatures ranging from 800° to 1,350° C. The impurities are removed by reaction of SiF_4, with trace metals, particularly with Al and B, contained in the silicon chunks. The process can be further improved by introducing CO to form volatile metal carbonyls with the remaining metals to obtain higher purity. The low-cost approach could improve silicon production for silicon solar cells.

Stephen W. Thompson of Motorola, Inc., for **NASA's Jet Propulsion Laboratory.** *For further information Circle 54 on the TSP Request Card.*

This invention is owned by NASA, and a patent application has been filed. Inquiries concerning nonexclusive or exclusive license for its commercial development should be addressed to the Patent Counsel, NASA Resident Legal Office-JPL [see page A5]. Refer to NPO-14474.

Compact Reactor for Onboard Hydrogen Generation

Hydrogen, chemically stored as methanol,
is a promising internal-combustion fuel.

Lewis Research Center, Cleveland, Ohio

Hydrogen has been suggested as an alternate fuel for internal-combustion engines. Major problems associated with its use are the requirements for onboard storage and handling. An alternate approach is to store hydrogen in a chemical compound that can be safely handled and easily converted into gaseous hydrogen. One such compound is methanol, which has attractive characteristics: (1) methanol is readily obtainable from natural products such as wood, compost, or various organic wastes; (2) a mixture of methanol and water is readily converted into hydrogen at moderate temperatures by catalytic reaction; (3) methanol can be handled and stored easily by conventional

methods; (4) the amount of hydrogen per unit volume of liquid is 40 to 50 percent greater for methanol or methanol/water mixture than for liquid hydrogen; and (5) if the energy necessary for the reformation process is captured from otherwise waste energy (e.g., engine exhaust), the dissociation of methanol provides a means of converting waste thermal energy into useful chemical energy.

The steam reformation of methanol as a source for hydrogen is a relatively simple operation. The problem is to develop a catalytic reactor of permissible size and weight that will generate the desired quantity of hydrogen (260 to 460 stdft^3/h for automotive applications).

Several catalysts were tested, and a copper chromite type (78 percent CuO, 20 percent Cr_2O_3, and 2 percent graphite) was found to give the best results. Data were taken for various reactor temperatures and several feed-flow rates. These data indicated that a catalyst bed temperature of 600° F (589 K) would yield the maximum amount of hydrogen for a given volume of methanol without damaging the catalyst.

Empirical equations, relating the hydrogen flow rate to the reactor temperature and to the amount of methanol converted, have been developed to aid in designing a compact reactor for onboard hydrogen generation. A reactor that would produce 270

stdft^3/h (1.5 pounds per hour) of hydrogen was estimated (see figure). This reactor requires about 4 pounds of catalyst, which fills nine tubes, each 1 in. (2.5 cm) in diameter and 7 in. (17.8 cm) long. Such a reactor would have an overall size of 3 by 3 by 7 in. (7.6 by 7.6 by 17.8 cm). By utilizing waste heat, the reactor products would contain 12 to 13 percent more energy than the incoming methanol/water feed.

*This work was done by Theodore A. Brabbs of **Lewis Research Center.** Further information may be found in NASA TP-1247 [N78-23256/NSP], "Catalytic Decomposition of Methanol for Onboard Hydrogen Generation," [$6.00] a copy of which may be obtained at cost [prepayment required] from the National Technical Information Center, Springfield, Virginia 22161.*
LEW-13033
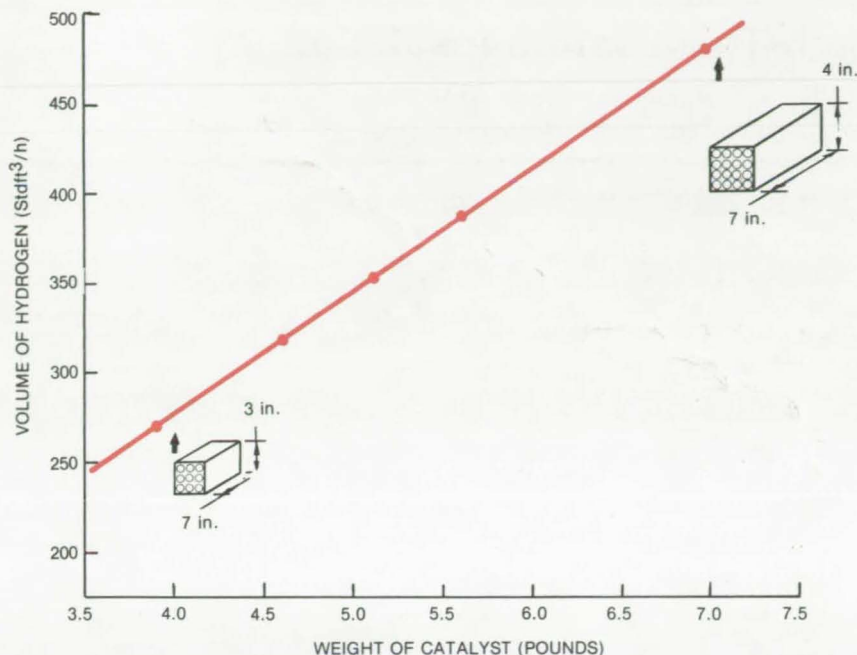
Volume of Hydrogen is shown vs. the weight of catalyst. Two reactors are sketched to show the size required to produce the indicated amounts of hydrogen.

Water-Cooled Insulated Steam-Injection Wells

Water is proposed as an insulated coolant and heat-transfer medium for steam-injection oil wells.

NASA's Jet Propulsion Laboratory, Pasadena, California

Using water as a coolant and heat-transfer medium has been suggested as another way of extending the depth from which oil may be recovered from wells by steam injection. [See "Double-Wall Tubing for Oil Recovery" (NPO-14606) on page 375 of this issue.] Water is injected into the annulus between the insulated central steam-feeding tube and the well casing. The water heats up on its way down the well and is mixed with steam when it is injected into the oil formation at the bottom of the well.

This approach is somewhat analogous to the cooling system in a liquid-propellant rocket. It could possibly help solve the main problem in extending the depth of steam-injection wells: heat loss to the surrounding rock. (A variety of solid, liquid, and gaseous insulations have been tried, but economic or technical problems have precluded their general use.)

In addition to trapping and delivering heat to the steam-injection point, the water will also keep the casing cooler, preventing or reducing casing failures caused by thermal stresses. It is expected that the waterflow would keep steam from running back up the annulus between the steam feedpipe and casing.

Although the water would deliver much of the otherwise-lost heat to the injection point, there may be some loss in the quality (temperature) of the delivered steam. This could be compensated for by keeping the heat supplied to the steam generator constant, while slightly reducing the amount of water fed to it, to increase the initial steam quality.

*This work was done by Lloyd H. Back and Leonard D. Jaffe of Caltech for **NASA's Jet Propulsion Laboratory.** For further information, Circle 55 on the TSP Request Card.*
NPO-14605

High-Temperature Insulation

Lightweight insulating material works
over a very broad temperature range.

Marshall Space Flight Center, Alabama

A new insulating material developed for NASA's Space Shuttle main-engine nozzle protects the nozzle skin from engine plume heat. The material is unaffected by moisture or hydraulic oil and is usable at temperatures ranging from 2,200° F (1,200° C) to cryogenic levels. It could be readily applied to a number of high-temperature and cryogenic processes.

The material is a partially sintered batting using 2-percent-dense [10 lb/ft^3 (189 kg/m^3)] 8-μm wire blanket available in 1/8 in. (3.2 mm) thickness. Two commercially-available wire materials that may be used include CRES (corrosion-resistant steel) for operation up to 1,400° F (760° C) or 80Ni-20Cr Nichrome for operation up to 2,200° F (1,200° C) temperature.

In both cases, the material was successfully tested for 10 cycles of dipping in liquid nitrogen (LN$_2$) and thawing at 300° F (150° C). It also withstood two cycles of hydraulic liquid soaking, LN$_2$ dipping, and 1,600° F (870° C) oven thawing.

Other tests included prolonged thermal exposure to 2,200° F (1,200° C), emissivity tests prior to and after the thermal exposure, thermal-conductivity tests to 2,000° F (1,100° C), vibration to simulate anticipated nozzle-operation levels, and salt-spray and corrosion tests. No other lightweight insulation was found to withstand all of these tests.

This work was done by R. E. Mowers and A. C. Peterson of Rockwell International Corp. for **Marshall Space Flight Center.** *No further documentation is available.*

Inquiries concerning rights for the commercial use of this invention should be addressed to the Patent Counsel, Marshall Space Flight Center [see page A5]. Refer to MFS-19498.

Books and Reports

These reports, studies, and handbooks are available from NASA as Technical Support Packages (TSP's) when a Request Card number is cited; otherwise they are available from the National Technical Information Service.

Mossbauer Study of FeSi$_2$ and FeSe Thin Films

A report discusses new information about film structure.

Structural studies of FeSi$_2$ and FeSe thin films have been conducted via Mossbauer spectroscopy as a continuation of earlier investigation of FeTe films. [See "Mossbauer Studies of Bulk and Thin-Film FeTe," (MFS-23773) on page 64 of *NASA Tech Briefs*, Vol. 3, No. 1.] Results of this work are published in a short report discussing the structures of bulk and thin-film FeSi$_2$ and bulk and thin-film FeSe. The thin-film samples of the FeSi$_2$ had 10-, 85-, 190-, and 380-Å thicknesses deposited on amorphous substrates (Mylar, or equivalent), while the FeSe films were 500, 1,000, and 2,000 Å thick deposited on aluminum substrates.

Results for the FeSi$_2$ show that the isomer-shift (IS) values of the observed doublets decrease with increasing thickness and are constant beyond 190 Å. This initial decrease is indicative of an increase in the s-electron density at the iron site with increasing film thickness. The 4s-electron contribution to iron coming from silicon ions increases when the number of Si near-neighbors increases or when the Fe-Si distance decreases. At low thicknesses the dangling-bond density is high. This leads to a lowering of the number of Si near-neighbors for some iron sites. As a result, a lowering of the s-electron density at these iron sites could be possible. The other possible reason for the observed behavior of the IS values could be that the Fe-Si distances for low-thickness films are greater than those for films of higher thicknesses. On the basis of IS variation alone, it is difficult to say which phenomenon is dominant. However, quadrupole-splitting (QS) data, as indicated below, favor greater Fe-Si distances at lower thicknesses.

It is observed that the QS values gradually increase with increasing film thickness up to 380 Å. Variation in QS values could be due to either of the two above-mentioned causes. It is possible that both effects are present; however, since the net observed effect in the low-thickness range is a decrease in the QS value with decreasing thickness, it is concluded that changes in Fe-Si distances play the dominant role at lower thicknesses. Such changes in lattice constants at very low thicknesses have been reported by other workers. The decrease of QS values at 760 Å is indicative of the disappearance of dangling bonds.

The Mossbauer spectrum of 100 Å FeSi$_2$ film deposited on aluminum did not show any quadrupole splitting; a single line corresponding to an IS value of 0.0051±0.0142 mm/s was observed. A similar effect was observed with FeTe also deposited on

aluminum. The result suggests that even if the structure and bond nature in the bulk samples are different, their thin films deposited on aluminum substrates show structural similarity. This observation reflects on the influence of the substrates on the film structure.

Results with bulk and thin films of FeSe having thicknesses of 500, 1,000, and 2,000 Å deposited on aluminum substrates show that the lines, though broadened, could not be split. The large line width can be due to (a) the presence of a small internal field and (b) the disorder due to the dangling bonds.

As explained in the earlier study of FeTe thin films, the disorder due to the dangling bonds becomes less as the film becomes thicker. The observed decrease in the line width suggests the lowering of the disorder due to the dangling bonds. The observation that at 2,000 Å the line width is close to that of the bulk shows that the dangling-bond disorder disappears at this thickness.

The FeSe IS values are almost constant for all film thicknesses. This is due to the fact that this part of the study was confined to films of high thickness ($\geqslant 500$ Å) only. It was observed from studies on FeTe and FeSi$_2$ systems that beyond a certain thickness, the IS values do not change appreciably. This is because in films of higher thickness the dangling-bond density is low, and it does not vary much with the film thickness.

This work was done by Kamna Aggarwal, W. T. Escue, and R. G.

Mendiratta of **Marshall Space Flight Center.** *To obtain a copy of the report, "Mossbauer Study in Thin Films of FeSi$_2$ and FeSe Systems," Circle 56 on The TSP Request Card. MFS-25088*

Stress Corrosion in High-Strength Aluminum Alloys

Marine-environment tests compare new alloys with older ones.

A report describes the results of stress-corrosion tests on aluminum alloys 7075, 7475, 7050, and 7049. The tests were conducted to compare the performance of the original stress-corrosion-resistant (SCR) aluminum, 7075, with newer, higher-strength SCR alloys.

The tests were performed in a coastal marine environment near Daytona Beach, Florida, on both smooth and precracked specimens. The smooth specimens were tensile rounds 3.175 millimeters in diameter and were stressed in "window-frame" jigs. The precracked specimens were double cantilever beams 25 millimeters wide, 25 millimeters high, and 125 millimeters long with a chevron-shaped notch. These specimens were precracked by a pair of stainless-steel bolts turned into a machined slot at the end of the specimen. The precracks were propagated about 2 to 3 millimeters beyond the end of the chevron.

The report covers the first 26 months of the tests, which are to continue for a total period of 6 years. Initial crack-length measurements were made 1 day, 2 days, 4 days, 1 week, 2 weeks, 1 month, 2 months, 4 months, 6 months, 1 year, and 2 years after the tests were begun. Subsequent measurements are to be made annually.

The report concludes that alloys 7050 and 7049 are superior in short-transverse cross-corrosion resistance to the older 7075 alloy. The report also finds that all the alloys are subject to a self-loading effect caused by the wedging of corrosion products in the cracks. This effect causes cracks to continue to grow, even at very-low externally applied loads.

The report includes crack-growth plots and plots of crack growth rate vs. stress intensity (V-K) for the specimens. The experimental methods are described, and the test results are discussed.

This work was done by R. C. Dorward and K. R. Hasse of Kaiser Aluminum & Chemical Corp. for **Marshall Space Flight Center.** *To obtain a copy of the report, "Flaw Growth of 7075, 7475, 7050, and 7049 Aluminum Alloy Plate in Stress Corrosion Environments: 2-Year Marine Atmosphere Results," Circle 93 on the TSP Request Card. MFS-23986*

Computer Programs

These programs may be obtained at very reasonable cost from COSMIC, a facility sponsored by NASA to make new programs available to the public. For information on program price, size, and availability, circle the reference letter on the COSMIC Request Card in this issue.

Temperature and Moisture Analysis in Composites

Program to study environmental effects

Advanced fiber-reinforced polymeric matrix composites have emerged as strong candidate materials for airframe applications. The favorable aspects of these materials include their high strength, stiffness, and low density. However, studies have shown that these materials pick up moisture from the atmosphere with a resultant degradation of the matrix-sensitive mechanical properties at elevated temperature.

The structural integrity and life-cycle durability of composites must be well understood before they can be

confidently incorporated into airframe designs and other uses. The Temperature and Moisture Analysis in Composites (TMAC) program was developed to study the effects of variations in diffusion coefficients, surface properties, panel tilt, ground reflection, and geographical location on the moisture-concentration profiles and average moisture contents of composite laminates. Studies have shown that the absorption and desorption of moisture can introduce significant stress into the outer plies of the laminate. With TMAC, the materials

analyst should be able to develop a better understanding of the effect the environment has on composites.

The TMAC program performs the analysis as a one-dimensional diffusion problem described by Fick's Second Law, treating the composite as an isotropic material with an effective temperature-dependent diffusion coefficient given by the Arrhenius equation. The diffusion equation is solved by an explicit finite-difference method. The moisture concentrations on both surfaces are assumed equal and are specified as a function of the relative humidity of the air next to the panel. The panel temperature is assumed uniform and is calculated from an energy-balance algorithm, which includes both direct and diffuse solar radiation. The boundary layer of air next to the panel is assumed to be at the same temperature as the panel. This temperature and the dewpoint of the ambient air are used to calculate the relative humidity of the air next to the panel. The user supplies data concerning the panel properties, orientation, weather, environment, and time span. The time span of the simulation may cover many years to accommodate life-cycle studies. Outputs include moisture-concentration profiles through the panel thickness and a history of total moisture content.

This program is written in FORTRAN IV and has been implemented on a CDC 6000-series computer with a central memory requirement of approximately 48K (octal) of 60-bit words. TMAC was developed in 1978.

Life
Sciences

Hardware, Techniques, and Processes

Improvement of CAT Scanned Images

Digital image-enhancement procedures improve
the definition of computerized axial tomograms.

Lewis Research Center, Cleveland, Ohio

Computerized axial tomograms (CAT scans) of human anatomy suffer from inherently poor definition. A digital enhancement procedure has been developed to improve the definition of the images. A tomogram is generated from a large number of X-ray beams. The beams are collimated and small in diam. . A scanning device passes the :ams sequentially through a human bject at many different angles. A battery of transducers opposite the subject senses the attenuated signals. The signals are transmitted to a computer where they are used in the construction of an image on a transverse plane through the body.

The poor definition of the image is the result of several factors. Resolution of the constructed image is necessarily coarse, because the total X-ray dose applied to a human subject must be kept low for health reasons. Similarly, the scanning time must be kept short to minimize the effects of motion due to respiratory and circulatory functions. Moreover, if the entire range of values of X-ray attenuation from air to bone is recorded, local contrast is low. The combination of low contrast, coarse resolution, and body motions produces unsharp edges on the various image elements. Finally, the low X-ray voltages are responsible for a low signal-to-noise ratio. Therefore, the task of improving the definition of CAT scanned images becomes that of increasing resolution, sharpening edges, filtering noise, and increasing local contrast.

Resolution cannot be increased for the obvious reason that information not originally a component of a signal may not be added later. However, the remaining three tasks can be performed digitally. Unfortunately the desired results sometimes conflict with each other. Image smoothing reduces noise at the expense of blurring edges. Image sharpening enhances the edges at the expense of increasing the relative amplitude of the noise. However, the selection of

(continued on next page)
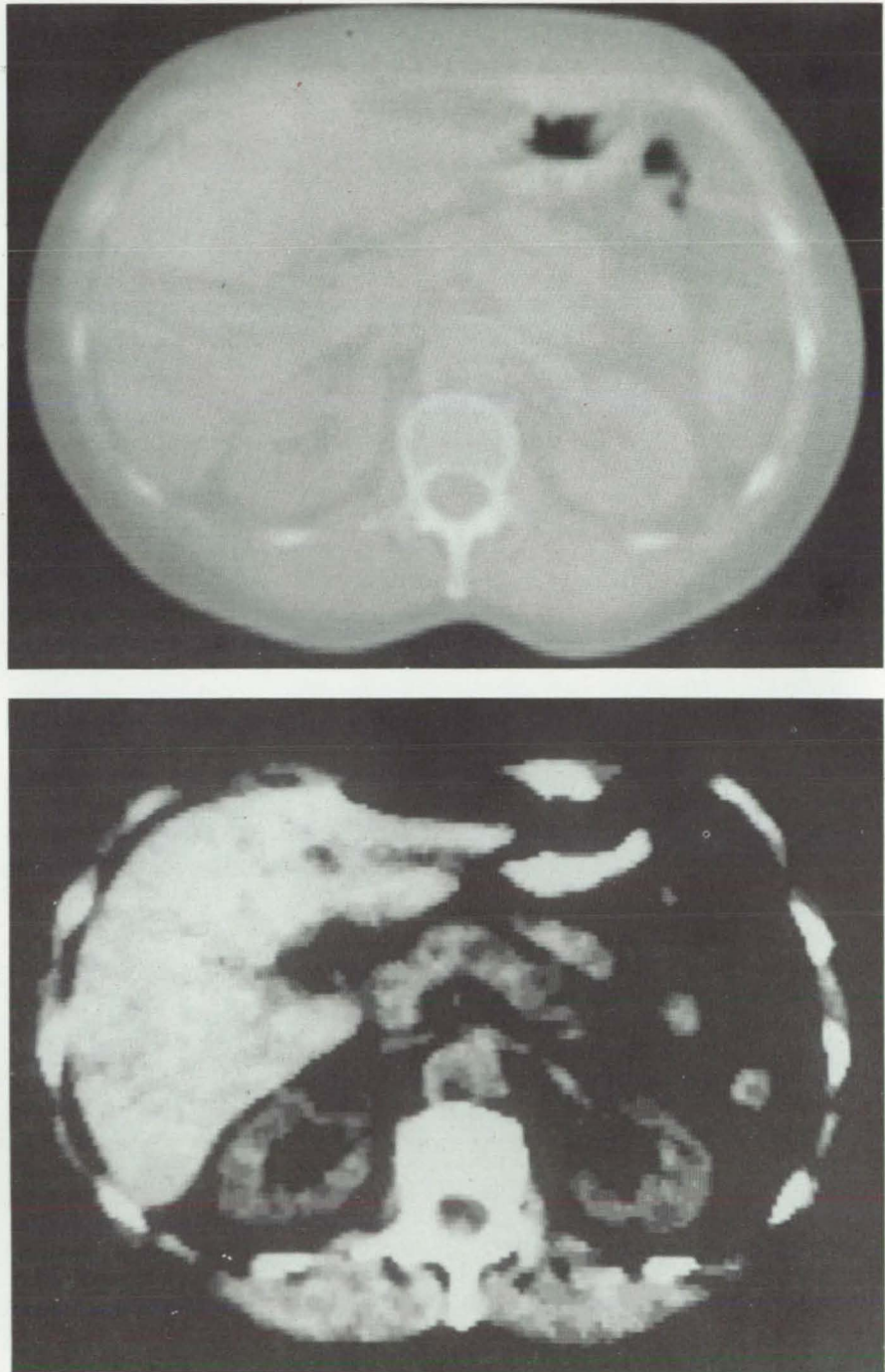
Figure 1. The **Effects of Digital Processing on Tomograms** are shown in the examples above. For the typical tomogram on the top, the range of gray values to be expanded is determined, and the smoothed and contrasted image on the bottom is produced. The associated histogram is shown in Figure 2.

appropriate functions, applied in the proper sequence, reveals information not otherwise obtainable.

NASA technology development has resulted in a repertoire of digital image-enhancement functions originally evolved for use in a radiographic inspection facility for aerospace structures. Presently, these functions are applied directly to the radiographic images, rather than first using various mathematical transforms on the images.

The results produced by an image-enhancement procedure depend heavily on the type of image being processed. For CAT scanned images, the following procedure has been most effective. First, noise is reduced, then image contrast is modified.

The noise is reduced by selective smoothing. Two processes have been found to be effective. The first examines the immediate neighbors of every picture element, one each to the top, bottom, sides, and diagonals for a total of nine including the central picture element. If the value of the central element lies outside a specified multiple of the range of values of its neighbors, it is replaced by the arithmetic mean of the values of its neighbors. Otherwise, it is not modified. An alternative is to replace the value of every picture element with the median of the values of its neighbors. In this case, arbitrary weighting functions may be associated with the neighbors. Both procedures minimize random noise spikes without excessively blurring edges.

After the smoothing operations, limited portions of the contrast range
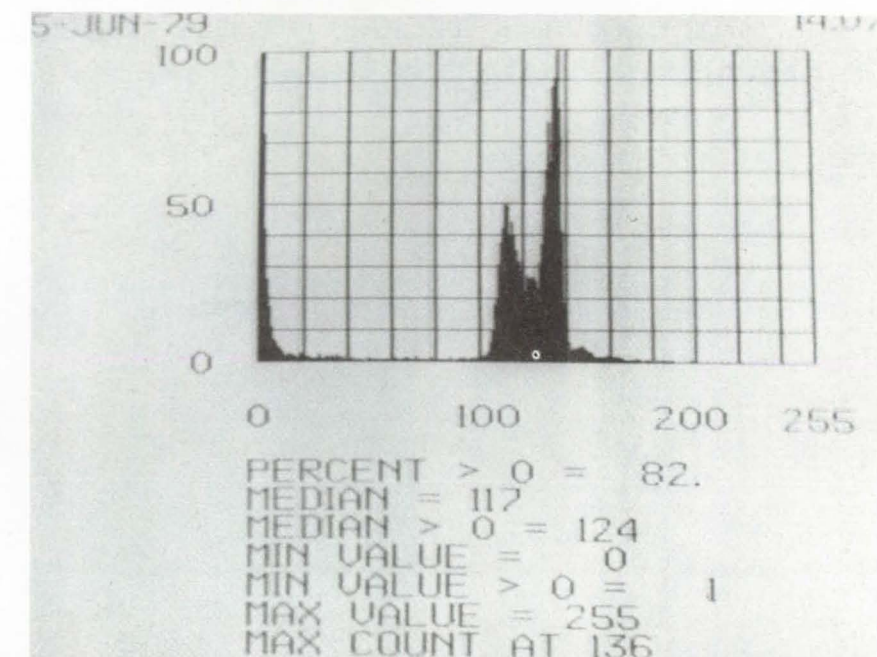
Figure 2. **Gray Scale Histogram** above is used to determine the range of gray values to be expanded.

of the image are expanded. Each expansion highlights a different feature of the image. A complete analysis of the image requires several different expansions, each producing a different processed image. The range of gray values to be expanded is determined from a gray-scale histogram. Examples of an unenhanced image, an enhanced image, and a histogram are shown in the figures.

The result of the application of these procedures is a sequence of processed images. The sequence clearly reveals details that are difficult to discern by eye in the unenhanced images.

Improved Optics for an Ultracentrifuge

Changes in the optics can make the readouts
more exact and easier to interpret.

NASA's Jet Propulsion Laboratory, Pasadena, California

The ultracentrifuge is an important tool in the study of polymers, biomolecules, and cell structures. In a typical ultracentrifuge, shown schematically in the figure, the rotor supports a pair of optically matched vials; one contains a sample mixed in a solvent, and the other is a reference

that contains only the solvent. A double-slit optical system, transverse to the rotor, creates an interference pattern on a photographic plate each time the vials pass through the optics. The medium in the sample vial displaces the interference maximums such that the shift gives a measurement of the density distribution along the length of the sample. A typical interference pattern is shown.

The accuracy and utility of the ultracentrifuge may be improved by several modifications to the basic design. The modifications may be grouped in two categories — those

that can be retrofitted to an existing optical system and those that require some modification of the existing optics. The retrofit modifications include:

1. The continuously emitting lamp can be replaced by a pulsed lamp that is synchronized to passage of the double slit. This would allow the intensity to be higher while maintaining a low average power level. It would also allow narrower slits to be used, reducing diffraction broadening of the lines.

2. An additional lens can be placed at the film plane to give an image that consists of two parallel lines (the displaced image of the double slit). This image is the superposition of the interference fringes and would be more intense and easier to measure than the individual fringes.

3. Since the optical density of the developed film is correlated with the logarithm of the exposure, the performance can be improved if the plates are given a low-level light exposure by "prefogging." The actual exposure would then have better contrast.

4. An isodensity tracer can be scanned over the photographic image to get a better measurement of the displacement of each fringe line.

5. A photoelectric readout could be added. This could include a servo feedback loop to seek signal maximums in the interference bands; or, direct photomultiplier inputs from the whole interference pattern could be processed by a computer.

Possible improvements that would require changes in the optical system are:

1. A three-slit optical system which would have one sample vial and vials on either side that would contain only the solvent, would translate differences in the sample density into light amplitude variations of the interference maximums (rather than to their displacement). This would allow the use of a fixed photoelectric pickup.

ULTRACENTRIFUGE, TOP VIEW
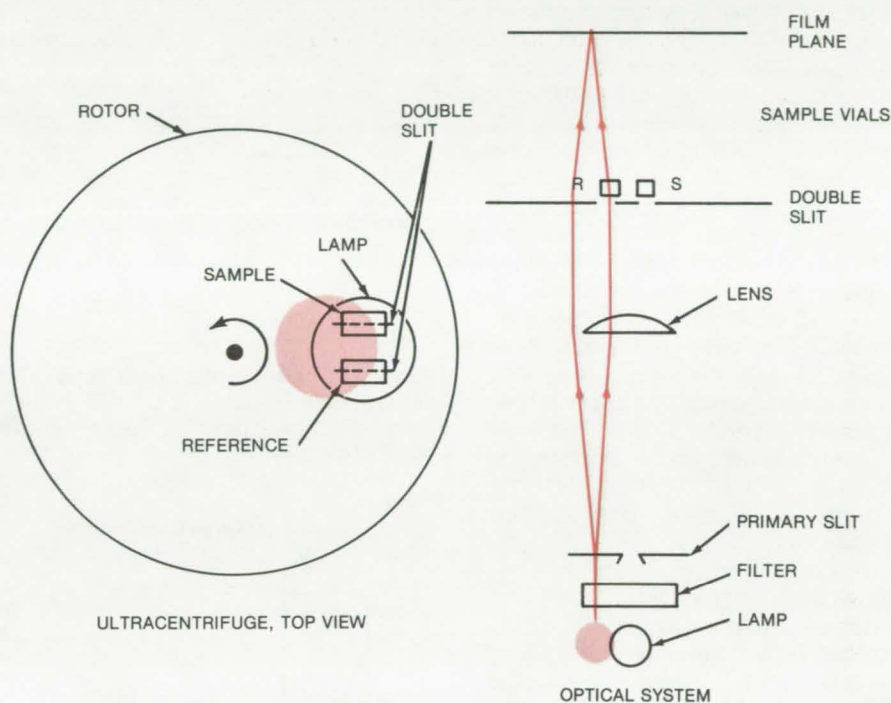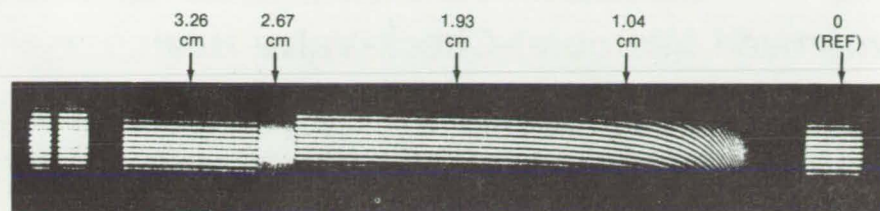
OPTICAL SYSTEM

In an **Ultracentrifuge System,** the light originates at the lamp and passes through a band-pass filter, a primary slit, a lens, and the double slit to give an interference pattern at the film plane. The optical path is changed by the density of the sample such that the displacement of the interference fringes measures the density. A typical diffraction pattern is shown at the top.

2. Replacing the slits with transmission gratings would give a series of spots rather than the series of interference lines. The lateral displacements of these spots may be easier to analyze.

3. A transmission holograph could be made of the sample vial.

4. A cylindrical sample cell or a cylindrical cavity in a rectangular cell could be used. For such a cell, refraction at the cell wall would measure the sample density.

Improved Microbial-Check-Valve Resins

New resins release small constant iodine
concentrations into drinking water.

Lyndon B. Johnson Space Center, Houston, Texas

Improved microbial-check-valve resins have been tested for their microbicidal effectiveness and long-term stability. The new resins give more-stable iodine concentrations than previous preparations and do not impart objectionable odor or taste to the treated water.

A microbial check valve is a small cylindrical device, packed with an iodide-saturated resin, that is installed in the water line where contamination by micro-organisms is to be prevented. The resin cartridge (see Figure 1) kills bacteria, fungi, and viruses by releasing small amounts of iodine into the water stream. The valve is totally passive, and it operates on flows in either direction (at the expense of a small loss of flow pressure).

In early versions of the check valve, the initial levels of iodine in the effluent water were high enough to impart an objectionable odor and taste. Using the new resins, however, the iodine concentration is maintained at about 2 ppm, a level that is both microbicidal and drinkable. Moreover, whereas previous resins did not have a constant washout characteristic, the new resins maintain a relatively-constant iodine concentration during their entire life cycle (see Figure 2).

The resins are prepared by converting a commercially-available quaternary ammonium anion-exchange resin from the chloride form to the iodide form. This is done by soaking in a 1N solution of potassium iodide that contains 3.5 times the number of equivalents of I- based on the theoretical capacity of the resin. Different iodine residual levels may be established by varying the process parameters.

A prototype microbial check valve was tested for stability and performance under harsh environmental conditions. In the test, a controlled mixture of pathogenic bacteria was prepared and passed through the valve. The valve was heated and
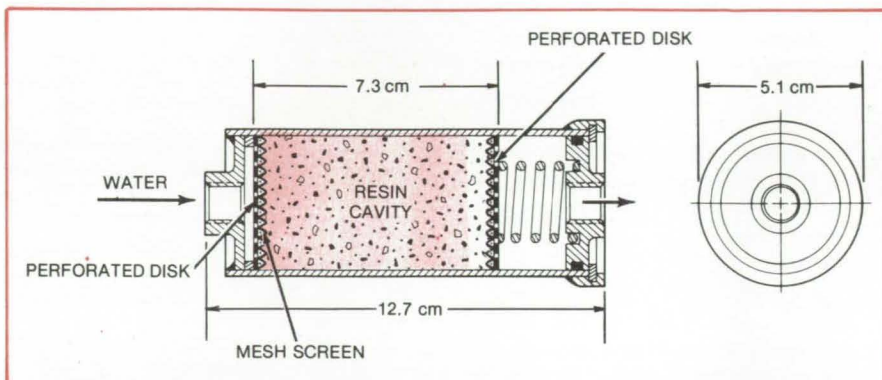
Figure 1. The **Microbial Check Valve** is a passive device that is installed in multiuser potable water systems. It is filled with an ion-exchange resin packed with iodine in the form of I_3^- and possibly I_5^- and I_2 at concentrations that exceed the stoichiometric occupation level.
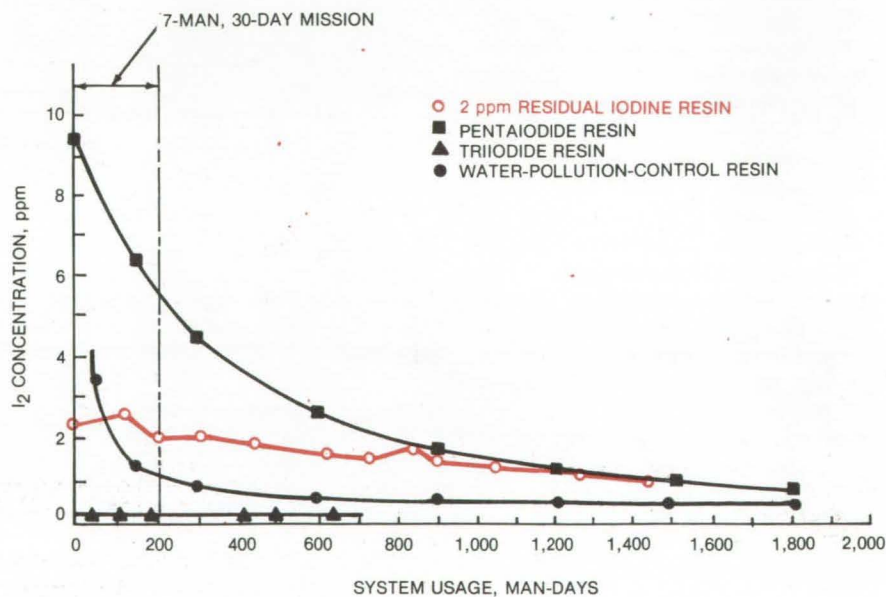
Figure 2. The **Improved-Resin Washout Characteristic** is shown in color. The other two curves stabilize to 2 ppm or less iodine residual level only after many hours of operation. During the initial 200 man-days, the iodine residual level for these resins is too high for drinking water.

cooled to various temperatures for various periods of time, and the effluent water was analyzed for bacterial content. The micro-organisms that were tested included species of *Escherichia, Strep, Staph, Pseudomonas, Clostridia,* and

Aspergillus. The effectiveness of the resin against these organisms was essentially 100 percent at 35°, 70°, and 160° F (2°, 21°, and 71° C).

This work was done by Gerald V. Colombo and David F. Putnam of Umpqua Research Co. for **Johnson**

Computer Measurement of Arterial Disease

X-ray angiograms are read
for the extent of atherosclerosis.

NASA's Jet Propulsion Laboratory, Pasadena, California

An image processing technique quantifies human atherosclerosis by computer analysis of arterial angiograms. X-ray film images are scanned and digitized, the arterial shadow is tracked, and several quantitative measures of lumen irregularity are computed. Computer estimates of atherosclerosis in femoral angiograms have been correlated with smoking level, age, cholesterol level, blood pressure, and other clinical factors. An extension of the analysis to coronary angiograms is underway.

Shown in Figure 1, the JPL system consists of the following:
- a commercial minicomputer with 64 kilobytes of bipolar memory and 192 kilobytes of core;
- an automated light microscope (also used for other biomedical image-processing research projects);
- a 35-mm film digitizer;
- an interactive memory/display system;
- a sonic-stylus digitizer;
- an electrostatic picture recorder; and
- magnetic tape, disk, and printer peripherals.

In contrast to previous systems in which the system operator traces the arterial wall and the computer quantifies the extent of atherosclerosis, this system performs both functions: It determines both the vessel outline and extent of stenosis from numerical measures of irregularities in the digitized intensity patterns (see Figure 2). As the computer tracks the artery, the operator uses the sonic stylus to point out artifacts, such as branches to or crossing of other blood vessels. In the recent work on coronary angiograms, the operator also traces the
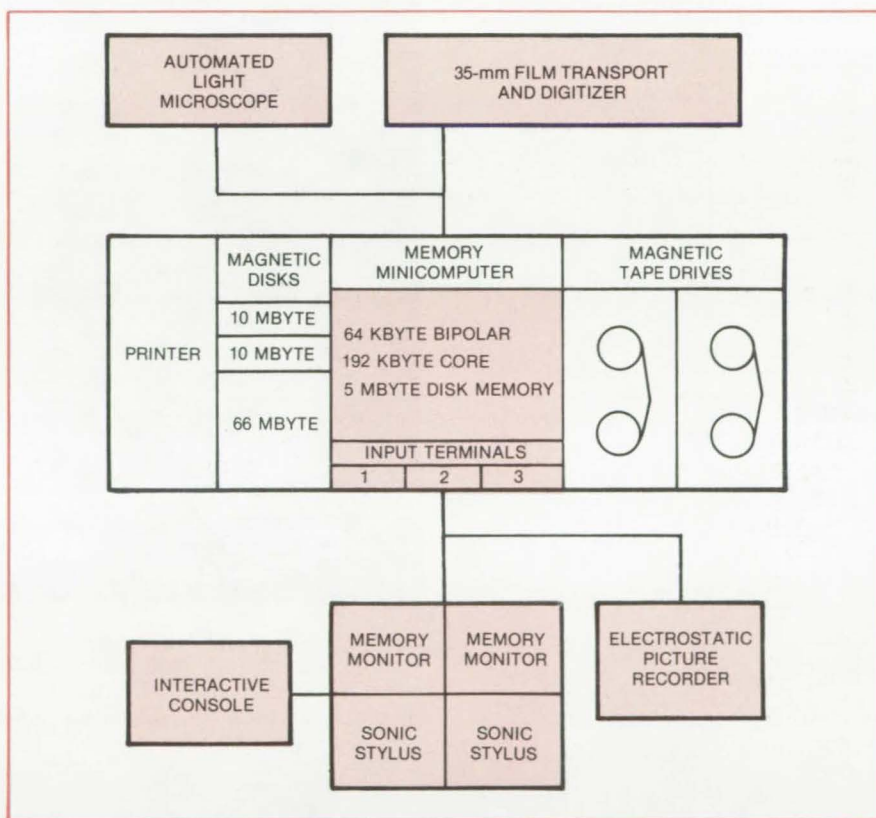
Figure 1. A **Minicomputer-Based System** evaluates 35-mm X-ray cineimages of arteries by calculating several numerical measures of lumen irregularity. These measures help to locate the vessel edges and extent of atherosclerosis.

approximate midline of the curved vessel. (This is not necessary in evaluating the relatively-straight femoral arteries.)

In one application, femoral angiograms of 21 cadavers were evaluated. After being angiogramed, the arteries were excised, opened, and color-photographed. In assessing the degree of atherosclerosis, the computer

agreed with human visual grading of the color photographs with very high correlation. Computer results were also highly correlated with a cholesterol analysis of the arterial wall.

In other tests, excellent agreement was found between computer evaluation of femoral angiograms on living subjects and evaluation by teams of trained angiographers. Correlations

were also found between femoral atherosclerosis progression, and blood cholesterol levels. Recent work with coronary angiograms also shows good agreement with the visual analyses of expert angiographers.

This work was done by James Armstrong and Robert H. Selzer of Caltech and Robert Barndt, David H. Blankenhorn, and Samual Brooks of the University of Southern California for the National Heart, Lung, and Blood Institute [of the National Institute of Health] and **NASA's Jet Propulsion Laboratory.** *For further information, Circle 58 on the TSP Request Card.*
NPO-14266
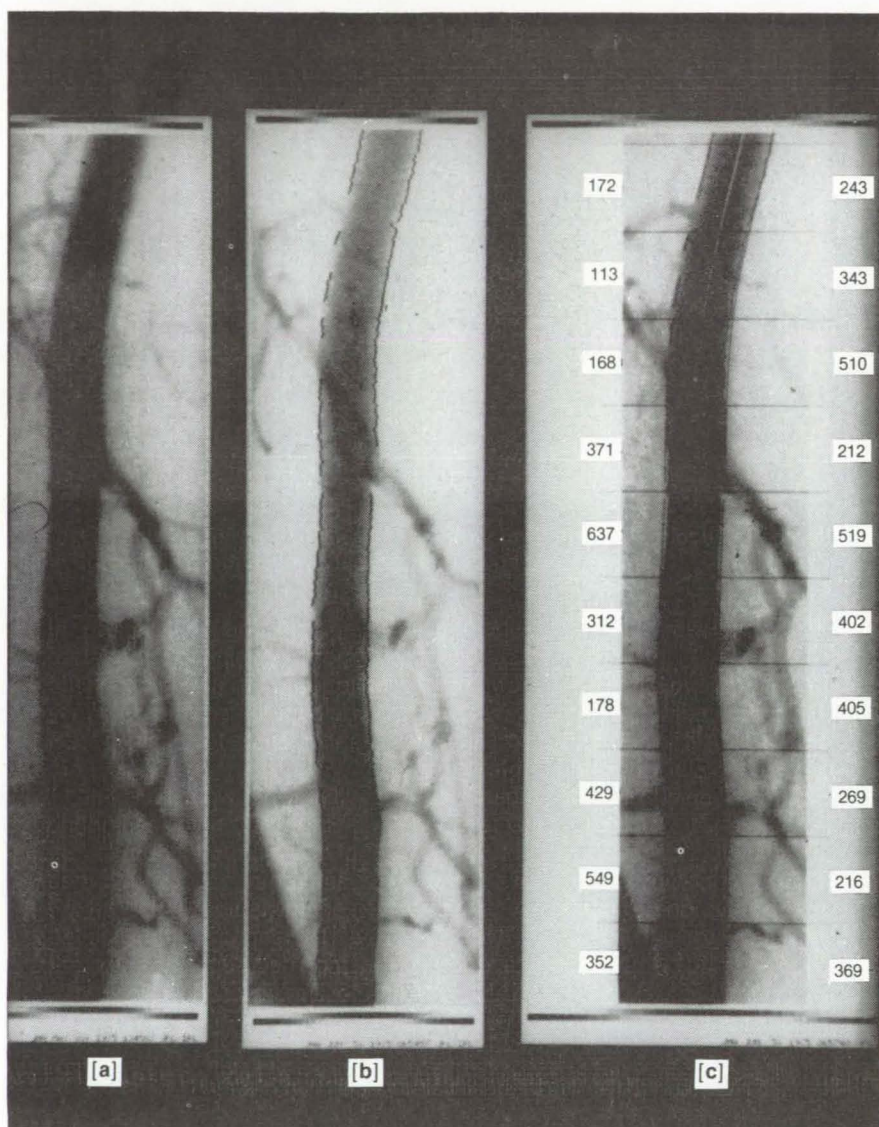
Figure 2. A **Femoral Angiogram** (a) is digitized for computer analysis. The lumen edge is tracked in (b), and the computer estimate of the original, or nondiseased vessel lumen, is shown in (c). Numbers are proportional to the root mean square of the displacement of the vessel wall within each 1-cm vertical interval.

Mechanics

Hardware, Techniques, and Processes

Books and Reports

Computer Programs

Improved Flaw-Detection Method

Use of helium improves flaw detection
by holographic interferometry.

Langley Research Center, Hampton, Virginia

Holographic detection of unbonded or delaminated surfaces of materials and structures is improved by using helium instead of air in the vacuum test chamber. Helium has an index of refraction closer to vacuum (unity) than air. Therefore, changes in the chamber pressure during the test do not alter the index of refraction as much as they do with air. The result is wider-spaced interference fringes more clearly outlining the flaws.

The nondestructive holographic interferometry involves placing a test object inside a vacuum chamber. A double-exposure photograph is made of two holograms of the object surface taken when the object is at atmospheric pressure and when the chamber pressure is reduced down to 10 mm Hg. When the pressure is reduced, stresses created on the object surface tend to exaggerate the flaws. These flaws become clearly outlined by the interference fringes as shown on the two photographs.

When air is used, there is a marked change in the index of refraction as the chamber is evacuated. This effect produces closely-spaced fringe lines of the object photograph. Flaw detection becomes very difficult, particularly on curved surfaces.

With helium, however, the change is not as marked because its index of refraction is close to that of vacuum. Thus fewer fringes are generated with a better outline of the flaws.

This work was done by Robert J. Platt, Jr., of **Langley Research Center.** *No further documentation is available.*
LAR-11866
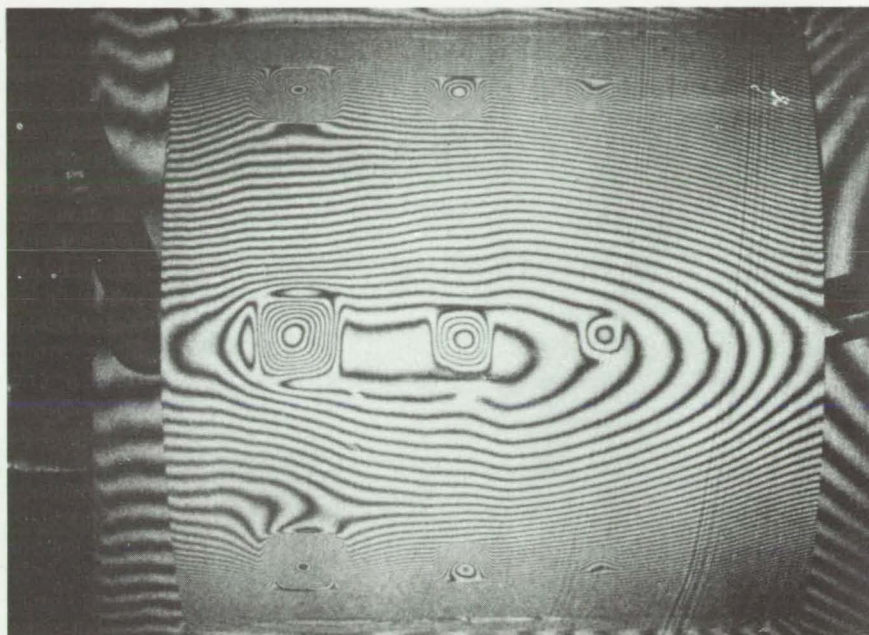
[a]
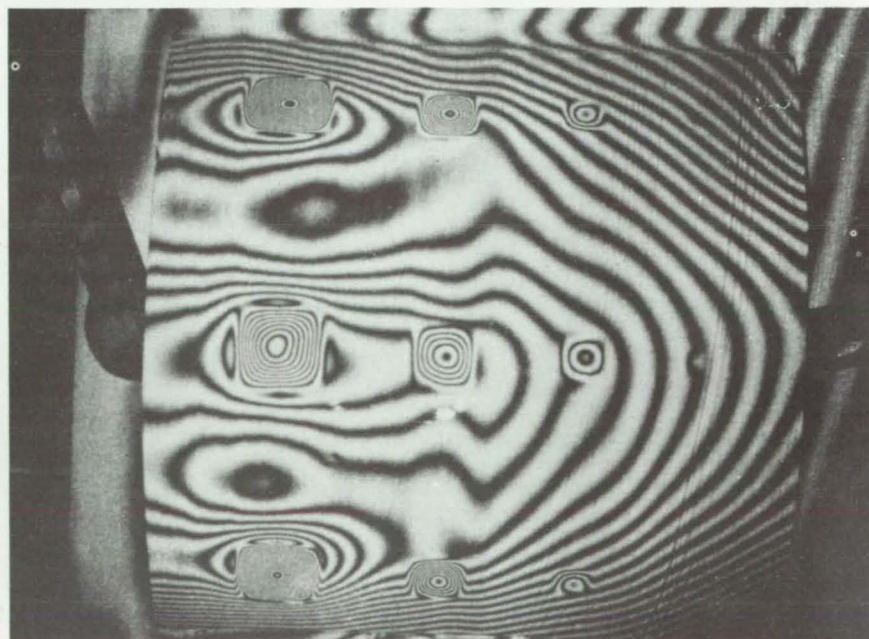
[b]

Improved Flaw Detection is demonstrated by using helium (b) in the test vacuum chamber instead of air (a). The two photographs of a curved, bonded plate of aluminum sheet 0.025 in. (0.635 mm) thick were taken by double-exposing its holograph at ambient and reduced pressures, respectively. Fewer interference fringes obtained in helium environment clearly outline the 12 built-in unbonded areas. With air, much of the detail is lost, particularly in the curved areas.

Solar-Cell Defect Analyzer

A nondestructive, automated scanning method can
test cells even after assembly and encapsulation.

NASA's Jet Propulsion Laboratory, Pasadena, California
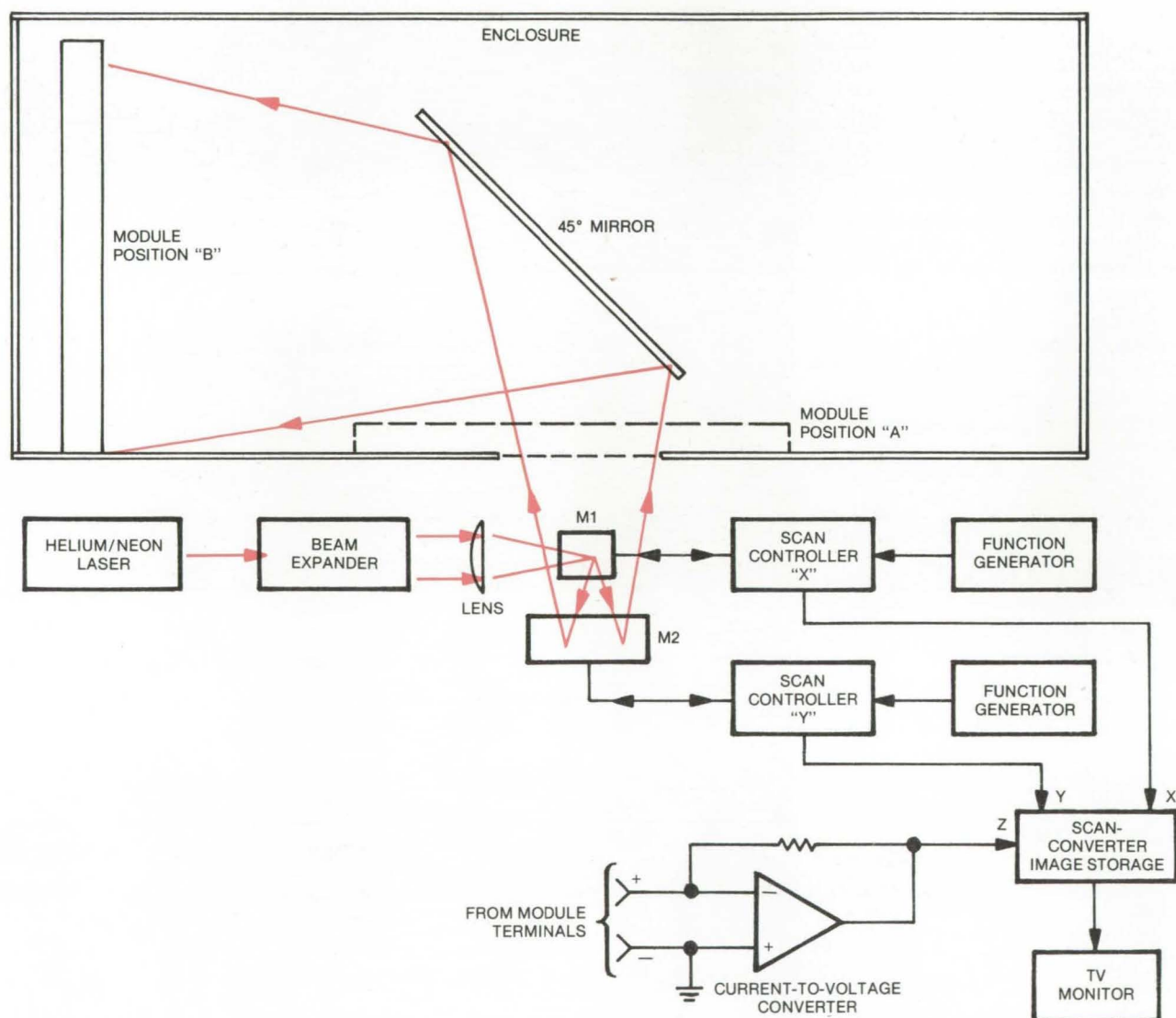
Figure 1. **Laser-Scanning System** pinpoints imperfections in solar cells. As laser light is scanned across the surface, the cell current is monitored and displayed as an electrical "image." Variations in the image intensity can be correlated with anomalies in the cell. Entire solar panels containing large numbers of cells can be scanned, even after encapsulation.

A laser scanner locates fine cracks and other imperfections in solar cells. Since the scanner can test individual cells within a large array, even after encapsulation, it could be used for quality-control checks during production runs.

To make a test, a laser beam is scanned over a selected region of the cell surface (see Figure 1). The photocurrent variations that occur in re-

sponse to the swept beam are recorded and stored along with the x-y coordinates of the moving spot of light. An electronic "image" of the cell surface is then generated from the current levels and coordinates and is displayed on a video monitor. The "operating point" of the cell can be adjusted by setting an external dc bias current through the solar panel or by setting the intensity of a steady back-

ground light. For comparison, a photodetector simultaneously develops an optical image of the cell from reflected light.

Although the technique is similar to the use of a scanning electron microscope (SEM) to locate microscopic imperfections, it differs in that large areas may be examined, including entire solar panels, and it is not necessary to remove cover glass or
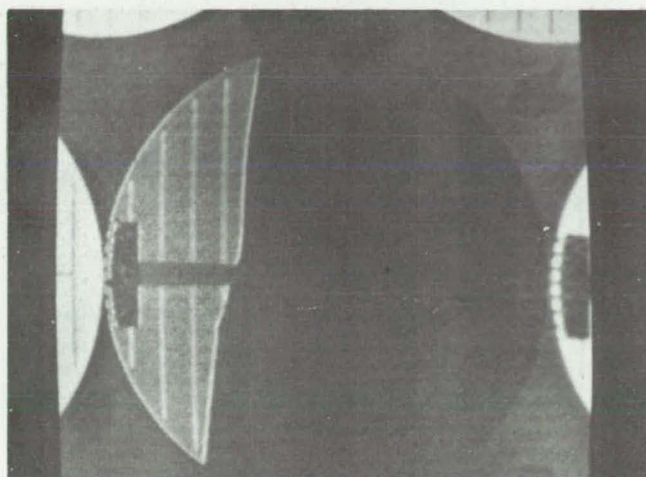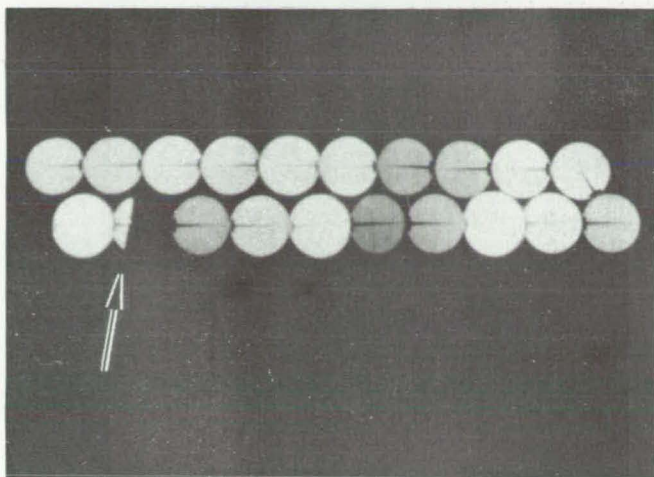
Figure 2. A **Cracked Solar Cell** is evident in these views obtained with the laser scanner. The array in the left figure consists of 20 cells, each 2 in. (5.1 cm) in diameter; a closeup of the damaged cell is seen at the right.

encapsulants. Other evaluation methods, which require visual inspection, masking, or detaching individual cells before a test can be run, are slower and less suitable for online testing.

A typical test procedure for a cell would begin by setting the bias light or current level. The laser beam is swept across the cell area in a raster pattern, and the cell is mapped by x-y coordinates as shades of gray, with lighter shades representing higher currents. The electrical image can be viewed on a video display and stored

for signal processing and image enhancement. The scanning beam may be focused down to a diameter of 20 microns to produce a magnified high-resolution image of a smaller area.

An ideal cell would show essentially uniform brightness over its active area. Areas of nonuniformity would appear as brightness variations. Figure 2 shows some typical images obtained by using the scanner. The performance profiles can be compared from cell to cell as a means of quality control, or they can be visually

inspected on a high-resolution TV screen.

This work was done by Michael K. Gauthier, Emmett L. Miller, and Alex Shumka of Caltech for **NASA's Jet Propulsion Laboratory.** *For further information, Circle 59 on the TSP Request Card.*

Title to this invention has been waived under the provisions of the National Aeronautics and Space Act [42 U.S.C. 2457(f)] to Caltech, Pasadena, California 91109.
NPO-14476

Detecting Leaks in Vacuum Bags

A simple low-cost chemical test identifies leaks in vacuum bags.

Lyndon B. Johnson Space Center, Houston, Texas

Small leaks in a vacuum bag can be readily detected by eye, using a simple chemical reaction: the combination of ammonia and acetic acid vapors to produce a cloudy white smoke. The technique has been successfully used to test the seam integrity and to identify minute pinholes in a vacuum bag used in the assembly of the ceramic-tile heat shield for the Space Shuttle Orbiter.

The assembly bag was a heat-sealed container made of a sheet of Mylar laminated between two sheets of heat-sealable polyethylene sheet. However, since the ammonia and

DILUTE ACETIC-ACID VAPOR APPLIED OVER EXTERNAL SURFACE

VISIBLE CLOUD AT DEFECT LOCATIONS

BAG MATERIAL LAMINATED POLYETHYLENE/MYLAR

AMMONIA VAPOR AT ABOUT 1 PSIG

HEAT-SEALED SEAM
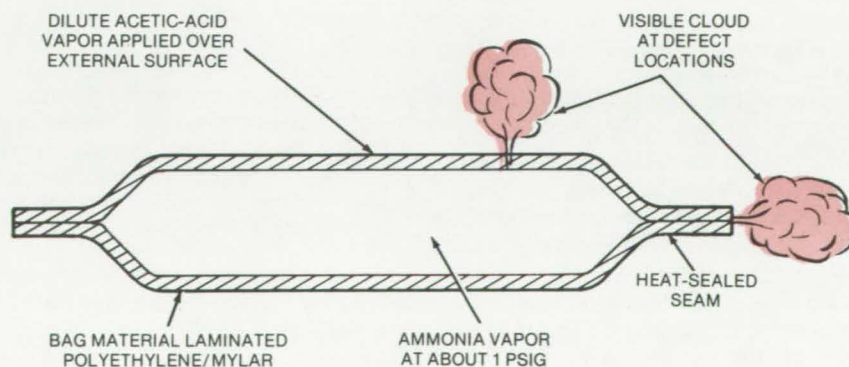
Leakage in Vacuum Bag Material is detected through the reaction of ammonia vapor with acetic acid vapor. Visible clouds of ammonium acetate smoke are produced, clearly showing the tiniest material defects. The previously-used ultrasonic detection method could not locate minute leakage points.

acetic acid vapor used in the leak test are relatively mild chemicals, the technique could be used in many other applications, such as checking packaging film. It has identified leaks that escaped detection by more sophisticated techniques, such as ultrasonic examination.

To check for leaks, the bag is filled with ammonia vapor at slightly-above atmospheric pressure. Then the vapor from a squeeze bottle partially filled with dilute acetic acid is squeezed out over the surface of the bag. Any ammonia vapor escaping through the bag will react with the acid to produce a white cloud of ammonium acetate, easily visible to the eye.

Crack-Opening Displacement Transducer

Accurately measures growth
of short, narrow slots

Langley Research Center, Hampton, Virginia

The effects of artificial flaws on the tensile strength of advanced composite materials (boron/aluminum and graphite/epoxy) are obtained from tests on specimens with cracklike slots machined in them. The specimens are typically 6 to 16 plies thick, vary from 0.75 to 12 inches (19 to 305 mm) wide, and are from 10 to 36 inches (254 to 914 mm) long. Transverse to the load direction, cracklike slots are machined in the center of the specimen through all the plies. These slots are typically 0.007 inch (0.18 mm) wide and vary from 0.02 to 2 inches (0.51 to 51 mm) long.

Clip-on displacement-gage arms do not fit into this narrow slot. In the past, this problem has been overcome by using reference marks 0.2 inch (5 mm) apart and mounting blocks to attach the gage. Thus, the displacement of the mark is measured, instead of the slot edges. This works well for long slots, but not for slots less than 0.4 inch (10 mm) long.

The new crack-opening displacement transducer shown in the diagram consists of a 30° cone, a coil spring, and a linear-displacement transducer. The apex of the cone is inserted into the center of the slot and is held firmly by the spring. The cone is connected to the core of the linear-displacement transducer. A bracket holds the body of the transducer a constant distance from the specimen. When the specimen is loaded, the slot opens. The spring forces the cone into the slot as the opening grows larger. This motion changes the voltage output of the
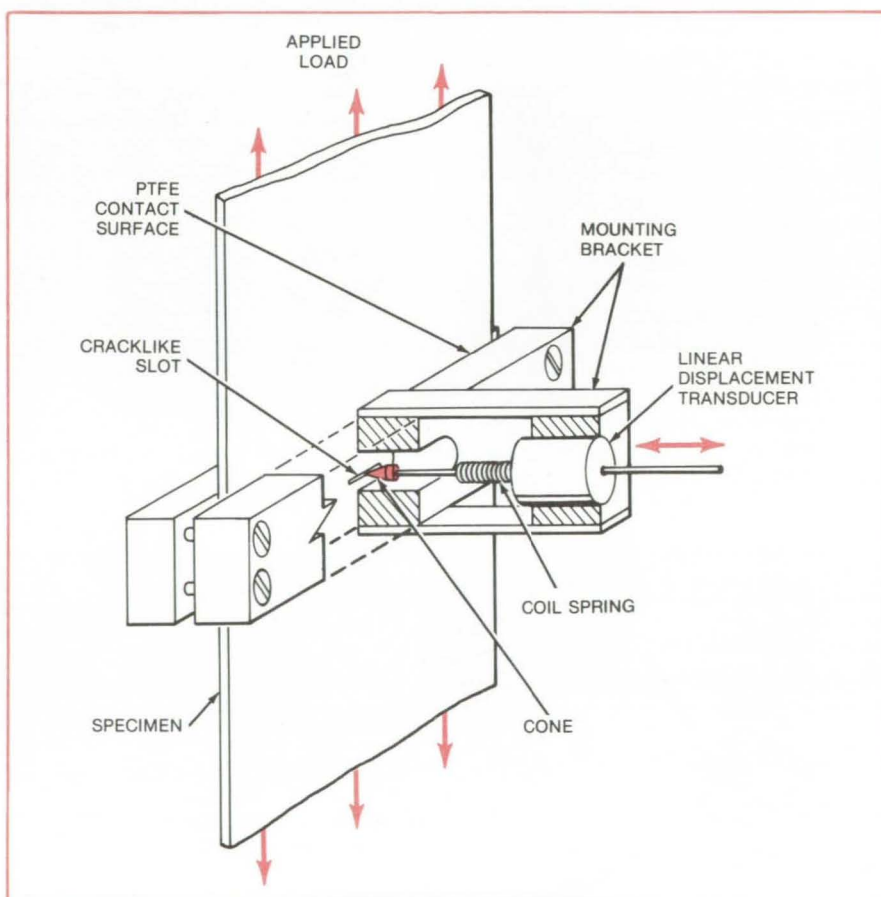
A **Conical Probe** is used to measure crack opening. The cone is pressed firmly into the crack by a spring. As an applied load causes the crack to open up, the cone is pushed further into it. The movement of the cone, and thus the crack growth, is monitored by a linear-displacement transducer.

linear-displacement transducer, which can be converted into displacement of the slot edges.

This method gives more accurate measurement of the crack-opening displacement of very narrow slots.

Peel Testing Metalized Films

Flimsy ultrathin sheets are mounted on
glass for peel-strength measurements.

NASA's Jet Propulsion Laboratory, Pasadena, California

A new technique makes it easier to perform peel tests on metalized plastic films. The technique was developed for determining the peel strength of thin (1,000 Å) layers of aluminum on Kapton film. Previously, this material has been difficult to test because it is flimsy and tends to curl up and blow away at the slightest disturbance.

The technique consists of the following steps (see figure):

a. The metalized plastic film is pressed smoothly onto a wet glass plate, aluminum side against the glass.

b. A fast-setting epoxy resin is pressed between the metalized film and another clean, dust-free glass plate.

c. The first (wet) glass plate is removed, and the aluminum surface is prepared for bonding by a soak in aqueous carbonate solution at 80° C for 1 minute. This step exposes fresh aluminum by removing about 100 angstroms of material from its surface.

d. Another layer of epoxy is pressed between the aluminum and an unmetalized plastic film 1 mil (0.025 mm) thick. The new layers are squeezed back and forth until a uniform wrinkle-free thickness is obtained.

e. The final film/epoxy layer is sliced into strips 0.2 centimeter wide and peeled back slightly.

The glass plate is placed in one of the grips of a peel-test machine (instron, or equivalent). An adhesive tape is attached to the film/epoxy strip, is inserted in the other grip on the test machine, and is pulled away at 180°. The aluminum metalization peels away from its plastic film.

The procedure can be used to measure the effects on metalization bond strength of handling, humidity, Sunlight, and heat.

This work was done by Lawrence Bivins and Tennyson Smith of Rockwell International Corp. for **NASA's Jet Propulsion Laboratory.** *No further documentation is available.* NPO-14672
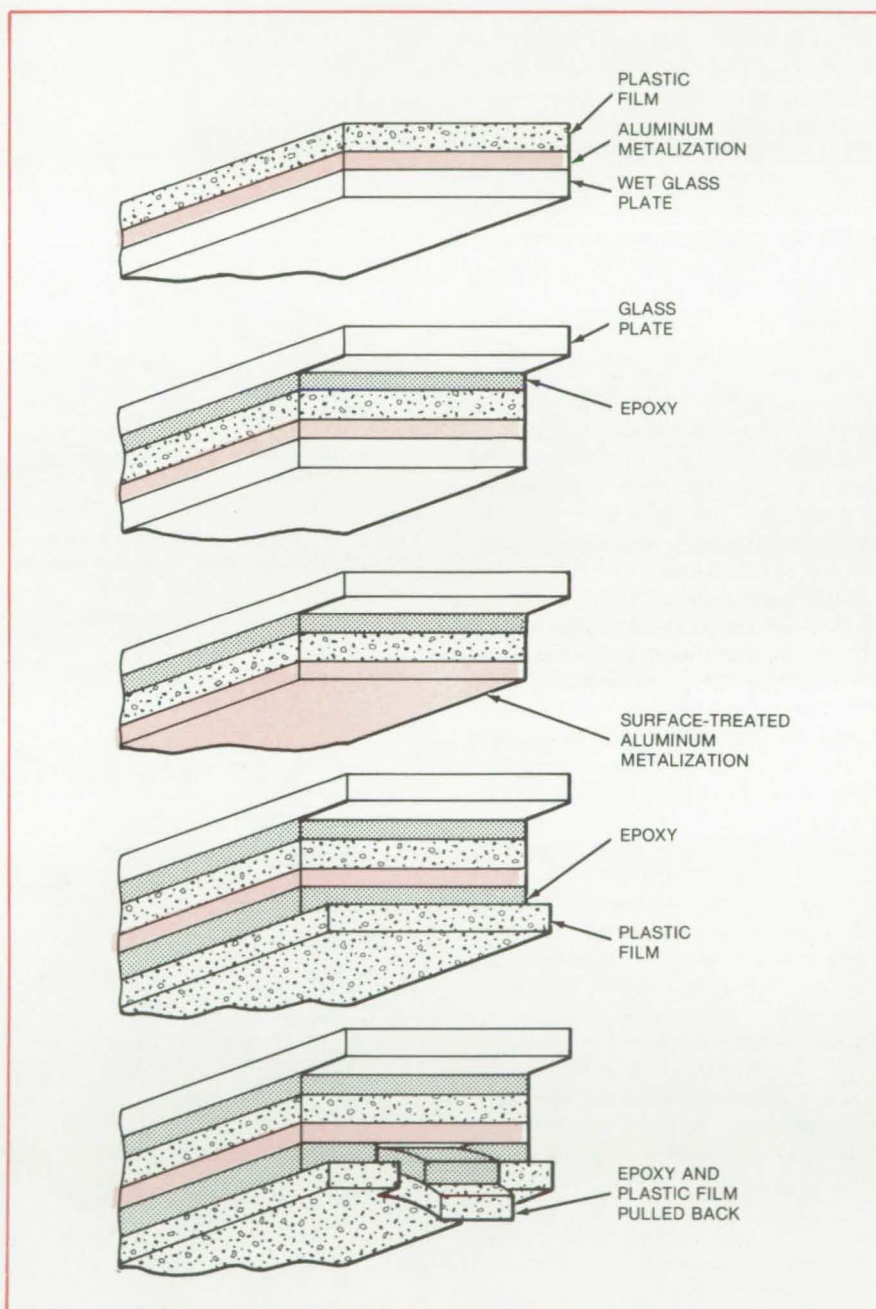
A **Layered Structure** is built up around the metalized plastic film. The topmost glass plate fits in one grip of the peel-testing machine, and the bottommost layers of pulled-back epoxy and plastic film form a tab for connection of the other grip.

Gage for 3-D Contours

A calibrated wedge and a template measure
conformance to a required shape.

Lyndon B. Johnson Space Center, Houston, Texas

A simple gage, used with a template, can help inspectors determine whether a three-dimensional curved surface has the correct contour. The gage was developed as an aid in explosive forming of the Space Shuttle emergency-escape hatch. The hatch is shaped from a machining blank by repeated explosions. The gage is used after each step to determine the proper weight and placement of the next explosive charge.

The gage consists of a wedge-shaped wooden block, calibrated to read in 1/16-in. increments of height. To make a contour measurement, the inspector slips the point of the wedge through one of the holes in the template (Figure 1) and observes the point at which the lower surface of the template coincides with the scale.

The template is a glass sheet curved in the required contour and perforated with holes 3 inches (7.6 centimeters) in diameter, as shown in Figure 2. Small buttons of precise thickness support the template and keep it above the surface to be measured.

Zero on the gage scale corresponds to the button thickness. Thus, a reading above or below zero indicates the distance by which the measured surface is above or below its required contour. For even greater accuracy, the wedge can be made of metal and calibrated by an indexing machine.

*This work was done by Cyrus C. Haynie of Rockwell International Corp. for **Johnson Space Center**. No further documentation is available.*
MSC-19589
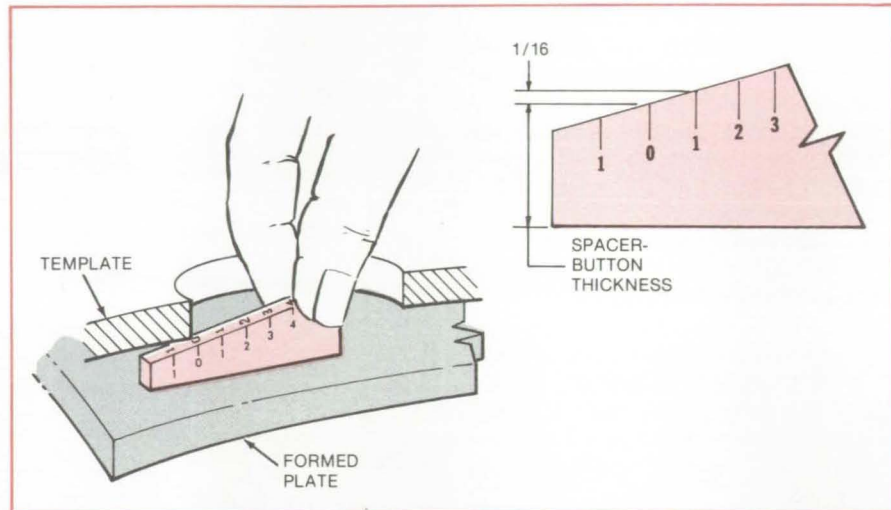
Figure 1. The **Template Touches the Gage** at a point that indicates how far the formed plate deviates from the required contour. Here, the zero indication means that the contour is correct.
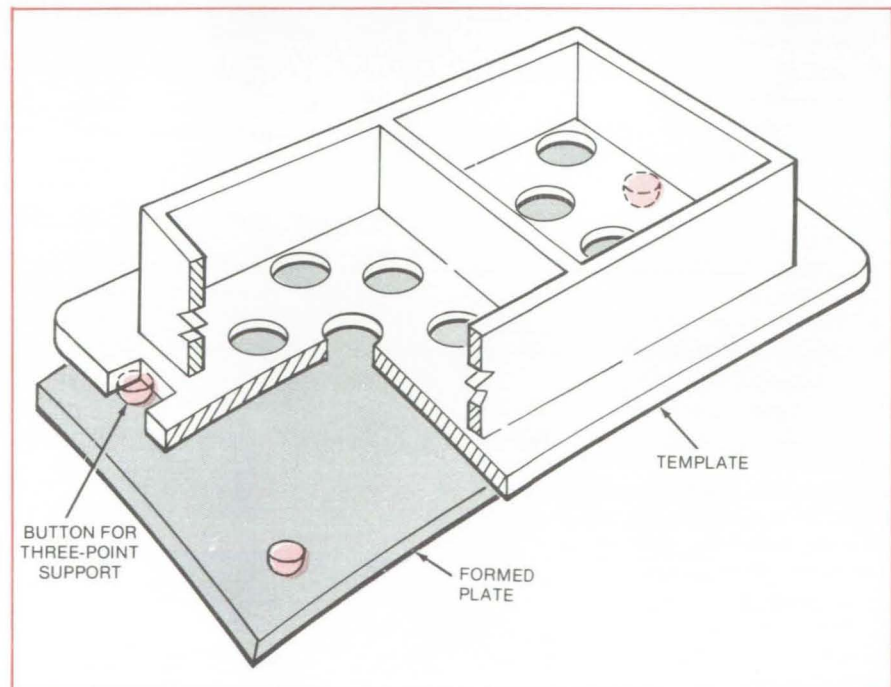
Figure 2. The **Glass Laminate Template** is shaped on a plaster master. It is stiffened by a box frame. Small buttons of precise thickness give three-point support.

Automatic Inspection of Silicon Wafers

Laser machine scans wafers for contaminating particles and transfers
the good wafers to integrated-circuit processing equipment.

Marshall Space Flight Center, Alabama

Silicon wafers can be checked for particle contamination quickly and automatically by a new laser-beam scanning machine. The machine is much faster and more accurate than a human operator using a light-field/dark-field microscope.

The scanner detects particles in the size range from 1 to 20 micrometers. It is used before the wafers are processed into integrated circuits so that wafers with excessive contamination can be rejected. Such particles can cause open circuits, short circuits, and other defects in integrated circuits that have conductor path widths and spacings as small as 2.5 micrometers. For economical manufacturing, it is important to remove particle-contaminated wafers from the production line before they are processed. (Particles below 1 micrometer are not harmful, and those above 20 micrometers are easily removed by standard cleaning procedures.)

The scanner fits into the air-track wafer-transportation system in an automated integrated-circuit production line. It can easily keep up with the 100-wafer-per-hour rate of such lines, and it can be controlled by the same computer that runs the processing equipment.

A helium/neon laser beam scans the wafer (see figure). Particles on the wafer reflect light from the beam into a photodetector, but the photodetector receives no light from the smooth silicon surface. The number of light pulses received by the photodetector is the particle count for a wafer, and the intensity of a pulse indicates the size of the particle.
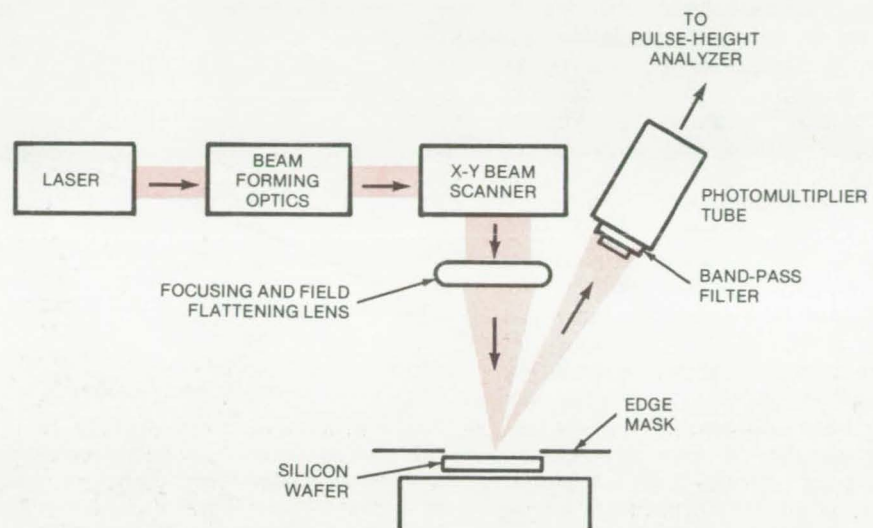
A Particle on the Surface of a silicon wafer reflects light into a photomultiplier tube. A clean surface, however, reflects no light into the tube.

An electromechanical device sweeps the beam in a straight line across the wafer in the x direction and indexes the beam at a frequency of 800 Hz in the y direction. The total scan time for a wafer 3 inches (7.6 cm) in diameter is 2 seconds. A lens focuses the beam to a 50-micrometer spot on the wafer. A highly reflective mask with an opening slightly smaller than the wafer diameter is placed over the wafer during scanning to delineate its edge sharply. A filter on the photodetector aperture discriminates particle-reflected light from background room illumination.

The photomultiplier output passes to a preamplifier, a pulse-height analyzer, and finally a display circuit. Wafer scanning results are displayed on a cathode-ray tube as a map of the wafer, with particles appearing as bright spots on the screen, or as a histogram of particle count vs. particle size. Wafers that fail to meet preselected maximum particle-size and particle-quantity standards are automatically ejected by the machine, and those that pass are automatically sent on to the processing equipment.

This work was done by M. Martin of TAI Inc. for **Marshall Space Flight Center.** *For further information, Circle 61 on the TSP Request Card.*

Inquiries concerning rights for the commercial use of this invention should be addressed to the Patent Counsel, Marshall Space Flight Center [see page A5]. Refer to MFS-25124.

Faired Instrumentation for Aerodynamic Tests

Streamlined package can be installed and removed without
altering the aerodynamic properties of the structure being tested.

Langley Research Center, Hampton, Virginia

Test instrumentation can be installed on helicopter blades without causing damage or significantly affecting airflow. When testing has been completed, the instrumentation can be stripped away without damaging the blade.

Flat electronic circuit boards and sensors are contained in an aerodynamic fairing, which is bonded to the rotor blade (see figure). This instrumentation-mounting technique was developed for measuring the pressure profile and determining noise sources on rotor blades. The adhesive bonds are unaffected by spilled fuel, hydraulic fluid, or synthetic lubricant during the relatively-short test period. Previous attachment methods altered the aerodynamic shape of the blade and damaged the blade surface, thereby reducing its life expectancy. The new method has neither of these disadvantages and, moreover, uses lightweight materials so that the blade balance is maintained.

The first step in the installation procedure is to remove paint from the area of the blade where the instrumentation is to be attached. The paint remover is thoroughly rinsed away with a solvent, and a layer of contact adhesive is applied to the blade. A rectangle of fiberglass cloth 4 mils (0.1 mm) thick is pressed in place over the adhesive.

Next, plastic foam is contoured to fit over the leading edge of the blade and extend about 6 inches (15 cm) toward the rear of the blade, and is bonded to
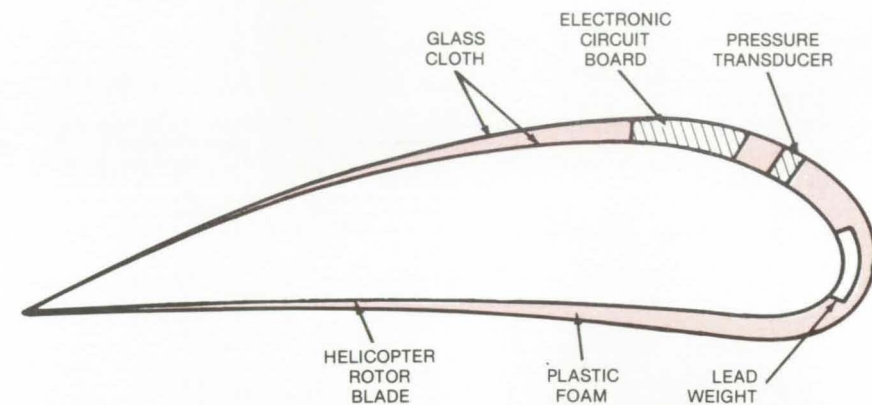
Test Instrumentation consisting of pressure sensors and an electronic circuit board is adhesive-bonded to smoothly-contoured plastic foam, which in turn is bonded to an aerodynamic surface — in this case, a helicopter rotor blade. The addition to the blade is greatly exaggerated in this drawing; the thickness of the instrumentation fairing is only about 0.1 inch.

the fiberglass cloth with an adhesive. The outer face of the foam is cut to present a smooth aerodynamic shape. The forward, rear, and side edges of the foam are sanded to a feathered edge. Maximum thickness of the plastic foam is only about 0.1 inch (0.25 cm).

Holes are cut in the foam to accommodate the circuit board, pressure transducers, and lead wires. These components are inserted in their holes and adhesive-bonded in place. Finally, glass cloth is bonded over the assembly. This covering is trimmed away over the transducer diaphragms, and the instrumentation

package is ready for use.

This work was done by Walt C. Long and Milton L. Williams of **Langley Research Center.** *Further information may be found in the U. S. Patent referenced below, which may be purchased from the U.S. Patent and Trademark Office, Washington, DC 20231, for $0.50 a copy.*

This invention has been patented by NASA [U.S. Patent No. 4,082,001]. Inquiries concerning nonexclusive or exclusive license for its commercial development should be addressed to the Patent Counsel, Langley Research Center [see page A5]. Refer to LAR-11201.

Deflectometer for Precracked Charpy and J$_{Ic}$ Bend Tests

Bend-deflection measurement
for standardized tests

Lewis Research Center, Cleveland, Ohio

In the development of a standardized precracked Charpy slow-bend test, the need arose for a small deflectometer to measure bend deflection. A deflectometer was developed that

uses the ASTM Standard Test E-399 clip-in displacement gage as the sensing element; this gage is available in most fracture-testing laboratories and has good sensitivity and accuracy.

Since the deflectometer uses the same electronics as employed for fracture-toughness testing according to ASTM E-399, laboratories already equipped for standard fracture-tough-
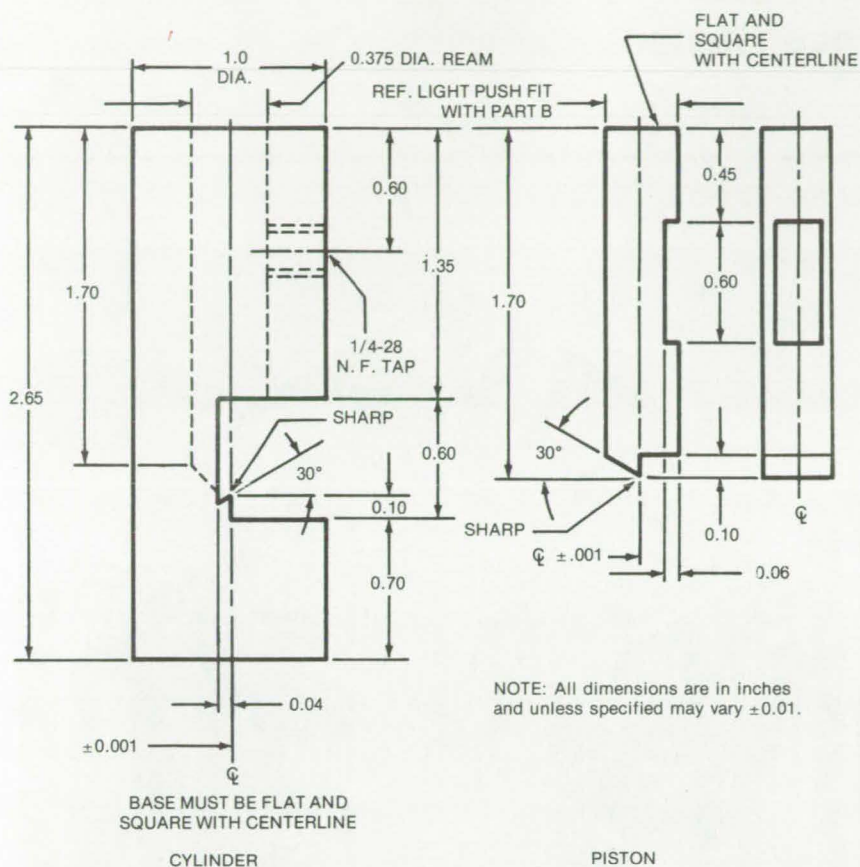
Figure 1. **Detailed Deflectometer Drawing** showing cylinder and piston

Dimensions shown:
- 1.0 DIA.
- 0.375 DIA. REAM
- REF. LIGHT PUSH FIT WITH PART B
- FLAT AND SQUARE WITH CENTERLINE
- 0.60
- 1.35
- 0.45
- 0.60
- 1.70
- 1/4-28 N. F. TAP
- SHARP
- 2.65
- 30°
- 0.60
- 0.10
- 0.70
- SHARP
- 30°
- 0.10
- 0.06
- 0.04
- ±0.001
- ±.001

NOTE: All dimensions are in inches and unless specified may vary ±0.01.

BASE MUST BE FLAT AND SQUARE WITH CENTERLINE

CYLINDER

PISTON

Figure 2. **Assembled Deflectomer**

Figure 3. **Bend-Test Setup** shows application of deflectometer with clip-in displacement gage.

ness testing require no additional expense for electronic equipment to use the deflectometer.

The deflectometer directly measures the change in distance between the bend-specimen undersurface and the base of the test fixture and can be used for sensitive and accurate measurement of distance change in J_{IC} bend tests and other not-necessarily related applications. The device consists only of a cylinder and piston, with knife-edge attachment of the ASTM clip-in gage for sensing relative motion between the two components. It is shown in detail in Figure 1 and assembled in Figure 2. Figure 3 is a schematic of a typical bend-test setup incorporating the deflectometer.

Zone-Controlled Resistance Heater

Temperature varies with time and
location under computer command.

Lyndon B. Johnson Space Center, Houston, Texas

A geodesic array of heaters pro-
duces controlled temperatures over
many independent zones. The array
can be arranged to conform to and
enclose virtually any shape, with close
thermal coupling; and it can be
programed to reproduce almost any
desired time/temperature distribution.
Each of the 18 graphite resistance
heaters in the array is powered by a
separate electrical supply unit and
silicon-controlled-rectifier (SCR) con-
trol unit. Under the command of a
computer the SCR's produce the time-
varying temperature distribution.

The heating system was developed
to simulate reentry temperatures in
tests of the Space Shuttle nose cap
(see figure). The computer-controlled
heater array may also be useful in
producing zone-controlled heat reac-
tors for coal gasification, in testing
ceramic materials, and as a simulated
heat source for testing energy gener-
ators and collectors. The heaters can
create temperatures up to 2,600° F
(1,400° C).

Two types of graphite heater ele-
ments are used in the array. Serpen-
tine elements are used in 12 zones
over the nose-cap semihemispherical
surface. Straight rectangular bars are
used around the nose-cap skirt. The
serpentine heaters were specially
developed to produce the required
power density with minimum separa-
tion between the heater and the nose-
cap surface.

The zone temperatures are sensed
by thermocouples affixed to the back
surfaces of the nose cap — one
thermocouple in the center of each
cap. The thermocouples furnish
closed-loop feedback to the controller.
Air blowers on the back surface allow
the heating elements to be cooled off
quickly in response to commands from
the controller.
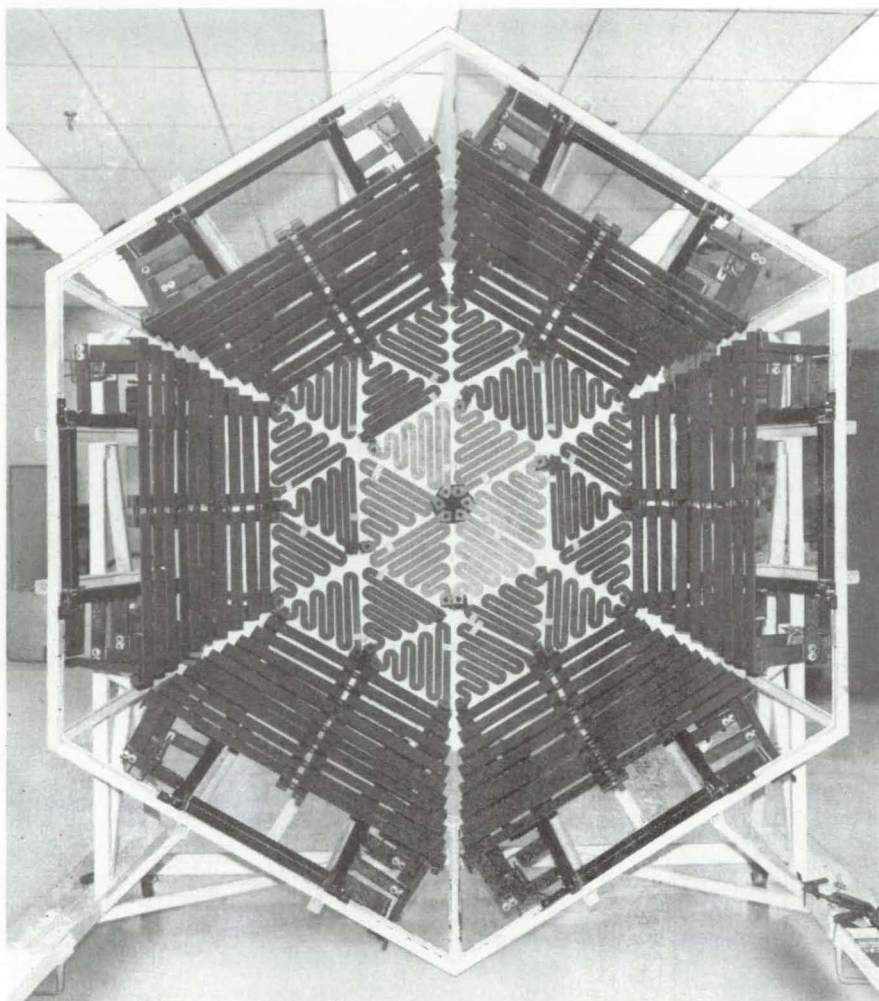
Heater Array for Testing Nose Caps utilizes serpentine graphite elements at the
curved end of the cap and straight graphite bars around the skirt of the cap.

The graphite elements were select-
ed over quartz lamps and silicon
carbide bars because those heaters
cannot produce the required high
temperatures and cannot be oriented
to produce the required temperature
distribution. With a thin ceramic
coating, the graphite heaters can be
used in an oxidizing environment.

*This work was done by Phillip R.
Bagwell of Vought Corp. for* **Johnson
Space Center.** *No further documen-
tation is available.*
MSC-16251

Energy Saver for Industrial Lighting

An electronic controller switches lights on or off
in response to the amount of Sunlight available.

John F. Kennedy Space Center, Florida

NOTES:
a. All resistors are in ohms and 1/4 W, 10%
   unless otherwise stated.
b. The variable resistors are 2 W, 10%.
c. $D_{1,2,3}$ are 1N4001.
d. D_4 is a Zener diode rated at 5.1 V, 1 W.
e. $Q_{1,2,3,4}$ Triac 1.6 A rms minimum
   (TECCOR L2001M3 or RCA 2300A)
f. $Q_{5,6}$ are 2N2222
g. All components may be replaced by equivalent
   parts.
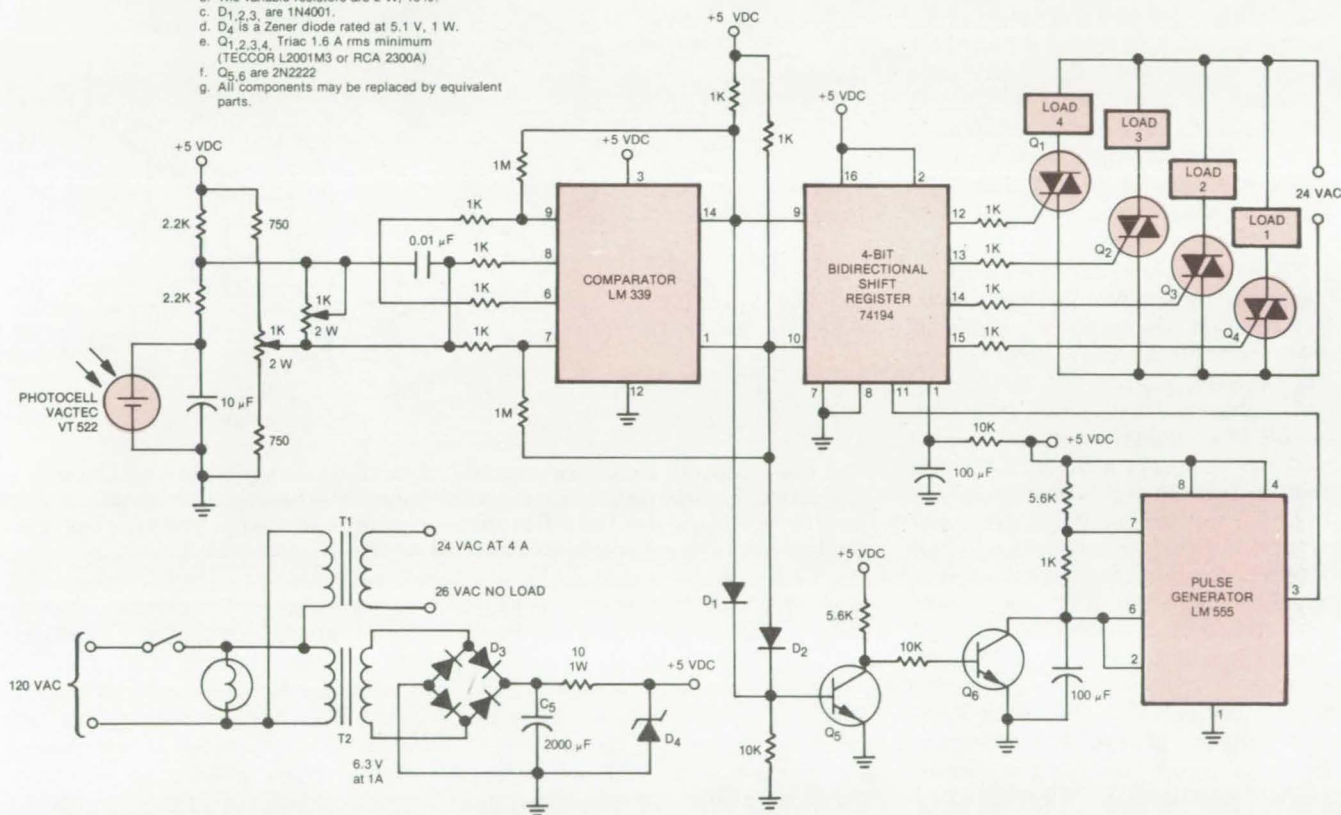
The **Sunlight Intensity Monitor** adjusts artificial lights according to the amount of Sunlight available inside the building. Lights
are turned on or off selectively via the photocell/comparator/shift register, which responds to the photocell monitoring the area.

Many offices and industrial installations waste electrical energy by using artificial light in Sunlit areas. This can be corrected with a compact inexpensive electronic monitor that varies artificial lighting according to the amount of Sunlight available to a given area. It serves essentially the same function for a lighting system that a thermostat serves for heating and air-conditioning.

The unit, as shown, incorporates a photocell that detects changes in Sunlight level over a monitored area. The changing illumination increases or decreases the cell resistance, causing voltage imbalance across a quad comparator (gate). The change in voltage activates the gate, which in turn, triggers the pulse generator. The output pulse signals are fed into a shift register. The shift register responds to comparator and pulse generator inputs by actuating a switching circuit determined by the register input. The switching circuit may incorporate Triacs, SCR's, thyristors, or relays, each connected to a corresponding bank of lights. The lights are turned on or off in sequence until the preselected intensity is reached.

The cell is usually mounted on a ceiling and pointed to an area of the room where the illumination is representative of the entire room. Care is taken to prevent direct cell exposure to Sunlight or artificial light. The controller operates at a low voltage and requires little current. The circuit is idle much of the time and is only actuated as the Sunlight intensity is changing.

Compact Thermocouple Reference for Vacuum Chambers

Self-contained reference includes
its own heater and power controller.

Lyndon B. Johnson Space Center, Houston, Texas

The standard setup for transferring thermocouple signals through a vacuum-chamber wall requires a custom feedthrough with pins made of the same material as the thermocouple wire. To complete the connection between the thermocouple junction inside the chamber and a commercial reference-junction box outside, thermocouple wires terminated by matched plugs are connected to both sides of the feedthrough.

A simpler, less costly approach, particularly when many thermocouples are required, utilizes a compact, self-contained reference-junction box that is installed inside the vacuum chamber. Shown in the accompanying figure, this unit accommodates up to 300 thermocouple signals. Since the box is installed inside the chamber, only a short length of thermocouple wire is required between it and each junction. Connections to outside monitoring instruments are made with conventional copper wire, so standard connectors and feedthroughs may be used.

The thermocouple reference junction consists of four basic components: a power controller, a radiant heater, terminal-block reference junctions, and thermal insulation. The main element of the power controller is a common gate-controlled semiconductor switch. It is energized by a 110-Vac, 10-A power source.

The resistance-heating coil is mounted on the outer shell of the junction box. The heater is backed with reflective tape to minimize
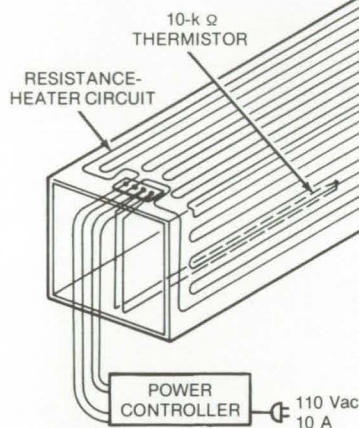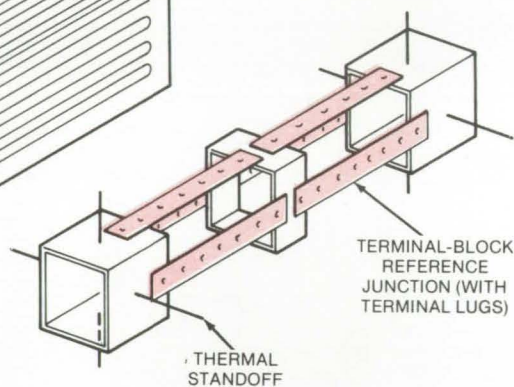
The **Thermocouple Reference Junction** is installed within a vacuum chamber. It consists of a power controller, a radiant heater, terminal-block reference junctions, and thermal insulation. The inside absorbing surface of the outer radiating shell and the terminal lugs are coated to obtain an emissivity of about 0.9.

radiation losses. The shell is fabricated from aluminum, and its outer surface is left untreated.

The terminal-block reference junctions are commercially-available terminal strips, and the thermal insulation consists of a minimum of eight layers of aluminized polyester film. The film completely encompasses the outer shell and is sealed at the cable penetrations.

To operate the unit, thermocouple wires are attached to the terminals, and copper wires are mated to them through the terminals. The inner assembly is mounted within the radiant heater, and the thermal insula-

tion is installed. The copper cables are terminated with a commercial connector at the chamber bulkhead. The power controller is energized to set the reference-junction temperature [150° F (65° C) in the present design]. The unit has been used at vacuum levels of less than 1×10^{-6} torr and at temperature extremes of $+450°$ F (230° C) and -320° F (-195° C).

This work was done by John C. Fay and John D. Glover of Rockwell International Corp. for **Johnson Space Center.** *No further documentation is available.*
MSC-19651

Fiber-Optic Proximity Sensor

Proximity sensors are more
sensitive using fiber optics.

NASA's Jet Propulsion Laboratory, Pasadena, California

A proposed proximity sensor for the mechanical hand of a remote manipulator incorporates fiber optics to conduct signals between the light

source and the light detector. The fiber optics are not prone to noise from electromagnetic interference (EMI) and radio-frequency interference

(RFI) as are sensors using long electrical cables [up to 100 ft (30 m)] for the same purpose. Noisy environment significantly reduces the sensitivity of conventional sensors.
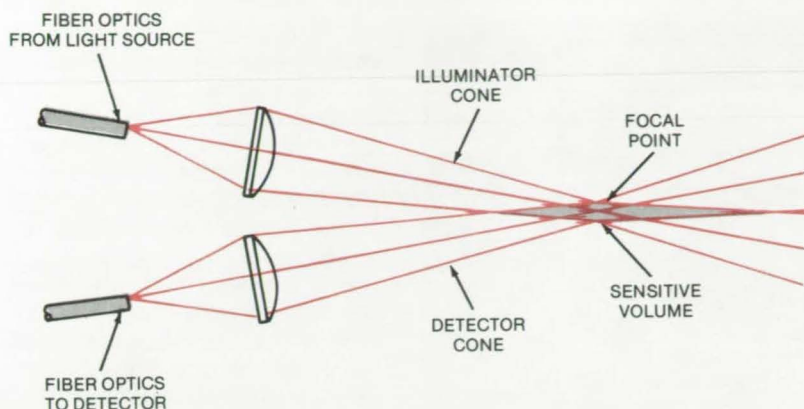
Figure 1. **Fiber Optics** connecting light source and detector with respective lenses of a proximity sensor are immune from "noisy" environment (EMI and RFI), unlike electronic cables that were used previously for the same purpose. This immunity makes the system more sensitive to objects in adverse environment.

The proposed sensor (see Figure 1) uses two lenses mounted on a finger of the mechanical hand. One lens connected to the light source via fiber optics projects an infrared beam ahead of the hand. The other lens connected by the same means to a photodetector is aimed in a direction intersecting the beam. The intersection forms an imaginary volume that defines the region of sensitivity to objects. The volume can be modified depending on how the lenses are positioned to detect farther or closer objects.
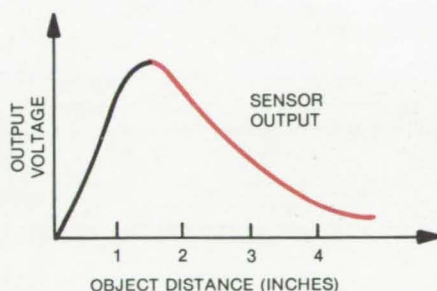
Figure 2. **Typical Detector Response Curve** to detected objects: Only the right half of the curve is used for detection.

One or several proximity sensors (one on each "finger") may be mounted on the mechanical hand. Several sensors of course make a more versatile system. Each sensor generates a voltage signal in response to the detected object. Since the response curve is bell shaped (see Figure 2) as a function of object distance, the sensor heads are moved inside the "fingers" by a distance equaling the distance projection of the inner leg of the signal curve. The object distance then becomes a single-valued function of the voltage output.

The proposed system will use low-attenuation (0.5 dB/m) fiber-optic cables cut to 5.5-m lengths. The lenses are 2 mm in diameter separated by 8 mm between the optical axes. The system will use an infrared light source pulsed for 6 μs at a 6-kHz rate. The system sensing range will be about 7 to 8 cm.

This work was done by Antal K. Bejczy, Wilbert A. Hermann, and Howard C. Primus of Caltech for **NASA's Jet Propulsion Laboratory.** *For further information, Circle 63 on the TSP Request Card.*
NPO-14653

Safety Shield for Vacuum/Pressure-Chamber Windows

An optically-clear shatter-resistant shield
reduces implosion and explosion hazard.

Goddard Space Flight Center, Greenbelt, Maryland

An optically-clear shatter-resistant safety shield (see figure) protects workers from the implosion and explosion of vacuum and pressure windows. In tests, a plastic (Plexiglas, or equivalent) plate, 1/2 inch (1.2 cm) in thickness, spaced 1 in. (2.54 cm) from a chamber viewing port, was not broken when bombarded by explosive fragments from a shattered port window.

In high-vacuum and pressure-chamber systems, the cycling of the chamber pressure can damage the

viewing-port seal and weaken the window. Unlike built-in double-pane or mesh-reinforced viewing ports, however, stresses placed on the window do not affect the safety shield because it is not a part of the seal.

Conventional reinforced viewing ports are costly to manufacture; and because of the double refraction of light passing through dual windows or interference from a reinforcing grid, they restrict the view. The plastic shield, in contrast, is inexpensive, and it allows an unobstructed view of the

interior of the chamber. A bevel edge around the shield prevents chipping.

As shown, the safety shield can have the same shape as the viewing port, although this is not essential. For a circular port, the radius of the shield should exceed the radius of the porthole viewing area by about 1 inch. This allows holes to be drilled for attaching the shield to threaded rods extending from the viewing-port collar.

These shields can be added to vacuum chambers, pressure chambers, and gas-filling systems. They
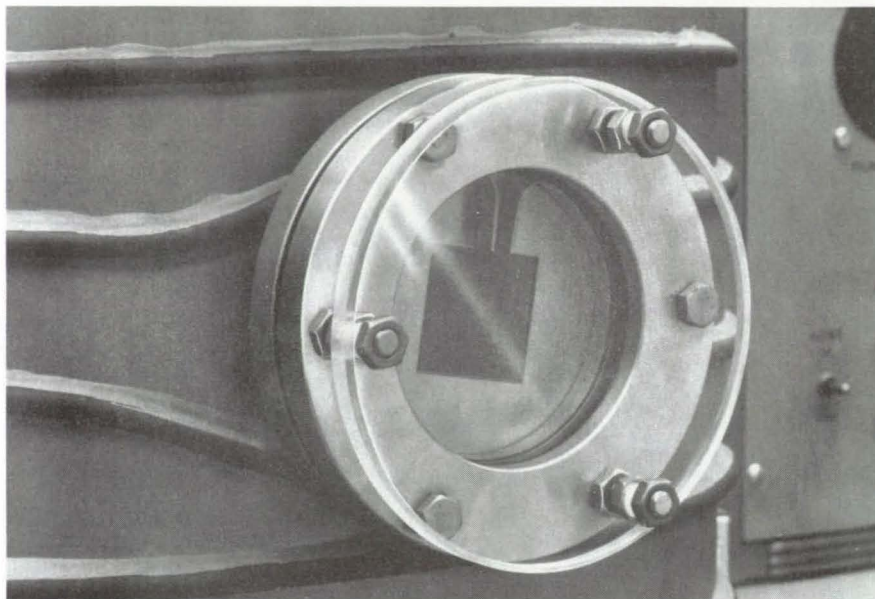
The **Safety Shield** is slightly larger than the viewing window so that holes can be drilled along the periphery to receive the ends of threaded rods. The shield is fastened to the rods by inner and outer locknuts, which allow adjustment of the airgap between the shield and the window.

can also be modified for use as an enclosure for ionization gages.

This work was done by Richard A. Shimansky and Rodney Spencer of **Goddard Space Flight Center.** *For further information, Circle 64 on the TSP Request Card.*

This invention is owned by NASA, and a patent application has been filed. Inquiries concerning nonexclusive or exclusive license for its commmercial development should be addressed to the Patent Counsel, Goddard Space Flight Center [see page A5]. Refer to GSC-12513.

Books and Reports

Lightning Protection for Aircraft

Special emphasis on the consequences of modern nonmetalic materials

A reference book has been published that summarizes current knowledge concerning the potential lightning effects on aircraft and the means available to designers and operators to protect against these effects. This book is of particular importance because of the increasing use of nonmetallic materials in aircraft structural components and the increasing use of electronic equipment for control of critical flight operations and navigation.

Nonmetallic structures are inherently more susceptible to lightning-strike damage. They also provide less shielding against the intense electromagnetic fields of lightning than do metallic structures. These fields have been known to cause damage to or upset electronic equipment.

In the past decade, these and other concerns (such as fuel system vulnerability to lightning) have led to increased research into lightning effects on aircraft. The results of these research activities have been reported in the technical literature, in conferences and symposiums, and in informal exchanges between scientists and engineers. This book organizes and summarizes much of this current body of information. Emphasis is placed upon those facts that are of most use and benefit to the aircraft designer and operator in achieving flight safety in the lightning environment.

The book is organized into 17 chapters. The first chapter reviews the nature of lightning and how it originates. The second chapter describes how aircraft become involved with lightning flashes and why aircraft may

sometimes "trigger" a flash. Chapter 3 looks at lightning-strike statistics and reviews avoidance procedures now in use by operators and their degree of success. The fourth chapter summarizes the various consequences of lightning-struck aircraft. Chapters 5, 6, and 7 discuss protection against direct physical damage effects. Chapter 6 addresses lightning effects on aircraft fuel systems and design approaches to protect against these effects. The seventh chapter deals with the protection of aircraft from structural damage with emphasis on nonmetallic materials.

The remainder of the book deals with indirect effects. Basic mechanisms by which induced voltages occur in aircraft electrical circuits are introduced in chapter 8, and chapters 9 through 14 treat these mechanisms in greater detail. The impact of induced voltages on solid-state devices and how these devices may be protected are considered in chapters 15 and 16. Chapter 17 describes testing methods for determining the susceptibility of the aircraft and the vulnerability of equipment to indirect

effects. Methods for assessing the effectiveness of protection techniques are also discussed.

Although this book is primarily oriented to the aircraft designer and operator, much of the information may be useful to mitigating lightning problems associated with terrestrial facilities.

This work was done by F. A. Fisher of General Electric Co. and J. A. Plumer of Lightning Technologies, Inc., for **Lewis Research Center.** *Further information may be found in*

NASA RP-1008 [N78-11024/NSP], "Lightning Protection Aircraft" [$16.25]. A copy may be purchased [prepayment required] from the National Technical Information Service, Springfield, Virginia 22161. LEW-12981

Computer Programs

Fan Noise-Mode Structure in a Duct

Method and computer package for analysis

Two new computer programs help the analyst meet low-noise limits on turbofan engines. The first, the Microphone Location Program, computes the optimum locations in the turbofan duct for the placement of microphones. The number of microphone locations must equal the number of sound modes to be determined. Inputs to this program are the sound-field model including the desired number of modes, the geometry of the placement region including duct radius and hub/tip ratio, and the test parameters such as frequency, axial-flow mach number, and the speed of sound. The output is the locations where the microphones are to be placed, selected such that use of these positions will result in numerically stable solutions of the subsequent mode-structure determination. The suitability of an already-existing set of locations can also be assessed by the Microphone Location Program.

After the tests have been run with the microphones placed at the calculated positions, inputs used in the Microphone Location Program plus the measured acoustic phase, amplitude, and pressure are used as inputs to the second program — the Modal Calculation Program. This program is then used to determine the fan sound-mode structure by calculating the modal amplitudes and phases. A set of influence coefficients is also calculated for use in determining the sensitivity of the modal calculations to errors in both microphone placement and microphone readings.

Since the number of pressure measurements equals the number of modes, a like number of equations result, which are treated in matrix form, inverted to solve for amplitude and phase, and then reduced to a triangularized matrix by Gaussian elimination to obtain the complex modal coefficients.

These programs are written in FORTRAN IV and have been implemented on the IBM 360 computer, with the larger program having a central memory requirement of approximately 366K of 8-bit bytes. Both programs were developed in 1977.

This program was written by R. A. Love, G. F. Pickett, and R. A. Wells of Pratt & Whitney Aircraft Group for **Lewis Research Center.** *In addition to the computer program available by using the COSMIC Request Card [Circle E], related information on this technique may be found in:*

NASA CR-135295 [N78-17066/ NSP], "Method of Fan Sound Mode Structure Determination Computer Program User's Manual, Modal Calculation Program" [$5.25];
NASA CR-135294 [N78-17065/ NSP], "Method of Fan Sound Mode Structure Program User's Manual, Microphone Location Program" [$5.25];
NASA CR-135293 [N78-17064/ NSP], "Method of Fan Sound Mode Structure Determination, Final Report [$8.00].

Copies of the three documents above may be purchased [prepayment required] from the National Technical Information Service, Springfield, Virginia 22161. LEW-13129

Electric-Car Simulation

Interactive-program for designers

PARAMET, an interactive simulation program for parametric studies of electric vehicles, guides the user through a simulation by a menu and a series of prompts for input parameters. The program provides the actual Ripp Electric Vehicle parameters as default parameters. It considers aerodynamic drag, rolling resistance, linear and rotational acceleration, and road gradient as the forces acting on the vehicle.

For maximum performance simulation, there are two choices of acceleration models: One assumes linear acceleration; the other assumes that the vehicle is torque-limited below a certain speed and is power-limited above that speed (a Larrabee model). Both acceleration techniques consider rotational inertia when calculating acceleration. A modified fractional-utilization battery model is used for the vehicle battery; the model is based on a Ragone equation technique with coefficients that are user-controlled inputs. The battery model accounts for regenerative braking and battery recuperation while the vehicle is idle.

An efficiency function covers the effects of the motor/controller, transmission, differential, and shift logic. This drive-line efficiency function can have up to 9 straight-line segments and 10 breakpoints. One has a choice of using a driving-cycle approach or a constant speed with an optional road grade. Information that defines the SAE J227 driving cycles for schedules B, C, and D is incorporated into the program.

PARAMET accepts data from an external file to define the EPA highway and urban driving cycles. There are 12

menu items available: total vehicle weight, battery weight, drag coefficient, frontal area, drag coefficient/frontal area product, tire coefficient of resistance, drive-line rotating-mass factor, drive-train efficiency characteristics, battery charge/discharge polynomial coefficients, driving cycle or constant speed and grade, regenerative braking factor, battery recuperation factor, and a code to restart solicitation of model parameters.

The parameters that will be used in the simulation are all printed as part of the results. Output from the program for a simulation consists of: the vehicle range, the energy consumed, the cost in dollars per mile (at $0.04 per kWh for energy), efficiency, and the peak required power. The peak required power is broken down into the following parts: aerodynamic power requirements, rolling resistance, and power used in climbing a grade. There is an option to print the total power, acceleration power, aerodynamic power, rolling power, speed, acceleration, and efficiency in 1-second increments for an entire driving cycle.

This program is written in FORTRAN IV and has been implemented on an IBM 360 with a central memory requirement of 74K bytes. Development of this program was completed in April 1978.

This program was written by C. Phil Chapman and Ronald A. Slusser of Caltech for NASA's Jet Propulsion Laboratory. For further information, Circle F on the COSMIC Request Card.
NPO-14570

Phase Changes in Liquid Face Seals

Simplified program produces accurate predictions.

A simplified computer program predicts boiling (phase change) in liquid face seals. The program determines if and when boiling occurs; then it calculates the location of the boiling interface, the pressure and temperature profiles, and the load.

The main assumption, which allows for a simplified analysis, is the assumption of an isothermal gas phase. The results compare almost identically with a previously-developed more-exacting computer program.

This much simpler program should be of immediate use to the design engineer.

A liquid face seal may be placed in one of two general categories: (1) hydrodynamic seals, in which the principal agent responsible for fluid migration is pumping within the clearance space due to irregularities in the mating seal-plate surfaces, and (2) pressure seals, in which the driving force for fluid migration is an externally applied pressure differential across the seal. Because the analysis is simpler in the case of pressure seals, this computer program deals exclusively with pressure seals.

The program incorporates a conceptual model having the following features: (1) The seal plates are modeled as uniform semi-infinite solids having identical thermal conductivity (if the actual seal being modeled has plates of differing conductivity, the average of the conductivities of the two plates is used in the computer model); (2) the fluid flow regime in the film space between the seal plates is divided into two annular regions — a liquid region where viscous heating due to high fluid shear rates and high absolute viscosity occurs and a gas region where the vapor phase of the fluid is assumed to behave like a perfect gas (because of low gas viscosity the viscous dissipation in the gas region is neglected); (3) the properties of the fluid and the seal plates are assumed to be uniform and constant; (4) the temperature of the seal plates at infinity is assumed to equal the temperature of the fluid reservoir or the structure of the machine, of which the seal is a part, far from the seal; and (5) the change of phase occurs over a region of negligible width compared to the seal-plate width, and the heat required for vaporization is negligible compared to the heat generated by viscous dissipation in the liquid.

The program uses the data, and it outputs pressure and temperature distributions, leakage rates, and absolute load. It is capable of handling liquid seals and gas seals in addition to mixed-phase seals.

The program is written in both FORTRAN IV and BASIC-PLUS for use on a PDP-11 computer. With the use of the BASIC-PLUS program, the interaction between the person running the program and the computer is

conversational in nature, so that someone unfamiliar with the program may run it with a minimum of difficulty. All output is given in both English and SI units.

This program was written by William F. Hughes of Carnegie-Mellon University for Lewis Research Center. For further information, Circle G on the COSMIC Request Card.
LEW-12994

Coupled-Cavity Traveling-Wave Tubes

TWT analysis and design

A computer program has been developed for the analysis of coupled-cavity traveling-wave tubes (TWT's). Traveling-wave tubes are used in a variety of radar and communications applications.

Coupled-cavity TWT's differ from conventional TWT's in that the helix delay line is replaced by a chain of cavities connected by apertures in the common cavity walls. Consequently, coupled-cavity tubes are quite rugged and have high power-handling capability. However, they do not have large bandwidth capability and are more expensive to fabricate than conventional helical TWT's. Coupled-cavity TWT's are used primarily in high-power radar and communications applications where the bandwidth capability of helical TWT's is not needed and the power-handling capability of helical TWT's is inadequate.

The computer program was developed to provide an analytical tool for the evaluation of coupled-cavity TWT efficiency-enhancement schemes (e.g., through velocity resynchronization or other methods that improve the efficiency of the basic interaction process in these devices). It may also be used for routine TWT design.

The program provides a flexible, accurate, large-signal, one-dimensional TWT analysis. The beam is described by a disk model, and the slow-wave structure is described by a sequence of cavities or cells. The computational approach is arranged so that each cavity may have geometrical or electrical parameters different from those of its neighbors. This allows the program user to simulate a tube of almost arbitrary complexity.

Input and output couplers, severs, complicated velocity tapers, and other features peculiar to one or a few cavities may be modeled by a correct choice of input data. The beam-wave interaction is handled by a new approach in which the radio-frequency fields are expanded in space harmonic solutions to the transverse magnetic-wave equation. All significant space harmonics are retained.

The program was used to perform a design study of the traveling-wave tube developed for the Communications Technology Satellite (CTS). Good agreement was obtained between the predictions of the program and the measured performance of the flight tube.

This program is written in FORTRAN IV for use on an IBM 360/67 time-sharing system.

This program was written by Denis J. Connolly and Thomas A. O'Malley of **Lewis Research Center.** *For further information, Circle H on the COSMIC Request Card.*
LEW-12861

Natural Modes of Helicopter Rotor Blades

An improved computational procedure

The accurate calculation of the undamped natural frequencies and mode shapes of rotor blades is an important first step in analyzing the dynamic behavior of helicopter rotor systems. A computer program based on the Holzer-Myklestad approach calculates the coupled vertical (out-of-plane), horizontal (in-plane), and torsional characteristics of a wide variety of hub and blade configurations of practical interest. The Holzer-Myklestad approach represents the helicopter blade by a lumped-mass system that includes the effects of rotary inertia, blade geometric pitch, and inertial and elastic coupling among the five degrees of freedom at each mass station. Shear deformation, aerodynamic effects, and built-in coning are not included in the analysis. The accuracy of the program has been demonstrated in comparisons with exact solutions to classical problems and experimental data.

The rotor blade is considered as a discretized system of finite elements with each element representing a segment of the blade. The user supplies data pertaining to the average structural properties for each segment. The blade segments are modeled by a finite-element representation with all the inertia lumped at the inboard end and a stiffness element extending over the segment length. It is assumed that the cross-sectional principal structural-stiffness and mass axes are parallel.

Deflections, slopes, forces, and moments at the inboard end of each segment due to conditions at the outboard end of each segment are calculated by a series of recursion equations. The hub configuration and support-system impedance characteristics are expressed as boundary conditions. Thus, an eigenvalue problem is formed where the vibratory frequency may be systematically varied and conditions along the blade calculated for each unity tip displacement. These conditions are used to determine that the boundary conditions are satisfied. In the analysis, three basic sets of boundary-condition equations are used, and the resulting modal characteristics are designated as pertaining to collective, cyclic, and scissors modes. Using an iterative procedure, the relative tip deflections for a mode are determined. From this, the span-direction distributions of deflections, slopes, shears, and moments for each unit tip deflection; the mode shapes; and the associated shear and moment distributions are calculated. Output includes plots for visual analysis and punched output for input to rotorcraft simulation programs.

This program is written in FORTRAN IV and has been implemented on the CDC CYBER 175 with a central memory requirement of approximately 64K (octal) of 60-bit words. For plotted output, access to a CALCOMP plotting system is required. The program was developed in 1978.

This program was written by Raymond E. Mineck and William H. Weller of the U.S. Army R&T Laboratories [AVRADCOM] for **Langley Research Center.** *For further information, Circle J on the COSMIC Request Card.*
LAR-12501

Interfering Surfaces in Subsonic, Transonic, and Supersonic Flow

A steady and oscillatory kernel-function method

Interest in aircraft designed to operate efficiently in the high subsonic regime has grown considerably. This has increased the need for better unsteady, transonic, aerodynamic analysis techniques so that flutter and dynamic response characteristics can be predicted accurately in this flow regime. The characteristic of transonic flow, which causes the greatest difficulty when attempting to apply uniform flow theory to such problems, is the presence of shocks embedded in the flow. Linear theory cannot account for this phenomenon, and finite-difference approaches often require extremely costly amounts of computer time.

A computer program was developed to provide an analysis method based on a kernel-function technique that uses assumed pressure functions with unknown coefficients. With this technique, generalized forces can be calculated in unsteady flow, and pressure distributions can be obtained in both steady and unsteady flow. Once the aerodynamic matrices are computed and inverted, they may be saved and used on subsequent problems at very little cost as long as mach number, reduced frequencies, and aerodynamic geometry remain unchanged. This method should be particularly useful for design applications where the structural mode shapes change continually due to structural changes and payload variations while the aerodynamic parameters remain constant.

A wing over which the flow has mixed subsonic and supersonic components with embedded shocks is treated as an array of general aerodynamic lifting-surface elements. Each element is allowed to have mutual interference with the other elements. Each element is assigned the appropriate mach number, and its downwash is modified accordingly. The mach number distribution and shock geometry may be obtained either experimentally or by a finite-difference technique.

The solution proceeds in a manner identical to ordinary aerodynamic interference methods based on a collocation technique. The unknown pressure function is assumed to be composed of a series of polynomials weighted by a user-selected weighting function that is characteristic of each lifting surface. The nonplanar kernel function is computed using a mach number, and a reduced frequency is determined from values at a downwash control point. To link subsonic and supersonic linear-theory solutions, it is assumed that the appropriate mach number for computing downwash at a point is the mach number at that point. It is further assumed that the reduced frequency is modified according to the local velocity such that the physical frequency is held constant.

Thus, the computation procedure becomes a problem of testing the mach number of the downwash point. If the downwash point is supersonic, the self-induced downwash and all interference effects at that point are computed with the supersonic kernel function. Likewise, if the downwash point is subsonic, the subsonic kernel function is used. The presence of a normal shock is simulated by a line doublet that represents the load induced by shock movement. The appropriate steady or unsteady normal-shock boundary conditions are satisfied across the shock along the surface of the wing. The computed aerodynamic matrices may be saved on magnetic tape for use in subsequent analyses.

In practice, the program has been found to be most useful in the subsonic and supersonic flow regimes. The inherent problems associated with supersonic box methods have been eliminated, and it is possible to use a single program to calculate the generalized aerodynamic forces at both subsonic and supersonic speeds. The usefulness of the program for transonic applications has yet to be demonstrated.

This program is written in FORTRAN IV and has been implemented on the CDC CYBER 175 computer with a central memory requirement of approximately 111K (octal) of 60-bit words. The program is overlaid to reduce core requirements. The program was developed in 1976.

This program was written by Atlee M. Cunningham, Jr., of General Dynamics Corp. for **Langley Research Center.** *For further information, Circle K on the COSMIC Request Card.*
LAR-12524

Low-Aspect-Ratio Wings

Partial leading-edge separation for low speeds

In recent years, low-aspect-ratio wings have been increasingly considered for aircraft designs. These wings, designed to be efficient at high subsonic or supersonic speeds, must also perform effectively in off-design flight regimes such as takeoff and landing. One promising design approach to this problem is to have fully attached flow at cruise conditions and controlled leading-edge separation at takeoff and landing conditions. To simulate these off-design conditions, a computer program has been developed to predict the aerodynamic characteristics of wings having attached flow across part of the wing and vortex flow across the remainder. The program uses a quasi-vortex lattice method to formulate the wing boundary conditions so that the leading-edge boundary condition may be satisfied exactly. Calculations made with the code show reasonably good agreement with experimental data.

In steady symmetric flight at a high angle of attack, the flow over a thin, low-aspect-ratio, swept-back wing separates along the leading edge and the tips. In this analysis, the wing is represented by a bound-vortex sheet across which a pressure difference exists. The separated flow along the leading edges and the wake is represented by discrete free vortex elements.

The quasi-vortex lattice method is used to simplify the induced-velocity expressions. The flow is assumed to be tangential to the wing camber surface, with the leading-edge boundary conditions and trailing-edge Kutta conditions satisfied. Also, the vortex elements are assumed to be force free.

The initial locations of the leading-edge vortex elements are estimated by letting them leave the leading edge in the undisturbed free-stream direction up to a height of about 10 percent of the root chord, beyond which the elements are parallel to the wing plane. By satisfying the wing boundary conditions, the bound-vortex density on the wing and the strengths of the free vortex elements are obtained.

The aerodynamic characteristics of the wing and the forces acting on the free vortex elements of the leading-edge vortex system are calculated. The leading-edge vortex elements and the wake vortex elements are alined in the direction of local velocity vector to satisfy the force-free condition. This procedure is performed iteratively until a converged solution is obtained. The expressions for the evaluation of the pressure distribution are obtained by applying the Kutta-Joukowski theorem to the vortex system on the wing.

This program is written in FORTRAN IV for batch execution and has been implemented on the CDC 6600 with a central memory requirement of approximately 56K (octal) of 60-bit words. This program was developed in 1978 and is restricted to delta wings with zero thickness and no camber.

This program was written by C. Edward Lan and Sudhir C. Mehrotra of the University of Kansas Center for Research, Inc., for **Langley Research Center.** *For further information, Circle L on the COSMIC Request Card.*
LAR-12490

Machinery

Hardware, Techniques, and Processes

Computer Programs

Automatic Thermal Switch

Self-powered switch opens
and closes heat-flow path.

Goddard Space Flight Center, Greenbelt, Maryland

An automatic thermal switch closes and opens a heat-flow path in response to temperature changes. The thermal switch controls the flow of heat from one object to another to regulate the temperature in electronic circuitry or cryogenic refrigeration equipment, for example.

The combined sensor and actuator in the switch is a phase-change capsule, which contains a material that changes phase (for example, changes from a liquid to a gas). In so doing, the material changes enough in volume to actuate a mechanical linkage. The material can be formulated to change phase at any temperature over a wide range. The switch is self-powered and thus requires no electrical energy. It is simple and reliable and functions even in a high-vibration environment.

The phase-change capsule is in contact with an upper conductive plate so that it can readily exchange heat with the plate (see figure). The capsule is linked mechanically by a sliding tube to a pivoted arm that has articulated heat-transfer panels at its ends. When the temperature of the upper plate rises to the phase-change temperature, the capsule material expands against a piston, forcing the pivoted arm to turn slightly clockwise and press the heat-transfer panels against upper and lower plates. Heat can then pass readily from the hot upper plate to the cool lower plate, via the upper panel, the pivoted arm, and the lower panel. All these components are made of copper for good conductivity.

When the upper plate cools below the critical temperature, the capsule material condenses, moving the pivot-

Thermal Switch closes when upper-plate temperature rises, creating a path for heat flow between the top and bottom through the transfer panels and copper arm.

ed arm slightly counterclockwise. This action pulls the panels away from the plates, preventing further heat transfer between upper and lower plates.

The switch exists in two versions; the first (shown in the figure) passes heat when the upper, or temperature-control, plate is above the phase-change temperature. The second (not shown) passes heat when the temperature-control plate is below the phase-change temperature.

The automatic thermal switch was developed for regulating the temperature of a tape recorder in a spacecraft. In this application, the upper plate in the figure is the spacecraft skin and the lower plate is a mounting plate for the recording instrument. When the recorder portion of the spacecraft is in Sunlight, the skin temperature is high enough to keep the thermal switch closed so that heat can flow between the upper and lower plates. The upper-plate exposed surface coating is se-

lected so that the plate equilibrium temperature when viewing full Sun is comfortably below the allowable maximum temperature of the recorder. Thus, heat will flow from the lower (recorder mounting) to the upper (skin) plate.

On the other hand, when the recorder portion of the spacecraft is in shade, its skin temperature drops and the thermal switch opens to prevent an excess of heat flow to the surrounding space, which would result in cooling the recorder to intolerable levels.

Compact Rotary Sequencer

Two coaxial rotations, one clockwise and one counterclockwise,
are derived from a single clockwise rotation.

Lyndon B. Johnson Space Center, Houston, Texas

A proposed rotary sequencer is assembled from a conventional planetary differential gearset and a latching mechanism. Its single input and two rotary outputs (one clockwise and one counterclockwise) are coaxial, and the output torque is constant over the entire cyle. Housed in a lightweight, compact, cylindrical package, the sequencer requires no bulky ratchets, friction clutches, or cam-and-track followers. Among its possible applications are sequencing in automated production-line equipment, in home appliances, and in vehicles.

The sequencer is shown in Figure 1. A Sun gear connects with four planetary gears that engage a ring gear. With the ring gear held stationary, clockwise rotation of the Sun gear causes the entire planetary-gear carrier also to rotate clockwise. If the planetary-gear carrier is held fixed, the ring gear will rotate counterclockwise when the Sun gear rotates clockwise.

SECTION A-A
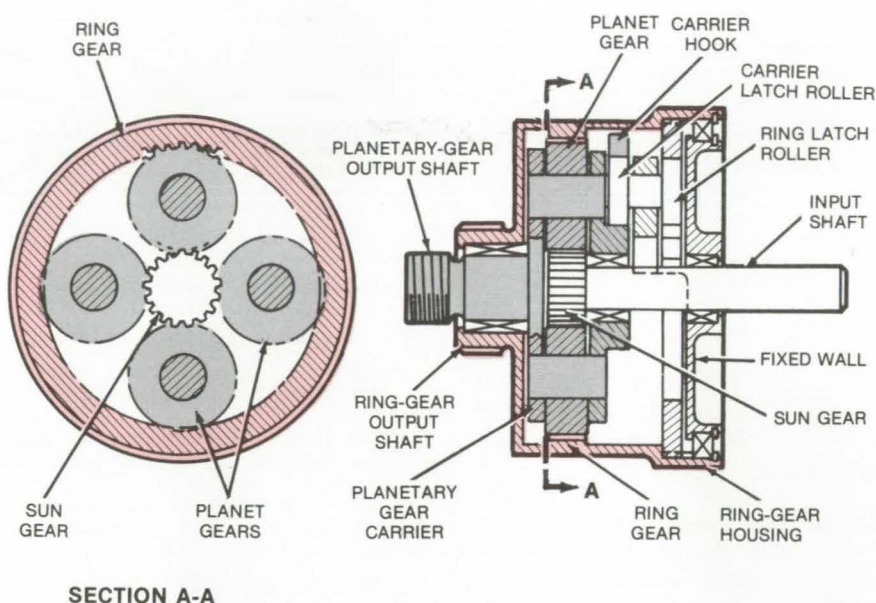
Figure 1. The **Rotary Sequencer** has a ring-gear output (in color) coaxial with a planetary-gear output (in gray). Clockwise rotation of the input is converted to clockwise rotation of the planetary-gear output followed by counterclockwise rotation of the ring-gear output. The sequence is controlled by the latch action described in Figure 2.

[a]   [b]   [c]   [d]
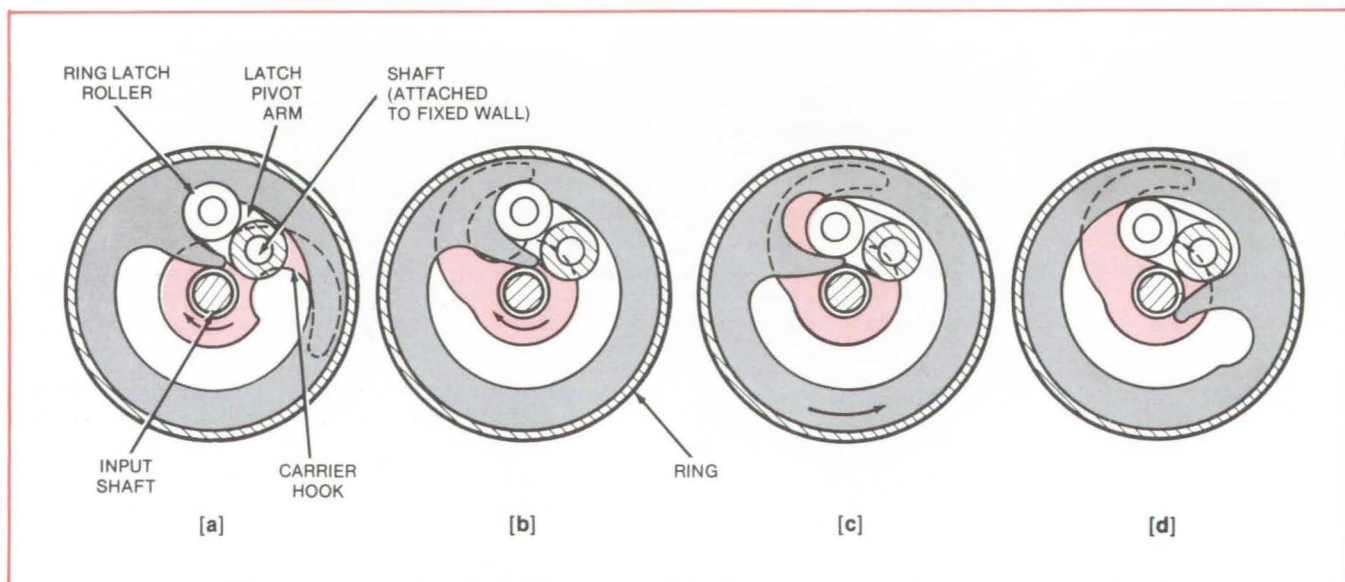
Figure 2. The **Latch Sequence** is shown in four steps: (a) The input shaft rotates the carrier clockwise while the ring latch roller holds the ring gear stationary; (b) the carrier hook begins to engage the carrier latch roller; (c) the ring latch roller begins to move out of its slot, and the carrier motion ceases while the ring begins to move; and (d) the sequence has ended with the ring in its final position.

Figure 2 shows the latch. It consists of a hook (the carrier hook) that is rigidly attached to the planetary-gear carrier, a ring that is rigidly attached to the ring gear, and a latch pivot arm with a pair of latch rollers attached to one end. The other end of the pivot arm rotates about a short shaft that extends from the fixed wall of the housing.

The sequencer cycle starts with the ring latch roller resting in a slot in the ring. This locks the ring and causes the planetary-gear carrier to rotate clockwise with the input shaft (Figure 2a). When the carrier hook has rotated approximately three-quarters of a complete cycle, it begins to engage the planet-carrier latch roller (Figure 2b), causing the latch pivot arm to rotate and the ring latch roller to slip out of its slot (Figure 2c). This frees the ring and ring gear for counter-clockwise motion, while locking the carrier. After a short interval of concurrent motion, the planetary-gear output shaft ceases its clockwise motion, and the ring-gear output shaft continues its clockwise motion.

When the ring reaches the position in Figure 2d, the cycle is complete, and the input shaft is stopped. If required, the input can then be rotated counterclockwise, and the sequence will be reversed until the starting position (Figure 2a) is reached again.

In a modified version of the sequencer, the latch pivot arm is shortened until its length equals the radii of the rollers. This does away with the short overlap of output rotations when both are in motion. For this design, the carrier motion ceases before the ring begins its rotation.

This work was done by Walter T. Appleberry of Rockwell International Corp. for **Johnson Space Center.** *For further information, Circle 66 on the TSP Request Card.*

This invention is owned by NASA, and a patent application has been filed. Inquiries concerning nonexclusive or exclusive license for its commercial development should be addressed to the Patent Counsel, Johnson Space Center [see page A5]. Refer to MSC-19514.

Sealed-in-Quartz Resistance Heater

A quartz sheath prevents hotspots
and premature failure.

NASA's Jet Propulsion Laboratory, Pasadena, California

An electric resistance heater encapsulated in quartz operates at temperatures as high as 1,400° F (760° C) without developing excessively hot spots that can fail prematurely. Because the resistance element is sealed in the quartz, the heater can be used in hostile environments. The sealed construction also keeps the heater from contaminating the heated object. This could be an advantage in the thermal decomposition of ammonia, hydrocarbons, and other gases. The original application was to heat the catalyst in hydrazine rocket engines.

The heater is fabricated by winding a resistance wire, such as tungsten, around a fused-quartz rod. A thin tube of fused quartz is slipped over the helical windings and is heated until it softens and conforms to the wire-wrapped substrate (see figure). The tube forms a tight sheath, leaving no voids into which the wire can creep or evaporate. A representative tungsten heater uses wire 0.020 in. (0.05 cm) in diameter, a quartz rod 3/32 in. (0.24 cm) in diameter, and a quartz tube with a wall 0.01 in. (0.25 mm) in thickness.

The lead wires to the unit can be made of platinum, Chromel, or an
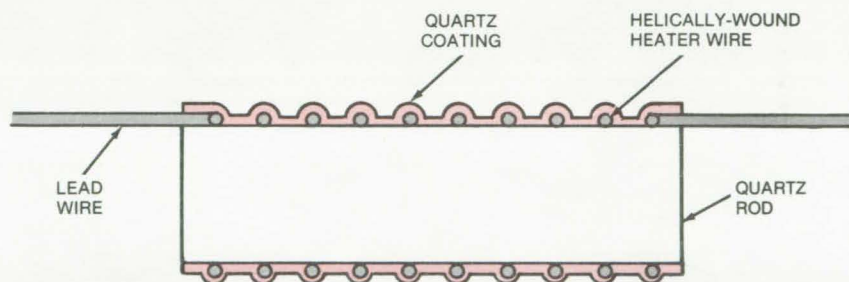
A **Thin Quartz Tube Is Heat-Shrunk** around the resistance wire in this encapsulated heater, shown in cross section. The sealed construction prevents hotspots that could lead to an early failure.

equivalent metal to prevent them from oxidizing. It is also advisable to use a heavier gage wire for the leads than for the heater element so that the leads do not become as hot.

In the hydrazine rocket engines, the new heater replaced previous designs in which the resistance wire was embedded in aluminum oxide or magnesium oxide powder and encapsulated in a metal case. At high temperature, the powder tended to separate from the wire, exposing bare wire sections that were vulnerable to failure.

In addition to its use in resistance heaters, quartz-encapsulation is suitable for zero-temperature-coefficient resistors, since the quartz covering would improve the stability of the thin-film resistance layer at high temperatures. The structure is also suitable for high-temperature thermocouples.

This work was done by Charles G. Miller and James B. Stephens of Caltech for **NASA's Jet Propulsion Laboratory.** *For further information, Circle 67 on the TSP Request Card. NPO-14529*

Remotely Controlled Latch

A simple mechanism engages and disengages parallel
plates carrying couplings and connectors.

Lyndon B. Johnson Space Center, Houston, Texas

A new latch mates two parallel plates in one continuous motion (see Figure 1). On the Space Shuttle, the latch connects (and disconnects) plates carrying 20 fluid couplings and electrical connectors. (The coupling/connector receptacles are on one plate, and mating plugs are on the other plate.) Designed to lock items in place for handling, storage, or processing under remote control, the mechanism also has a fail-safe feature: It does not allow the plates to separate completely unless both are supported. Thus, plates cannot fall apart and injure people or damage equipment.
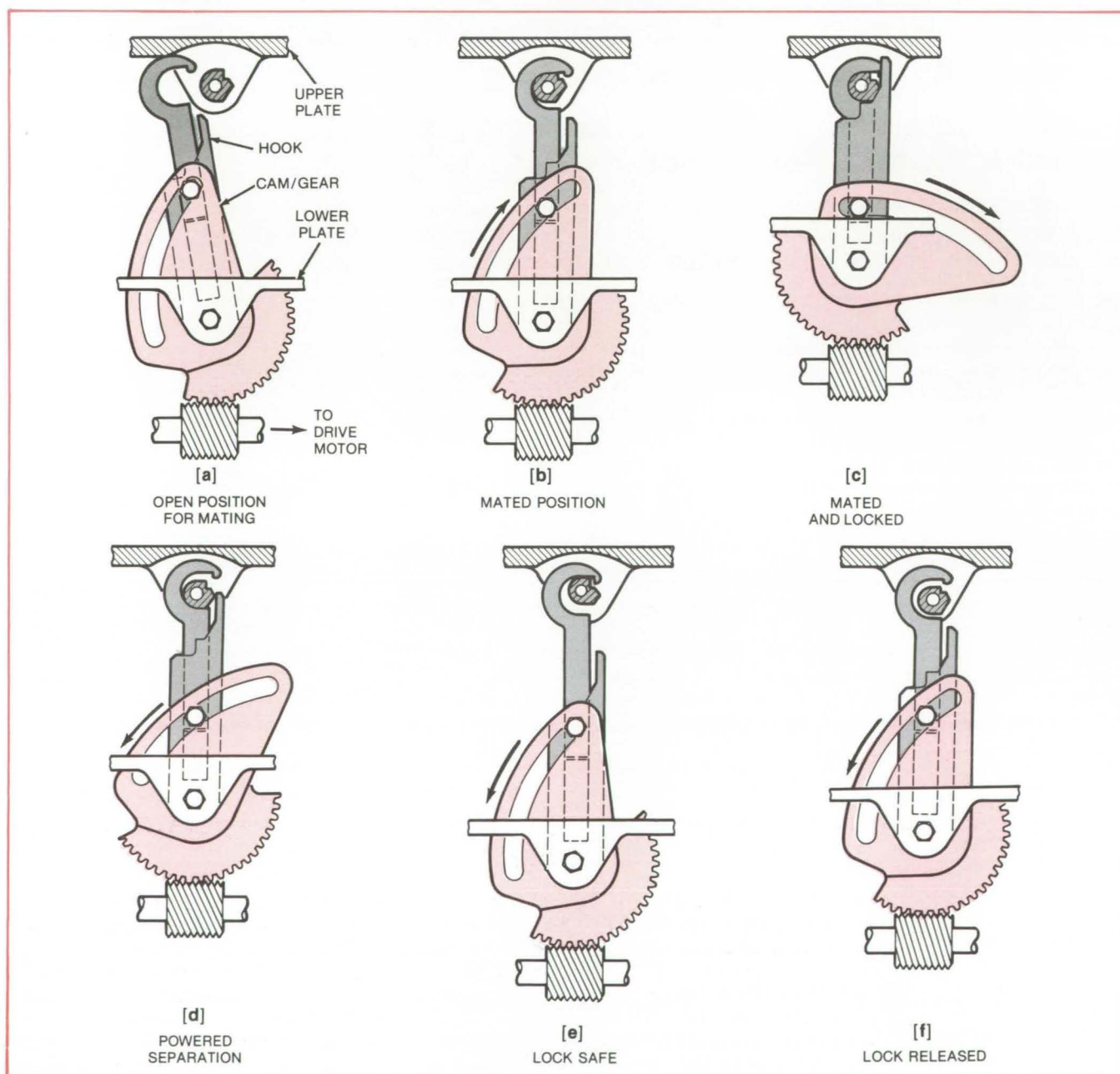
Figure 1. The **Latch Operation Sequence** is shown for locking in steps (a) through (c) and for unlocking in steps (d) through (f).

The mechanism employs four cam/gear assemblies, one at each corner of the lower plate (the photo in Figure 2 shows two cam/gears). The gears on each side of the plate face inward to balance the loading and help aline the plates. Worm gears on the cam/gear assemblies are connected to a common drive motor.

Figure 1 illustrates the sequence of movements as a pair of plates is latched and unlatched. Initially, the hook is extended and tilted out. The two plates are brought together, and when they are 4.7 in. (11.9 cm) apart, the drive motor is started (a). The worm gear rotates the hook until it closes on a pin on the opposite plate (b). Further rotation of the worm gear shortens the hook extension and raises the lower plate (c). At that point, the couplings and connectors on the two plates are fully engaged and locked.

To disconnect the plates, the worm gear is turned in the opposite direction. This motion lowers the bottom plate and pulls the couplings apart (d). However, if the bottom plate is unsupport-
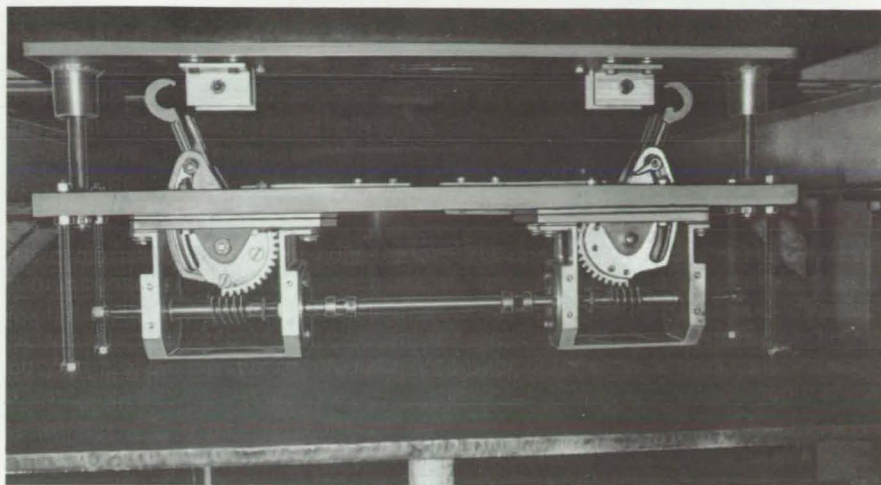
Figure 2. The **Prototype Latches** are shown with hooks in the unlatched position. When latched, the hooks secure themselves to pins (behind flanges) on the upper plate.

ed, the latch safety feature operates. The hook cannot clear the pin if the lower plate hangs freely (e). If the bottom plate is supported, the hook extension lifts the hook clear of the pin (f) so that the plates are completely separated.

This work was done by Clifford J. Barnett, Paul Castiglione, and Leo R. Coda of Rockwell International Corp. for **Johnson Space Center**. *For further information, Circle 68 on the TSP Request Card.*
MSC-18365

Torque-Wrench Extender for Hard-to-Reach Fasteners

Sturdy universal-joint linkage delivers
precisely calibrated torque.

Lyndon B. Johnson Space Center, Houston, Texas
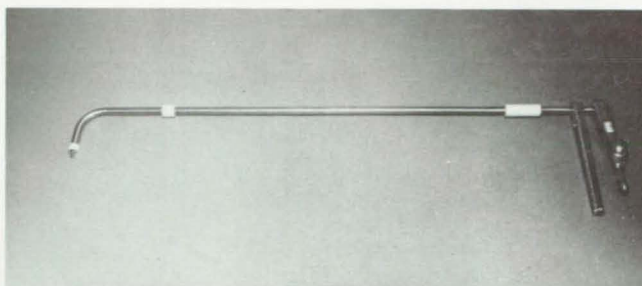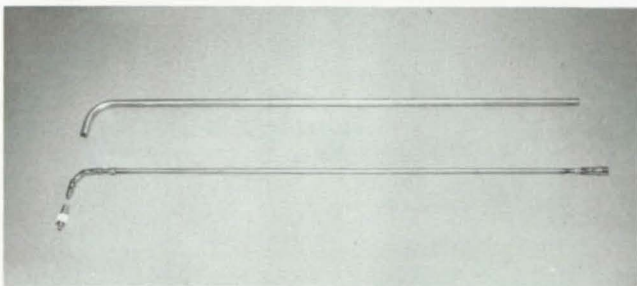
Universal Joints and Extender Bar fit in lubricated sheath (left photo). A countertorque handle holds the sheath while a torque wrench turns the extender bar (right photo).

An extension kit for a torque wrench tightens and loosens captive fasteners in hard-to-reach places. The kit consists of four universal socket joints and an extender rod enclosed in a greased-packed tube. The universal joints fit in the 90° bend at the end of the steel tube (see figure).

A countertorque handle grips the steel tube so that the tube can be held securely while a torque wrench is used to turn the extender-rod and universal-joint assembly, thereby tightening a nut, bolt, or screw to the prescribed torque, or loosening it.

Because of the universal joints, the extender delivers less torque than the input torque, so each unit must be calibrated empirically. The resulting calibration chart gives the user the proper torque-wrench setting for a desired torque on the fastener. Two plastic bumper-guard rings on the tube prevent equipment from being damaged by the extender kit.

The extension kit replaces a snap-on adapter and flexible drive shaft formerly used with a torque wrench to get to hard-to-reach fasteners. The flexible drive delivered erratic torque and was difficult to calibrate accurate-ly. Moreover, the shaft was often damaged by the torque required to tighten or loosen fasteners.

This work was done by Sol Selik and John A. Stein of Rockwell International Corp. for **Johnson Space Center.** *For* *further information, including assembly and detail drawings, Circle 69 on the TSP Request Card.*
MSC-18488

Slip Sensor

Slippage in any direction is
sensed by a magnetic pickup.

NASA's Jet Propulsion Laboratory, Pasadena, California

The slippage of one surface, relative to another is detected by a "ball-bearing" magnetic sensor. Originally developed for a mechanical claw manipulator, this omnidirectional sensor responds to slippage in any direction.

A nonmagnetic sphere embedded with magnetic pins rotates in a bearing at the tip of the new sensor (see figure). When the sphere is rotated, the pins move past a magnetic pickup that generates a series of electrical pulses. If the sensor is pressed against an object, slippage of the object turns the sphere to generate the pulses. A warning light, a buzzer, or a slip-control circuit could be actuated by the electrical output.

The sensor is mounted in the "finger" of the mechanical claw manipulator. When an object gripped by the claw begins to slip, the sensor signals the operator, who tightens the grip by remote control.

This work was done by Antal K. Bejczy of Caltech and Sur Park for **NASA's Jet Propulsion Laboratory.** *For further information, Circle 70 on the TSP Request Card.*
NPO-14655

The head of the **Slip-Sensor** is a nonmagnetic sphere (e.g., brass) that is embedded with magnetic pins. It rotates in a tetrafluoroethylene bearing and is held by a brass retaining ring. The housing is aluminum.

Coupler for Remote Manipulators

A reliable, low-cost coupler alines and
grasps moving and rotating objects.

Goddard Space Flight Center, Greenbelt, Maryland
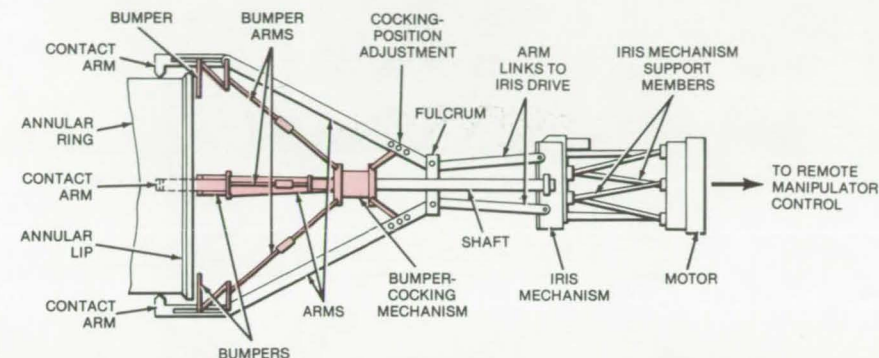
Figure 1. A **Remote-Manipulator Coupler** automatically alines and grasps satellites by the use of arms driven by an iris mechanism. The device is guided toward a satellite annular ring with arms widespread and bumpers cocked at an angle away from the ring. The ring is grasped by the converging contact arms driven by an iris mechanism. The released spring-loaded bumpers aline the annular lip, pushing it into position just before final grasp.

Figure 2. The **Coupler Operates** as follows: (a) It is guided toward the annular ring in a fully open position with the bumper arms cocked, (b) once in contact the bumper arms are released, (c) pressure from the bumper arms alines the ring, and (d) the alined ring is grasped firmly with the contact arms.

A new coupler alines and grasps satellites in the vicinity of the Space Shuttle. The device, remotely manipulated from inside the Shuttle, is extended outward by the remote-manipulator arms to grasp the annular coupling ring protruding from the satellite. The satellite can then be alined and positioned with respect to the Shuttle. This same coupling mechanism could be scaled down and modified to handle radioactive materials and used for deep underwater explorations and other remote manipulations.

The coupler has four contact arms (see Figure 1) equally spaced 90° apart—at least three arms must be used spaced at 120° apart for structural integrity. Each contact arm is connected to an extension that is mounted on a fulcrum. Each is further linked to an electrically driven iris. The iris moves back and forth to bring the arm links together (grasping) or apart (releasing).

The action of the coupling device depends on the fulcrum design. One version has rotatable arms pin-mounted on the fulcrum and operates on the "negative pliers" effect; i.e., the device uncouples as the arm links are brought together by the iris. An alternate "positive pliers" approach also utilizes fulcrum-to-iris arms that cross through the center bolt. The choice depends on whether the greater force is needed to disengage the mechanism or to grip the object.

On the Shuttle, when the coupling device is guided toward the annular ring (see Figure 2), it is in a wide-open position (a), the bumper arms are cocked, forming a larger than 90° angle with the contact arms. A separate mechanism on the center shaft automatically cocks and releases the bumper arms (b).

Just before the annular ring is fully engaged, the iris is driven to close the rotating contact arms around the ring while the loaded bumper arms are released to push the annular lip into alinement (c) with the coupler. Once axially alined, the contact members close firmly around the ring (d).

This work was done by Arthur A. Rudmann of **Goddard Space Flight Center**. *For further information, Circle 71 on the TSP Request Card.*

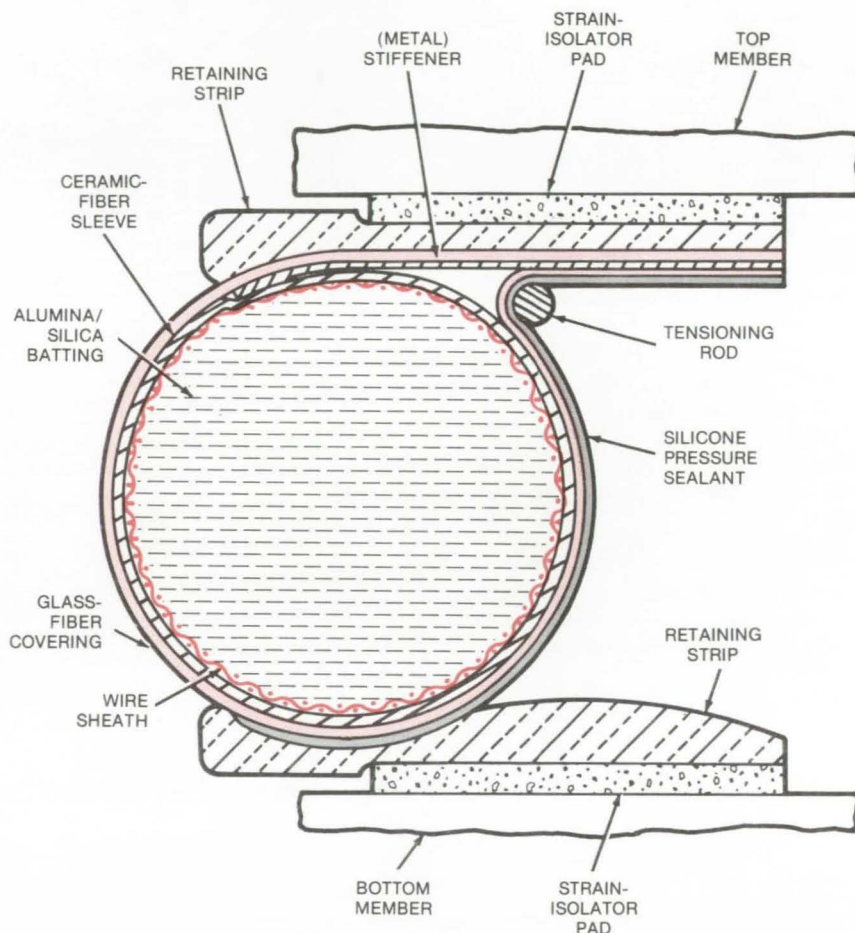*This invention is owned by NASA, and a patent application has been filed. Inquiries concerning nonexclusive or exclusive license for its commercial development should be addressed to the Patent Counsel, Goddard Space Flight Center [see page A5]. Refer to GSC-12429.*
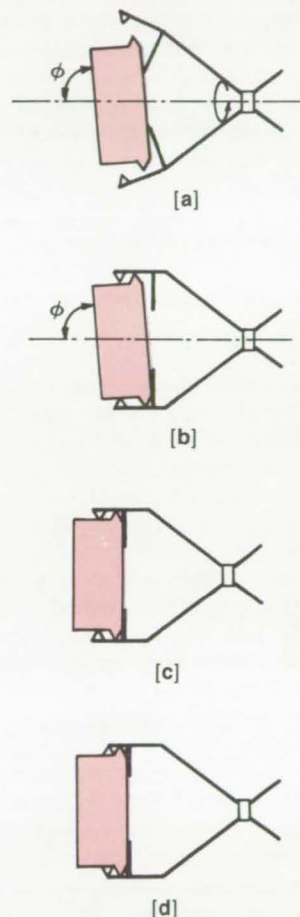
Centrifugal Reciprocating Compressor

Efficient compressor uses centrifugal
force to compress a gas.

NASA's Jet Propulsion Laboratory, Pasadena, California

A proposed reciprocating compressor for cryogenic applications incorporates a cylinder with two free pistons. The pistons are driven in unison by centrifugal forces as the entire assembly is rotated inside a low-pressure chamber. The compressor may utilize large pistons driven at a low reciprocating speed so that dry lubricated components are used for compressing pure fluids. Conventional single-piston compressors would require heavy parts and large torques for low-speed operation.

The proposed compressor consists of a cylinder assembly and two free pistons. The entire assembly is contained in a chamber (see the figure) maintained at low pressure P_0, which is less than the minimum operating pressure of the compressor. The area between the pistons is also held at P_0 through openings in the cylinder. The difference between P_0 and the compressor pressure provides necessary restoring force during the intake cycle, and conventional springs are not required.

The cylinder is driven by a motor inside the chamber. As the cylinder is accelerated, centrifugal force pushes the pistons into compression, forcing the refrigerant gas through a passage in the shaft. The housing is then decelerated to reduce centrifugal force to accommodate the intake cycle.
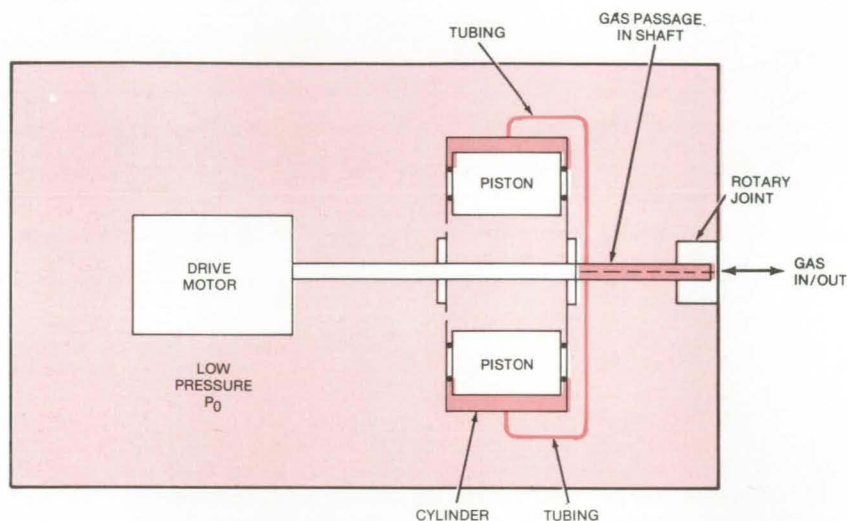
The **Cylinder** is located in a low-pressure chamber. The minimum piston pressure is larger than P_0 and acts as a restoring force during the intake stroke as the cylinder is decelerated.

An energy-efficient method of driving the compressors utilizes dynamic or regenerative braking by employing a dc shunt motor as the prime mover. This system incorporates two coupled dc motors, each driving a separate centrifugal reciprocating-compressor assembly. The motors are synchronized to accelerate and decelerate alternately. Thus when one device decelerates, it acts like a generator feeding power to the second one, which is accelerating and acting like a motor, and vice versa.

*This work was done by Walter H. Higa of Caltech for **NASA's Jet Propulsion Laboratory.** For further information, Circle 72 on the TSP Request Card.*

This invention is owned by NASA, and a patent application has been filed. Inquiries concerning nonexclusive or exclusive license for its commercial development should be addressed to the Patent Counsel, NASA Resident Legal Office-JPL [see page A5]. Refer to NPO-14597.

Angular-Displacement Mechanism

A reliable system uses
two redundant motors.

Marshall Space Flight Center, Alabama

A redundant-motor drive system generates angular displacement to rotate mechanical or optical components in a limited arc. Two reversible electric motors are used; either one can drive the system while the other remains stationary. (The stationary motor is not back-driven, which effectively reduces the system energy requirement.)

As shown in the figure, the system

output shaft is a rotatable sleeve that rests on bearings around a concentric axle shaft. The axle shaft is permanently fixed to a disk-shaped worm gear. One of the two motors is fixed to

the system baseplate, and the other is mounted on the rotatable output shaft (sleeve). Each motor is connected to the disk-shaped worm gear by its own three-gear drive train: two spur gears and a "vertical" worm gear that meshes with the disk-shaped worm gear.

With this arrangement, the disk-shaped gear and axle rotate together, and the one "rotatable" motor and the output sleeve rotate together. The operation of the system relies on the fact that worm gears cannot be back-driven; i.e., either of the vertical worm gears can drive the disk gear, but the disk gear cannot drive the vertical worm gears.

Thus when the sleeve-mounted "rotatable" motor is turned off, the disk-shaped gear cannot rotate with respect to the output sleeve, but the disk and the sleeve may still rotate about the axle. When the fixed motor is turned off, the disk-shaped gear cannot rotate relative to the baseplate (in other words, not at all). However, the output sleeve is free to rotate about the axle.

When the fixed motor is on and the rotatable motor is off, the torque transmitted through the fixed-motor drive train causes the disk to rotate and carry the inactive, rotatable motor with it. The output sleeve is thus rotated. When the rotatable motor is operating and the fixed motor is off, the disk gear is stationary. The output torque moves
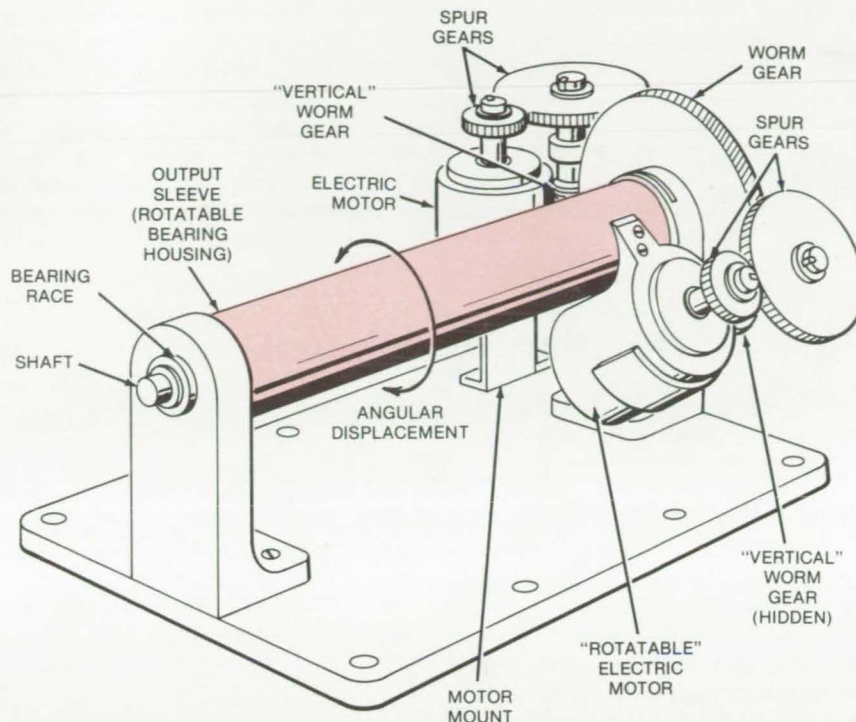
A **Reliable Angular-Displacement System** uses two redundant electric motors. Each motor can rotate the output sleeve in a limited arc, angularly displacing optical or mechanical components rigidly connected to the sleeve.

the rotatable-motor worm gear around the rim of the disk gear. Thus the rotatable motor and the output sleeve are rotated.

This work was done by John A. Calvert of **Marshall Space Flight Center**. *For further information, circle 73 on the TSP Request Card.*

This invention is owned by NASA, and a patent application has been filed. Inquiries concerning nonexclusive or exclusive license for its commercial development should be addressed to the Patent Counsel, Marshall Space Flight Center [see page A5]. Refer to MFS-23777.

Long-Wearing TFE/Metal Bearings

A surface of polytetrafluoroethylene in a metal matrix can be formed on a broad range of surface shapes and compositions.

Lyndon B. Johnson Space Center, Houston, Texas

A new method for making metal/polytetrafluoroethylene (TFE) bearing surfaces embeds a long-wearing layer of TFE in microscopic pits in the metal. Previously, such surfaces were made by compressing powdered metal and TFE and applying the compressed mixture to a metal substrate. The new method allows a metal/TFE surface to be formed on a solid metal part and on complex shapes. Moreover, it is not limited to metals that are available as powders.

To make the bearing surface, the part is first roughened by blasting it with aluminum oxide grit. The surface is sprayed with a TFE dispersion, and this coating is dried and fused in an oven at 730° F (390° C). Next, the coating is burnished with a non-abrasive cloth to a thickness of from 0.0001 to 0.0004 inch (0.003 to 0.01 mm). In the final step, the coating is feathered to the level of the grit-blasted surface so that the TFE remains only in the grit-eroded pits.

The method was originally developed to treat poppets in a gaseous-helium check valve for the Space Shuttle. The poppet is a very hard part made of chemical-vapor-deposited tungsten containing dispersed tungsten carbide. This composition is very difficult to produce as a powder. Thus, the previous powder-metallurgy method could not be applied.

The poppet in the check valve is guided by three sapphire pins, one of which is spring-loaded. However,

rubbing of the pins against the poppet caused wear and early failure of the valve. The addition of TFE by the new grit-blast method extended the valve life expectancy to 100,000 on/off cycles, as required for the Shuttle application.

The new coating technique has potential applications in automotive gears, ball joints, and roller chain components. It also might be used to make unlubricated bearings in chemical, pharmaceutical, and food-processing equipment or bearings for hard-vacuum environments in which lubricants would be a source of contamination. Other possible applications include release coatings on dies and molds.

This work was done by Richard A. Brass and Williard A. Gillon, Jr., of Rockwell International Corp. for **Johnson Space Center.** *For further information, Circle 74 on the TSP Request Card.*
MSC-15994

Positive Isolation Disconnect

A device prevents leakage or spillover when two fluid lines are disconnected.

Lyndon B. Johnson Space Center, Houston, Texas

The positive-isolation-disconnect (PID) device shown in Figure 1 has two mating halves, each attached to a separate fluid line. The mating halves connect or disconnect the fluid lines quickly without leakage or spillover. Each half has a shutoff poppet to stop the fluid flow. When the flow is shut, the poppets are flush against each other, leaving no space for fluid to remain in.

Fluid is isolated by individually opposing poppets. Each poppet is attached to the poppet shaft through a yoke section near midlength. The poppet shaft is centered and supported by guide rings that are held in position by the internal bore of the valve body. The poppet is opened or shut by rotating the valve-stem cap.

An eccentric cam lobe on the valve stem moves the poppet shaft by leaf springs fixed inside the yoke section. When the cam lobe is in its top-dead-center position, the leaf springs are under maximum compression, depressing the poppet to a closed position. When the cam lobe is turned 180°, the compression is released, opening up the fluid flow.

The poppets may be fitted with either elastomer or PTFE seals, depending on the type of fluid in the lines. Ethylene propylene elastomer seals are the choice on systems flowing high-purity water, coolant water, and gaseous systems (e.g., nitrogen). PTFE is best on systems flowing Freon-21, or an equivalent, and ammonia.

The mating halves are connected and disconnected by a handle-operated coupling mechanism (see Figure

TOP VIEW

FRONT VIEW
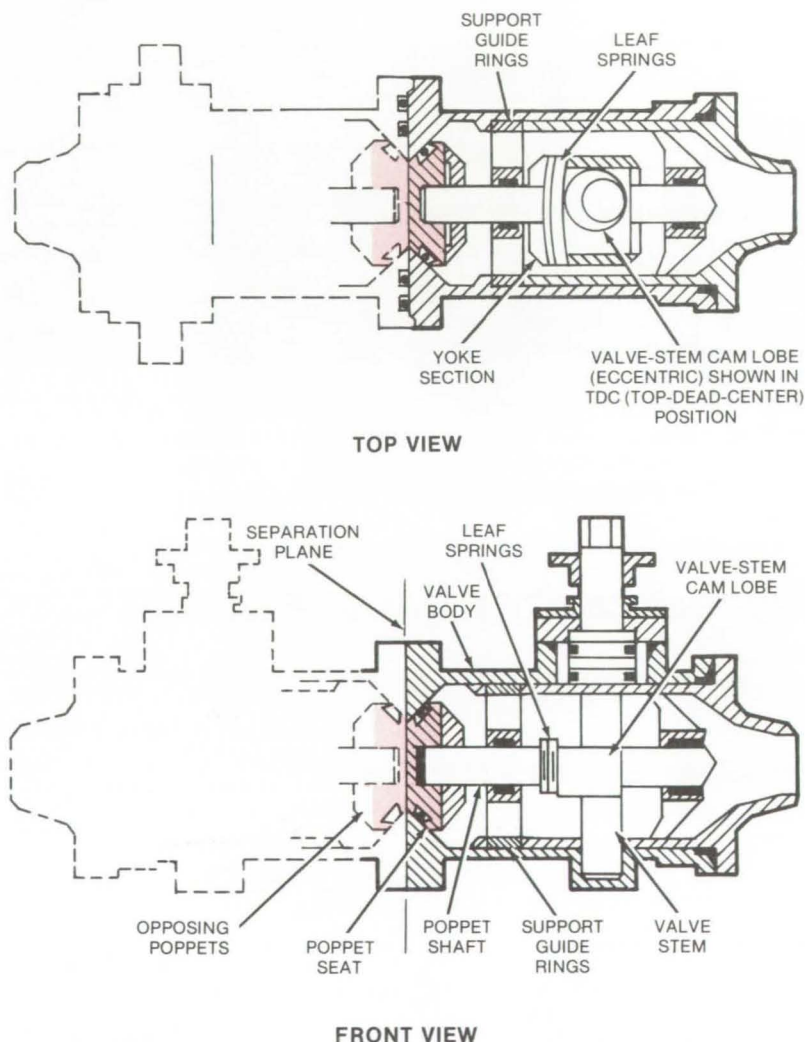
Figure 1. This **Disconnect Device** prevents fluid leakage or dripping when two fluid lines are disconnected. Two opposing poppets at the line junction are shut tightly against each other, leaving no clearance for the fluid to be trapped between the lines. The lines then are disconnected neatly without spillover or dripping.

2). The handle rotates 90° about a pivoting cam fixed to one mating half. The cam is connected to a yoke translating the handle movement to a clamp. The clamp interlocks with two tabs fixed to the other mating half. The clamping tension is adjustable by two screws on the clamp assembly.

The device may not be disengaged unless both valves are shut. The valve caps are keyed to two handle slots, preventing accidental lifting of the handle when the fluid is on.

This work was done by Morley V. Friedell of Martin Marietta Corp. for **Johnson Space Center**. *Further information may be found in NASA CR-144634 [N76-14187/NSP], "Positive Isolation Disconnect" [$9]. A copy may be purchased [prepayment required] from the National Technical Information Service, Springfield, Virginia 22161.*

This invention has been patented by NASA [U.S. Patent No. 4,103,712]. Inquiries concerning nonexclusive or exclusive license for its commercial development should be addressed to the Patent Counsel, Johnson Space Center [see page A5]. Refer to MSC-16043.
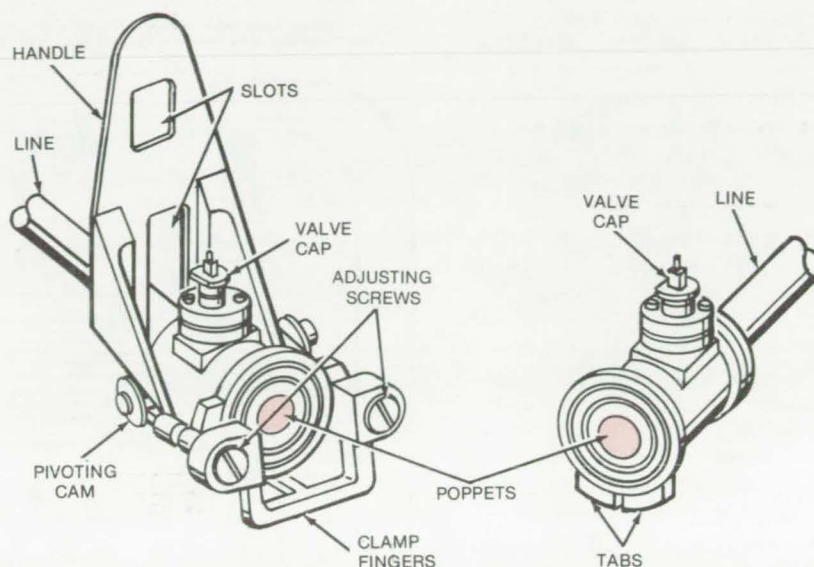
Figure 2. A **Handle-Actuated Coupling Mechanism** utilizes a clamp to join the two fluid lines. The clamp grasps two tabs of the mating opposite line to lock the lines together by a simple throw of the handle. The handle has two slots keyed to fluid-shutoff valve caps on both ends of the junction. This prevents accidental disconnection unless both line ends are shut off.

Heated Tool for Autoclaves

Improved technique
for curing composites

Lewis Research Center, Cleveland, Ohio

Components made of composite materials can be heated in autoclaves by employing electrical resistance heating blankets, thus avoiding the need to heat the entire autoclave volume. Conventional pressurized and heated autoclaves have been used for many years to provide compacting pressure and heat for the fabrication and cure of thermosetting resin-matrix composite materials and objects such as epoxy/fiberglass aircraft structures. The process used generally involves the layup or assembly of plies of pre-impregnated reinforcement onto a tool of the desired configuration.

The tool may be flat or highly contoured and made of steel, aluminum, or a similar material. Conventionally this subassembly is then covered with a number of bleeder or venting layers of dry glass fabric or other suitable material and with a layer of porous release material such as nylon or PTFE-coated glass separating the work from the bleeder plies. The subassembly is then covered with an impermeable membrane of rubber, Mylar, Kapton, or the equivalent, with a suitable sealant to isolate the workpiece inside the bag.

The total bagged assembly is then placed in an autoclave connected to a vacuum system such that the inside of the bag is isolated from the autoclave environment. Through a prearranged cure schedule, the autoclave pressure is raised, and the total autoclave volume is heated. Following the cure, the necessary finishing operations are per-

formed to complete the desired end-product item.

The fabrication of higher temperature materials, such as graphite/polyimide resin composites, generally necessitates higher temperatures and/or faster heat-up rates than are usually found in conventional or existing autoclaves in the industry. A new method has been developed to provide the necessary high temperatures and rapid heating rates. The method involves a tool into which the heat is supplied by heating blankets. The electrical power supply for the blankets is external to the autoclave.

The figure describes the basic elements of the tool with its heating blankets. In this case, an aluminum plate acts as the tool onto which the com-

posite workpiece and necessary bleeder and release layers are assembled. The impermeable membrane is a silicone-rubber sheet, and the sealing mechanism is a rubber O-ring and aluminum sealing frame. Other tooling materials, membranes, and sealing mechanisms can, of course, be incorporated. Heating is provided by insulated resistance heating blankets both above and below the assembly, although heat from the bottom is more than adequate if sufficient insulation is provided on top. The workpiece is then cured in the autoclave to the predetermined time/temperature/pressure/vacuum schedule. Thermocouples in the heating elements or workpiece govern external controllers.

The heated tool described here is used on a regular basis in curing graphite and glass-reinforced PMR polyimides and other resin systems.

In addition to providing high temperature and rapid heating rates, the method offers greater versatility in tool design, particularly on complex contour hardware. Heating blankets can be segmented to provide as many zones of control as needed, and any number of thermocouples can be woven directly into the heating blanket to assure temperature uniformity and rapid control response time.

The low-heat-capacity tooling assembly provides not only significant energy savings compared to heating the entire pressure vessel but offers time savings in accelerated heat-up and cool-down cycles.
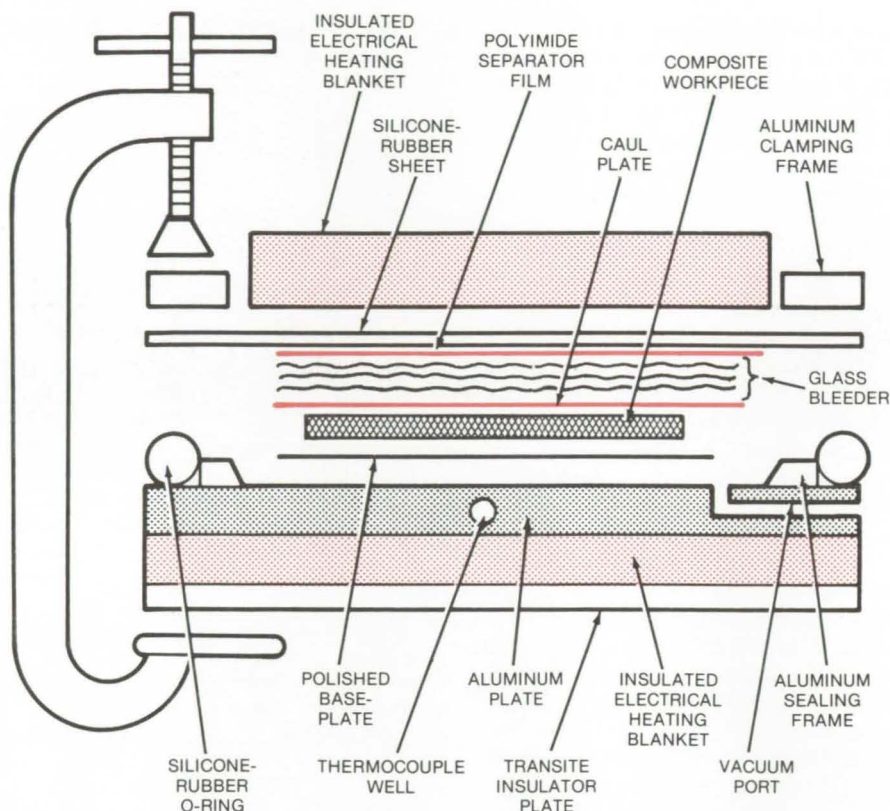
The **Layup of Heated Tool for Autoclaves** shown above makes it possible to use a low-temperature autoclave to cure resins at around 600° F (316° C).

Improved Piston Rings for a Stirling Engine

Antifriction coatings and a cast-iron core improve piston ring life.

NASA's Jet Propulsion Laboratory, Pasadena, California

Cast-iron piston rings coated with commercially-available antifriction materials could improve the cylinder life of a high-performance Stirling engine. Conventional rings have low heat conductivity and high thermal expansion, which reduced their service life. Stirling-engine piston rings must operate without lubricants because conventional lubricants degenerate at the high operating temperatures of the working gas (such as helium, argon, or hydrogen) in current high-performance engines. These temperatures can reach 1,600° F (870° C).

The proposed new design (see figure) incorporates two cast-iron piston rings, similar to the standard automobile ring, except that the surface in contact with the cylinder is first coated with polytetrafluoroethylene and then Xylan (a commercial fluoropolymer) or an equivalent. The

first coating acts as a conformal resilient support for the second. With the ring gaps set at 180°, a Viton (or equivalent) O-ring under the cast-iron rings effectively seals the ring gap.

The cast-iron ring is an efficient heat conductor between the piston and the cylinder. It has low thermal expansion which maintains a minimum gap in the ring, good radial force characteristics, and essentially indefinite life.

Because of its antifriction characteristics and high heat conductivity, the new ring is not expected to exceed the 210° F (100° C) cylinder-wall temperature by any significant amount, even though the working gas is at a much higher temperature. Conventional rings have heated up to 500° F (260° C) at the piston contact surface.

This work was done by Allan R. McDougal of Caltech for **NASA's Jet Propulsion Laboratory.** *For further information, Circle 75 on the TSP Request Card.*
NPO-14497

ANTIFRICTION COATING BONDED TO POLYTETRAFLUOROETHYLENE, OR AN EQUIVALENT, COATING

CYLINDER WALL

PISTON

CAST-IRON PISTON RINGS

"O" RING ACTS AS PRESSURE AND RING GAP SEAL
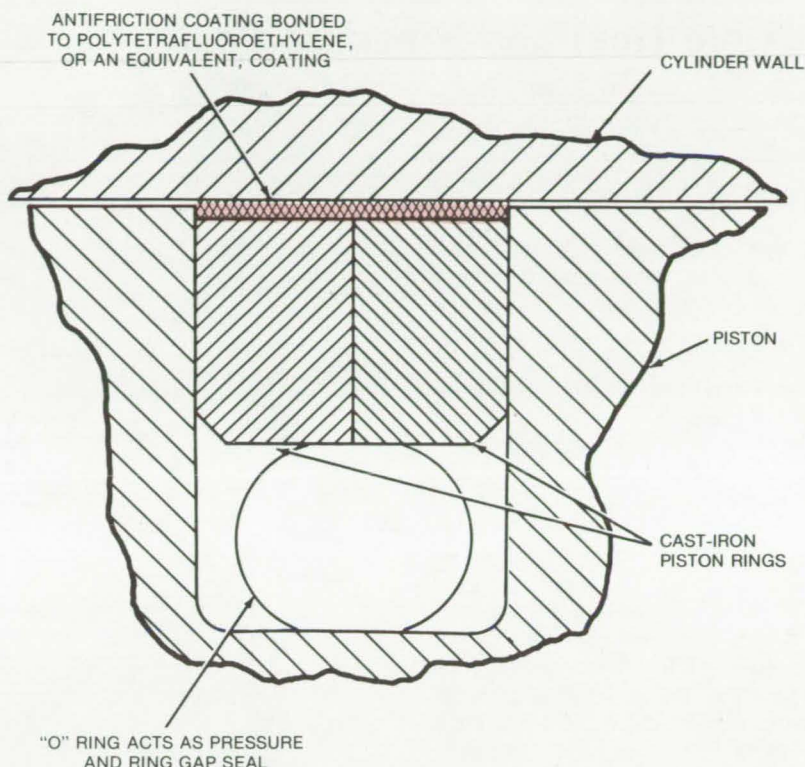
Cast-Iron Piston Rings coated with commercially-available antifriction materials should work reliably in a high-performance Stirling engine. The cast-iron core has good thermal conductivity, to minimize thermal gradients in the ring, and the outer coating reduces friction. The inner coating, which acts as a resilient support, may not always be necessary.

Thermal Seal for High and Low Temperatures

A composite seal remains flexible between -423° and +500° F.

Lyndon B. Johnson Space Center, Houston, Texas

A composite bulb seal can sustain temperatures ranging from −423° to +500° F (−253° to +260° C). The seal (see figure) incorporates a knitted-wire tubular spring core surrounded by a thin-wall flow barrier of polytetrafluoroethylene or polyolefin. Because of its wide temperature capability, the seal outperforms conventional elastomeric seals used in industrial freezers, environmental chambers, refrigerated trucks and railcars, and aircraft doors.

The knitted-wire tubular spring is resilient and can be deflected to an extreme without permanently deforming. The 304 stainless-steel wire has a constant modulus of elasticity over a very wide temperature range, and the spring force can be easily adjusted for

THIN-WALL FLOW BARRIER

KNITTED-WIRE SPRING

MOUNTING FLANGE
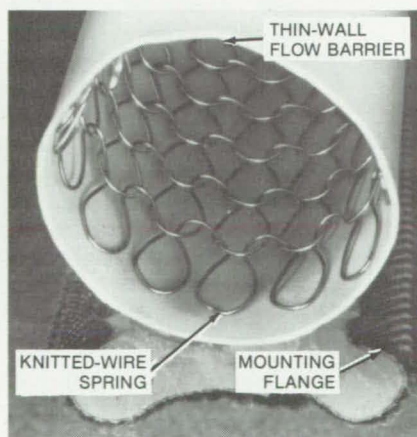
The **Bulb Seal,** designed for a wide temperature range, is made from a tubular knitted-wire spring core surrounded by a thin-wall polytetrafluoroethylene or polyolefin flow barrier.

specific applications by varying the wire diameter and knit density.

The flow barrier remains flexible down to −423° F, which exceeds the performance of silicone-rubber seals. The latter are limited to about −150° F (−101°C), below which the material undergoes a glass transition [at approximately −170° F (−112° C)].

The seal can be used as is with the flow barrier and the spring, or it can have a mounting flange or facet bonded to the flow barrier.

This work was done by James E. Collipriest, Jr., and Donald M. Fell of Rockwell International Corp. for **Johnson Space Center.** *For further information, Circle 76 on the TSP Request Card.*
MSC-16151

Flexible Heat-and-Pressure Seal

A thermal/pressure seal accommodates transverse
and lateral motion between the sealed surfaces.

Lyndon B. Johnson Space Center, Houston, Texas

A new seal withstands both heat and pressure and accommodates relative motion between the sealed surfaces. It consists of a flexible tube filled with a thermally insulating material and coated with a pressure-resistant material.

The new seal withstands temperatures of 1,950° F (1,066° C) on one side while maintaining the temperature on its "cool" side at less than 350° F (177° C). It seals gases at pressures up to 5.0 psi (34×10^3 N/m²). One such seal, fabricated for a 1.5-inch (3.8-cm) gap, accommodates about 2.5 cm of side-to-side movement of the surfaces and transverse motion of about 3.5 cm without disrupting the heat and pressure barrier.

As shown in Figure 1, the core of the tube is filled with alumina/silica batting for heat insulation. The batting is held in a sheath of knit iron/nickel-alloy wire, which gives the necessary strength, flexibility, and resilience. A ceramic-fiber sleeve is braided snugly around the wire sheath for further insulation, and the sleeve is enclosed in a glass-fiber cover coated on the outside with a layer of silicone as a pressure sealant.

The tube is held in place by a ceramic retaining strip on both of the sealed members and by a tensioning rod. The seal nests between the ceramic strips with the end flaps of the outer covering held in place by the rod.

If the sealed members move, the seal deforms (Figure 2), changing shape to accommodate the relative motion. A synthetic felt strain-isolator pad is bonded between each member and its retaining strip.

This work was done by John Bellavia, Jr., and John O. Kane of Rockwell International Corp. for **Johnson Space Center.** *For further information, Circle 77 on the TSP Request Card.*

This invention is owned by NASA, and a patent application has been filed. Inquiries concerning nonexclusive or exclusive license for its commercial development should be addressed to the Patent Counsel, Johnson Space Center [see page A5]. Refer to MSC-18134.

Figure 1. The **Heat/Pressure Seal,** shown here in cross section, uses an outer silicone layer to keep out gases. The pressure limit, 5 psi in the original design, can be raised by increasing the thickness of the silicone layer. The ceramic fibers and inner batting block heat flow. A wire sheath is the structural framework for the seal.
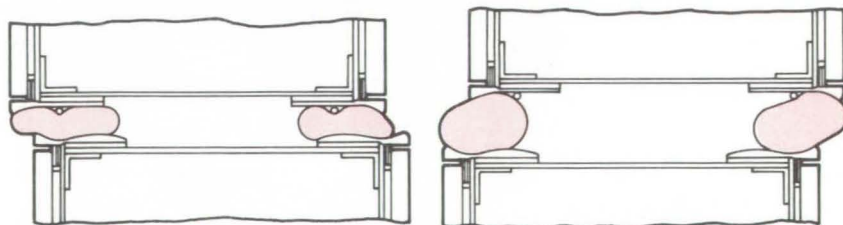
Figure 2. The **Seal Deforms To Accommodate Relative Movement** of the sealed members — left: lateral movement with minimum spacing between the members; right: lateral movement with maximum spacing between the members.

Insulating Seal for Cryogenic-Liquid Transfer

Shims and shrinkable tubing insulate
an O-ring seal to prevent leakage.

John F. Kennedy Space Center, Florida

A simple modification to the male bayonet on a cryogenic transfer line prevents freezeup of the transfer-line coupling and leakage of the cryogenic liquid. Originally used on the liquid-oxygen transfer line for the Space Shuttle fuel cell, the procedure could help to reduce leakage in plumbing for other cold fluids.

The male bayonet for the Shuttle transfer line is shown in the photograph. When the bayonet is fully inserted in the female portion of the coupling, the O-ring butts against a flange, creating a leakproof seal. The flange is maintained at near ambient temperature because a gaseous barrier keeps the liquid from entering the annular space between the male and female bayonet. However, during transfer, the annular space and its envelope gradually became colder permitting liquid to move toward the flange. This resulted in cooling the O-ring beyond its operating temperature range, destroying its sealing capability and allowing the liquid to escape.

The leakage is prevented by wrapping strips of stainless-steel shim stock 5 mils (0.13 mm) in thickness around the outside of the bayonet and then slipping a length of heat-shrinkable tetrafluoroethylene tubing over the bayonet and shim. The shim spacing and alinement are held as the tubing is shrunk. [A winding of
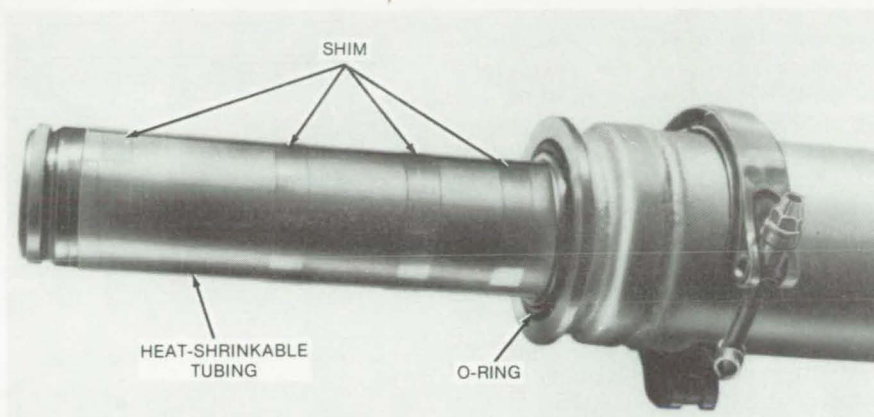
The **Cryogenic Transfer-Line Bayonet** is shown with four shims in place. Clear tubing has been heat-shrunk around the outside of the bayonet. (The shim near the tip was slightly twisted when the bayonet was installed.) Without the shim, the tubing did not keep the O-ring seal warm enough to prevent leakage. The seal would operate above -20° F (-6.6° C).

stainless-steel wire 0.032 in. (0.81 mm) in diameter around the outside of the tubing helps to hold the shim in place.]

The shim and tubing create pockets of liquid and gas around the bayonet. These have an insulating effect that prevents the region around the O-ring from cooling as the cryogenic fluid is transferred. In tests on two bayonets insulated this way, the O-ring region remained at ambient temperature or only slightly cooled, and the seals remained intact.

Further testing showed that excellent results could be obtained by using one or two layers of stainless steel shims the full length of the bayonet and preformed to the outside diameter of the male bayonet. This sleeve was inserted into the female bayonet and pressed tightly against the inside diameter prior to inserting the male bayonet. Shim thickness is selected so that the annular space between male and female bayonet is only sufficient to permit mating of the bayonet.

This work was done by I. M. Kroenke of the Beech Aircraft Corp. for **Kennedy Space Center.** *No further documentation is available.* KSC-11105

Cryogenic Seal for Instrument Wires

Double-plug tube prevents
leakage and avoids splices.

Lyndon B. Johnson Space Center, Houston, Texas

A seal allows electrical wires to pass directly from sensors inside of a liquid-nitrogen storage vessel to outside instruments. No splices or connectors are required, so errors created by contact resistance are avoided. Measure-

ments with highly sensitive instrumentation (such as strain-gage measurements) can thus be made with greater accuracy.

The seal is contained in a corrosion-resistant steel tube welded in the ves-

sel wall (see figure). Two perforated metal disks, located about 1 inch (2.54 centimeters) from either end of the tube, are tack-welded in place. The instrumentation wires pass through the disk perforations, which keep the wires

separate and allow a silicone sealing compound (such as RTV 511, or equivalent) to seep completely around each wire. The silicone compound is poured into both ends of the tube and also, through a fitting, into the inside of the tube so that it forms plugs around each disk with a void at the center of the tube.

The void between the silicone plugs is pressurized to prevent seepage of cryogenic fluid past the inner plug. When the liquid nitrogen contacts the inner plug, it tends to shrink the plug in relation to the tube, thereby creating a leakage path around the plug. However, with the void at a slightly higher pressure than the cryogenic vessel, the fluid is held back. The outer plug thus remains warm and maintains its seal.

The size of the tube and disks depends on the vessel pressure. For a vessel containing liquid nitrogen at 90 lb/in.^{2} (620×10^3N/m^2) gage, a steel tube 2 inches (5.1 centimeters) in diameter with a 0.04-inch (1-millimeter) wall is used. The disks are 0.08 inch (2 millimeters) thick and contain fifty 0.12-inch (3 millimeter) perforations. The void between the silicone plugs is pressurized at 95 lb/in.^{2} (656×10^3N/m^2) gage.

This work was done by Herbert V. Massey of Federal-Mogul Corp. for **Johnson Space Center**. *No further documentation is available.*
MSC-18450
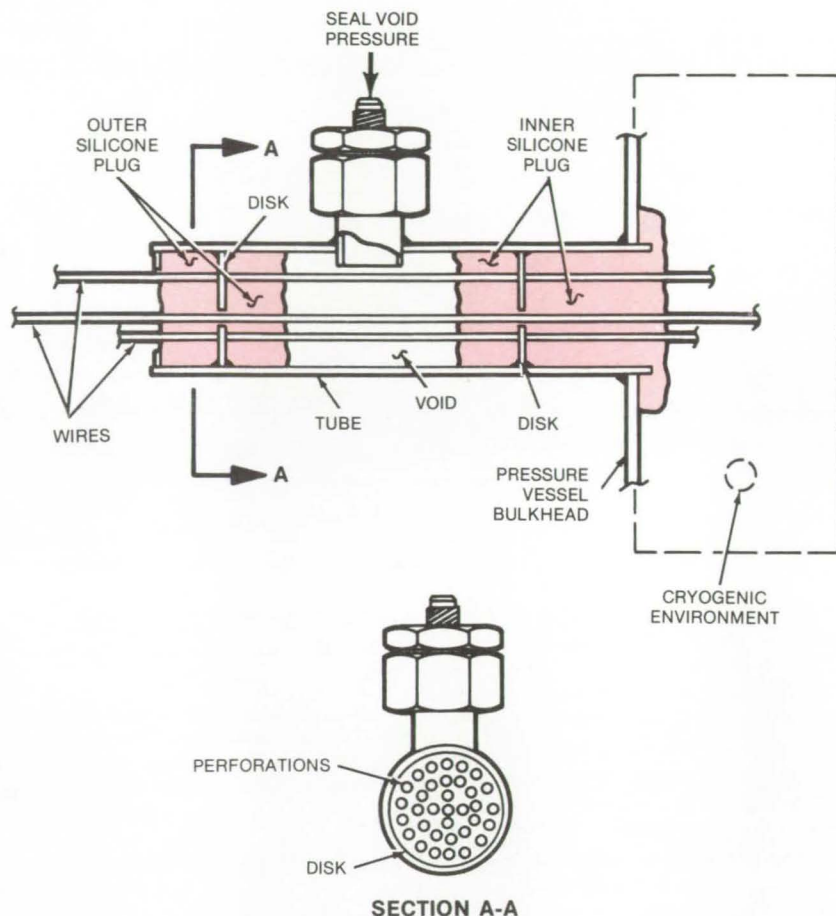
The **Pressurized Void** at the center of the instrument-wire tube prevents the cryogenic fluid from contacting — and shrinking — the outer silicone plug.

Strong, Corrosion-Resistant Aluminum Tubing

If its chemical composition is carefully controlled, 5083 alloy can be drawn into thin-wall tubing with excellent mechanical properties.

Lyndon B. Johnson Space Center, Houston, Texas

When aluminum tubing having good corrosion resistance and postweld strength is needed, type 5083 alloy should be considered. Although this 4-percent magnesium, 0.30-percent manganese alloy is not usually regarded as drawable into tubing, by careful control of the metallurgical composition of the master ingot, it is possible to fabricate large-diameter, thin-wall tubes in H32 (strain-hardened, one-quarter hard) temper.

Type 5083 alloy is being used in the Space Shuttle radiator manifold, where 6061 aluminum alloy has insufficient postweld strength to meet design requirements and where size limitations and adhesive bonds make heat treatment impractical. The postweld tensile yield strength of type 5083 is in the 20-ksi (138×10^6-N/m^2) range. Moreover, whereas type 6061 is prone to cracking in thin-wall, low-penetration weld configurations [the radiator manifold wall thickness is only 0.035 in. (0.089 cm)], type 5083 does not crack if drawn from carefully-prepared master ingots.

A chemical and mechanical specification for 5083 aluminum thin-wall tubing can be obtained by requesting the Technical Support Package referenced at the end of this article. Possible uses of the tubing are in aircraft, boats, docks, underwater platforms, heat exchangers, chemical process equipment, and other assemblies requiring high strength in the as-welded condition.

This work was done by Madison W. Reed and Frank E. Adams of Vought Corp. for **Johnson Space Center.** *For further information, Circle 78 on the TSP Request Card.*
MSC-18040

Dynamic-Pressure Regulator

Servo/transducer accurately controls
gas pressure as a function of time.

Lyndon B. Johnson Space Center, Houston, Texas

A computerized pressure regulator controls the gas pressure in a fixed-volume container, increasing, maintaining, and decreasing pressure according to preprogramed instructions. An existing model, which is used for dynamic-pressure testing in the range between 0 and 90 psi (0 and 0.6×10^6 N/m^2), gives a pressure-vs.-time profile that is reproducible within 5 percent, whether the pressure is increasing or decreasing; the hold pressure is reproducible within 0.5 percent.

Unlike controllers that set the pressure by using mechanical regulators or orifices that are calibrated for a given container, the new controller can be adapted (by reprograming) for virtually any volume size or shape. The pressure variation can also be synchronized with selected process parameters. In chemical processing, for example, the regulator could control the pressure in pipes, tanks, and other containers as the chemical reaction progresses.

As shown in the figure, digital pressure-vs.-time commands are generated by a computer and converted to analog voltages by a digital-to-analog converter (DAC). The analog signals enter a servoamplifier, which converts them to current signals. An adapter
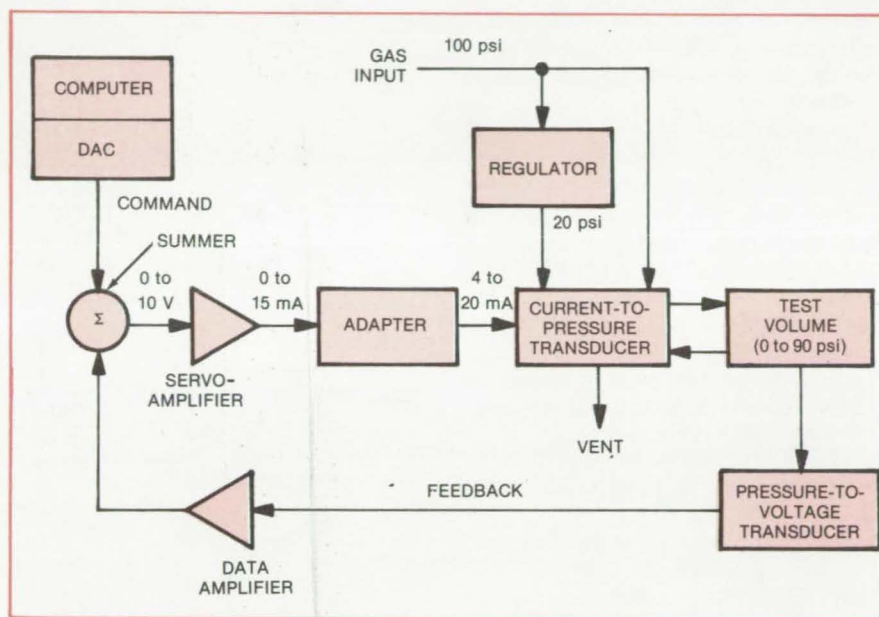
As Directed by a Computer, the dynamic-pressure regulator admits or vents air to control the pressure in a test volume.

corrects the current for scale and offset and sends it to a current-to-pressure (I/P) transducer, which then supplies the required pressure to the test volume. The pressure in the volume is sensed by a transducer and fed back as a voltage to the servosummer to form a closed-loop feedback system.

This work was done by Robert R. Walker of Rockwell International Corp. for **Johnson Space Center.** *For further information, including a diagram of the adapter circuit, Circle 79 on the TSP Request Card.*
MSC-18415

Balanced-Force Flow-Regulator Valve

Porous control element reduces surfaces
that cause unbalanced flow forces.

Lyndon B. Johnson Space Center, Houston, Texas

A new valve regulates fluid pressure or flow by means of a porous barrier. Unlike conventional regulating valves, which employ flat, conical, or spherical poppets as closure elements, the new valve reduces the surfaces exposed to the liquid or gas flow that causes unbalanced pressure forces. Unlike other regulators designed specifically to minimize unbalanced forces, such as curtain-flap valves and piston-metering valves, the new regulator can operate with low leakage over a wide range of pressures.

Essentially, the new regulator valve (see figure) controls fluid flow by alternately exposing solid and porous barriers to the fluid in response to pressure differences within the valve assembly. When the porous barrier is exposed, the fluid can flow from the valve inlet to its outlet. When the solid barrier is exposed, the fluid cannot flow.

A hollow stem with a disk piston at

its top separates the lower (inlet) and upper (outlet) chambers of the valve. The disk piston is spring-loaded to bias it toward a high (open-valve) position.

The stem wall contains a section of porous material near its base. This portion of the stem is formed by welding a cylindrical section of high-porosity sintered metal between solid-wall tubular sections of the stem. (Alternatively, other porous metals, plastics, or ceramics can be bonded between stem sections.)

When the stem is in its low (closed) position, illustrated in the main figure, a solid section of the stem blocks the flow of fluid. However, when the pressure in the upper valve chamber drops, the piston moves upward and uncovers part of the porous stem section (as shown in the detail portion of the figure). Fluid can then flow from the inlet through the porous section, the hollow center of the stem, and the upper chamber to the valve outlet.

When the pressure in the upper chamber rises, it forces the piston downward again. The porous section of the stem is covered once more, and the fluid flow stops. The various valve parts are equipped with plastic or elastomeric rings to seal them against leakage of the fluid.

In addition to its application in regulator valves, the porous stem principle can be used in simple hand valves, spool valves, and other devices that meter or control gases or liquids. A variation of the porous regulator valve has been designed with a fixed porous element. Instead of being part of the stem, the porous element is part of the valve body and is alternately covered and uncovered by a shoulder on a sliding plug.

This work was done by William C. Huber of **Johnson Space Center**. *For further information, including more details of design, construction, and operation, Circle 80 on the TSP Request Card.*

This invention has been patented by NASA [U.S. Patent No. 4,073,380]. Inquiries concerning nonexclusive or exclusive license for its commercial development should be addressed to the Patent Counsel, Johnson Space Center [see page A5]. Refer to MSC-12731.
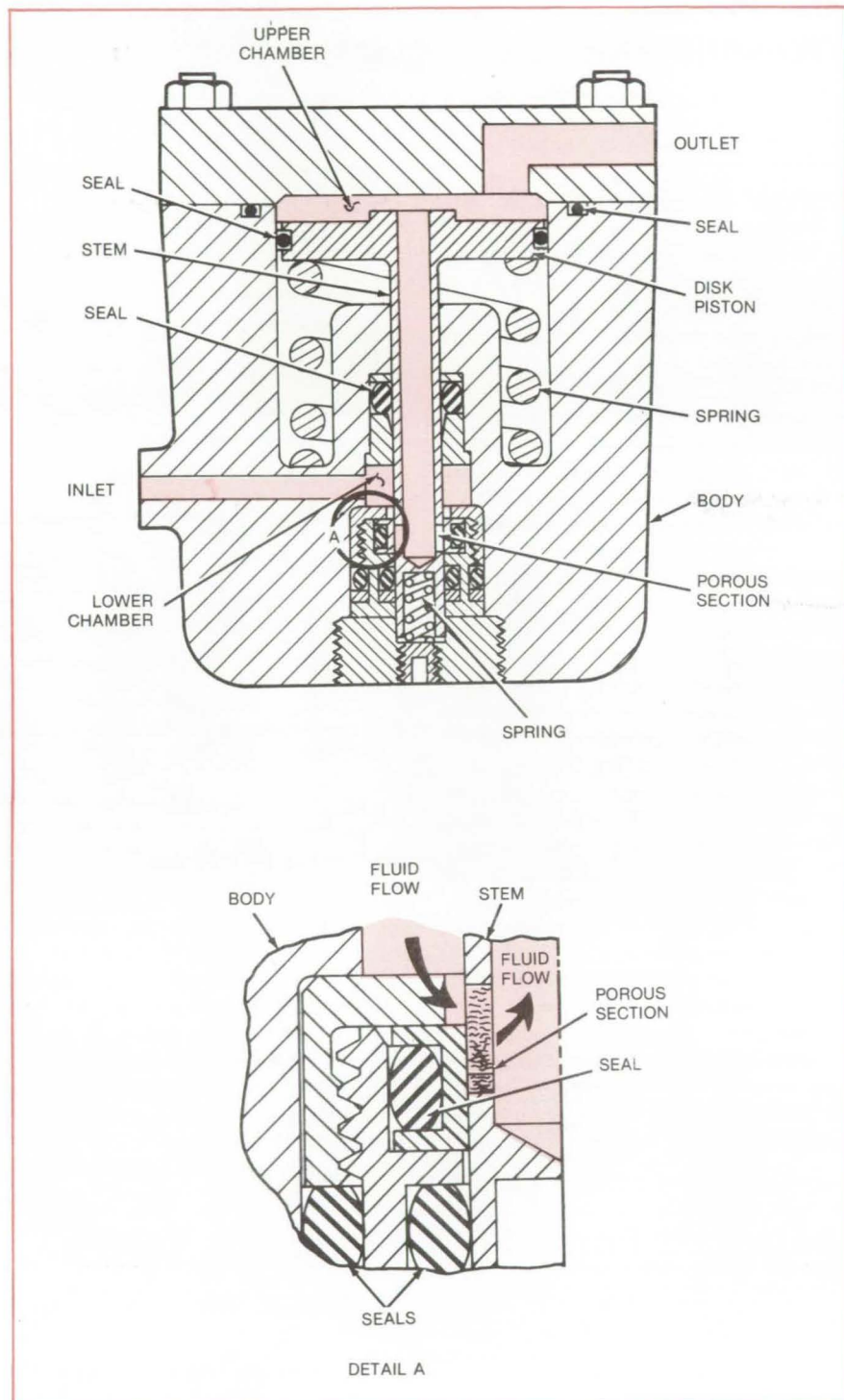
A Porous Section is built into the stem of this regulator valve. When the stem is in the closed position (large diagram), the porous section is covered, and there is no flow of fluid from inlet to outlet. However, in the open position (detail diagram), part of the porous section is exposed, and fluid flows through it. Because the porous section extends around the outside circumference of the stem, fluid enters the stem radially from all sides.

Improved Wrapped-Curtain Seal

A foam pad improves the reliability
of a simple thermal seal.

Lyndon B. Johnson Space Center, Houston, Texas

An improved wrapped-curtain thermal seal for the gap between the fixed wing and movable elevon on the Space Shuttle could be modified to seal spaces around doors, windows, partitions, and other movable assemblies. Designed for simplicity, the seal uses no springs or other mechanical devices and is easily installed on already-existing structures. It will fit in small gaps without interfering with the operation of the moving parts, and with a proper choice of materials, the seal can be used in high- or low-temperature applications. (The Shuttle seal operates from -95° to +260° C.)

As shown in the figure, a flexible material or "curtain" is attached to the fixed surface on one side of the seal. A low-density silicone foam, or a similar material, is bonded to the inside surface of the curtain. The curtain then wraps around a tube and is fastened to the movable surface on the other side of the seal.

When the surface on the right side of the seal moves, the curtain is pulled tightly against the tube, compressing the foam. Since the curtain is the only moving part in the seal and is cushioned by the pad (previous wrapped-curtain seals did not use a foam pad), it can withstand repeated cycling without creasing, wrinkling, or tearing.

BEFORE MOTION   **AFTER MOTION**
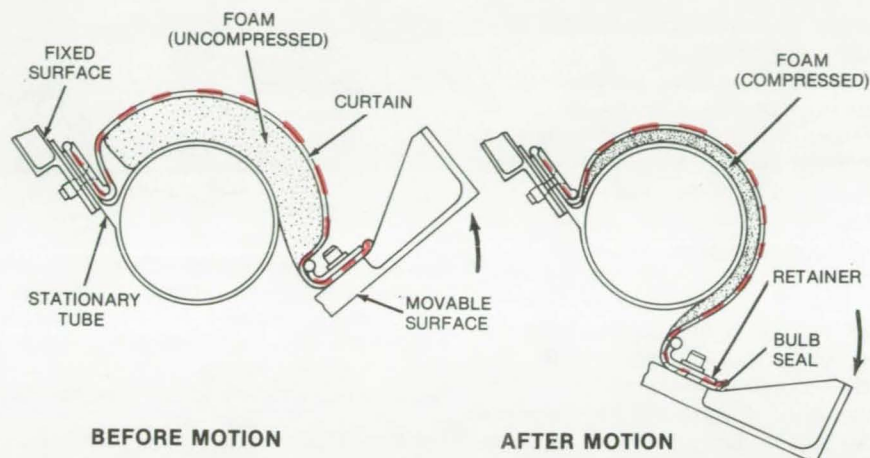
This **Wrapped-Curtain Seal** includes a foam pad that absorbs flexure in the curtain and prevents wrinkling. Possible applications range from aerothermal seals on aircraft and other vehicles to seals around doors and windows in homes.

In the Shuttle seal, a silicone-coated, modified-nylon-fiber felt curtain allows operation at elevated temperatures, and the bias weave of the curtain absorbs shear stresses. At the pad inner surface, a coating of tetrafluoroethylene could be added to reduce sliding friction between it and the tube.

Reliable fastenings at the points where the curtain attaches to the two surfaces are critical to satisfactory operation of the seal. The bulb seal shown is one relatively simple approach to making the attachment. The bulb is an integral part of the curtain edge and is compressed tightly against the retainer flange as the curtain is pulled taut. For greater stiffness and strength, a reinforcing batten could be added to the curtain edge.

This work was done by Paul M. Schroeder of Rockwell International Corp. for **Johnson Space Center.** *For further information, Circle 81 on the TSP Request Card.*
MSC-16647

Zero-Leak Valve

A relatively simple design could reduce
fabrication costs for a zero-leakage valve.

NASA's Jet Propulsion Laboratory, Pasadena, California

A proposed zero-leakage valve has a fluid-sealing diaphragm support and a flat sievelike sealing surface. When the valve (see figure) is closed, the diaphragm is flat and rests lightly on the valve seat. When fluid begins to flow into the valve, it lifts the diaphragm, flows over the valve seat with very little pressure drop, and then leaves the valve.

Zero-leakage valves typically have a forged body, all-welded construction, and are fabricated to very close tolerances. As such, they are expensive and require constant surveillance to ensure proper operation. The diaphragm-support valve, on the other hand, is easy to fabricate and should require minimum maintenance. It has potential applications as an isolation

valve for waste systems and as a remote air-actuated valve. It is expected to be useful in controlling the flow of liquid fluorine and other corrosive fluids at high pressures.

The incoming fluid passes through several small passages drilled in a flat plate. The fluid spreads across the face of the valve seat, lifting the
(continued on next page)

diaphragm against the top element. The fluid then leaves the valve through a second set of small passages. Because the critical sealing surface of the valve is flat, it can be easily lapped to any tolerance.

The fluid-sealing diaphragm is placed across the flat valve seat. Stacked on top of the diaphragm are a number of flexible disks capped by a second diaphragm.

The valve is closed (or opened) by applying mechanical pressure or fluid pressure to (or removing pressure from) the second diaphragm via the actuator port in the valve top. The pressure is transmitted through the stacked flexible disks, which distribute the applied pressure uniformly across the sealing diaphragm. The disks lie loosely within a ring so that they are free to move in response to the pressure applied to them.

For liquid fluorine and high temperature applications, the valve could be constructed entirely of metal. For less

severe applications, other materials such as plastics could be used.

This work was done by William F. MacGlashan, Jr., of Caltech for
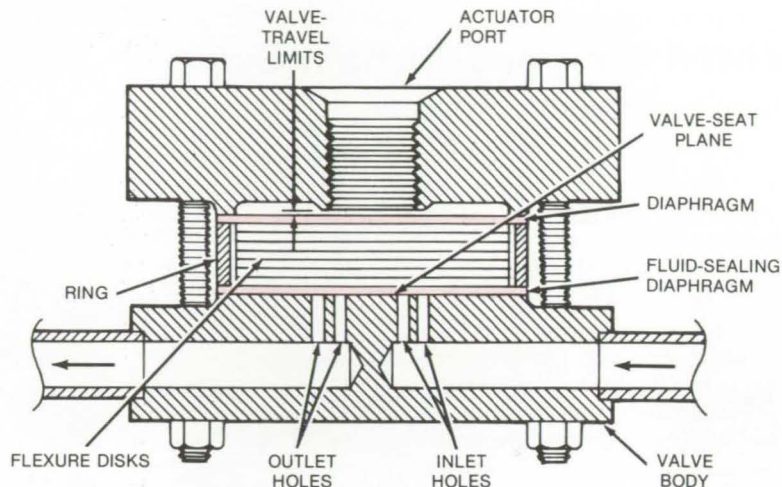
In a **Diaphragm-Supported Valve,** fluid passes through a large number of small intake holes drilled in the flat sealing surface, into a very small chamber above the plate, and then leaves the valve through a second set of small outlet holes. Stacked above the valve body are a fluid-sealing diaphragm, a number of flexible disks loosely contained within a ring, and a second diaphragm. Top, diaphragms, ring, and body are rigidly bolted together, forming a gastight configuration.

NASA's Jet Propulsion Laboratory.
For further information, Circle 82 on the TSP Request Card.
NPO-14717

Computer Programs

Separation Region on Boattail Nozzles

Analytical model for subsonic speeds

Boundary-layer flow separation often occurs on the afterbody of an aircraft, increasing the drag and decreasing the aerodynamic performance. A computer subroutine package, VISCUS, offers the flow analyst a practical engineering computational procedure to model the viscous effects of separated reverse flow on afterbody pressures and drag. The package includes an aerodynamic interface setup so that VISCUS can be coupled iteratively with an inviscid-flow calculation, thereby creating a full flow-analysis system. A special discriminating streamline calculation accounts for displacement effects of the reverse flow in separated regions with and without a flowing jet.

VISCUS uses the modified Reshoto-Tucker method with the Ludweig-Tillman skin-friction law to calculate the boundary layer. In the first iteration, the boundary layer is calculated over the original contour. Four different separation pressures can be calculated based on the control-volume criterion, Goldschmied's criterion, the modified Page's criterion, or Stratford's criterion. The user selects the criterion, and the program calculates the separation point. After the second iteration, the separation point locations are averaged. Additional restraints on the movement of the separation point improve convergence.

The separation point is used as the starting point for calculating the discriminating streamline. An axisymmetric control-volume calculation is used to account for changes in pressure, skin friction, and shear stress. The user may also specify that jet entrainment effects from the nozzle exit are to be included. VISCUS calculates the aerodynamic contour by adding the boundary-layer displacement thickness to the original contour or to the separated contour, if separation occurs. This contour may then be used in an inviscid program to recalculate the external inviscid solution.

The VISCUS subroutines are written in FORTRAN IV for batch execution and have been implemented on a CDC 6000-series machine with a central memory requirement of approximately 103K (octal) of 60-bit words. This program was developed in 1978.

This program was written by J. D. Buteau, R. W. King, and W. M. Presz, Jr., of United Technologies Corp. for **Langley Research Center.** *For further information, Circle M on the COSMIC Request Card.*
LAR-12453

Fabrication Technology

Fixture for Winding Transformers

Toroid-shaped transformer cores are
firmly held in place for manual winding.

NASA's Jet Propulsion Laboratory, Pasadena, California

A bench-mounted fixture assists the operator in winding toroid-shaped transformer cores. The toroid is rigidly held in place as the wires are looped around. The arrangement frees both hand for rapid winding. Frequent untangling of the wires that occurred when the core was hand held is eliminated.

The fixture (see figure), easily adjusted to accommodate various toroid sizes both in height and in diameter, is supported by a structure clamped to a working bench. A toroid core is placed on a nonslipping pad flush against two vertical bumpers. The bumpers prevent the core from falling during the winding process.

The fixture height is adjusted by removing two wingnuts on the back of the cam mechanism. One or two blocks are slipped underneath the mechanism, raising it, and the nuts retightened. To lower the fixture, some of the bottom blocks are removed. For large core diameters, the wingnuts are loosened, and the cam mechanism is slid back.

A spring-loaded cam mechanism locks the toroid in place. The mechanism is controlled by a lever moved to vertical position to release the mechanism and returned to horizontal position to lock the toroid in place.

Once the toroid is in place and the fixture adjusted, the cam mechanism
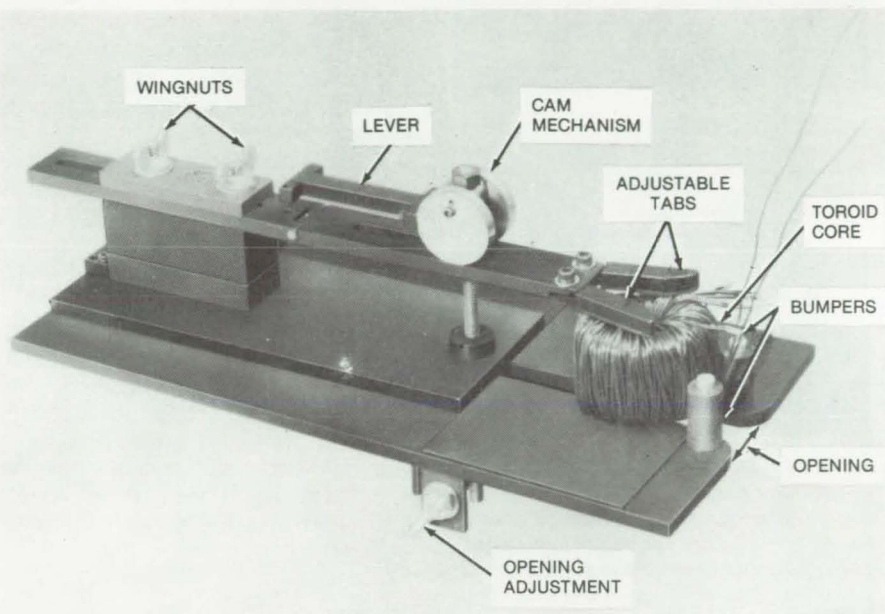
A **Convenient Fixture** for winding toroid-shaped transformer cores locks the core in place, freeing both hands for looping the wires around the core. The toroid is held in place by a lever-operated cam mechanism. By raising the lever, the core is unlocked, turned, and locked again for further winding. An adjustment on the back end of the fixture held by wingnuts slides the cam back for large-diameter cores and raises or lowers it for various core heights.

is lowered. The operator makes sure that one of the two tabs pinches one end of the wire so that he can pull against it as he winds the loops. After several loops are wound, the toroid is released, turned, and locked again for further winding. The process is re-

peated until the core is wound.

This work was done by Colonel W. T. McLyman of Caltech for **NASA's Jet Propulsion Laboratory.** *For further information, Circle 83 on the TSP Request Card.*
NPO-14146

Fabrication of a Pillowed Airbag

Compartmented rubber bag
makes a conformal cushion.

Lyndon B. Johnson Space Center, Houston, Texas

A rubber airbag composed of many small air "pillows" can be used as a cushion for equipment during shipment. Pressures in the pillows can be adjusted individually to suit a given cargo. Developed to simulate air-pressure loads on the Space Shuttle

nose cap, the pillowed airbag can also be used to apply uniform pressure to plastics or composites during curing.

The airbag is fabricated from two rubber sheets that are bonded only at the boundaries of the individual pillows. The first sheet of semicured

rubber is placed over a mold containing the pattern of the pillow compartments. Pressure is applied to the sheet, through the medium of a vacuum bag, so that the sheet surface conforms to the pillow pattern and the
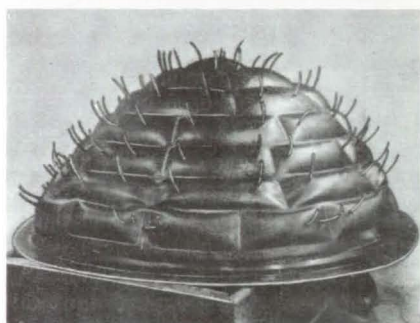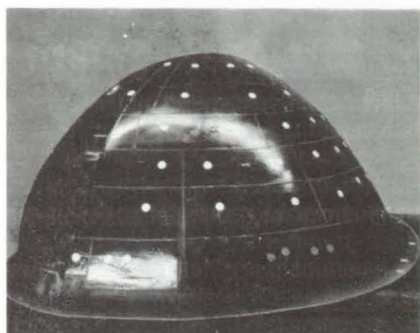
To make a **Pillowed Airbag,** one rubber sheet is bonded to another along the lines marked with tape in the top photo. Holes for inflation tubes are cut in the second rubber layer at the sites marked by disks. The pillow compartments in the finished airbag (bottom photo) can then be pressurized individually for packing any particular object.

divisions between pillow compartments become clearly visible (see upper photograph).

The vacuum bag is removed, and a strip of aluminum-foil adhesive tape, 1/4 inch (0.64 centimeter) wide, is placed around the compartments to delineate the pillows. A mold-release agent is sprayed over the sheet. The aluminum strips are peeled away, leaving blocks of the release agent separated by strips of clean rubber (Toluene is used to remove traces of the tape adhesive.)

Two small tetrafluoroethylene (TFE) disks are placed in each pillow rectangle. Later, these disks will provide a hard surface for cutting tube holes in an outer rubber layer without damaging the inner rubber layer.

Next, a second layer of semicured rubber sheet is placed over the mold. A glass-cloth bleeder layer is then placed over the second rubber sheet, and the mold is covered with a vacuum bag and placed in an autoclave. There the rubber sheets are cured at a pressure of 70 to 80 lb/in.^{2} (500x10^3 N/m^2) and a temperature of 340° F (170° C) for approximately 3 hours.

After the cure, the vacuum bag and bleeder cloth are removed. The second rubber sheet then adheres to the first sheet in the narrow strips where there is no release agent, thereby forming pillows (as yet uninflated).

Holes are cut through the top rubber layer of each pillow, with the TFE disks as a backup for the cutting tool. The disks are removed through the newly cut holes. Rubber tubes are inserted in the holes and bonded to the outer rubber sheet with an adhesive. The pillows can then be inflated through the rubber tubes and the tubes sealed (lower photograph).

This work was done by Leon M. Lambert and George Okamoto of Rockwell International Corp. for **Johnson Space Center.** *For further information, including details of the processing, Circle 84 on the TSP Request Card.*
MSC-18455

Technique for Mounting Pyroelectric Detector Arrays

Silicon integrated-circuit technology is used to form
quasi-free mounts that eliminate wire bonding.

Langley Research Center, Hampton, Virginia

A new technique has been developed at Langley Research Center for mounting pyroelectric detector arrays on silicon integrated circuits. It is desirable to mount pyroelectric detector elements so that they are as close to "free hanging" as possible, in order to minimize thermal conductance and consequently to improve responsivity. Many single-element detectors are mounted in this way. The new technique incorporates normal silicon integrated-circuit technology to form quasi-free mounts for detector arrays.

Previously, pyroelectric detector arrays have been produced by cementing the pyroelectric chip to a ceramic substrate and wire-bonding the individual detector elements to the

load resistors and to the FET's, which are also cemented to the ceramic substrate. This method has the disadvantages of creating thermal contact over an entire side and of requiring a minimum of three wire bonds per element.

The new mounting technique applies integrated-circuit technology to form the mounting fixture for a linear array of pyroelectric detectors, to attach the detectors to the mounts, and to deposit the biasing resistor for these detectors. The mounting fixture is formed by etching (through a photolithographically formed mask) a series of holes in the silicon dioxide, which has been thermally grown and/or pyrolytically deposited on the silicon

substrate. This step forms the nearly-free-hanging mounting supports that are desirable for pyroelectric detectors.

The detector strip is mounted over these holes by coating and patterning (with photolithography and metal-etching) a soft metal such as indium on both the silicon dioxide and the pyroelectric material. These two materials are then cold-welded together. The ground connection for the detectors is formed by depositing, patterning, and etching a thin film of gold or chromium on the upper surface of the pyroelectric film and then wire-bonding to a metalized pad on the silicon dioxide surface.

The biasing resistor is formed by the pyrolytic decomposition of silane gas to deposit polycrystalline silicon on the surface of the silicon dioxide. Undoped polycrystalline silicon has a resistivity of approximately 2×10^5 ohm-cm. Hence, by using standard silicon device dimensions, a biasing resistor as large as 1×10^{12} ohms can be integrated on the chip.

The advantages of this technique over prior art appear to include lower cost, better image registration, improved reliability, and quasi-free mounting for improved responsivity.

This work was done by Roger A. Breckenridge, Archibald L. Fripp, and James B. Robertson of **Langley Research Center.** *No further documentation is available.*

Inquiries concerning rights for the commercial use of this invention should be addressed to the Patent Counsel, Langley Research Center [see page A5]. Refer to LAR-12363.
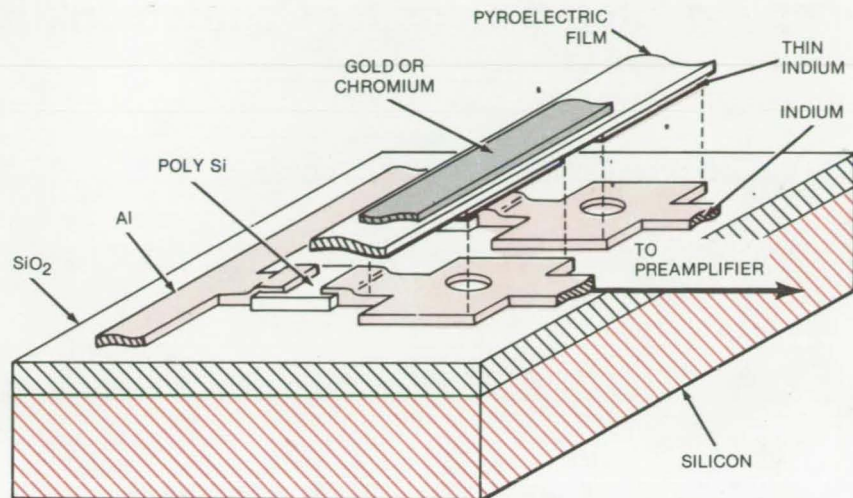
A **Pyroelectric Detector** can be mounted on a silicon substrate using integrated-circuit technology. A quasi-free mount is obtained by etching a series of holes in the SiO_2 and joining the detector and SiO_2 by cold-welding a thin film of indium formed on each.

Repairing Ceramic Insulating Tiles

A press-fit plug repairs glazed silica tiles.

Lyndon B. Johnson Space Center, Houston, Texas

Fused-silica tiles containing large voids or gouges can now be repaired without adhesives by a plug-insertion method. The tiles, which are potentially useful in conduits for high-temperature gases, in furnaces, and in other applications, are the protective heat-insulating outer surface of the Space Shuttle. Previously, tiles containing defects deeper than 0.02 in. (0.05 cm) and longer than 0.5 in. (1.35 cm) had to be discarded. (Powder patches in such defects tended to dislodge when they were glazed.)

In the new repair method, the damaged area is bored out, and a matching plug, machined to an interference fit from the same fused-silica material, is inserted in the hole. When the tile is later glazed and fired, the high firing temperature (220° F, 105° C) shrinks the tile around the plug, locking it in the hole. Tiles repaired this way have withstood 100 simulated Space Shuttle missions. The scrap rate in tile manufacturing has been reduced by 8 percent, and costs and delivery problems have been significantly reduced.

The defect is machined out of the tile with a flat-bottom diamond drill with a diameter at least 0.06 in. (0.15 cm) larger than the defect. The drilled hole is flat-bottomed and is at least 0.75 in. (1.9 cm) in depth.

The fused-silica plug is flat-bottomed and is machined to a diameter 0.005 to 0.010 in. (0.013 to 0.025 cm) greater than the hole diameter and a length 0.25 in. (0.64 cm) longer than the hole depth.

The plug is press-fit to the bottom of the hole. Then the portion of the plug protruding above the tile surface is cut off with a knife. The plug is sanded flush with the surface, and the tile is ready for glazing.

This work was done by Ben R. Dunn and Earnest L. Laymance of Rockwell International Corp. for **Johnson Space Center.** *No further documentation is available.*

Inquiries concerning rights for the commercial use of this invention should be addressed to the Patent Counsel, Johnson Space Center [see page A5]. Refer to MSC-18368.

Dimpling Aircraft Skins for Countersunk-Head Rivets

Hand-operated tool replaces
bulky pneumatic devices.

Langley Research Center, Hampton, Virginia
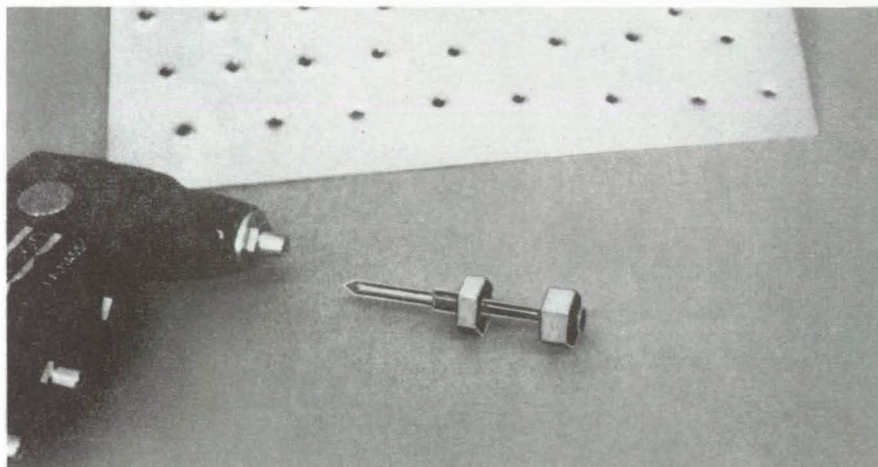
Figure 1. **Dimpling Tool** is shown with a sample of riveted airframe skin.
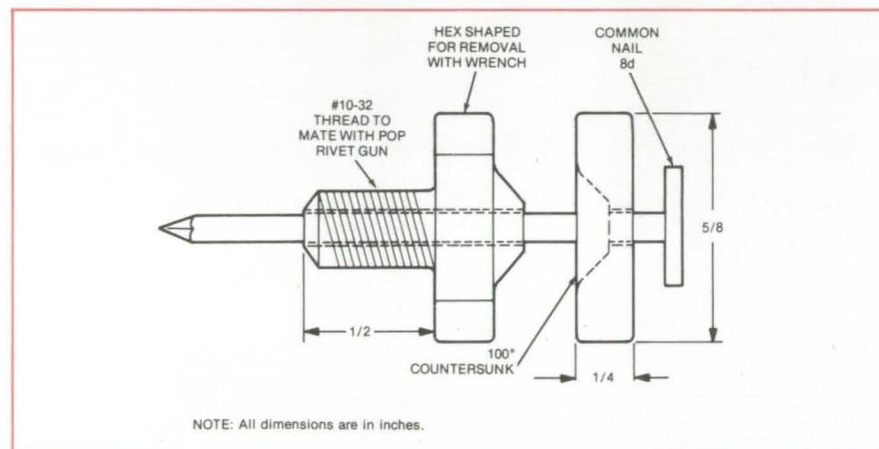
Figure 2. **Adapter** for the dimpling tool is made from 174PH bar stock that has been heat-treated. If the threading does not match the rivet gun, a larger set, which comes with the gun, can be annealed, drilled, tapped, reheated to cherry red, and quenched in water to harden.

An inexpensive hand-operated tool is used at Langley Research Center to dimple airframe skins to receive countersunk-head rivets. New male and female mandrel dies were designed to fit a commercially-available pop rivet gun.

The tool, as shown in Figures 1 and 2, replaces bulky pneumatic equipment normally used for dimpling. It compresses an airframe skin 100° to receive 100° rivets.

Since no air supply is necessary, this new tool will permit dimpling in many structures where the mandrel on a pneumatic tool cannot be used because of throat-depth restrictions. Furthermore, the specially-designed stainless-steel dies are inexpensive and can be readily fabricated in any machine shop. In most instances, one man can perform the dimpling process without assistance, thereby saving considerable time and manpower.

This work was done by Jack G. Barbour of **Langley Research Center.** *No further documentation is available.* LAR-12240

Safe Bending of Boron/Aluminum Sheets

Aluminum backing sheets protect a boron/aluminum
sheet from cracking during bending.

Lyndon B. Johnson Space Center, Houston, Texas

An expensive process of diffusion-bonding a steel facing sheet to a boron/aluminum sheet to prevent the latter from cracking or stretching during bending (parallel to the boron/aluminum fiber) can be replaced by a simpler low-cost procedure. Two aluminum facing sheets are epoxy/polyamide-bonded on each side of the boron/aluminum sheet. After the bending, the protective sheets are removed by heating the assembly. When steel facing is used, it is removed by chemical milling. The new process utilizes low-cost universal-brake bending dies rather than special hydroforming dies.

The process has been utilized in making the Space Shuttle avionics
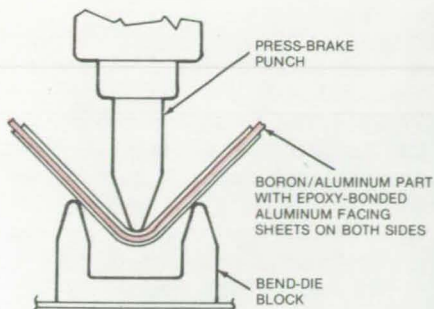
Figure 1. **Two Aluminum Facing Sheets** protect a fragile boron/aluminum sheet from cracking or stretching during the brake bending process. The facing sheets are adhesive-bonded on each side of the boron/aluminum blank and are easily removed by heat. In some cases, a single aluminum facing sheet may be used on the outside of the bend and the punch nose covered with a polytetrafluoroethylene tape.

Figure 2. The **Finished Boron/Aluminum Channel** is shown in the foreground of the new Space Shuttle avionics shelf. The boron/aluminum reduces the shelf weight by 50 percent.

shelves out of boron/aluminum channels and facesheets. The material is 50 percent lighter and equally as rigid and strong as the previously-used 6061-T6 aluminum. Boron/aluminum channels 0.014 in. (0.36 mm) thick are bent 90° with a press-brake bend die having a minimum inside radius of 1/8 in. (3.2 mm) (see Figure 1).

Two 0.030-in. (0.76-mm) aluminum facing sheets are epoxy/polyamide-bonded on each side of the boron/aluminum sheet, using a commercial epoxy mix (e.g., 50/50 Epon 828, or an equivalent, and Versomid 120, or an equivalent). The applied adhesive coating is 0.004 to 0.006 in. (0.10 to 0.15 mm) thick. The sheets are held under contact pressure and cured at room temperature for 1 to 2 days.

The bonded sheet is placed on a conventional bend-die block and bent 90° by a press-brake punch. The bent assembly is removed and placed into an oven set at a maximum temperature of 400° F (205° C) to remove the facing sheets. Figure 2 shows the finished boron/aluminum shelf channel.

This work was done by Geza G. Liskay and Stanley Y. Yoshino of Rockwell International Corp. for **Johnson Space Center.** *No further documentation is available.*
MSC-19525

Heat-Shrinkable Film Improves Adhesive Bonds

A shrinkable film applies
pressure during the cure cycle.

Lyndon B. Johnson Space Center, Houston, Texas

Pressure can be applied during adhesive bonding by wrapping the parts in a heat-shrinkable plastic film. The film eliminates the need to vacuum bag or heat the parts in an expensive autoclave.

The procedure begins with the prefit, prime, and layup steps normally followed in adhesive bonding. Then, the layup is wrapped in a layer of nylon polyamide film followed by a layer of polyvinyl alcohol (PVA) film.

The wrapped parts are heated in an oven to cure the adhesive. In the oven, the PVA film shrinks, applying uniform pressure to the bond. The nylon wrap ensures that, after the cure, the parts can be released easily from the shrunken PVA film.

The shrinkable-film method has been used with success to bond metal tubes to curved half-tube doublers. Previously, the parts had to be placed in a vacuum bag and then cured at high pressure [45 psig (0.31x10^6 N/m^2)] in an autoclave. The new method can be carried out with much simpler and less costly equipment. Operators can be trained in the new procedure quickly, and no special skills are required.

This work was done by Joe M. Johns and Madison W. Reed of Vought Corp. for **Johnson Space Center.** *No further documentation is available.*
MSC-18437

Books and Reports

Design Rules for CMOS/SOS Circuits

Layout guidelines for integrated-circuit designers

A report presents design rules for advanced-technology integrated circuits made by the self-alined silicon-gate complementary-metal-oxide-semiconductor/silicon-on-sapphire (CMOS/SOS) process.

The report specifies spacing and width requirements for contacts, conductors, and other elements on these high-speed, low-power devices. Specifications are furnished for seven distinct masking levels:

1. P-type epitaxial islands,
2. N-type epitaxial islands,
3. Polysilicon areas,
4. N^+-type diffusion,
5. Contact areas,
6. Metalization, and
7. Protective oxide.

In addition, design rules are established for bonding pads for input and output leads.

At masking level 2, for example, the minimum allowable width of an n-type island is 0.3 mil (7.6 μm), while minimum spacings are 0.3 mil between n-type islands and 0.4 mil (10.2 μm) between n- and p-type islands. It is further stipulated that contour lines of n-type islands must be orthogonal.

For level 5, examples of correct and incorrect contacts are presented. This information is particularly valuable to designers of integrated circuits because there are so many possible arrangements, sizes, and shapes of contact openings. The guidelines cover both in-line and right-angle contacts.

The design rules are applicable to a variety of CMOS/SOS fabrication techniques and to double-epitaxial diffusion as well as single-epitaxial ion implantation. The report includes a standard color code and standard symbols for integrated-circuit layouts.

This work was done by the Government Systems Division of RCA Corp. for **Marshall Space Flight Center.** *For a copy of the report, Circle 62 on the TSP Request Card.*
MFS-25132

CMOS/SOS Processing

Alternatives and variations in fabrication processes are described.

A report describes processes used in making complementary-metal-oxide-semiconductor/silicon-on-sapphire (CMOS/SOS) integrated circuits. The report lists processing steps ranging from the initial preparation of sapphire wafers to the final mapping of "good" and "bad" circuits on a wafer.

Two alternative methods of forming transistors are presented: double epitaxial growth and ion diffusion. Several variations of the ion-diffusion process are presented, and the relative merits of each alternative are discussed.

Regardless of the transistor-formation process to be used, all sapphire substrates are prepared in the same way. First they are visually inspected for scratches, cracks, and chips. Then they are checked by X-ray diffraction for proper crystal orientation. Finally, they are cleaned and annealed. The report describes each of these procedures briefly.

A particular transistor-formation process — the single-epitaxial/single-ion-implant process — is recommended because it requires only six photolithographic steps. Consequently, this process is described at somewhat greater length and is illustrated by a detailed process sequence and by cross-sectional diagrams of the CMOS/SOS device at progressive stages in its fabrication. The transistors are formed in 0.6-μm-thick epitaxial silicon islands by implanting the islands with phosphorus ions and then diffusing boron and phosphorus into the islands to delineate sources, channels, and drains. A sample "lot card" for tracking the progress of wafers through the fabrication process is also included in the report.

This work was done by P. Ramondetta of RCA Corp. for **Marshall Space Flight Center.** *For a copy of the report, Circle 85 on the TSP Request Card.*
MFS-25176

Low-Cost Production of Solar-Cell Panels

A proposed manufacturing sequence combines state-of-the-art techniques to produce solar-cell panels at low cost.

A new large-scale production model combines the most modern manufacturing techniques in a facility to produce silicon-solar-cell panels at low costs by 1982. The model proposes a facility capable of operating around the clock with an annual production capacity of 20 MW of solar-cell panels. Each manufacturing step is defined with corresponding cost where applicable. All the costs are given in 1975 sollars per watt.

The modeled process is initiated by growing silicon crystal ingots by the Czochralski technique. A total of thirty-three 25-kg-capacity Czochralski furnaces is needed with melt replenishment apparatus to handle 428.2 metric tons of polycrystalline-silicon raw material per year. Five crystals weighing 100 kg can be grown from one crucible utilizing the melt replenishment.

The ingots are cropped, sectioned, and ground to a diameter for efficient packing of the cells during encapsulation. Next, the ingot sections are epoxy-bonded to ceramic and sliced into wafers by a multiblade slurry saw. A total of 39 900-blade saws is needed to meet the projected solar-panel production rate.

At this point, the majority of production costs have been incurred, at an estimated $1.358/W. Further processing

steps command significantly smaller cost increments. These include (a) treatment of the optical surface, (b) formation of the junctions, and (c) metalization of electrical connectors.

Texture-etching the active solar-cell surface with hot NaOH solution was judged the most practical optical surface treatment in mass panel production. Cell junctions are formed utilizing the $POCl_3$ gaseous diffusion process. The proposed metalization process is etching through a silk-screened wax pattern mask and immersing in electroless gold and electroless nickel. The entire cell-manufacturing sequence costs $0.302/W.

The plated cells are laser-trimmed and assembled into modules. The cells are interconnected in batches on a fixture in a vapor-phase solder reflow chamber. The finished panel has a low-iron front-surface glass plate and a standard float-glass backplate. Module fabrication amounts to $0.285/W.

After totaling the three major production costs, wafer making, cell manufacturing, and module fabrication, the total manufacturing costs are expected to be $1.945/W. The proposed processing sequence may be easily modified to include new developments in the manufacturing technology, leading to further cost reductions.

This work was done by Donald B. Bickler, Brian D. Gallagher, and Lloyd E. Sanchez of Caltech for **NASA's Jet Propulsion Laboratory**. *For further information, Circle 86 on the TSP Request Card.*
NPO-14453

RF-Sputtered and Ion-Plated Solid Lubricants

A review of recent advances

The recent advances in the tribological uses of RF-sputtered and ion-plated films of solid film lubricants (laminar solids, soft metals, organic polymers) and wear-resistant refractory compounds (carbides, nitrides, silicides) are reviewed in a current report.

This report illustrates and evaluates sputtered and ion-plated films, both soft and hard, in terms of friction, wear, and film durability. It also evaluates the manner in which such coating characteristics as adherence, coherence, density, thickness, internal stresses, growth morphology, and substrate conditions, such as surface temperature, topography, and chemistry, affect coating behavior.

The lubricating coatings were divided into two main groups based on their chemical, physical, and mechanical properties: the hard wear-resistant coatings (e.g., carbides, nitrides, and silicides) and the soft lubricating coatings with low shear strength (e.g., graphite, molybdenum disulfide, gold, and polytetrafluoroethylene).

Past experience has shown that virtually any coating can be stoichiometrically sputter-deposited without a binder, with strong adherence, and with a controlled thickness on curved and complex-shaped surfaces, such as retainers, races, balls, and gears. In addition, the sputtering technique is not limited by thermodynamic criteria and therefore offers a great flexibility to form coatings with graded interface compositions, laminated layers, dispersion strengthening, and other desirable additives. This technique permits tailoring film properties in ways not available with the other deposition methods. Available are many sputtering modes and configurations and the ability to prepare the sputtering targets in any desired chemical ratio by powder metallurgy techniques.

RF or dc diode sputtering systems with RF or dc substrate biases are the most widely used configurations for depositing solid lubricant coatings. Sputtering is essentially the only deposition technique that offers a high degree of operational flexibility and does not depend of the melting point and vapor pressure of refractory compounds (carbides, nitrides, silicides, and borides). Films of these compounds can be directly sputtered onto surfaces without alteration of the desirable properties of the bulk material.

The factors affecting film adherence and coherence that should be recognized and carefully controlled are: tar-

get preparation, type of interface formed, residual or internal stresses, film thickness, and interal and surface defects. All of these factors can contribute to premature failure of the film, and the coating may not wear by normal, relatively slow attrition but rather by a more accelerated wear mechanism such as spallation or delamination. The wear debris formed under these accelerated wear conditions can act in an abrasive manner, thereby accelerating the wear process.

Ion plating is the only plasma deposition technique where a direct potential (3 to 5kV) is applied directly across the specimen to be coated and the evaporation source. The specimen to be coated is made the cathode of the high-voltage dc circuit, and the evaporation source is made the anode. This technique differs from the other vacuum-deposition processes in that the plating material is partially ionized and strikes the specimen as charged or excited atoms rather than as neutral atoms.

In the report, the sputtering and ion-plating potentials and the corresponding coatings formed are evaluated relative to the friction coefficient, wear endurance life, and mechanical properties. The tribological and mechanical properties for each kind of film are discussed in terms of film adherence, coherence, density, grain size, morphology, internal stresses, thickness, and substrate conditions, such as temperature, topography, chemistry, and dc-biasing.

This work was done by Talivaldis Spalvins of **Lewis Research Center**. *Further information may be found in NASA TM-78841 [N78-20333/NSP], "Coatings for Wear and Lubrication," [$4.50]. A copy may be purchased [prepayment required] from the National Technical Information Service, Springfield, Virginia 22161.*
LEW-13147

Computer Programs

Photomask and Pattern Programs

Program helps engineers design masks and patterns.

A photomask is a photographic plate or film that carries a geometrical pattern representing part of the design of a device to be fabricated. It can be thought of as a link between design and fabrication. The use of a photomask is particularly suited to applications involving fine detail, reproducibility, repetition, and fabrication on the planar surface of a material. Items fabricated with photomasks include semiconductor integrated circuits, printed circuit boards, magnetic bubble devices, and integrated optics circuits.

A new package of computer programs helps designers with the layout and graphics of photomasks. They are not automated design or simulation programs; a design and an initial geometrical layout must be provided by the user. The programs help the designer with documentation, graphical verification, alteration, and updating. They also create data tapes that can be used to plot the mask geometry on a graphic device or to produce the finished photomask on a numerically-controlled pattern generator.

The programs also allow simplified specifications of pattern scaling, repetition, shifting, and image reversal. They can be used to generate certain complex geometries, alphanumeric characters, and alinement marks.

Basic geometrical specifications are input to the mask programs on punched cards, which may either be prepared by hand or by a drawing digitizer. Once the initial geometrical data have been processed, the mask pattern may be displayed on a CALCOMP plotter or on a Tektronix graphics terminal for visual inspection and verification. The design can easily

be altered or updated and new displays generated. Once a final design is obtained, the program generates a driver tape for the Mann model 1600 pattern generator.

The programs in this package are written in FORTRAN V for batch processing and have been implemented on a UNIVAC 1108 with a central memory requirement of approximately 38K of 36-bit words. The programs are intended for use with CALCOMP plotters or Tektronix graphics terminals.

This program was written by Randall K. Kirschman of Caltech for **NASA's Jet Propulsion Laboratory.** *For further information, Circle N on the COSMIC Request Card.*
NPO-14419

Solar Array Manufacturing Industry Simulation

Program models a multicorporation industry.

The Solar Array Manufacturing Industry Simulation (SAMIS) program is a standardized model of an industry to manufacture silicon solar modules for use in electricity generation. SAMIS simulates a hypothetical industry based on a structure that is developed interactively by the user.

The model is used to develop financial reports that detail the requirements, including amounts and prices, for materials, labor, facilities, and equipment required by the various companies and processes that comprise the industry. The "costs of doing business" (return on equity, interest on debt, and taxes, for instance) are also estimated.

Although SAMIS was developed to simulate the manufacture of solar arrays, it could be useful for producing price estimates for other types of production-line manufacturing. It serves as a consistent and reliable way of comparing manufacturing processes being developed by numerous independent efforts. It could also be used to assess the industry-wide impact of changes in such financial parameters as the cost of resources or services, inflation rates, interest rates, tax policies, and the required rate of return on equity.

The SAMIS methodology is simple, general, and expected to be useful in virtually any manufacturing industry. The program contains several important assumptions. Perhaps the most important is that demand is assumed to be known and steady; the resultant prices and expenses correspond to operation at that assumed scale.

A second major assumption is that all manufacturing processes are operated in a production-line mode. Thirdly, in order to calculate a definite annual cost rate, SAMIS assumes that the modeled factories have reached a steady-state operating condition but that a variety of "one-time costs" (startup expenses, interest during construction, and so on) are still being recovered.

The structure of the industry is defined by specifying who buys what from whom. Each hypothetical company is defined by listing its manufacturing processes and by specifying values for a variety of financial parameters. Each manufacturing process is defined in terms of performance and cost parameters along with a detailed list of direct requirements (such as floorspace, labor and energy requirements, and raw materials).

The user specifies the annual market production quantity; the SAMIS analysis is then initiated. All product and direct requirement quantities are calculated, using the industry structure and the process descriptions. Within each company, direct requirements are collected and used to develop a set of indirect requirements. Starting at the raw materials stage, all of the annual expenses of each company are calculated. Annual expenses include direct and indirect expenses as well as such financial expenses as profits and taxes. To facilitate detailed study, all expenses are allocated back to the manufacturing processes. A price that will just cover all expenses (and include profit) is calculated for the product of each manufacturing process, until the final product price is obtained.

This program was written by Robert G. Chamberlain, Paul J. Firnett, and Bruce Kleine of Caltech for **NASA's Jet Propulsion Laboratory.** *For further information, Circle P on the COSMIC Request Card.*
NPO-14747

Mathematics and Information Sciences
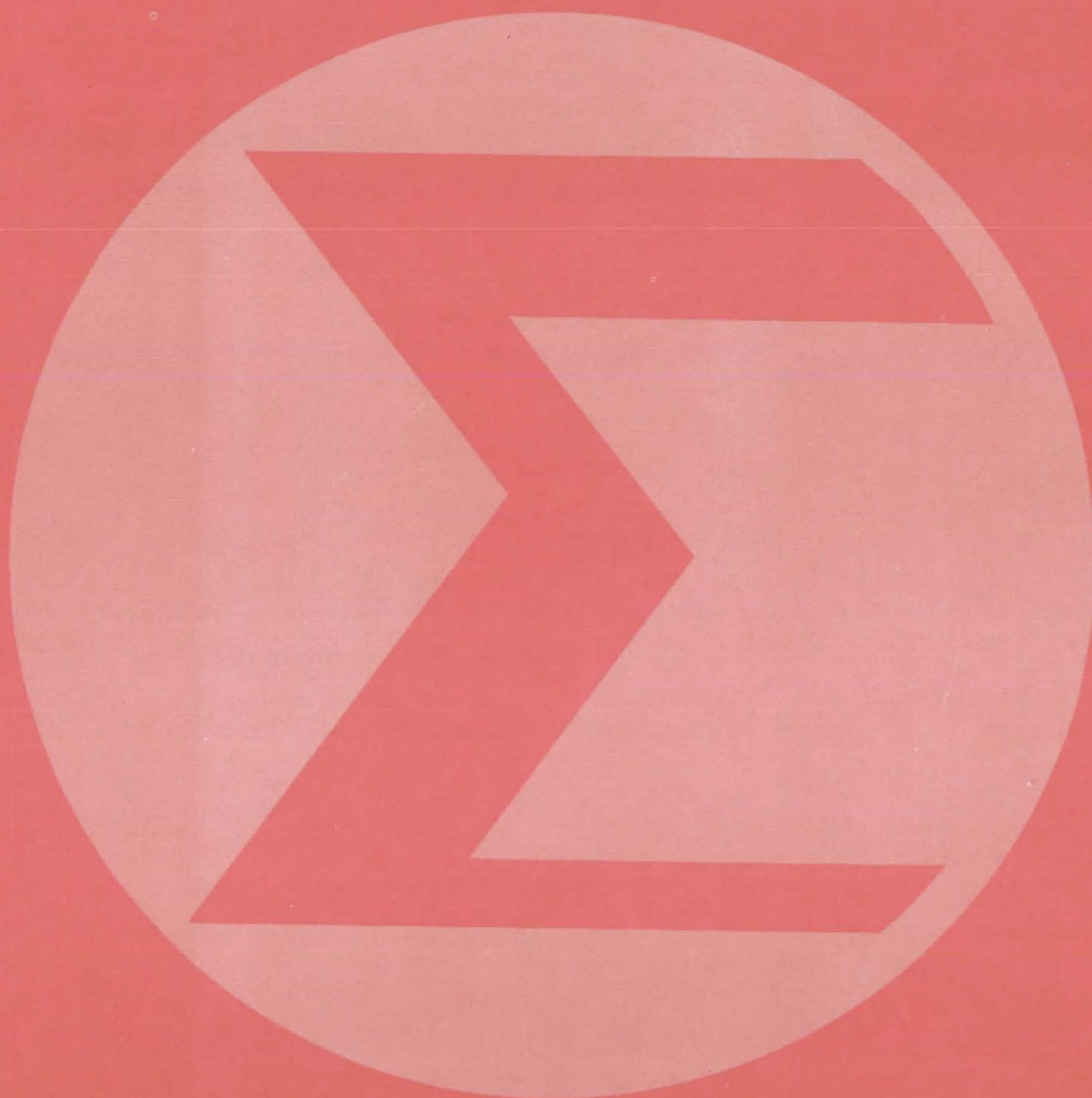
Revised Adage Graphics Computer System

Bootstrap loader and mode-control
options simplify operations.

Langley Research Center, Hampton, Virginia

Revised bootstrap loader and mode-control options for the Adage Graphics Computer System significantly simplify operations procedures. All normal load and control functions are performed quickly and easily from one work station — the control console — instead of four stations as previously required.

The prior procedure for loading the system monitor program included placing the bootstrap paper tape into the reader, reading and loading the tape and program with teletype instructions, proceeding to the DPR4 mode control panel to exercise mode control, and then going to the user work station to utilize the graphics computer system. Prior procedures required significant user activity and time, utilized slow and complex electromechanical paper tape and teletype systems, required storage of the bootstrap routine on a nonpermanent paper tape, and provided no redundancy of load and control capability.

The hardware bootstrap loader and mode control subsystem developed to provide alternate load and control capabilities consists of bootstrap enable and control input circuits, a timing chain and initialization circuit, a memory address register, an address decoder/memory select circuit, a read-only memory, and an output data multiplexer. The subsystem includes mode control buttons at the control console that are functionally parallel with the DPR4 mode control buttons. The subsystem serially transmits a set of instructions stored in programable read-only memory to the DPR4 computer in place of the former paper-tape/teletype loading sequence. Mode control is thus achieved at the control console as well as at the DPR4 control panel. The engineering specifications for this design conform to the DPR4 hardware reference manual with respect to TTL compatibility, voltage levels, channel transmission characteristics, and circuit-timing requirements.

The primary operating characteristics of the revised system include greatly increased speed, convenience, and reliability. The new system uses existing teletype-timing circuits and also the DPR4 system clock signals to reduce system loading time dramatically by a 4,000:1 ratio. Maintenance requirements are decreased because utilization of a complex electromechanical paper-tape reader and teletype system is reduced. Operations are generally conducted through a single board solid-state electronics system. Reliability is increased due to the use of solid-state electronics and the redundancy available through the parallel paper-tape and teletype system. Safety is slightly improved through the reduced use of mechanical elements.

This work was done by John S. Tulppo of Sperry Rand Corp. for **Langley Research Center.** *For further information, Circle 87 on the TSP Request Card.*
LAR-12492

Compiler Validates Units and Dimensions

Usage and compatibility of units
are checked by flexible program.

John F. Kennedy Space Center, Florida

Software added to the compiler for an automated test system for the Space Shuttle decreases computer run errors by providing offline validation of engineering units used in system command programs. The compiler checks for errors in the use of engineering units and for the compatibility of units used in arithmetic operations, in comparisons, and with data exchanged between the program and input/output devices. The validation procedures are general, though originally written for GOAL, a free-form language that accepts "English-like" statements, and may be adapted to other programing languages.

Unit	Mass	Length	Time	Temperature	Charge
°F	0	0	0	1	0
°C	0	0	0	1	0
In.	0	1	0	0	0
g/cm^3 (density)	1	-3	0	0	0
cm/s (velocity)	0	1	-1	0	0

Vector Representations of typical dimensions are shown in this table.

The engineering units validation has also been designed for flexibility and satisfies the following criteria:

• Units validation is open ended to allow easy addition and construction of new units;

• Automatic scaling is provided so that decimal values other than those consistent with an internal set may be used;

• The internal working units are converted back to those originally specified, and an abbreviated version of the original units is displayed; and

• The self-documentation provisions of the GOAL language are enhanced by the engineering units and their usage validation.

The compiler represents units by a "vector" that has 10 components: mass, length, time, temperature, charge, revolutions, angles, radians, counts, and mach. The first five components are basic physical quantities (see table); the remaining five are derived from the first five.

A unit of momentum, slug-feet per minute (or, dimensionally, mass-length-time^{-1}), is represented in the compiler by the vector (1,1,-1,0,0). This combination of components is automatically formed whenever velocity is multiplied by mass, regardless of the units specified or how the factors in the multiplication are formed.

Only compatible quantities (those having the same vector representation) may be used for input, output, comparison, and parameter passing. Arithmetic compatibilities are determined as follows:

• Only compatible quantities may be added or subtracted; the resulting quantity has the same vector representation;

• A new quantity results from multiplication; its vector is formed by vector addition of the multiplied quantities;

• A new quantity results from division; its vector is formed by vector subtraction of the divided quantities;

• A new quantity results from exponen-

tation; its vector is formed by scalar multiplication of the exponent by the original vector.

The compiler also distinguishes between "absolute" and "relative" quantities. Absolute quantities, such as meters, seconds, and miles per hour, may be multiplied and divided to produce other absolute quantities. Relative quantities, such as degrees (temperature) and gage pressure (psig), are subject to arithmetic restrictions. For example, gage pressure has different meanings on different days (since the atmospheric pressure changes). Thus, care must be exercised when these quantities are subtracted.

This work was done by F. E. Levine of IBM Corp. for **Kennedy Space Center.** *To obtain a report that describes the engineering units validation in more detail [not including a program listing], Circle 88 on the TSP Request Card.*
KSC-11054

Books and Reports

A Flexible Data Base

A centralized data base organized for easy access, understanding, and flexibility

A 102-page report describes a hierarchical multilevel, multientry-point data file, and the methodology of developing such a file for a unit-record-oriented system. The data base structure was prepared for the Goldstone Energy Project where it is used in analyzing past energy consumption, predicting future consumption, and aiding design of buildings. The methodology should be applicable to many of the data-base requirements, especially in the area of monitoring energy consumption.

The Goldstone Energy Data Base is a collection of organized "raw data"

grouped into electrical, mechanical, architectural, environmental, and other energy-related data. All of these groups consist of one or more files that are structured into three levels: primary, secondary, and tertiary. Files at the primary level contain the basic logical data records. The secondary-level files are detailed breakdowns of information in the corresponding primary files. The tertiary files are similar breakdowns of the secondary-level files.

The first, or initial, file of each level has a maximum record length of 80 characters. When the logical data record exceeds this length, from one to eight continuation files are available, each with an 80-character capacity.

For group identification, all files are given a three-character acronym preceding each numbering sequence. The first file of each group is given the number 100 and is referred to as the Initial Primary File. The Continuation Files (maximum of eight) are numbered 200 to 900 by increments of 100. Each Continuation File can have its own secondary and tertiary levels. The first secondary-level file of the Initial Primary File is numbered 101

and is referred to as the Initial Secondary File. Continuation Secondary Files (maximum of eight) are numbered from 102 to 109. The first tertiary file corresponding to the Initial Secondary File is numbered 110 and is referred to as the Initial Tertiary File. Continuation tertiary files (a maximum of nine) are numbered from 111 to 119.

Each file incorporates two records. The first entitled Identification Record contains the information identifying the file in relation to others, comparison documentation, and a person responsible for contents. The second entitled Header Record contains column headers alined over the field of each data item. The remainder of the file, the data records, all has the same column format.

The companion documents called out on the Identification Record describe the corresponding data group, include the names of the people responsible for data in the group, revision and control procedures, narrative information, and data for each file within the group.

This procedure has been developed for all of the groups in the program; building and utilities, exterior lighting,

interior arhitecture, interior electrical equipment, interior lighting, interior occupancy, powerplant, and weather group.

Computer Programs

Computing Time- and Frequency-Domain Analysis

Computation of several types of statistical descriptors

Time-series data (normally a collection of numerical observations made at specified time intervals) are often subjected to two kinds of statistical analyses. First, the time series may be treated as a set of independent observations using a time-domain analysis to derive the usual statistical properties, including the mean, variance, and distribution form. Secondly, the order and time intervals of the observations may be used in a frequency-domain analysis to examine the time series for periodicities.

In almost all practical applications, the collected data are actually a mixture of the desired signal and a noise signal that are collected over a finite time period with a finite precision. Therefore, any statistical calculations and analyses are actually estimates. A computer program, Spectrum Analysis (SPA), was developed to perform a wide range of such statistical-estimation functions. It is a rigorous tool for time- and frequency-domain studies.

In a time-domain statistical analysis, the SPA program will compute the mean variance, standard deviation, mean square, and root mean square. It also lists the data maximum, data minimum, and the number of observations included in the sample. In addition, a histogram of the time-domain data is generated, a normal curve is fitted to the histogram, and a goodness-of-fit

test is performed. These time-domain calculations may be performed on both raw and filtered data.

For a frequency-domain statistical analysis, the SPA program computes the power spectrum, cross spectrum, coherence, phase angle, amplitude ratio, and transfer function. The estimates of the frequency-domain parameters may be smoothed with the use of Hann-Tukey, Hamming, Barlett, or moving-average windows. Various digital filters are available to isolate data-frequency components. Frequency components with periods longer than the data-collection interval are removed by least-squares detrending. As many as 10 channels of data may be analyzed at one time. Both tabular and plotted output may be generated by the SPA program.

This program is written in FORTRAN IV and has been implemented on a CDC 6000-series computer with a central memory requirement of approximately 142K (octal) of 60-bit words. This core requirement can be reduced by segmentation of the program. The SPA program was developed in 1978.

Linear Continuous and Sampled-Data Systems

For analysis of linearized control systems

A new program performs general analysis of linear and continuous, discrete and sampled-data systems using the state-variable techniques. The program is especially suited for the analysis of linearized control system problems. It can be used to model a system described by a combination of differential equations and Laplace transform blocks, such as an aircraft control system. This

mixed-formulation capability facilitates the analysis of continuous systems and is indispensable in the analysis of sampled-data systems.

The analysis is based on plant equations, output equations, and control laws. For flexibility, additional matrix equations are used for the definition of feedback-control laws. State-variable-matrix operations are used to find system eigenvalues, transfer functions, root contours, root loci, frequency responses, power spectra, and transient responses. Input data may be entered in matrix form, block diagram form, general-parameter input form, or a combination of these.

This program is written in FORTRAN IV and has been implemented on a CDC 6000-series computer with a central memory requirement of approximately 140K (octal) of 60-bit words.

Mass Properties of a Rigid Structure

Simplified technique requires minimal input.

The program MASPROP rapidly calculates the mass properties of complex, rigid structural systems. Its basic premise is that complex systems can be adequately described by a combination of basic elementary structural shapes. Thirteen, widely-used basic structural shapes are used: discrete mass, cylinder, truncated cone, torus, beam (arbitrary cross section), circular rod (arbitrary cross section), spherical segment, sphere, hemisphere, parallelpiped, swept trape-

zoidal panel, symmetric trapezoidal panels, and a curved rectangular panel. With this approach, minimal inputs are required to calculate mass properties, such as the center of gravity and moments of inertia, of a complex structure.

Rigid-body analysis is used to calculate mass properties about component axes that have been rotated to be parallel to the system coordinate axes. The system center of gravity is calculated, and the mass properties are transferred to axes through the system center of gravity by using the parallel-axis theorem. System weight, moments of inertia about the system origin, and the products of inertia about the center of mass are calculated and printed. From the information about the center of mass, the principal axes of the system and the moments of inertia about them are calculated and printed.

The only inputs required are simple geometric data describing the size and location of each element and the respective material density or weight of each element.

This program is written in FORTRAN for execution on a CDC 6000-series computer with a central memory requirement of approximately 62K (octal) of 60-bit words. The development of this program was completed in 1978.

This program was written by John L. Gilbert, Reid A. Hull, and Phillip J. Klich of **Langley Research Center.** *For further information, Circle T on the COSMIC Request Card.*
LAR-12454

Image-Analysis Library

Collection of math and statistics routines

The MATHPAC image-analysis library is a collection of general-purpose mathematical and statistical routines and special-purpose data-analysis and pattern-recognition routines for image analysis. The MATHPAC library consists of six packages of routines based on widely accepted algorithms:

Linear Algebra Package: generalized matrix-manipulation routines, including matrix inversion, matrix decomposition, and eigenvalue computations

Optimization Package: a collection of routines for optimizing functions, including calculation of zeros, maximums, and minimums, least-squares problems, and linear and quadratic programing problems

Statistical-Summary Package: routines for computing statistical information, including moments, coefficients, ordering data, means, and deviations

Densities and Distribution Package: a means of determining probabilities related to various distributions, including incomplete-beta, binomial, chi-square, Fisher's, Poisson, gamma, and hypergeometric distributions

Regression Package: routines for finding solutions to multiple linear-regression analysis problems and for nonlinear least-squares-parameter estimation

Statistical-Test Package: statistical-test routines, including Fisher-exact test, goodness-of-fit tests, multiple-range test, and analysis-of-variance capabilities

The routines in MATHPAC are written in DEC FORTRAN IV PLUS for batch execution on the DEC PDP 11/45 using RSX 11D. The entire library requires a disk space of approximately 99K of 16-bit words. With some modifications the MATHPAC routines should compile on other FORTRAN IV compilers. MATHPAC was developed in 1977.

This program was written by the College of Science of Texas A. & M. University for **Johnson Space Center.** *For further information, Circle U on the COSMIC Request Card.*
MSC-18178

Modern Programing Language

Structured-programing for assembly language

A new structured-programing language is especially-tailored for producing assembly language programs for the MODCOMP II and IV minicomputers. The language, modern programing language (MPL), consists of a set of simple yet powerful control structures that include sequencing, alternative selection, looping, submodule linking, comment insertion, statement continuation, and compilation termination capabilities.

A basic function of MPL is to facilitate the expression of flow of control within a program. MPL allows programers to concentrate on program structure and logic while freeing them from certain limitations and inconveniences of standard assembler programing. The programer constructs codes using MPL control statements and assembly language instructions. The MPL control statements are translated into assembly language statements to perform the desired functions. This generated assembly code is combined with the user-supplied assembly code and passed to the assembler. MPL should enhance the development of assembly language programs for use on the MODCOMP minicomputers.

The MPL is implemented by use of the MPL preprocessor. This preprocessor is divided into three functional phases: editing, parsing, and code generation. The first action of the preprocessor is to edit the first statement of the input. If the statement is not an MPL structure, it is passed through to the appropriate output area, and the next statement is edited. When an MPL structure is encountered, the syntax is checked and any error condition messages generated. Structures containing errors are not passed for further processing.

The parsing phase of processing breaks an MPL structure into a set of appropriate table entries. The code generation phase accesses the tables built by the parsing phase and generates the appropriate assembly code. Upon completion of code generation, a return to the editing phase initiates processing of the next input statement. The input is processed in this manner until an MPL terminator is detected. The output from the preprocessor is a complete assembly-language program ready for the assembler.

The MPL preprocessor is written in FORTRAN IV and generates assembly code for use on the MODCOMP II and IV. The preprocessor has a core requirement of approximately 139K of 8-bit bytes. The MPL preprocessor was developed in 1976.

This program was written by Gail H. Feldman and John A. Johnson of Caltech for **NASA's Jet Propulsion Laboratory.** *For further information, Circle V on the COSMIC Request Card.*
NPO-14105

SUBJECT
INDEX

THIRD-CLASS BULK

NASA

Using rocket-engine insulation technology to treat sewage sounds farfetched, but nonetheless that is what is done at this pilot plant built in Huntington Beach, California, with the help of NASA engineers. Activated carbon, produced pyrolytically by a process developed at the Jet Propulsion Laboratory to make lightweight insulation, is applied to remove organic contaminants and to accelerate settling in secondary sewage treatment. The process could help municipalities and industry save money when building facilities to meet new Environmental Protection Agency standards. [See the bottom of page A1.]